Assessing and Predicting Distribution Shifts of Canopy-Forming Marine Macrophytes in the Northwest Atlantic with Remote Sensing and Species Distribution Models

by

Kristen Lynn Wilson

Submitted in partial fulfilment of the requirements
for the degree of Master of Science

at

Dalhousie University
Halifax, Nova Scotia
December 2017

Table of Contents

List of Tables

List of Figures

Abstract

This thesis quantified the distribution of several ecologically and commercially important canopy-forming marine macrophytes in the Northwest Atlantic using species distribution models (SDM) and satellite remote sensing. Firstly, correlative SDMs and physiological thresholds were used to determine current and projected distributions by 2100 under different climate change scenarios for six seaweed species common to the Northwest Atlantic. Species ranges will shift north with continued warming where fucoids and kelps were projected to have a net loss of latitudinal range, while other species gain latitudinal range. Secondly, SPOT 6/7 imagery was classified with two different classification techniques and modest ground-truthing effort to determine the distribution of eelgrass (*Zostera marina*) in three bays in Nova Scotia. Only one bay successfully classified eelgrass distribution, highlighting the need for excellent satellite image quality, and clear water. The two approaches can inform conservation and management of canopy-forming marine macrophytes on different spatial and temporal scales.

List of Abbreviations and Symbols Used

AUC	Area under the curve
AUG	August
CMIP	Climate Model Intercomparison Project
CO_2	Carbon dioxide
DFO	Department of Fisheries and Oceans
DNR	Department of Natural Resources
FEB	February
GFDL	Geophysical Fluid Dynamics Laboratory Earth System Modular Ocean Model; mild warming
GPS	Global positioning systems
IPSL	Institute Pierre Simon Laplace Earth Systems Low Resolution Model; strong warming
ISOCLUST	Iterative self-organizing unsupervised classifier
LTA	Long term average
Max	Maximum
Mea	Mean
Min	Minimum
NE	Northeast
NIR	Near infrared
NS	Nova Scotia
NW	Northwest
PT	Physiological thresholds
RCP	Representation concentration pathways; four carbon concentration pathways indicating different levels of radiative forcing by 2100
SAT	Surface air temperature
SE	Standard error
SDM	Species distribution model
SIC	Sea ice area coverage
SMR	Summer
SRS	Satellite Remote Sensing
SSS	Sea surface salinity
SST	Sea surface temperature
SW	Southwest
USA	United States of America
VIF	Variable inflation factor
WNT	Winter

°C	Degree Celsius
°	Degree cell
%	Percentage
m	Metres
nm	Nanometres
PSS	Practical salinity scale

Acknowledgments

First and foremost, I wish to thank my supervisors Drs. Heike Lotze and Marc Skinner, this thesis would not have been possible without their support and guidance over these past few years. I'd like to thank my committee members: Drs. Derek Tittensor and Boris Worm, and my external committee member: Dr. Melissa Wong, for all their thoughtful insights to improve this thesis. To my volunteers Adrienne Chan and Alicia Pérez Aparico, thank you for your help collecting seaweed occurrence records. To Monica Boudreau, Drs Anthony Chapman, Gary Saunders, Ricardo Scrosati, David Garbary, Philippe Archambault, Kyle Matheson, Robert Hooper, Scott Caine, Jordan Nathan Musetta-Lambert, and Thierry Chopin, for your contribution of personal seaweed occurrence records and area descriptions. Thank you to Dr. William Cheung for regridding the CMIP5 climate data out of the native tripolar grid. Thank you to Dr. Alana Westwood and Shannon Bale for their advice and guidance for building SDM and running Maxent. Thank you to Heather Ward for her advice with the remote sensing analysis. To my lab mates: Andrea Buchholz, James Scott McCain, Nakia Cullain, Reba McIver, Lauren Kay, Liz Nagel, Isabelle Hurley, Faelan Prentice and Dr. Tyler Eddy for their help with field work, and making the lab a great place to come to work. To my partner, Paul Dickson, with his help with writing code and continued support. Lastly, I'd like to thank the National Science and Engineering Council of Canada, Dalhousie University, Killam Laureates, and Nova Scotia Graduate Scholarships for funding this research.

Chapter 1 Introduction

1.1 Importance of Marine Macrophytes

Canopy-forming marine macrophytes, including seagrasses, kelp, and fucoids, are important components of coastal ecosystems. As ecosystem engineers (Jones et al. 1994), they provide shelter and food to a multitude of different marine taxa through their complex three-dimensional structure (Schmidt et al. 2011; Krumhansl and Scheibling 2012; Kay et al. 2016). Despite covering only 0.2% of the surface area of the world's oceans (Duarte et al. 2013a), marine macrophytes are estimated to contribute 2 to 6% of global net primary productivity, and are the predominant primary producers in coastal ecosystems (Duarte and Cebrián 1996; Field et al. 1998). They form large quantities of primary producer biomass which allows them to store large amounts of carbon and nutrients (Smith 1981; Schmidt et al. 2011). Recognizing this importance, eelgrass (*Zostera marina*) has been designated as an ecologically significant species in Eastern Canada (DFO 2009) with a policy of no net loss of habitat function (Hanson et al. 2008), and is protected by the Clean Water Act in the USA (Nelson 2009). Yet the canopy-forming seaweeds, such as kelp and fucoids, which perform similar ecosystem functions as eelgrass, are not protected by similar policies. Several seaweed species are impacted by direct commercial exploitation (Seeley and Schlesinger 2012; Vandermeulen 2013; Arbuckle et al. 2014). Furthermore, the ecosystem functions provided by canopy-forming macrophytes in the Northwest (NW) Atlantic are also affected by anthropogenic activities including the spread of invasive species (Garbary and Miller 2006; Schmidt and Scheibling 2006, 2007), nutrient loading (Worm and Lotze 2006; Waycott et al. 2009; Schmidt et al. 2012), and climate change (Harley et al. 2006, 2012; Wilson et al. 2015; Kay et al. 2016). Consequently these anthropogenic impacts can alter the abundance and

distribution of canopy-forming macrophytes with potentially negative consequences for the functions and services they provide, and the species communities that depend on them (Schmidt et al. 2012, 2017; Seeley and Schlesinger 2012; Wilson et al. 2015).

1.2. Marine Macrophyte Distribution in the Northwest Atlantic

The rocky shores of the NW Atlantic are dominated by perennial, canopy-forming seaweeds with distinct zonation patterns from Long Island Sound into the Arctic (Lüning 1990; Adey and Hayek 2011). South of Long Island Sound, seaweed distribution is limited due to the predominance of soft sediment shores (Schneider and Searles 1991). Fucoids dominate the mid-intertidal with rockweed (*Ascophyllum nodosum*) in more sheltered and *Fucus vesiculosus* in more exposed regions (Adey and Hayek 2011). The low-intertidal is dominated by smaller bushy red-algae, predominantly Irish moss (*Chondrus crispus*). In the subtidal, laminarian kelps can form dense forests and includes species such as *Alaria esculenta*, *Agarum clathratum, Laminaria digitata*, *Saccharina latissima*, and *S. longicruris*.

In 1957, the invasive *Codium fragile* was first introduced to the NW Atlantic in Long Island Sound (Carlton and Scanlon 1985). Originating from Japan (Provan et al. 2008), *C. fragile* has since spread south to North Carolina and north to Newfoundland (Matheson et al. 2014). *Codium fragile* competes with native kelp species; if a disturbance removes kelp canopy cover, *C. fragile* can quickly colonize the exposed substrate and inhibit the recruitment of kelp (Scheibling and Gagnon 2006). The spread of *C. fragile* has not been as extreme as at first anticipated; *C. fragile* had an average percent coverage of 28.5% in 2000 along the exposed Atlantic coast of Nova Scotia,

which had decreased to 11.70% by 2007, compared to 24.7% of coverage for kelps in 2007 (Watanabe et al. 2010).

By comparison, the soft sediment shores of the NW Atlantic from South Carolina into the Arctic are dominated by one perennial, canopy-forming seagrass species: *Zostera marina* (eelgrass), with occasional small patches of widgeon grass (*Rupia maritima*; Gosner 1978). This unique dominance of just one canopy-forming species on most soft-sediment habitat underscores the importance of eelgrass being recognized as an ecologically significant species (DFO 2009).

1.3. Assessing and Projecting Shifts in Species Distribution

Understanding the spatial distribution of any species is important for many conservation and management applications. Two techniques that can be used to estimate or project a species' distribution are species distribution models (SDM; Elith and Leathwick 2009; Franklin 2009), and satellite remote sensing (SRS; Pettorelli et al. 2014), both of which have been used to quantify the distribution of marine macrophytes (Klemas 2011; Hossain et al. 2015; Marcelino and Verbruggen 2015).

1.3.1 Species Distribution Models

SDMs are used in a wide variety of applications to make predictions about a species' present distribution. They can also be used to project a species distribution using historic data, or its future distribution using projected environmental data, to examine temporal changes in a species' range (Elith and Leathwick 2009). The development of SDMs relies on the niche concept, where a species persists and maintains a stable population size under a given set of abiotic and biotic conditions (Hutchinson 1957). There are two types of SDMs: correlative and mechanistic, which have been used to

predict the distribution of seaweed and seagrass species (Valle et al. 2014; Boscutti et al. 2015; Marcelino and Verbruggen 2015). Correlative SDMs are used to classify a species' realized niche; the range of environmental conditions a species occurs over that is constrained by dispersal capabilities and biological interactions. Whereas mechanistic models are used to classify a species fundamental niche; the entire range of environmental conditions that a species can persist in (Marcelino and Verbruggen 2015).

Correlative SDMs are more common, and are built by relating known instances of species presence (occurrence records) with biologically significant environmental variables to determine a species' distribution (Franklin 2009). Correlative SDMs can then be projected onto a new set of environmental variables (novel environments), to examine how a species' distribution may change (i.e. how a distribution changes with future climate data). There are two main disadvantages with correlative SDMs. The first is that both occurrence records and environmental data needed to build the model may be limited. The second is that they have difficulty making projections into novel environments, as the range of environmental conditions used to build the SDM may not match new projected environmental conditions (Elith et al. 2011).

Mechanistic models are less common as they require detailed physiological data to predict species presence, often collected through extensive laboratory studies (Franklin 2009). The physiological data is used to determine physiological tolerances, which classify environmental variables into areas of suitable habitat. Mechanistic models are typically more robust when making predictions into novel climate outside the range of environmental conditions the species is currently observed in, as they include physiological responses (Kearney and Porter 2009). Hybrid approaches, where a

correlative SDM is built, and added to a mechanistic model, can improve model projections for novel environment (Elith et al. 2010). This can be done simply by including information on a species' warm-water tolerance on its growth rate and mortality, indicating thermal physiological thresholds (Martínez et al. 2014; Franco et al. 2017).

1.3.2 Remote Sensing

There are several types of optical SRS which can be active (e.g. sensor emits a light source, including lidar) or passive (e.g. sensor uses light from the sun, including commercial and governmental satellites platforms such as WorldView, SPOT, IKONOS, and Landsat) to measure a features reflectance as each feature has different spectral properties (Horning et al. 2010; Hossain et al. 2015). Since the creation of Landsat satellites in 1972, passive, optical SRS have been used to successfully quantify marine macrophyte coverage (e.g. Casal et al. 2011; Hossain et al. 2014; Uhl et al. 2016). All passive, optical SRS rely on the same principles where ground reflectance is measured at different wavelengths (Horning et al. 2010). This is known as the spectral resolution, where one sensor (known as a band) measures a very specific grouping of electromagnetic radiation, typically corresponding to a colour (e.g. blue light). Multispectral imagery typically has between 4 to 12 bands. This reflectance is measured by a defined range of numbers, known as the radiometric resolution (i.e. 256 unique values for an image with 8-bit resolution), at a defined spatial resolution (pixel size on the ground; i.e. 1.5 x 1.5 m). The SRS image is then classified into ground cover with (supervised) or without (unsupervised) the use of known ground cover points. The resulting classification can be used in several applications including mapping species

distribution, habitat management, and if imagery exists across years, a temporal change analysis (Klemas 2011; Pettorelli et al. 2014; Rose et al. 2015).

1.4 Research Objectives

This thesis examined how passive optical SRS and SDMs can be used to estimate or project marine macrophyte distribution. In Chapter 2, I focus on projecting the large-scale, continental response of common canopy-forming seaweed distribution to continued climate warming. Since large-scale patterns for seaweed growth and survival are mainly controlled by sea surface temperature (SST; Lüning 1990), seaweed distributions closely follow SST isotherms (van den Hoek 1975). As the NW Atlantic continues to warm due to human-induced climate change (Barnett et al. 2001; Lee et al. 2011), seaweed distributions will be impacted across their entire geographic range, likely resulting in northward range shifts. I used species distribution models (SDMs) in combination with physiological thresholds (hybrid SDMs, see section 1.3.1) and climate model projections to investigate the extent of this shift in the NW Atlantic over the next century.

In Chapter 3, I focus on quantifying eelgrass distribution at a smaller, bay-wide scale. With the recent declines of eelgrass in Nova Scotia (Hanson 2004) and globally (Orth et al. 2006; Waycott et al. 2009), baseline knowledge of eelgrass distribution is critical to understand the extent of these declines. I used high-resolution multispectral satellite imagery in combination with ground truthing, local ecological knowledge, and substrate data to compare two methods for classifying remotely sensed data.

Note that while the general introduction (Chapter 1) and conclusion (Chapter 4) are written in the first person, the two data chapters (Chapters 2 and 3) are written as manuscripts and therefore include the use of ‘we’ in acknowledgement of my co-authors.

Chapter 2 Projected 21st Century Distribution of Canopy-Forming Seaweed Species in the Northwest Atlantic

2.1 Introduction

Since 1750, the exponential increase in greenhouse gas emissions, particularly CO_2, has resulted in sea level rise, ocean acidification, and ocean warming (IPCC 2013). Consequently the NW Atlantic has significantly warmed since 1980 (Barnett et al. 2001), at a faster rate than other ocean basins (Lee et al. 2011). Since 1982, sea surface temperature (SST) has significantly increased at latitudes of 42°N to 60°N (Baumann and Doherty 2013), and SST isotherms have been moving north at a rate of 40 km/year since 1975 (Hansen et al. 2006). By 2100, there is an anticipated 3°C further increase in SST expected, with the Arctic anticipated to warm by 4.9°C up to 9.3°C, under RCP 4.5 (representative concentration pathways; IPCC 2013). Therefore, coastal ecosystems in the NW Atlantic, including seaweed communities, will continue to be affected by increasing SST over the coming century.

SST is the major factor influencing seaweed survival and growth on large spatial scales (Lüning 1990), resulting in seaweed distributions which closely follow SST isotherms (van den Hoek 1975). In the NW Atlantic, there are four distinct phytogeographic regions representing common distribution limits: warm-temperate, cold-temperate, Subarctic, and Arctic regions (Figure 2.1; van den Hoek 1975; Adey and Hayek 2011). The warm-temperate region runs from Cape Hatteras, North Carolina to Cape Cod, Massachusetts. The cold-temperate/boreal region runs from Cape Cod to western Newfoundland, the Subarctic region from western Newfoundland to southern Labrador centered on the Strait of Belle Isle, and the Arctic region runs from mid-Labrador to the North Pole.

All study species are found in the warm-temperate region, where rockweed *Ascophyllum nodosum* (Gosner 1978), Irish moss, *Chondrus crispus* (Lüning 1990), and the kelps *Laminaria digitata* and *Saccharina latissima* (Merzouk and Johnson 2011) occur south to Long Island Sound, and *Fucus vesiculosus* and the invasive *Codium fragile* occur south to North Carolina (Taylor 1957; Carlton and Scanlon 1985). The Subarctic is the northern limit for *C. fragile*, *C. crispus*, and *L. digitata*, with the other three species existing into the Arctic (Lüning 1990; Adey and Hayek 2011).

Seaweeds are indicators of climate change in coastal ecosystems (Marbà et al. 2017) and will either need to adapt to a warmer climate, or shift their distribution to conserve their niche (Harley et al. 2012). Marine species are known to typically fill their thermal niche (Sunday et al. 2012), therefore present range limits likely indicate the true range of thermal tolerance for these species. If seaweed species fail to acclimate to increasing temperatures, range shifts are expected to occur (Müller et al. 2009; Jueterbock et al. 2013; Assis et al. 2014). As of yet, there have been no observed large-scale range shifts in the field for NW Atlantic kelp communities (Merzouk and Johnson 2011); however, smaller-scale decreases in abundance have occurred in many areas (Filbee-Dexter et al. 2015; Krumhansl et al. 2016; Dijkstra et al. 2017), which has been attributed to lack of baseline knowledge of kelp distribution (Merzouk and Johnson 2011). For rockweeds, there is anecdotal evidence suggesting that *A. nodosum* has had a small range shift at its southern edge from New Jersey to Long Island Sound (Keser et al. 2005), with decreases in abundance throughout the Canadian Maritimes (Ugarte et al. 2010).

The lack of observations of larger range shifts of seaweeds across the NW Atlantic despite significantly increasing SST is surprising. Range shifts of seaweeds have been observed elsewhere in Portugal (Lima et al. 2007), Spain (Duarte et al. 2013b), Britain (Gallon et al. 2014; Yesson et al. 2015), Australia (Wernberg et al. 2011), and Japan (Tanaka et al. 2012), and these shifts have been attributed to the impacts of climate change. Consequently, the NW Atlantic is also likely experiencing similar range shifts of seaweeds with continued warming.

The goal of this chapter was to assess how projected scenarios of future climate change will impact the distribution of common canopy-forming seaweed species in the NW Atlantic. To do so, we had three main objectives: (i) create a comprehensive database to determine where the seaweed species are currently observed; (ii) use these occurrence records in combination with environmental data to build a hybrid species distribution model (SDM) to predict current suitable habitat; and (iii) use this hybrid SDMs to make projections of future distribution under projected climate change. We chose six study species common in the NW Atlantic including mid-intertidal fucoids (*A. nodosum* and *F. vesiculosus*), low-intertidal Irish moss (*C. crispus*), and subtidal laminarian kelps (*L. digitata* and *S. latissima*), as well as the highly invasive *C. fragile*. It was hypothesized that each species would experience a northward shift of both the southern and northern distribution boundary. However, this shift will likely vary by species and as such, the seaweed community will not shift as an assemblage due to their varying thermal tolerances.

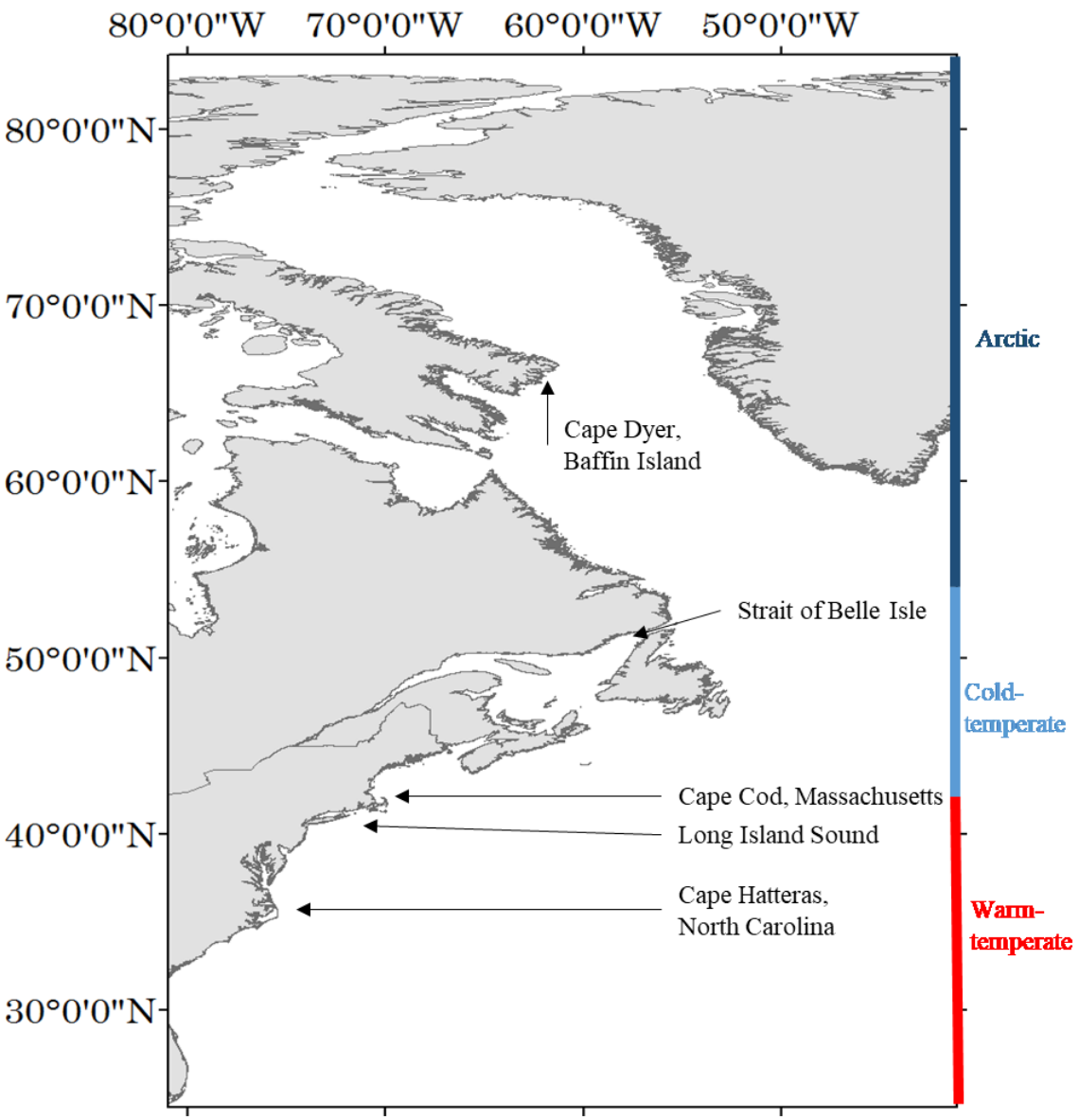

Figure 2.1 Phytogeographic regions of NW Atlantic from van den Hoek (1975) and Adey and Hayek (2011).

2.2 Methods

2.2.1 Species Occurrence Records

Presence-only occurrence records were collected from 1980 onwards to reflect the present-day distribution of six species of seaweeds within their current range in the NW Atlantic: *Codium fragile* (63 records), *Fucus vesiculosus* (134 records), *Ascophyllum nodosum* (86 records), *Laminaria digitata* (88 records), *Saccharina latissima* (122 records), and *Chondrus crispus* (72 records; Appendix B). These records were obtained through a literature search, correspondence with other research groups, personal observations, and online databases (Ocean Biogeographic Information System, Aquatic Biodiversity Monitoring Network, and Global Biodiversity Information Facility). If a study provided a map with sample locations, but no specific latitude and longitude coordinates, then these were obtained by matching the site in Google Earth. Generally, records were collected from 1980 onwards, as this was the first year significant increases in sea surface temperature were detected in the NW Atlantic (Barnett et al. 2001). However, due to the inaccessibility of the far north, very few occurrence records exist for the Canadian Arctic and Greenland. Therefore, records prior to 1980 were used in areas north of Newfoundland. It was assumed that along this northern range seaweeds who were present prior to 1980, could still occur after 1980 in these areas as any Arctic warming will promote northward range shifts.

2.2.2 Environmental Data

To inform species distribution models (SDMs), environmental parameters should be biologically relevant to the species examined at the study scale (Phillips et al. 2006). Environmental layers used in this study include sea surface temperature (SST), surface air temperature (SAT), sea ice area coverage (SIC), and sea surface salinity (SSS; Table

2.1). Monthly and seasonal long term averages (LTA) were determined in the statistical environment R (R Core Team 2014) for August, February, summer, and winter. The LTA of SAT at 0.5° resolution was interpolated using inverse distance weighting to extend over coastal areas, and resampled to a 0.25° resolution. All layers were projected into the North America Albers equal-area conic projection (Elith et al. 2011), and set to the same extent and cell size (0.25°x0.25°) using ArcGIS® v. 10.3 (ESRI, Redlands, USA). Occurrence records were processed to match the environmental data by projecting to the same equal-area projection, and duplicate records within a grid cell were removed. As the environmental layers do not perfectly match the coastline, occurrence records that did not overlay the environmental data were moved to the closest grid cell.

The variable inflation factor (VIF) was used to remove any correlated environmental variables, as correlations may change with future projected climate data (Elith et al. 2010). Variables were removed in a step-wise fashion by removing the variable with the highest VIF until all remaining variables had a VIF values less than or equal to 10 (Naimi and Araújo 2016).

2.2.3 Species Distribution Model

To build the correlative species distribution model (SDM) the software program Maxent v. 3.3.3k was used (Phillips et al. 2004, 2006) which determines areas of suitable habitat using machine learning techniques and the principle of maximum entropy. Maxent only requires the input of presence data to build a SDM, and it consistently performs well when compared to other correlative modelling algorithms (Elith et al. 2006). It assumes that (i) the occurrence records are unbiased (Elith et al. 2011), and from a source habitat (Phillips et al. 2006), (ii) the study area has been randomly sampled for

species presence (Phillips et al. 2006), (iii) the environmental data are independent of one another (Phillips et al. 2006), (iv) the probability of detecting a species is the same for all pixels (Yackulic et al. 2013) and, (v) that any pixel can be used as background as a species can occur anywhere in the study area (Merow et al. 2013). Criteria i and ii were not fully met due to limited occurrence records in northern areas, therefore it is likely that the niche breadth is these areas is under-estimated and therefore northern borders are predicted too far south.

Maxent is a deterministic model that tests against the null hypothesis that the study species shows no preference for a certain range of environmental conditions (Phillips et al. 2006; Elith et al. 2011). Entropy is a measure of dispersiveness, so maximizing the entropy results in a probability distribution which is maximally random based on the constraints. The probability distribution that most closely matches where a species occurs is the distribution with the maximum entropy subject to the same constraints. Maxent requires the input of occurrence records and environmental data. The area the environmental data covers defines the area the probability distribution is defined over. The environmental layers are transformed into feature classes, and then constrain the probability distribution so that the value expected from the environmental layers (i.e. August maximum SST) is the same as the empirical average. These constraints are regularized with L1-regularization to avoid over-fitting the model, for more detail see Phillips et al. (2006), and Elith et al. (2011).

Maxent also requires the use of random background points (default at 10,000), taken from the environmental data layers within the study area, which may or may not contain presence records. To determine a relative probability of presence, Maxent

transforms the raw model output into a logistic model, based on assuming a value of species prevalence (default at 0.5), to build the best model to determine the relative probability of presence of a species from background environmental data.

2.2.4 Model Building and Evaluation

We originally considered a large suite of environmental variables (Table 2.1) that were reduced using the VIF to only include uncorrelated environmental variables (see section 2.2.1). These uncorrelated environmental variables were input into the Maxent model, which was then run using k-fold cross-validation (Kohavi 1995). The number of folds (k) used depended on the number of occurrence records, where species with over 100 occurrences records (*F. vesiculosus* and *S. latissima*) k=5, and for the species with under 100 occurrence records (*A. nodosum*, *C. crispus*, *C. fragile*, and *L. digitata*) k=4. Feature classes were set to allow only linear (sample mean true to average conditions required), quadratic (sample range true to species tolerance range), and hinge (same as linear but constant past a threshold; Phillips et al. 2006; Elith et al. 2011) and the runs were set to 5000 iterations to ensure model convergence. As environmental layers had fewer than 10,000 pixels, all pixels were always used as background points.

A jackknife test was performed to determine the importance of each environmental variable, and the variable with the smallest decrease in average test gain when removed from the full model was dropped. This was repeated until only one variable remained to determine the most important variable for predicting a species distribution. To balance variables that performed well in training and testing, average regularized training gain was used to determine the best model for each species. This was done to balance model complexity and performance, where the best model was

determined to be the one with the fewest number of predictor variables that did not result in a significantly different training gain from the full model, based on 95% confidence intervals (Yost et al. 2008). Therefore, test gain was used to decide which variables to remove, while regularized training gain was used to decide when to stop removing variables from the model.

All continuous logistic model output was turned into binary presence/absence data based on the maximizing the sum of test sensitivity and specificity threshold (Liu et al. 2016). Sensitivity indicates where true presence occur (true positive rate), and specificity indicates where true absences occur (in this case, distinguishing presence from random background points; Phillips et al. 2006). This results in a model with the highest sum of correctly classified presences and pseudo-absences.

Model performance was evaluated using both threshold dependent and independent tests. A one-tailed binomial test requires the use of thresholds, and determines if test locations are predicted significantly better than random in the model. The null hypothesis states that the test values are predicted no better than a random model with the same proportional predicted area (Phillips et al. 2006). The associated p-value is exact since the number of test samples for each species was less than 25. This test uses the omission rate, the fraction of test samples which were not denoted as suitable habitat, and the proportional predicted area, the proportion of total pixels found to be suitable habitat, to determine this probability.

The threshold independent evaluation used was the area under the curve (AUC) of the receiver operator characteristics curve (ROC; Phillips et al. 2006). This curve plots 1-specificity (true negative rate) against sensitivity to determine the AUC as a value

between 0.5 (random prediction) and 1 (perfect model). Typically, specificity is determined using absence data points. In presence-only datasets, specificity is determined by determining presence from random, also known as pseudo-absence. This results in a decrease of the maximum value of the AUC to 1-*a*/2, where *a* is the fraction of pixels noting the species distribution. An AUC of 0.5-0.7 is indicative of poor, 0.7-0.9 of moderate, and >0.9 of high model performance (Franklin 2009).

2.2.5 Climate Model Data

Two representative concentration pathways (RCP) were used: RCP 2.6 represented a "best-case scenario" with a peak and then decline in CO_2 concentration, and RCP 8.5 indicated a "business as usual scenario" with a continual increase in CO_2 concentration by 2100 (Moss et al. 2010). Presently, CO_2 emissions are on target with the RCP 8.5 scenario (Sanford et al. 2014), which projects the highest magnitude of environmental changes by 2100 (Bopp et al. 2013).

Global climate models are available from the Coupled Model Intercomparison Project (CMIP5, Taylor et al. 2012). Each global climate model has its own bias, therefore multi-model ensemble means are frequently used to attempt to approximate the true range of environmental conditions expected under different climate scenarios (Bopp et al. 2013). Two climate models were used from CMIP5 (Taylor et al. 2012), indicating lower (GFDL-ESM2M; GFDL hereafter; Dunne et al. 2012) and higher (IPSL-CM5A-LR; IPSL hereafter, Dufresne et al. 2013) levels of SST warming (Bopp et al. 2013). LTAs of SST and SAT were calculated for current conditions (2006-2015), mid-century (2040-2050), and end-century (2090-2100). The combination of the two climate models and the two RCPs gives a range of best to worst-case scenarios of warming in the NW

Atlantic over the next century. All data were re-gridded to the same 0.25 x 0.25° grid used for the present-day environmental layers.

2.2.6 Future Projections

The best species distribution/Maxent model (determined in 2.2.4) was rerun using k-fold cross-validation to make projections about future changes under climate warming. First, to determine differences between present-day environmental data, and present-day climate model data, the best model was run and projected onto present-day climate model data (LTA of 2006-2015) for RCP 2.6 and 8.5. Next, to determine future changes in distribution, the Maxent model was projected onto future LTA over 2040-2050 and 2090-2100 for both GFDL and IPSL at RCP 2.6 and 8.5. Models were clamped to avoid training with data outside the species range and clamp grids were created to determine how clamping influenced the projection (Elith et al. 2010). A multidimensional environmental surface similarity plot was also created to determine areas of novel habitat.

To determine the present and future day northern and southern limit of the study species, the latitude for the furthest most northern and southern pixel of continuous distribution was determined. Continuous distribution was defined as pixels (grid cell) predicted to contain suitable habitat being separate by one or less pixels predicted to contain unsuitable habitat along the southern and northern edge. As many species exhibited a patchy distribution at their northern and southern limits, this was also done for the absolute most northern and southern pixel predicted, excluding outliers. Here, northern limit was defined as northern limit for the NW Atlantic, as such, no distinction was made as to whether the habitat was along the Canadian or Greenland coastline. This

was done for each model fold (k = 4 or 5) per model, time-period, and RCP to determine the standard error around the species range limits.

These absolute distribution limits were standardized to determine relative distribution limits and range shifts. First, the difference between present-day climate model data (LTA of 2006-2015) and future climate model data (i.e. LTA of 2040-2050) distribution limit (i.e. southern range limit) for one climate model (i.e. GFDL) was determined to find the magnitude of range shift expected (i.e. 3° shift north). This difference was added to the predicted present-day range limit (based on present-day environmental data) to determine the new relative projected distribution limit (i.e. 40°N to 43°N). This was repeated for all southern and northern distribution limits for both mid and end-century, RCP 2.6 and 8.5, and both GFDL and IPSL. Individual model responses of GFDL and IPSL are presented to assess the range of projected responses. The relative changes in distribution limits for GFDL (mild warming) and IPSL (strong warming) were averaged for each species to determine the most likely projection. Taking the average between the lower and higher increases in SST provides the most likely magnitude of range shift that can be expected by 2100 (Bopp et al. 2013).

2.2.7 Physiological Thresholds

A previous lab experiment (Wilson et al. 2015) provided information on the growth and survival of all study species except *S. latissima* between 12 and 29°C from Atlantic Canada populations found in the middle of each species respective range. This data were used to create physiological thresholds (PT) for heat-related survival to define the water temperatures (SST) at which each species grew well, experienced reduced growth, experienced reduced growth and partial mortality, and complete mortality.

Reduced growth was defined as the first temperature at which there was a significant reduction in relative growth rate, based on perANOVA post-hoc comparisons (Wilson et al. 2015). Partial mortality was defined as at least one individual dying during the experiment at a specific temperature, and complete mortality was defined as all replicates at a specific temperature dying. *Saccharina latissima* was assumed to experience similar PT as *L. digitata* based on experimental studies completed on Halifax (Bolton and Lüning 1982; Simonson et al. 2015) and Maine and Long Island Sound (Redmond 2013) populations. Cold-related survival was not tested but all species exhibit measurable photosynthesis in water temperatures of at least 0°C (Lüning 1990). Present-day and projected future climate model SST data were classified into these four categories in areas where August maximum SST was greater than 12°C, creating a layer for each species PT (Martínez et al. 2014).

The PT were combined with the correlative Maxent model to create a hybrid SDM. To do so, the predicted present-day and projected future climate Maxent distribution, binary coded for species presence absence, was multiplied by the corresponding species PT. Therefore, the resulting map denotes where Maxent predicted/projected each species to occur, while indicating where the PT agree and disagree with the model output. Areas where Maxent predicted/projected the species to occur, which correspond to PT for good and reduced growth, are likely to be areas with suitable habitat. Areas where Maxent predicted/projected the species to occur, which correspond to PT for partial and complete mortality, are less likely to be areas with suitable habitat. The PT provide empirical data help to improve model confidence in projecting a species distribution in a novel and changing environment (Elith et al. 2010).

Table 2.1 Original environmental data sources considered for building the Maxent model. Long term averages (LTA) per year range and parameter were determined for minimum (min), mean (mea), and maximum (max), for February (Feb), August (Aug), Winter (Wnt) and Summer (Smr). Winter is the combination of January-March and summer of June-August.

Environmental parameter	LTA	Unit	Year range	Resolution	Reference
Sea Surface Salinity (SSS)	Wnt mea Smr mea	PSS	1955-2012	0.25 x 0.25°	World Ocean Atlas 2013 version 2 (Zweng et al. 2013)
Surface Air Temperature (SAT)	Feb min Aug max Wnt mea Wnt max Smr mea Smr min	°C	1980-2011	0.50 x 0.50°	Climate Prediction Centre Land Surface Air Temperature Analysis dataset(Fan and van den Dool 2008)
Sea Surface Temperature (SST)	Feb min Aug max Wnt mea Wnt max Smr mea Smr min	°C	1982-2015	0.25 x 0.25°	National Oceanic and Atmospheric Administration (NOAA) optimum interpolation SST version 2 high resolution dataset (Reynolds et al. 2007) provided by the NOAA/OAR/ESRL PSD, Boulder, Colorado, USA, from their Web site at http://www.esrl.noaa.gov/psd/
Sea Ice Concentration (SIC)	Feb min Aug max Wnt mea Wnt max Smr mea Smr min	%	1982-1986, 1989-2015	0.25 x 0.25°	National Oceanic and Atmospheric Administration (NOAA) optimum interpolation SST version 2 high resolution dataset (Reynolds et al. 2007) provided by the NOAA/OAR/ESRL PSD, Boulder, Colorado, USA, from their Web site at http://www.esrl.noaa.gov/psd/

2.3 Results

2.3.1 Maxent Model

After removing correlated variables in a stepwise fashion based on the variable inflation factor (VIF), nine environmental variables were chosen to be included in the full Maxent model (Table 2.2). In the process of model selection, the least important environmental variables were removed from the model to determine the best model per species that balanced model complexity and performance (Appendix B: Table B.1). August maximum sea surface temperature (SST) was the most important predictor variable for *Chondrus crispus, Codium fragile,* and *Laminaria digitata.* Winter maximum sea ice area coverage (SIC) was the most important predictor variable for *Ascophyllum nodosum* and *Saccharina latissima*, and winter mean sea surface salinity (SSS) was the most important predictor variable for *Fucus vesiculosus*. Across all species, August maximum SST and winter maximum SIC were the only two variables consistently retained in all six models (Table 2.3). Figure 2.2 gives an example of how these variables were chosen to select the best model outlined in Table 2.3 (see Appendix B: Figures B.1-B.5 for similar figures for the other five species). As *C. crispus* test gain increased from drop 0 (full model) to drop 5 (five variables removed) there is a small but non-significant decrease in training gain. When the sixth variable was removed, there was a decrease in test gain, and a significant decrease (based on non-overlapping 95% CIs) in training gain, therefore for *C. crispus* the best model would be the one with only five variables removed. There was also a decrease in training and test AUC when the sixth variable was removed (Figure 2.2). All models had a significant binomial p-value, and an AUC >0.87 for training and test data (Table 2.3), indicating moderate to high model performance.

Each occurrence record was also plotted against its corresponding August maximum SST (Figure 2.3) to test if the physiological thresholds aligned with where the occurrence records were found. Most occurrence records occur in areas where the physiological thresholds indicate good and reduced growth for each species. However, some kelp occurrence records occur in SST that should indicate complete mortality.

Table 2.2 Variable inflation factor (VIF) for the nine environmental variables included in the full Maxent model and abbreviations used in subsequent tables.

Variable	Abbreviations	VIF
August Maximum SST	AugMaxSST	7.13
August Maximum SAT	AugMaxSAT	6.75
Summer Mean SIC	SmrMeaSIC	4.01
Summer Minimum SIC	SmrMinSIC	1.76
Winter Max SIC	WntMaxSIC	2.85
Summer Mean SSS	SmrMeaSSS	3.15
Summer Minimum SST	SmrMinSST	3.10
Winter Mean SSS	WntMeaSSS	3.27
Winter Maximum SAT	WntMaxSAT	4.28

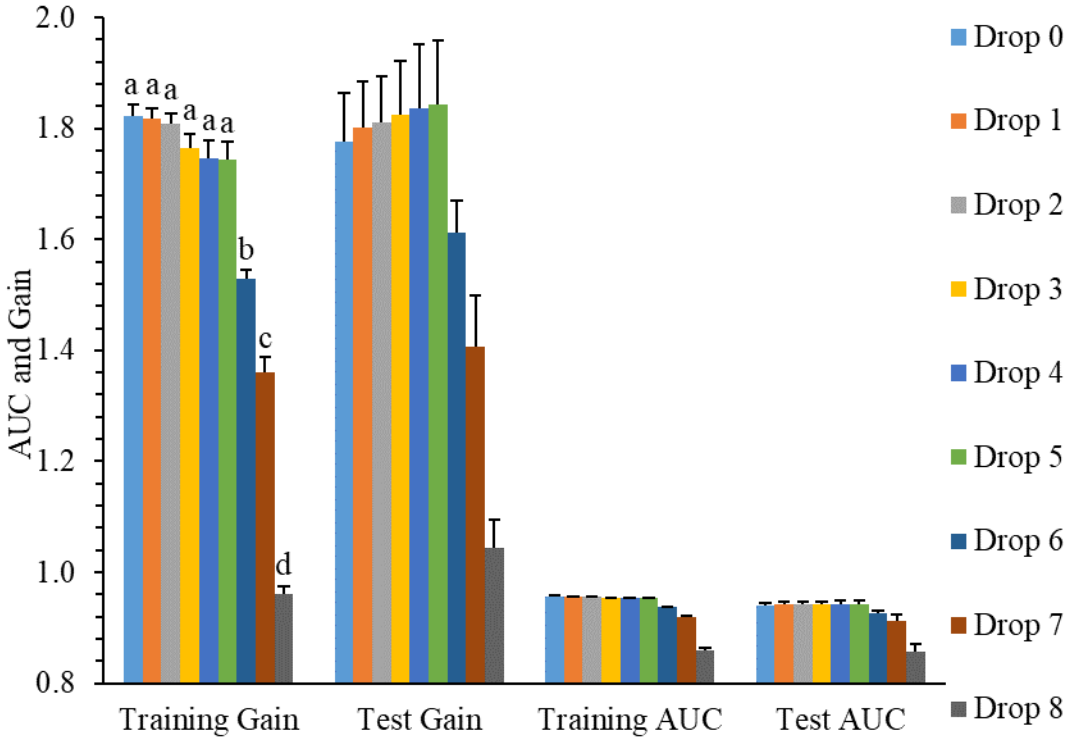

Figure 2.2 Change in *Chondrus crispus* average model regularized training and test gain (+SE) and AUC (area under the curve) when a variable is removed from the model (See text for detailed explanation). Letters indicate significant change in training gain based on whether 95% CI overlap or not, which was important to identify for training gain to decide when to stop removing variables, while test gain was used to decide which variable to remove.

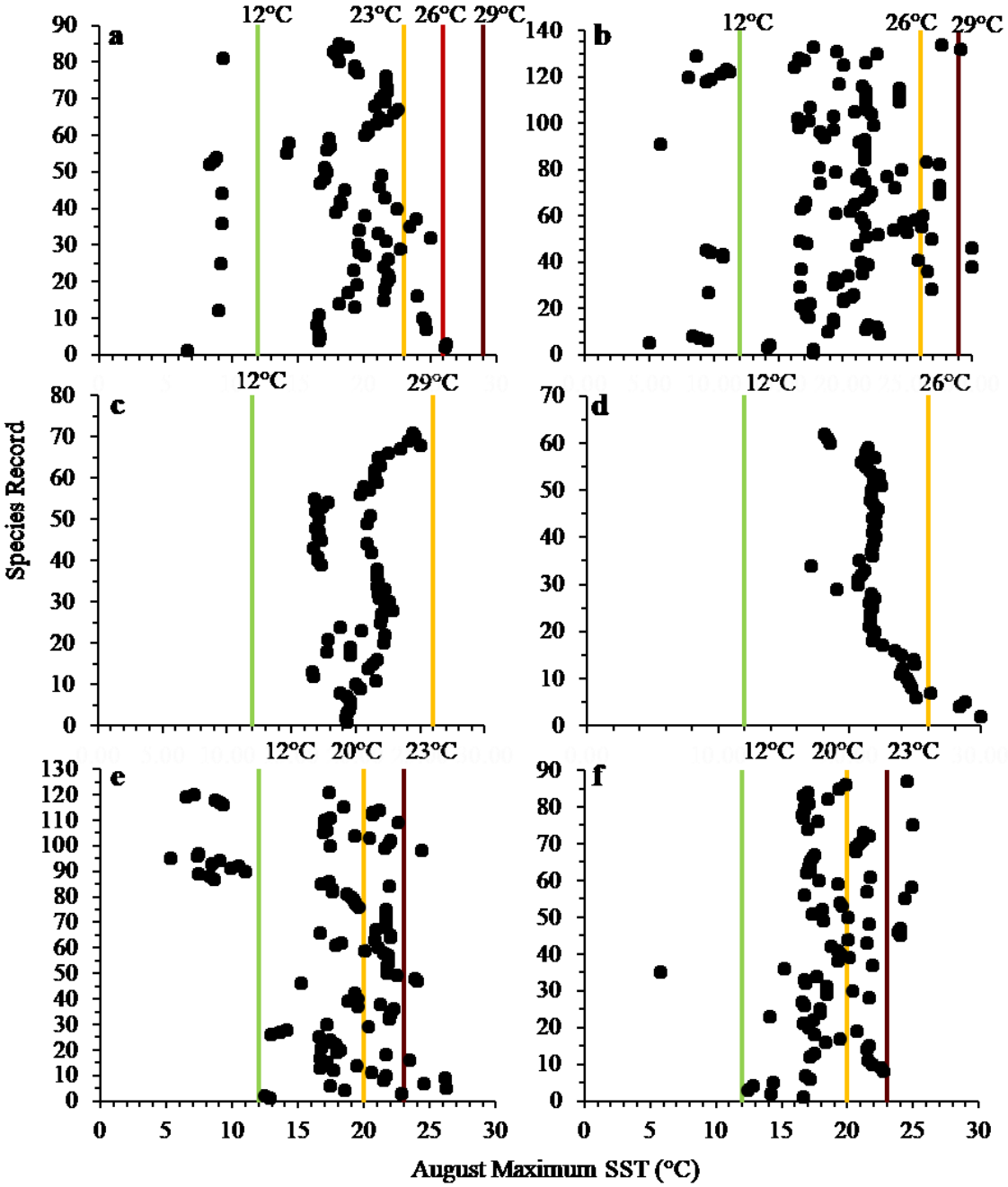

Figure 2.3 Occurrence records plotted against the corresponding August maximum sea surface temperature (SST) for **a** *Ascophyllum nodosum*, **b** *Fucus vesiculosus*, **c** *Chondrus crispus*, **d** *Codium fragile*, **e** *Saccharina latissima*, and **f** *Laminaria digitata*. Coloured lines indicate physiological thresholds where green is good growth, yellow is reduced growth, and dark red indicates complete mortality (Wilson et al. 2015).

Table 2.3 Variables included in the best model per species with the associated average training and test AUC (±SE), and maximizing the sum of test sensitivity and specificity threshold and binomial p-value. See table 2 for abbreviations.

		A. nodosum	*F. vesiculosus*	*C. crispus*	*C. fragile*	*S. latissima*	*L. digitata*
Variable	AugMaxSST	X	X	X	X	X	X
	AugMaxSAT		X				
	SmrMeaSIC	X	X		X	X	
	SmrMinSIC		X				X
	SmrMeaSSS	X					
	SmrMinSST		X	X			
	WntMaxSIC	X	X	X	X	X	X
	WntMeaSSS		X	X	X	X	
	WntMaxSAT	X	X				
Average Training AUC		0.9348 ±0.001	0.9162 ±0.002	0.9527 ±0.002	0.9618 ±0.002	0.8939 ±0.004	0.9150 ±0.004
Average Test AUC		0.9140 ±0.010	0.8792 ±0.009	0.9421 ±0.006	0.9479 ±0.006	0.8764 ±0.020	0.8954 ±0.013
Average maximum test sensitivity and specificity threshold and binomial p-value		0.2437 p <0.001	0.2084 p <0.001	0.1613 p <0.001	0.1891 p <0.001	0.2893 p <0.001	0.1630 p <0.001

2.3.2 Response of Fucoids: Ascophyllum nodosum and Fucus vesiculosus

Maxent predicted the present-day southern edge of the distribution of both fucoids within ~1° of known occurrence records (Figures 2.4-2.6, Table 2.4). The physiological thresholds (PT) used in this study suggest that *A. nodosum* grows well at SST of 12-22°C, with reduced growth at 23°C, partial mortality at 26°C, and complete mortality at 29°C (Appendix C: Table C.1). When the PT and Maxent results are combined, *A. nodosum*'s present distribution corresponds to a maximum August SST (SST hereafter) of ≤26°C, with the SST range for good growth (12-22°C) beginning at 42°N (Appendix C: Table C.2). The second fucoid species, *F. vesiculosus*, has a slightly higher thermal tolerance and grows well at SST of 12-25°C, experiences reduced growth and partial mortality at 26°C, and complete mortality at 29°C (Appendix C: Table C.1). Combining the PT and Maxent results for *F. vesiculosus*, the predicted present distribution extends south to 35.5°N, with SST for improved good growth beginning at 41°N (Appendix C: Table C.2).

The present-day northern edge is less clear for both species. Maxent predicted a continuous distribution further south, and patchy distribution further north, then *A. nodosum* is presently observed (Figures 2.4a, 2.6a, Table 2.4). For *F. vesiculosus* Maxent predicted suitable habitat marginally further north than the species is presently observed (Figures 2.5a, 2.6b, Table 2.4). The 12°C SST isotherm occurs at 56°N, therefore fucoids exist north of this study's lowest used PT (Appendix C: Table C.2) and the PT data cannot be incorporated to help denote fucoids northern range limit.

Regardless of the RCP scenario used, individual climate model projections for IPSL (strong warming) project a more drastic change in distribution than for GFDL (mild warming; Figures 2.4-2.6, Appendix D: Figures D.1-D.4). When climate model

projections are averaged to determine the most likely response between the mild and strong climate warming scenarios, the RCP 2.6 scenario projects minimal to no shifts of the southern and northern range limit of fucoids based on Maxent projections alone (Figure 2.6, Table 2.4). Presently, *A. nodosum* has a limited distribution (~1.5°) in areas where SST ranges from 23 to 26°C, indicating reduced growth and/or partial mortality (Figures 2.4a, 2.6a, Appendix C: Table C.2). By 2100, this area is projected to increase to ~2.5° under RCP 2.6. In both the present and future day models, SST reaches 26°C only along the most southern 0.5° of the range, indicating that the PT agrees with the Maxent model. In comparison, the PT for *F. vesiculosus* suggest that *F. vesiculosus* should not occur in areas where SST reaches 29°C, yet Maxent projections by 2100 define suitable habitat across 3.5° of latitude where SST reaches 29°C (Figures 2.5a, 2.6b, Appendix C: Table C.2). This would suggest a 3.5° range shift to the north based on the PT by 2100 at RCP 2.6.

The RCP 8.5 scenario results in a varying response in fucoids. Maxent projects an average southern range shift for *A. nodosum* of 1° to the north by 2050, and an overall 5.5° by 2100 (Figure 2.6a, Table 2.4). This new distribution includes 2.5° of latitude where SST reaches 26°C with expected reduced growth and partial mortality, much greater than the 0.5° presently observed (Appendix C: Table C.2). Consequently, adding together the average relative Maxent projected range shift of 5.5° to the north, with the 2.5° of projected habitat with reduced growth, *A. nodosum*'s southern border may move north by 8° by 2100. This would shift *A. nodosum*'s southern boundary from its current location in Long Island Sound, New York (~40.5°N), to somewhere between Cape Breton (~46°N) and southern Newfoundland (~48°N) by 2100. Along the northern edge,

continuous habitat is projected to shift north 1.5° by 2050, and an overall 2° by 2100. The patchy distribution limit shifts 3.5° to the north by 2050, and 7° by 2100. This shift in the northern distribution limit is expected to create new habitat along the rocky shores of northern Greenland, and potentially Baffin Island.

In contrast at RCP 8.5, Maxent projected *F. vesiculosus'* southern edge to only shift 1° to the north by 2100 (Figure 2.6b, Table 2.4). Again however, this corresponds to 4° of latitude where SST reach 29°C (Appendix C: Table C.2). When the Maxent average projected range shift is added to the PT, a total range shift of 5° to the north is expected. Therefore, the southern edge of *F. vesiculosus* may shift from Cape Hatteras, North Carolina (35.5°N) to Long Island Sound, New York (~40.5°N) by 2100. The northern border of continuous distribution is projected to shift north by 1.5° by 2050, and an overall 3° by 2100. The northern edge shifts less drastically resulting in mostly continuous habitat along the entire west coast of Greenland, and large areas of suitable habitat forming along Baffin Island.

Ultimately the relative average projected response of fucoids to continued warming by 2100 at RCP 8.5 is a range shift north and latitudinal contraction as *A. nodosum* southern edges shifts north by 8° (890 km), while the northern edge shifts less drastically north between 2° (223 km) to 7° (779 km), and *F. vesiculosus* southern edge shifts north by 5° (556 km), with a maximum northern range shift of 3° (334 km, Table 2.4, Figure 2.6).

2.3.4 Response of Chondrus crispus

Maxent predicted the present-day southern and northern distribution limits for *C. crispus* within ~1° of known occurrence records, which agrees with the PT, excluding

one outlier pixel in North Carolina (Figures 2.7, 2.9a, Table 2.4, Appendix C: Table 2). The PT used in this study suggests good growth for *C. crispus* at SST of 12-28°C, with growth reductions beginning at 29°C (Appendix C: Table C.1).

By 2050, regardless of RCP used, there is an average (between mild and strong warming climate models) projected southern range shift north by 1.0 to 1.5° (Figures 2.9a, Table 2.4). This is based off no projected range shift from the mild warming model (GFDL), and a 2° north range shift of the strong warming model (IPSL, Appendix D: Figures D.5-D.6). By 2100, at RCP 8.5 the relative average projected response increases to a potential 2.5° total shift north of the southern edge (Figure 2.9a, Table 2.4), which corresponds to the PT within SST for good growth. Interestingly, both GFDL and ISPL projected the same degree of range shift by 2100 at RCP 8.5 (Appendix D: Figures D.5-D.6). Therefore, *C. crispus* southern edge is projected to shift north from Long Island Sound (~40.5°N) to Southern Maine (~43°N) by 2100.

The northern boundary is likely to continually shift by 2100, corresponding to SST warmer than 11°C, although the magnitude of the shift is highly dependent on the RCP (Figure 2.9a, Table 2.4). At RCP 2.6, there is a relative average range expansion north of continuous habitat by 1.5°, and of patchy habitat by 2.5° by 2100. This is based off no projected range shift from the mild warming model (GFDL), and a northern range shift north of the strong warming model (IPSL, Appendix D: Figures D.5-D.6). At RCP 8.5, there is a relative average continuous northern edge shift north by 4°, and 12.5° of patchy habitat by 2100 (Figure 2.9, Table 2.4). The mild warming model (GFDL) projects suitable habitat to mid-Labrador (Figure 2.7), while the strong warming model (IPSL) projects suitable habitat throughout the Canadian Arctic and Western Greenland

(Figure 2.7). Therefore, it is likely by 2100 that the northern edge will shift further north into the Canadian Arctic. This would result in large areas of the Labrador coast, and potentially parts of Greenland and Baffin Island containing suitable habitat for *C. crispus* by 2100.

Ultimately, the relative average projected response of *C. crispus* to continued warming by 2100 at RCP 8.5 is a slight range shift and northern latitudinal expansion as the southern border shifts slightly north by ~2.5° (278 km), while the northern border shifts more drastically north by 4° (445 km) to 12.5° (1391 km, Table 2.4, Figure 2.9a).

2.3.5 Response of Codium fragile

Maxent defined a present-day southern edge for *C. fragile* within 1°, and a northern edge further north than present occurrence records (Figures 2.8, 2.9b, Table 2.4). The PT used in this study for *C. fragile* suggests good growth at SST of 12-25°C, with growth reductions beginning at 26°C (Appendix C: Table C.1). Presently *C. fragile* is found at SST of 12 to >29°C (Figures, 2.9b, Appendix C: Table C.2).

Neither RCP 2.6 or 8.5 project a relative average shift in *C. fragile*'s southern edge by 2100 (Figure 2.9b, Table 2.4) and, this is consistent across both the mild (GFDL) and strong (IPSL) warming climate models (Figure 2.8, Appendix D: Figures D.7-D.8). Furthermore, as *C. fragile* is presently commonly found within SST ≥26°C, the Maxent southern distribution likely represents its true southern limit. Therefore, continued warming is unlikely to result in a southern range shift for *C. fragile* by 2100.

For the northern distribution limit, regardless of RCP, the northern distribution corresponds to SST ≥12°C (Figure 2.9b). RCP 2.6 projects no change in the relative average northern edge of *C. fragile*'s continuous distribution by 2100, with patchy

distribution shifting north by 3°, which all remain within SST ≥12°C (Figure 2.9b, Table 2.4, Appendix C: Table C.2). The mild (GFDL) and strong (IPSL) warming climate models give similar projections for the continuous distribution, however IPSL projects a patchy distribution limit much further north (Appendix D: Figures D.7-D.8). RCP 8.5 projects the relative average continuous northern edge to shift north by 1.5° by 2050, to a total shift north of 2.5° by 2100 (Table 2.4, Figure 2.9b). More extreme shifts of patchy distribution are projected, with a 3° northward shift by 2050, to a total northward shift of 9.5°N by 2100. The RCP 8.5 projection have higher variation between the two climate models, where the mild warming (GFDL) projects small range shifts, and the strong warming (IPSL) projects large range shifts north (Figure 2.8, Appendix D: Figure D.7).

Ultimately, for the relative average RCP 8.5 scenario projections, there is the potential for a shift of the northern edge of *C. fragile* from northern Newfoundland (~51°N), to parts of Labrador by 2050 (~52.5°N), to Ungava Bay (~53.5°N) by 2100. Therefore, the relative average projected response of *C. fragile* to continued warming by 2100 at RCP 8.5 is a latitudinal range expansion north as the southern edge does not shift, while the northern border shifts north by 2.5 (278 km) to 9.5° (1057 km, Table 2.4, Figure 2.9b).

2.3.6 Response of Kelps: Saccharina latissima and Laminaria digitata

Maxent predicted *S. latissima* and *L. digitata* (hereafter kelp) present-day southern distribution limits within 1° of known occurrence records (Figures 2.10-2.12, Table 2.4). The PT used in this study suggest that kelps grow well at SST of 12-19°C, experience growth reductions and partial mortality at 20°C, and complete mortality beginning at 23°C (Appendix C: Table C.1). When the PT are overlaid over the Maxent

distribution, the predicted habitat corresponds to SST ≥26°C over 1° of latitude, and SST ≥23°C over 7°, therefore kelps exist in a narrow range of habitat with lethal SST, but are relatively common at SST with reduced growth (Figures 2.10-2.12, Appendix C: Table C.2). Maxent predicted *S. latissima* northern edge well, however *L. digitata* continuous distribution was predicted 7° too far south, and the patchy distribution was predicted 4° too far south (Figures 2.10-2.12, Table 2.4). Both kelp distributions exist north of the 12°C SST isotherm (Appendix C: Table C.2) and the PT data cannot be incorporated to help denote kelps northern range limit.

Looking to the future, there was no projected relative average shift of kelps southern edge by 2100 at RCP 2.6 (Figure 2.12, Table 2.4), with minimal changes in the 23°C and 26°C SST isotherms (Appendix C: Table C.2). This is consistent across the mild (GFDL) and strong (IPSL) warming climate models (Appendix D: Figure D.9-D.12). There was a small relative average projected shift of the northern edge of kelp distribution north by 1 to 2° by 2100 (Figure 2.12, Table 2.4). The response of the northern edge was varied across climate models with the strong (IPSL) climate warming model projecting suitable habitat much further north than the mild (GFDL) climate warming model (Appendix D: Figures D.9-D.12).

At RCP 8.5, kelps southern edge is projected to shift north by 3° based on the relative average response by 2100 (Figure 2.12, Table 2.4). While the PT shows that by 2050, the kelp projected Maxent distribution will be covering 3° of latitude at SST with complete mortality, by 2100 this increases to 6° of latitude (Appendix C: Table C.2). Therefore, adding together the 3° relative average projected range shift from the Maxent model, and the 6° projected range shift from the PT, kelps may experience a northward

range shift of the southern edge of 9° by 2100. This corresponds to a shift of its southern edge from Long Island Sound (~40.5°N) to southern Maine (43°N) by mid-century, and by end-century, kelps may not exist south of northern Newfoundland (~49°N).

Kelps have a varying response for the northern edge at RCP 8.5 where *S. latissima* is projected to shift 2° north by 2050, to give a total shift north of 3.5° by 2100, with patchy habitat shifting north as much as 4.5°, based on the relative average response (Figure 2.12a, Table 2.4). At this northern edge, *S. latissima* is likely to become more abundant along the shores of Baffin Bay by 2100. *Laminaria digitata* is projected to shift more during the latter half of the century, where there is a 1° shift north by 2050, to a total 4° shift by 2100, and patchy habitat shifting north by 8°, based on the relative average response (Figure 2.12b, Table 2.4). Yet, only the patchy distribution surpasses its current observed occurrence records. For *L. digitata*, there is likely to be a shift of the patchy distribution from its current distribution limit in Ungava Bay (60°N) to further north in the Canadian Arctic by 2100 (63.5°N) by 2100.

Ultimately the projected relative average response for kelps to continued warming by 2100 at RCP 8.5 is a range shift north and latitudinal contraction as the southern edge shifts north by 9° (1002 km), while the northern edge for both species shifts north by <9° (Figure 2.12, Table 2.4). However, this response is not consistent across climate models where the mild warming (GFDL) climate model projects a smaller range shifts, and the strong warming (IPSL) climate model projects a larger range shift further into the Arctic (Figure 2.10-2.11, Appendix D: Figures D.9, D.11).

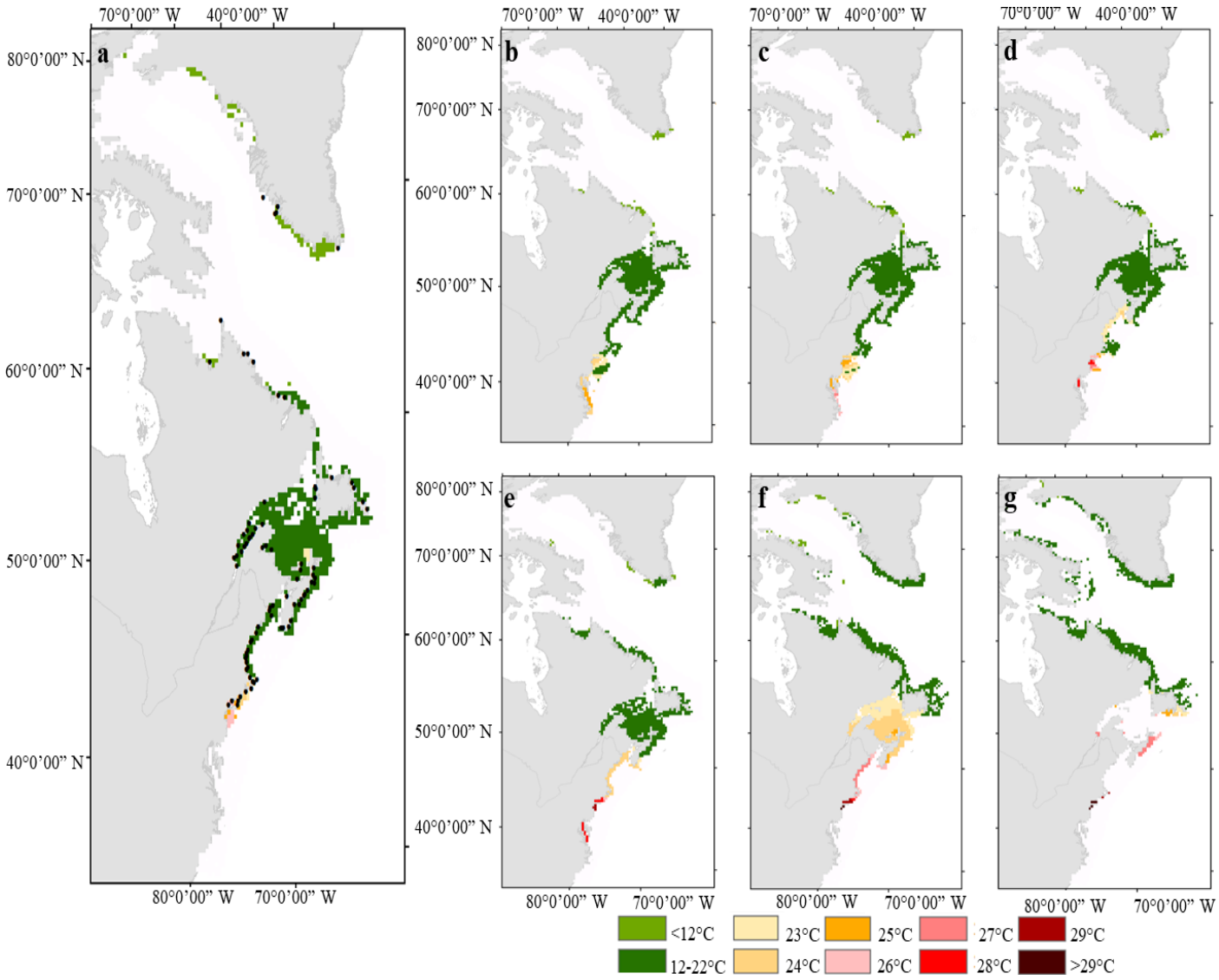

Figure 2.4 *Ascophyllum nodosum* **a** present distribution as predicted by Maxent. Black dots indicate the occurrence records used to build the Maxent model. Projected distribution for GFDL RCP 8.5 over **b** 2006-2015, **c** 2040-2050, and **d** 2090-2100, and for IPSL RCP 8.5 over **e** 2006-2015, **f** 2040-2050, and **g** 2090-2100. Physiological thresholds were overlaid over the distribution of a to show areas of good growth (green, 12-22°C), reduced growth (yellow-orange, 23-25°C), reduced growth and partial mortality (pink-red, 26-28°C), and complete mortality (dark red, ≥29°C). Data is in an equal-area projection.

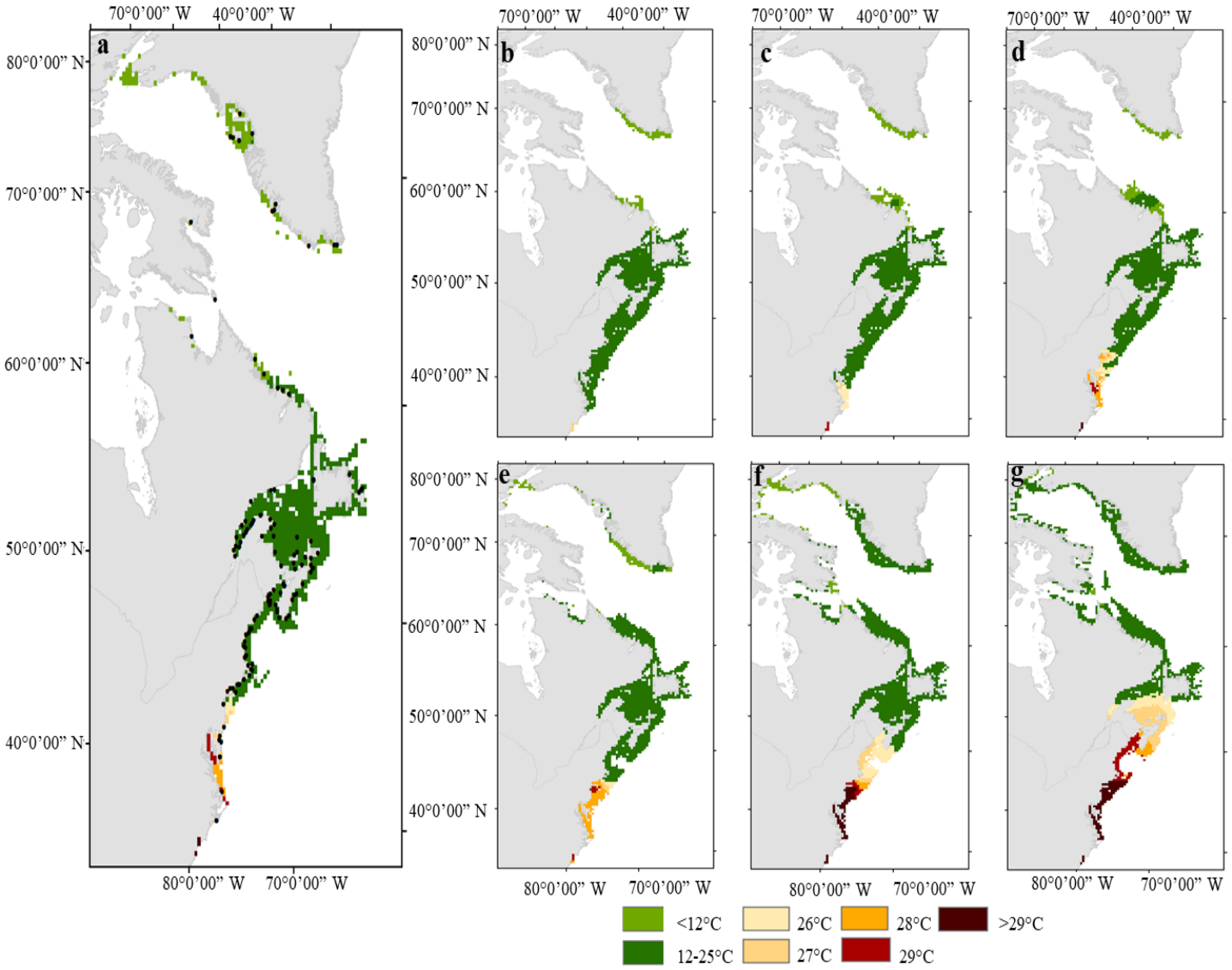

Figure 2.5 *Fucus vesiculosus* **a** present distribution as predicted by Maxent. Black dots indicate the occurrence records used to build the Maxent model. Projected distribution for GFDL RCP 8.5 over **b** 2006-2015, **c** 2040-2050, and **d** 2090-2100, and for IPSL RCP 8.5 over **e** 2006-2015, **f** 2040-2050, and **g** 2090-2100. PT were overlaid over the distribution to show areas of good growth (12-25°C), reduced growth and partial mortality (26-28°C), and complete mortality (≥29°C). Data is in an equal-area projection.

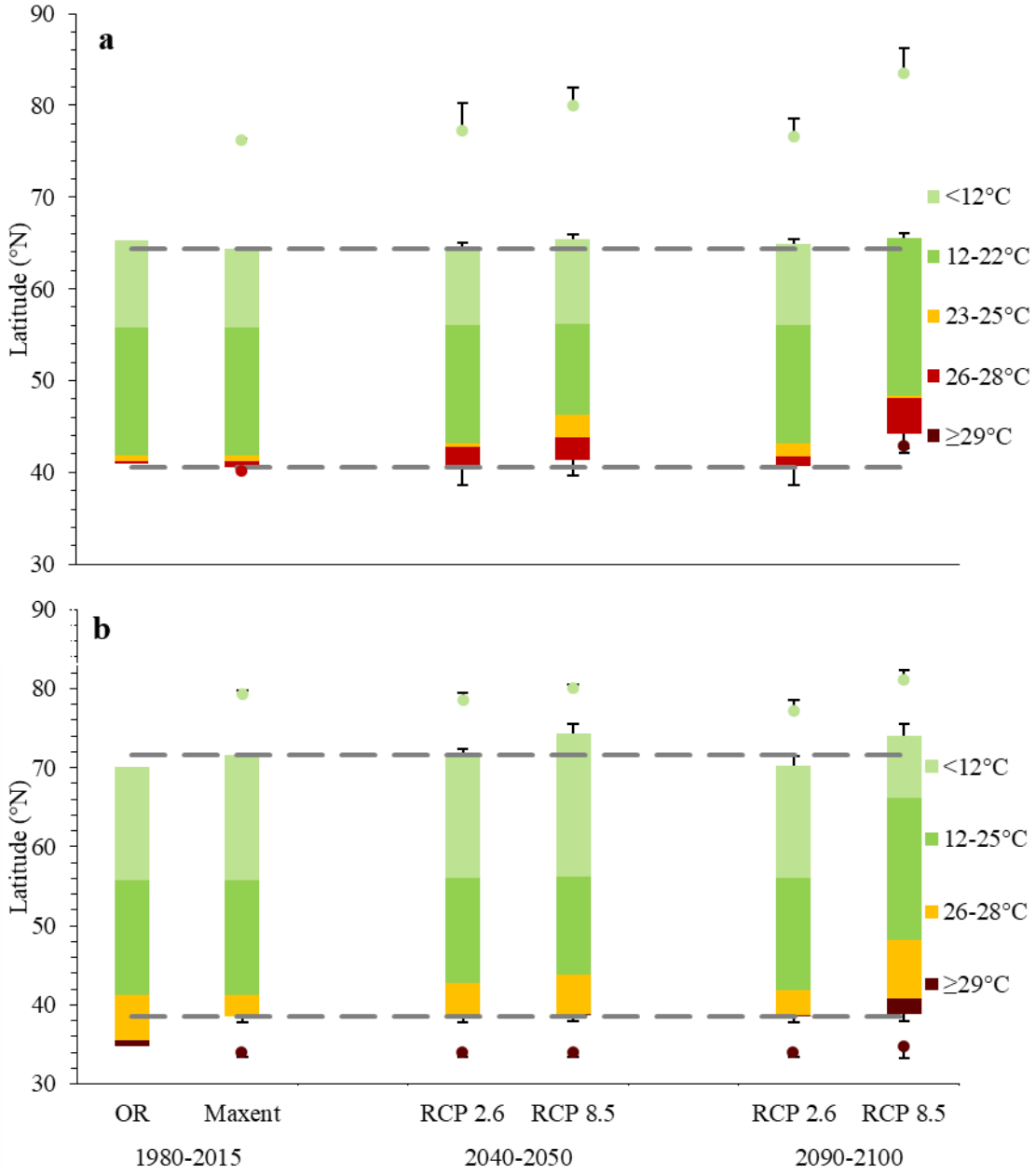

Figure 2.6 Relative northern and southern continuous (bars) and patchy (dots) distribution limits of **a** *Ascophyllum nodosum* and **b** *Fucus vesiculosus* based on occurrence records (OR), average Maxent (±SE) present-day (1980-2015), and average relative projected future limits at mid- (2040-2050) and end-century (2090-2100) based on two climate models (GFDL, IPSL) for two emission scenarios (RCP 2.6, 8.5). Physiological thresholds were overlaid to indicate areas of unknown growth (light green), good growth (green), reduced growth (yellow), reduced growth and partial mortality (red), and complete mortality (dark red). Grey hashed line indicates present-day Maxent continuous southern and northern limit.

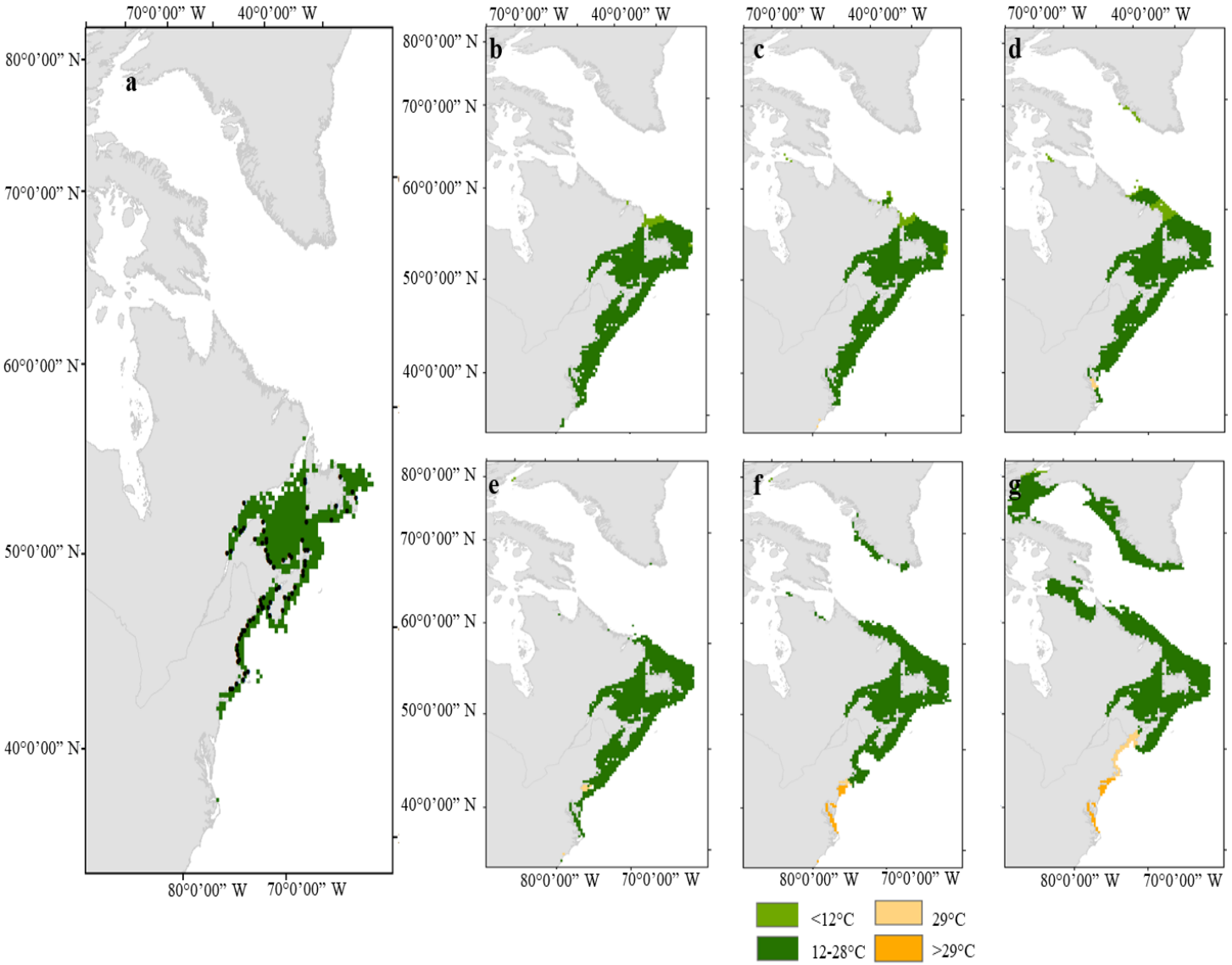

Figure 2.7 *Chondrus crispus* **a** present distribution as predicted by Maxent. Black dots indicate the occurrence records used to build the Maxent model. Projected distribution for GFDL RCP 8.5 over **b** 2006-2015, **c** 2040-2050, and **d** 2090-2100, and for IPSL RCP 8.5 over **e** 2006-2015, **f** 2040-2050, and **g** 2090-2100. PT were overlaid over the distribution to show areas of good growth (green, 12-28°C), and reduced growth (yellow-orange, ≥29°C). Data is in an equal-area projection.

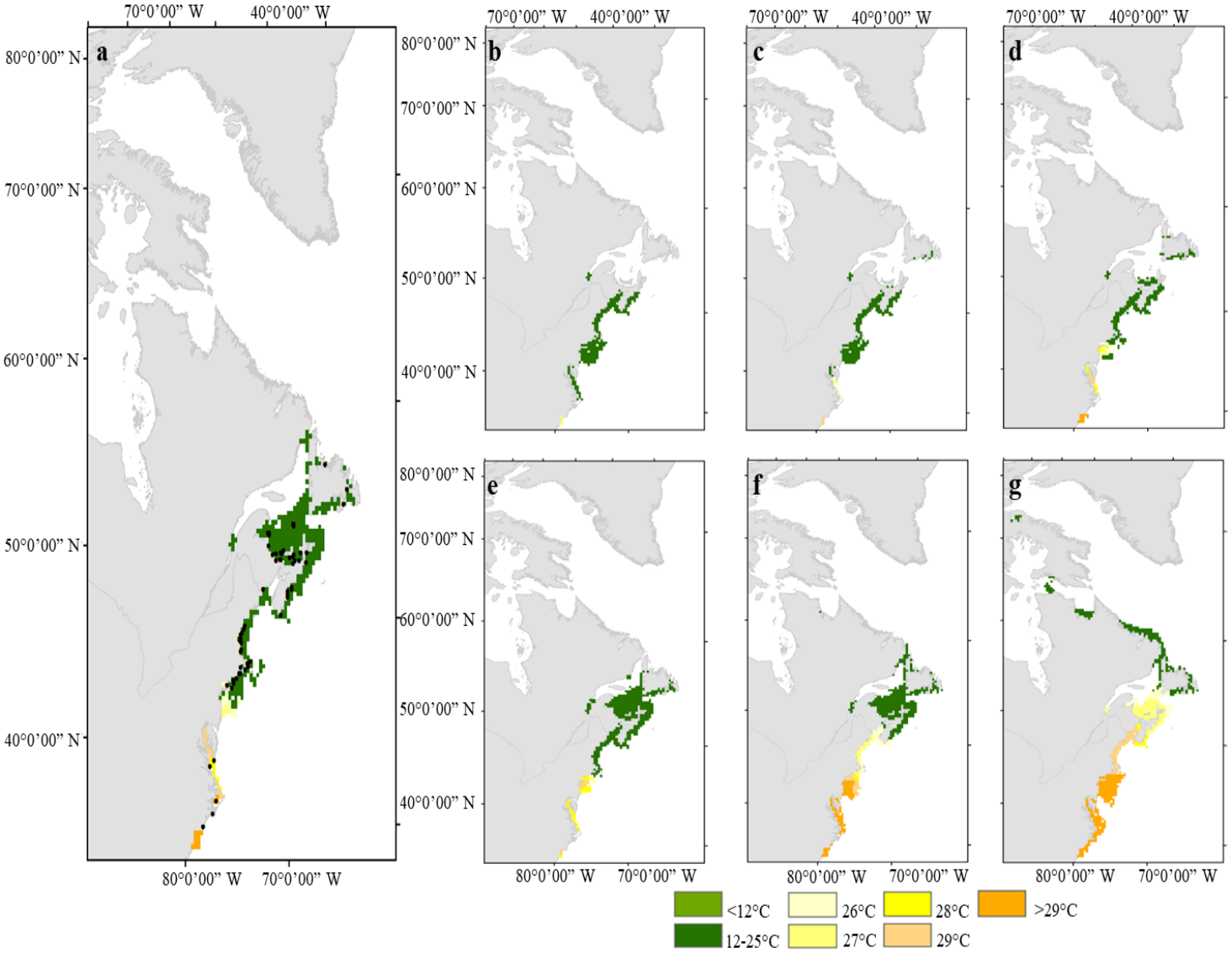

Figure 2.8 *Codium fragile* **a** present distribution as predicted by Maxent. Black dots indicate the occurrence records used to build the Maxent model. Projected distribution for GFDL RCP 8.5 over **b** 2006-2015, **c** 2040-2050, and **d** 2090-2100, and for IPSL RCP 8.5 over **e** 2006-2015, **f** 2040-2050, and **g** 2090-2100. PT were overlaid over the distribution to show areas of good growth (green, 12-28°C), and reduced growth (yellow-orange, ≥29°C). Data is in an equal-area projection.

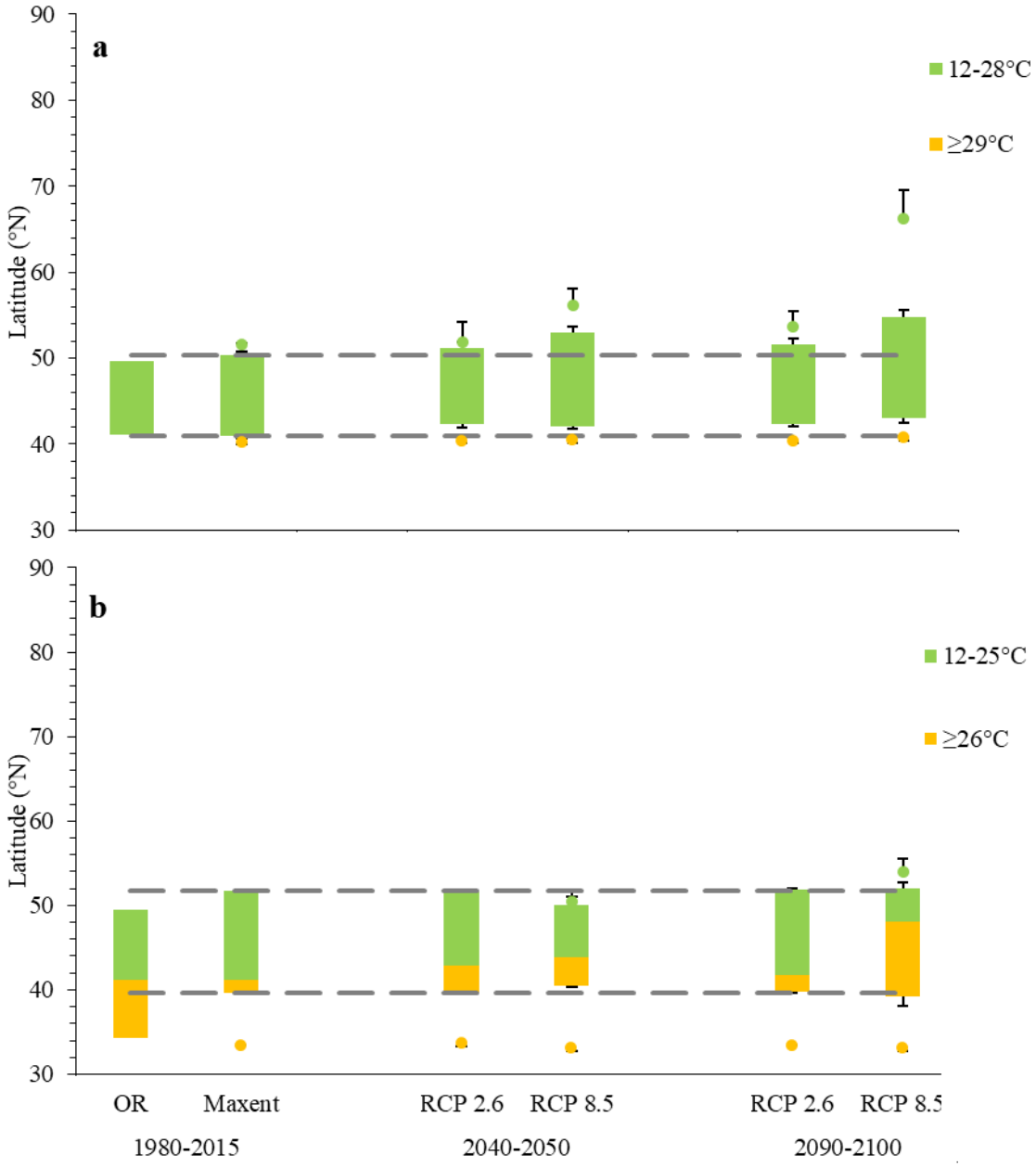

Figure 2.9 Relative northern and southern continuous (bars) and patchy (dots) distribution limits of **a** *Chondrus crispus* and **b** *Codium fragile* based on occurrence records, Maxent (±SE) present-day (1980-2015), and average relative projected future limits at mid- (2040-2050) and end-century (2090-2100) based on two climate models (GFDL, IPSL) for two emission scenarios (RCP 2.6, 8.5). Physiological thresholds overlaid to indicate areas of good growth (green) and reduced growth (yellow). Grey hashed line indicates present-day Maxent continuous southern and northern limit.

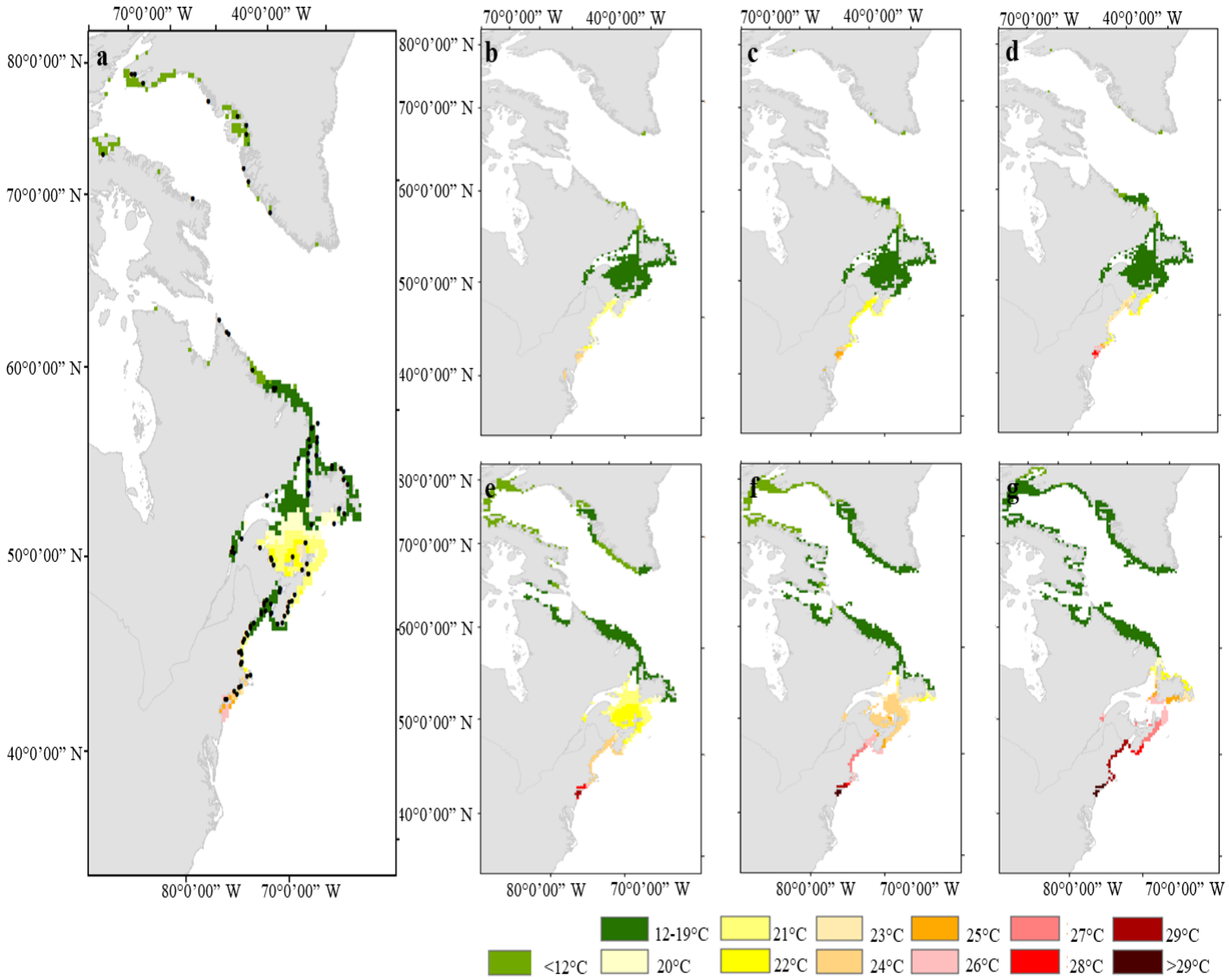

Figure 2.10 *Saccharina latissima* a present distribution as predicted by Maxent. Black dots indicate the occurrence records used to build the Maxent model. Projected distribution for GFDL RCP 8.5 over **b** 2006-2015, **c** 2040-2050, and **d** 2090-2100, and for IPSL RCP 8.5 over **e** 2006-2015, **f** 2040-2050, and **g** 2090-2100. Physiological thresholds were overlaid over to show areas of good growth (green, 12-19°C), reduced growth and partial mortality (yellow, 20-22°C), and complete mortality (orange-red, ≥23°C). Data is in an equal-area projection.

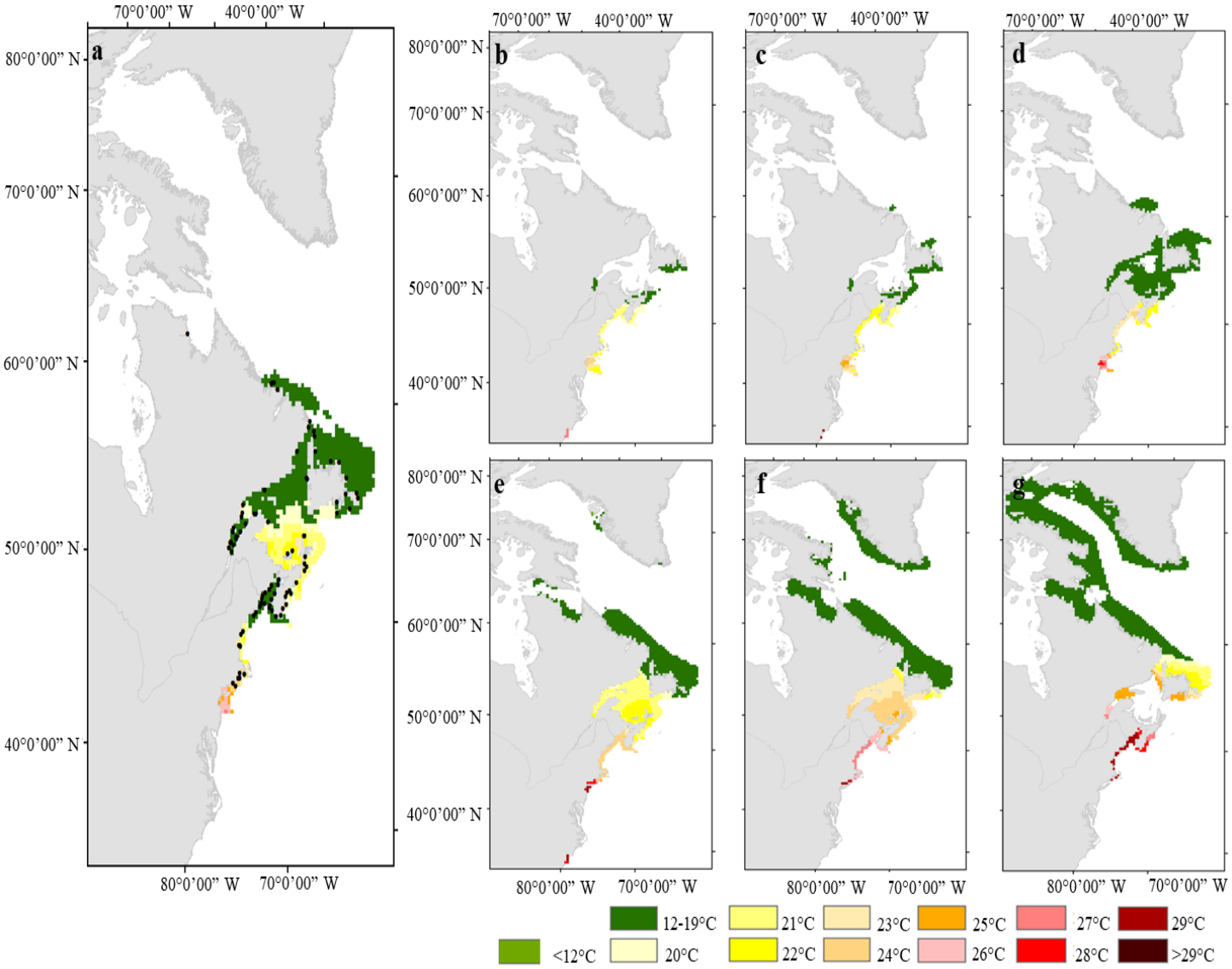

Figure 2.11 *Laminaria digitata* **a** present distribution as predicted by Maxent. Black dots indicate the occurrence records used to build the Maxent model. Projected distribution for GFDL RCP 8.5 over **b** 2006-2015, **c** 2040-2050, and **d** 2090-2100, and for IPSL RCP 8.5 over **e** 2006-2015, **f** 2040-2050, and **g** 2090-2100. Physiological thresholds were overlaid over to show areas of good growth (green, 12-19°C), reduced growth and partial mortality (yellow, 20-22°C), and complete mortality (orange-red, ≥23°C). Data is in an equal-area projection.

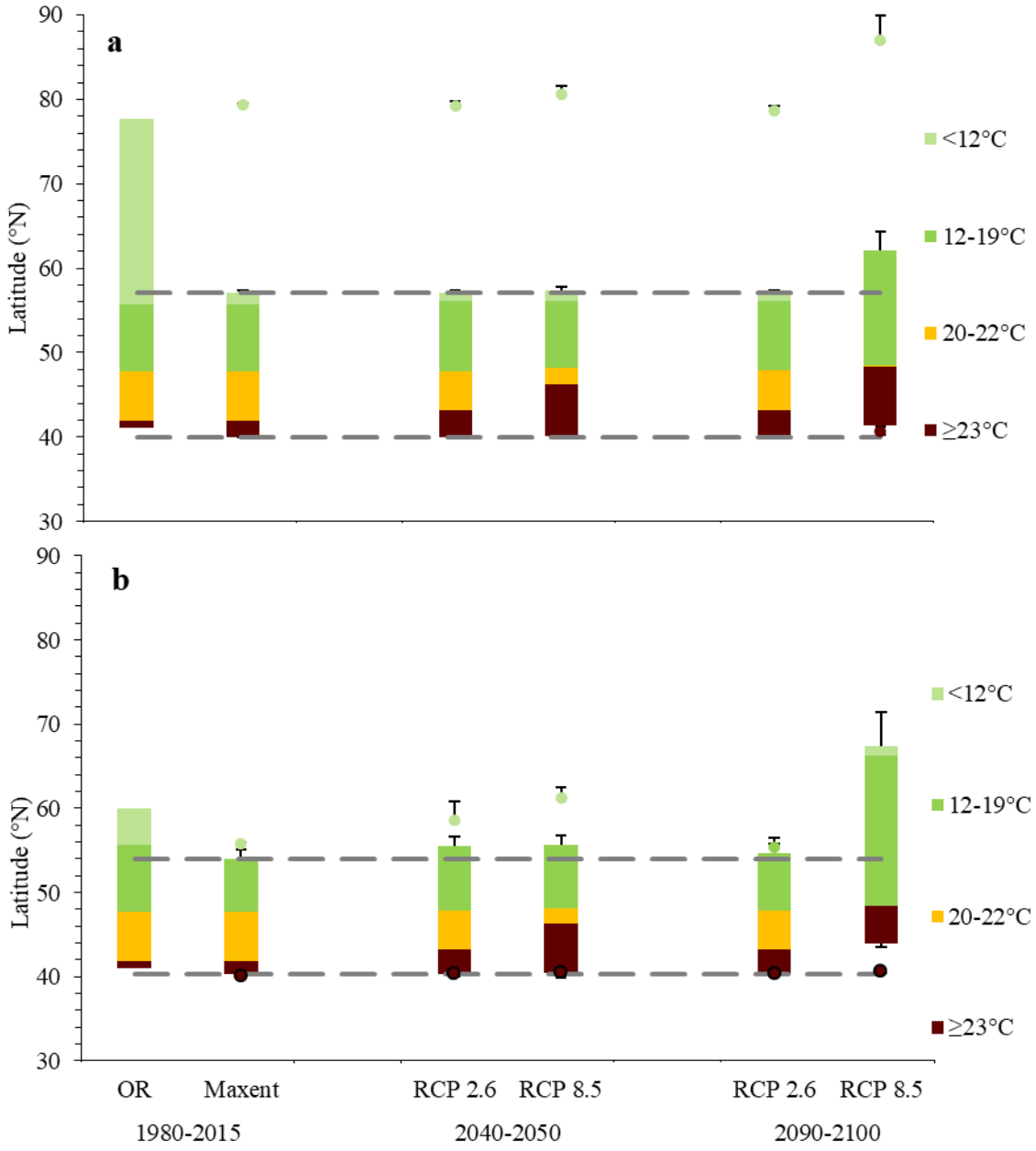

Figure 2.12 Relative northern and southern continuous (bars) and patchy (dots) distribution limits of **a** *Saccharina latissima* and **b** *Laminaria digitata* based on occurrence records, Maxent present-day (±SE, 1980-2015), and average relative projected future limits at mid- (±SE, 2040-2050) and end-century (±SE, 2090-2100) based on two climate models (GFDL, IPSL) for two emission scenarios (RCP 2.6, 8.5). PT were overlaid over the distribution to show areas of good growth (green), reduced growth and partial mortality (yellow), and complete mortality (red). Grey hashed line indicates present-day Maxent continuous southern and northern limit.

Table 2.4 Species average **S** southern limit and **N** northern limit (±SE) based on occurrence records and present-day Maxent model, with the relative average projected shift north per RCP and time period from the present-day Maxent model. Future projections are the average response from GFDL (mild warming) and IPSL (strong warming). A southern range shift is indicated with a negative sign. Latitude in brackets indicates patchy distribution limit if applicable.

		Present-day		2040-2050		2090-2100	
	Species	**Occurrence Records**	**Maxent**	**RCP 2.6**	**RCP 8.5**	**RCP 2.6**	**RCP 8.5**
S	*A. nodosum*	41.0°N	40.5°N ±0.4 (40.0°N ±0.0)	0.5 ±0.8	1.0 ±0.8 (1.0 ±0.8)	0.5 ±0.9	5.5 ±1.6 (3.0 ±1.0)
	F. vesiculosus	35.0°N	35.5°N ±0.1 (33.0°N ±0.0)	0.5±0.6 (0.0 ±0.3)	0.5 ±0.5 (0.0 ±0.5)	0.5 ±0.6 (0.0 ±0.3)	1.0 ±0.5 (1.0 ±1.0)
	C. crispus	41.0°N	40.5°N ±0.3 (40.0°N ±0.1)	1.0 ±0.9 (1.0 ±0.7)	1.5 ±0.9 (1.0 ±0.7)	1.0 ±0.8 (1.0 ±0.6)	2.5 ±0.6 (2.0 ±0.6)
	C. fragile	34.0°N	33.0°N ±0.0	0.0 ±0.1	0.0 ±0.1	0.0 ±0.1	0.0 ±0.5
	L. digitata	41.0°N	40°N ±0.0	0.0 ±0.1	0.0 ±0.1	0.0 ±0.0	3.0 ±0.15 (0.5 ±0.2)
	S. latissima	41.0°N	40.0°N ±0.2	0.0 ±0.3	1.0 ±0.5 (0.0 ±0.1)	0.0 ±0.2	3.0 ±1.5
N	*A. nodosum*	65.5°N	63.0°N ±0.9 (76.5°N ±0.5)	0.0 ±1.2 (2.5 ±2.0)	1.5 ±1.3 (3.5 ±2.2)	0.0 ±1.3 (1.5 ±2.0)	2.0 ±1.5 (7.0 ±2.8)
	F. vesiculosus	70.0°N	72.0°N ±0.0 (79.5°N ±0.5)	0.5 ±2.2 (-1.5 ±1.8)	1.5 ±1.3 (0.5 ±0.6)	-0.5 ±2.1 (-1.0 ±1.3)	3.0 ±1.9 (1.0 ±1.1)
	C. crispus	50.0°N	50.5°N ±0.1 (51.0°N ±0.3)	1.0 ±0.7 (0.0 ±0.9)	2.5 ±0.9 (4.5 ±1.6)	1.5 ±0.8 (2.5 ±1.8)	4.0 ±0.8 (12.5 ±3.9)

	Present-day		2040-2050		2090-2100	
Species	**Occurrence Records**	**Maxent**	**RCP 2.6**	**RCP 8.5**	**RCP 2.6**	**RCP 8.5**
C. fragile	49.5°N	51.0°N ±1.1 (52.0°N ±1.5)	0.0 ±1.0 (1.0±2.1)	1.5 ±1.7 (3.0 ±2.9)	0.5 ±1.3 (3.0 ± 3.0)	2.5 ±2.6 (9.5 ±4.9)
L. digitata	60.0°N	53.0°N ±0.9 (55.5°N ±0.1)	0.0 ±0.9 (2.0 ±1.2)	1.0 ±0.9 (4.5 ±1.1)	0.0 ±0.9 (1.0 ±0.8)	4.0 ±1.3 (8.0 ±3.0)
S. latissima	77.5°N	78.5°N ±0.3 (79.0°N ±0.3)	2.0 ±1.7 (0.5 ±0.7)	2.0 ±1.2 (3.5±2.6)	2.0 ±1.7 (0.5 ±0.3)	3.5 ±1.8 (4.5 ±2.4)

2.4 Discussion

The goal of this chapter was to project how future climate change may shift the distribution of common canopy-forming seaweeds in the NW Atlantic. To do so, we compiled a comprehensive database of occurrence records to determine current distribution, then used this data to build a hybrid species distribution model (SDM), and finally used this hybrid SDM to project future distributions under different climate change scenarios. We found that the future projections generally suggested northward shifts of the species' ranges. The addition of physiological thresholds (PT) suggested additional northward shifts of the southern edge relative to only the projected Maxent model.

2.4.1 Seaweed Distribution in the Northwest Atlantic

The quality of any species distribution model depends on accurate occurrence records, which are limited for seaweeds in the NW Atlantic. Present-day knowledge of seaweed distribution in the Subarctic to Arctic is limited; systematic surveys of seaweed distribution are either >30 years old (i.e. Wilce 1959; Lee 1980) or lacking entirely. However, recent efforts have aimed at documenting seaweed community composition along Baffin Island (Küpper et al. 2016) and Greenland (Høgslund et al. 2014). Surveys in other areas of the Arctic, such as Northern Alaska have found much higher seaweed diversity than anticipated (Wilce and Dunton 2014), and within the Canadian Arctic, kelps and fucoids have been observed as far north as Grise Fiord, Nunavut (~76°N; K. Krumhansl, personal communication), much further north than present-day published distribution limits. Therefore, it is likely that our present-day Maxent models and future projections could be improved and provide higher certainty for species' northern edges if

more detailed occurrence records become available. It is likely the northern border has been predicted too far south, due to an underestimated niche breadth, for each species.

2.4.2 Modelling Current Seaweed Distribution

When building the Maxent model, August maximum SST and winter maximum SIC were two of the most important environmental variables for predicting species distribution. Other SDMs in the NW Atlantic have considered some variation of maximum SST in their model (Müller et al. 2009; Jueterbock et al. 2013; Assis et al. 2014), yet this study was the second known study to include sea ice as an environmental variable (Assis et al. 2017). Seaweed distribution is primarily defined by water temperature, and closely follow SST isotherms (van den Hoek 1975; Lüning 1990). Consequently, August maximum SST coincides with southern distribution limits and therefore this variable was chosen to define the PTs used in this study. In northern areas, ice scouring strongly impacts the distribution of seaweeds, particularly for long lived species such as A. *nodosum* (Aberg 1992) with low dispersal capabilities (Vadas et al. 1990). Ice scour results in a bare intertidal zone and seaweed communities only beginning to occur in the subtidal below the lowest impacts of ice (Küpper et al. 2016). The presence of ice further decreases the amount of light that penetrates the water column, resulting in growth reductions (Krause-Jensen et al. 2012).

While all six SDMs had moderate to high model performance, fucoids, *C. fragile*, and *C. crispus* had higher AUC values than both species of kelp. These findings may be partially due to all environmental variables being associated with surface variables, while kelps are found from the low-intertidal into several meters of water depth, dependent on light availability (Krause-Jensen et al. 2012). While other studies examining range shifts

in kelp have also used surface environmental variables (Raybaud et al. 2013), the predicted distribution may differ if bottom environmental variables, such as bottom temperature and light availability, were used to build the SDMs.

Overall, Maxent present-day models predicted the southern border for all six species, and the northern borders for both *C. crispus* and *C. fragile* within one degree of known occurrence records, and published distribution limits (Taylor 1957; Gosner 1978; Carlton and Scanlon 1985; Lüning 1990; Merzouk and Johnson 2011). Yet for the kelp and fucoid species, which exist into the Subarctic/Arctic, the northern edge was not predicted well, likely due to the limited occurrence records from this region. The northern limits of *A. nodosum* and *L. digitata* were under predicted, while those of *F. vesiculosus* and *S. latissima* were predicted further north of known occurrence records.

2.4.3 Projected Distribution Shifts with Climate Change

As expected given the higher levels of projected warming (Bopp et al. 2013), IPSL typically projected a more drastic change in species distributions by end-century then GFDL. Interestingly, IPSL also typically projected the present-day distribution closer to the observed occurrence records. In contrast, GFDL typically projected the present-day distribution either further south or smaller in range with almost no change by end-century. Since the overall goal of this study was to determine the most likely response of the study species to continued climate change, the average of these mild and strong warming climate models was used in combination with different emission scenarios. Such multi-model means are increasingly being used to reflect the most likely climate change scenario given that each individual model has its own biases (i.e. Bopp et al. 2013; Raybaud et al. 2013).

If global CO_2 and other greenhouse gas emissions are greatly reduced or mitigated during this century, reflected by the RCP 2.6 scenario, our results suggest there will likely be no major shifts in the distribution of the studied seaweeds by 2100. In contrast, following the business-as-usual or worst-case RCP 8.5 scenario, there will likely be shifts in distribution by 2050 that continue up to 2100, but which vary by species. Based on our Maxent model results, average northward range shifts of up to 5° north of the southern edge by 2100 are possible. These shifts may be even more pronounced when combined with PTs to give northward shifts of the southern edge for kelps and *A. nodosum* of up to 9° (1002 km), *F. vesiculosus* up to 5° (556 km), *C. crispus* up to 2° (222 km), and no change for *C. fragile*. Maxent projections for the northern border also exhibited northward range shifts of up to 5° for each species, ultimately resulting in kelps and fucoids having an overall net loss of latitudinal habitat range and thus experiencing a range contraction. In contrast, warm-tolerant species (*C. crispus*, *C. fragile*) with smaller shifts of the southern, yet similar 5°C shifts of the northern edge, may experience a latitudinal range expansion.

Considering potential future changes under the RCP 8.5 scenario, the largest impacts on the seaweed community composition will likely occur in two major areas: the NE American seaboard from Long Island Sound north to the Canadian Maritimes, within the Canadian Arctic, and Greenland. Other studies projecting distribution shifts of fucoids (*F. vesiculosus, A. nodosum*), *S. latissima*, *L. digitata*, and *C. crispus* also found the NE American seaboard and southern Arctic (including Greenland) seeing the most drastic changes in species composition dues to species range shifts (Müller et al. 2009;

Jueterbock et al. 2013; Assis et al. 2014, 2017). No other known studies have made projections for *C. fragile* in the NW Atlantic.

There is large disagreement between studies about the magnitude of fucoids' responses to continued climate change. Jueterbock et al. (2013) projected a more extreme range shift of the southern edge of *F. vesiculosus* to Halifax, Nova Scotia, but a less extreme shift for *A. nodosum* to Delaware Bay by 2100 based off CMIP3 projections. Furthermore, both species' northern distribution limits were under projected in Jueterbock et al. (2013), resulting in minimal northern range shifts. Assis et al. (2014) used CMIP5 projections, for different climate models, to project *F. vesiculosus* southern range shift to southern Nova Scotia, with no change in species at the northern edge by 2100. These differences are likely due to: (i) differences between what was defined as present-day distribution limits, (ii) different environmental layers used to build the models (i.e. this study's use of SIC), (iii) the incorporation of PT in this study, and (iv) different climate models used to make future projections.

Müller et al. (2009) used February and August SST isotherms to make projections using CMIP3 data and observed very similar shifts in *S. latissimi*'s and *C. crispus'* southern and northern distribution limits. Lastly, Assis et al. (2017) used boosted regression trees, and CMIP5 projections for different climate models, and found similar shifts in the southern edge for both *S. latissima* and *L. digitata* at RCP 8.5 by 2100, with an overall decrease in habitat.

Part of the present-day warming of the NW Atlantic includes a northward shift of the Gulf Stream, which has resulted in significant warming along the NE American seaboard and Canadian Maritimes since 2004 (Pershing et al. 2015). Over this time,

decreases in kelp abundance have been observed in the Gulf of Maine and Scotian Shelf (Filbee-Dexter et al. 2016; Krumhansl et al. 2016; Dijkstra et al. 2017), while increases have been observed within the Gulf of St. Lawrence. Furthermore, a decrease of *A. nodosum* and increase of *F. vesiculosus* in the Canadian Maritimes has been related to increasing SST as well as harvesting of *A. nodosum* (Ugarte et al. 2010). Consequently, model projections in this study suggest the area impacted by the northward shift of the Gulf Stream, which includes the NE American seaboard and Canadian Maritimes, will experience changes in seaweed composition by 2100.

Marine life in the Arctic will be some of the most impacted by climate change, as this is one of the areas facing the largest increases in warming (Krause-Jensen and Duarte 2014). This study found that with increased warming, all study species will shift their range north, colonizing further into the Canadian Subarctic, Arctic, and western Greenland. Climate change is predicted to favour this northward expansion of seaweeds, particularly in the Arctic where there are large land masses connecting the temperate and Arctic regions (Krause-Jensen and Duarte 2014). Presently, climate change impacts have been observed in many Arctic ecosystems, impacting a variety of marine taxa (Wassmann et al. 2011), often with positive impacts on seaweed communities (Kortsch et al. 2012).

2.4.4 Species-Specific Responses and Implications

As there are projected species-specific responses, future climate change will not impact the seaweed community of the NW Atlantic equally, resulting in changes in both the intertidal and subtidal communities. The change in seaweed community along the NE American seaboard from Long Island Sound up to the Canadian Maritimes will likely

manifest itself in an increase in abundance of *C. fragile*, *C. crispus*, and *F. vesiculosus* with decreases in abundances for *A. nodosum* and kelps. Increasing SST will mostly drive this change along the southern limits as SST surpasses growth and mortality thresholds. Increasing SST and decreasing SIC will likely drive the change in seaweed community in the Subarctic, Arctic, and Greenland. This northward expansion is dependent on each species dispersal ability, where long-distance dispersal is possible in adult fucoids (Kalvas and Kautsky 1998; Olsen et al. 2010), adult *C. fragile* (Trowbridge and Todd 1999), and kelp zoospores (Reed et al. 1988). The combination of increasing temperatures, reduced ice scour, and increased light availability will positively impact seaweed communities in the Subarctic and Arctic (Krause-Jensen and Duarte 2014). Increasing temperatures may lead to range shifts, as well as increased growth and productivity in kelp and fucoids (Krause-Jensen et al. 2012; Marbà et al. 2017). Furthermore as nutrients (nitrate and phosphates) are limiting to seaweed growth during an Arctic summer (Chapman and Lindley 1980), increased nutrient input due to warming (Kortsch et al. 2012), such as upwelling due to ice shelf-break (Arrigo et al. 2008), may further promote increases in seaweed productivity at local scales throughout the Arctic (Krause-Jensen and Duarte 2014).

Along the mid-intertidal, *F. vesiculosus* is likely to replace *A. nodosum* from Long Island Sound up to PEI, to potentially Newfoundland by 2100. While *A. nodosum* typically outcompetes *F. vesiculosus, F. vesiculosus* is more tolerant to warmer SST then *A. nodosum* (Wilson et al. 2015). As temperatures continue to rise, *A. nodosum* is likely to experience reduced growth rates and partial mortality faster than *F. vesiculosus,* creating space for *F. vesiculosus* to settle. Consequently, the dominance of *A. nodosum* in

the mid-intertidal rocky shores along Long Island Sound into the Canadian Maritimes may shift to *F. vesiculosus* dominance. This has important implications for the rockweed harvest in both the Gulf of Maine (Arbuckle et al. 2014) and Canadian Maritimes (Ugarte et al. 2010), both of which may not be sustained with continued warming. As of yet, despite decreases in abundance on both sides of the Atlantic, currently there is only anecdotal evidence that *A. nodosum* has already experienced a small range shift in the NW Atlantic (Keser et al. 2005), with no range shift north of either species in the NE Atlantic (Lima et al. 2007; Yesson et al. 2015).

Fucus vesiculosus is more resistant to ice scour than *A. nodosum* (Aberg 1992; Ugarte et al. 2010), suggesting why *F. vesiculosus* is presently observed further north than *A. nodosum*. Typically, *A. nodosum* outcompetes *F. vesiculosus* for space along sheltered and ice-free shores. Yet, *A. nodosum* has difficulty settling in an already established *F. vesiculosus* bed (Thomas 1994). Furthermore, if both these species do exhibit a shift north, there will be competition with the already established *F. evanesces* species in the high Arctic (Küpper et al. 2016). *Fucus evanesces* typically occurs in the low-intertidal, and can be out-competed by *F. vesiculosus* along sheltered locations (Thomsen and Brandt 1999). In the high Arctic, where ice-scouring is common, *F. evanesces* is found in the subtidal starting at depths of 3 m (Küpper et al. 2016). Although, one isolated population was observed in the intertidal, and assumed to be protected from ice, suggesting the potential for intertidal colonization in the high Arctic with reduced sea ice. Consequently, SDM do not consider these biotic interactions, which may impact the northward range shifts of fucoids.

Along the low-intertidal, *C. crispus* is presently highly abundant throughout the southern reaches of its distribution, often forming monoculture beds (Adey and Hayek 2011). Older lab experiments for *C. crispus* found mortality occurred at water temperatures of 29°C (Lüning et al. 1986), yet the PT used in this study found that *C. crispus* grows at 29°C (Wilson et al. 2015). Moreover, growth reductions were not observed until 29°C, much higher than the previously reported 21°C (Kingsbury et al. 1973). As of yet, there is no indication that *C. crispus* distribution in the NW Atlantic has changed due to climate change, but there appears to be some acclimation to warmer SST (Wilson et al. 2015). In the NE Atlantic, along its southern distribution limit *C. crispus* has shifted its distribution 180 km north since 1971 (Lima et al. 2007) and populations along the southern edge in Spain have declined since 1998 (Piñeiro-Corbeira et al. 2016). Consequently, if *C. crispus* shifts northward as expected in the NW Atlantic, it may be replaced by the recently introduced invasive red-algae *Grateloupia turuturu*, which is presently found from Long Island Sound into the Gulf of Maine (Mathieson et al. 2008), and is able to tolerate warmer water temperatures than *C. crispus* (Kraemer et al. 2017).

Along its northern edge, *C. crispus* is likely to shift north. *C. crispus* is highly susceptible to ice-scour (Adey and Hayek 2011) and in areas throughout its range where ice-scouring is common, *C. crispus* exhibits a patchy distribution, finding refuge from ice impacts in rock cracks. Therefore, the northward shift will likely correspond to ice free shores, as well as increasing its abundance in Western Newfoundland/NW Gulf of St. Lawrence as SST continues to increase, resulting in decreases in ice coverage.

Along the subtidal, *C. fragile* may be able to replace kelp beds from Long Island Sound to potentially Newfoundland. *C. fragile* can form dense beds in the subtidal if a

disturbance creates exposed substrate within the native kelp community (Scheibling and Gagnon 2006). This disturbance may result from increasing water temperatures (Steneck et al. 2002), causing a northern distribution shift in kelp. *Codium fragile* mortality only occurs above 33°C (Hanisak 1979), but even under the most extreme warming scenarios, August maximum SST is not expected to be greater than 33°C by 2100 across the NW Atlantic. In contrast, kelp mortality occurs at 23°C with growth reductions at 20°C (Wilson et al. 2015). At its southern distribution limit, kelp becomes an annual plant, where growth stops at SST >20°C, and populations persist through annual production of gametophytes that "oversummer" (Lee and Brinkhuis 1986). Gametophytes of *S. latissima* and *L. digitata* are produced in spring and fall, and both gametophytes and adult plants experience mortality at SST >23°C (Bolton and Lüning 1982). Consequently, warm-water mortality has not changed since this older study, where Atlantic populations still exhibit mortality at 23°C (Wilson et al. 2015), despite increasing SST since 1980 (Lee et al. 2011).

In the high Arctic, kelp distribution is limited in the upper subtidal by the impacts of ice-scouring, and limited in the lower subtidal by the light reduction due to the presence of sea-ice (Krause-Jensen et al. 2012; Küpper et al. 2016). *S. latissima* blade biomass, area, and length were larger in populations at 64°N, and decreased in populations at 78°N (Krause-Jensen et al. 2012). This change was largely explained by a reduction in seasonal ice cover, and partially explained by slightly warmer temperatures at the more southern latitude (64°N). Therefore, Arctic warming should have positive effects on *S. latissima*. While *S. latissima* is only projected to have a minimal range shift north, it is likely to experience increases in production leading to larger plants, as well as

occupy a greater range of depths throughout the subtidal. *Laminaria digitata* will also benefit from Arctic warming through the potential to shift its range further into the Canadian Arctic and will likely see the same increase in production and depth range as *S. latissima*. Currently, within the shallow subtidal *Alaria esculenta* replaces *L. digitata* in the Arctic. Therefore, a northward migration of *L. digitata* may negatively impact the abundance of *A. esculenta* in the Subarctic and Arctic as *L. digitata* becomes more abundant. However, this has not been observed in the NE Atlantic, where *L. digitata* and *A. esculenta* have shown significant positive correlations in their changes in abundance since 1974, indicating that they are mirroring their response to increasing temperatures, and one is not causing a decrease in the other (Yesson et al. 2015).

The northern distribution limit of *C. fragile* is projected to shift north to northern Labrador by 2100. Since *C. fragile* is a tropical species, warming of the Subarctic will only facilitate the northward expansion of *C. fragile.* This species survives overwintering in areas with winter sea ice (Matheson et al. 2014), and as a subtidal species, would be minimally impacted by ice-scouring. At its northern distribution edge, *C. fragile* does not form dense beds throughout the subtidal (Matheson et al. 2014), suggesting it will co-exist with native kelp species as it expands its distribution northwards.

2.4.8 Limitations of this Study

The goal of this study was to determine how increasing temperatures will impact the distribution of common canopy forming seaweeds in the NW Atlantic. The use of physiological data gives confidence to model projections in novel environments (Elith et al. 2010; Martínez et al. 2014). The PTs used in this study were based on juvenile plants (10-15 cm) from the middle of their respective ranges, which are often more sensitive

than adult plants (Wilson et al. 2015). The PTs may change for larger plants and for individuals from populations at the most southern and northern distribution limits that may be locally adapted to warmer or cooler SST. Moreover, the used PTs were only able to denote the species southern edge, additional PTs for colder temperatures would help to give confidence to projections of the northern edge where known occurrence records are sparse.

The environmental data used to build the SDM was only available at quarter degree cell resolution, which does not allow for fine-scale discrimination of species distribution. As this study was only interested in determining species range limits, climate environmental variables were used to build the SDM as they denote species distribution on continental scales (Pearson and Dawson 2003). Presently, the data scale which predicts species distribution most accurately in coastal environments is unknown, however based on modelling of Canadian aquatic invasive species, finer scale does not necessarily result in increased model performance (Lowen et al. 2016).

Lastly, this study used global climate models with a coarse resolution. As such, these global models needed to be up-scaled to match the environmental data, extrapolated into coastal areas, and consequently do not capture fine-scale climate variations (Stock et al. 2011; Lowen and DiBacco 2017). To capture fine-scale variations, regional climate models are required. Unlike global models, regional models can resolve coastal upwelling, which may decrease the magnitude of warming expected (Lowen and DiBacco 2017). Furthermore, coarse global climate models are known to have a warm bias along the NE USA, due to the Gulf Stream being predicted too far north (Saba et al. 2015). Regional climate models exist for the NW Atlantic (Saba et al. 2015; Brickman et

al. 2016); however, these models were not used in this study as they did not encompass the entire study region, were calculated over limited temporal range, and project with fewer RCP scenarios.

2.5 Conclusions

Correlative SDMs are a powerful tool to make projections about how a species distribution may change with future climate change, and the addition of PT increases confidence in future projections of novel environments. Climate change will likely drive the large-scale response of the northern and southern latitudinal distribution limits of our study species. As such, results from this study suggest that the latitudinal ranges for canopy-forming seaweeds in the NW Atlantic will be impacted by continued climate warming, but the response will be species specific. Whereas local threats such as nutrient loading (Worm and Lotze 2006; Schmidt et al. 2012), change of biotic interactions through introduced species (Schmidt and Scheibling 2006, 2007, and commercial harvesting (Seeley and Schlesinger 2012; Vandermeulen 2013; Arbuckle et al. 2014) will likely drive the smaller-scale, local response of seaweeds throughout their range.

The NE coast of the USA and Canadian Maritimes will likely see a shift in community composition. If emission levels continue to correspond with the RCP 8.5 scenario, south of Newfoundland the mid-intertidal zone may see a transition to *F. vesiculosus* dominance and the subtidal may see a transition to *C. fragile* dominance. In the Subarctic, Arctic, and Greenland there may also be northward shifts as well as increases in abundance for all six species. Based on the relative average response these shifts would result in kelp and fucoids having an overall net loss of latitudinal habitat range, resulting in a range shift and contraction. These shifts are less drastic in *C. crispus*

and *C. fragile* with smaller shifts in the southern edge, while still shifting the northern edge resulting in a latitudinal range expansion.

These projected range shifts will impact the ecological services provided, as well as the commercial importance of harvested species in the NW Atlantic. Along the southern edge, this will likely translate into negative impacts of the commercial harvest of *A. nodosum* within Maine and Canadian Maritimes. In the subtidal, a possible transition from a kelp forest to a *C. fragile* meadow may result in a shift of the community of associated species as kelps and *C. fragile* support different species (Schmidt and Scheibling 2006, 2007). Along the northern edge, shifting distributions and changes in abundance will impact the native rocky shore community in the Arctic. Seaweeds are not expected to shift their distribution poleward in isolation, as fish and invertebrates are also experiencing poleward shifts (Poloczanska et al. 2013). As many species of fish and invertebrates depend on the ecosystem functions provided by canopy-forming seaweed species, it can be thought that an entire ecosystem is shifting poleward (Krause-Jensen and Duarte 2014), although not all species will respond in a similar way (Pinsky et al. 2013). In general, the poleward migration of canopy-forming seaweed species, such as the species in this study, may help to facilitate the poleward migration of associated fish and invertebrate species.

Chapter 3 The Usefulness of Satellite Remote Sensing as a Monitoring Tool for Eelgrass Distribution in Nova Scotia

3.1 Introduction

Eelgrass (*Zostera marina*) beds are the dominant perennial vegetation occurring along soft-sediment marine shores in Nova Scotia (Gosner 1978). As a subtidal species, eelgrass provides food and complex three-dimensional structure to the surrounding marine ecosystem (Schmidt et al. 2011). This includes supporting an increased abundance and diversity of fish and invertebrates compared to surrounding mudflats (Mattila et al. 1999), creating nursery habitat for many commercial species (Heck et al. 2003), and providing an important food source for migratory bird species (Hanson 2004). Furthermore, eelgrass beds slow currents, increase sedimentation rates, and help to stabilize coastlines (Bos et al. 2007).

Eelgrass beds are highly persistent through time in pristine environments (DFO 2009). They are only periodically disturbed through storms or sediment re-distribution events which can uproot or bury seagrass (Waycott et al. 2009), and ice rafting events where eelgrass blades freeze to the underside of sea ice and are lifted out of the sediment with ice break up (Schneider and Mann 1991). However, in Nova Scotia (Hanson 2004) and globally (Orth et al. 2006; Waycott et al. 2009) seagrass beds have been decreasing over past decades. These decreases have been attributed to human activities such as nutrient loading (Hauxwell et al. 2001, 2003; Schmidt et al. 2012), the spread of invasive species (Garbary et al. 2014; Carman et al. 2016), aquaculture activities (Holmer et al. 2008; Skinner et al. 2013), and climate change (Orth et al. 2006).

To monitor further eelgrass bed decline, detailed baseline knowledge of present-day eelgrass distribution is required, as well as long term monitoring programs (Hanson

2004). Presently, eelgrass beds in parts of Nova Scotia have been studied through dive transects (i.e. Schmidt et al. 2011; Wong et al. 2013), aerial photography (Hanson 2004), underwater camera tows or video transects (Vandermeulen 2017), side-scan sonar (Skinner et al. 2017 unpublished data; Vandermeulen 2014), as well as traditional local ecological knowledge (Lee 2014). Elsewhere in the Canadian Maritimes, topographic-bathymetric lidar has also been used to map eelgrass distribution (Webster et al. 2016). The use of dive transects allows for quantitative information on eelgrass bed extent, percent cover and shoot density, as well as the diversity and abundance of associated flora and fauna. However, dive transects are time consuming, and as such, can only quantify limited spatial areas at selected time intervals (Environment Canada 2002). Boat based video transects can provide similar information on eelgrass bed characteristics in clear water, and sonar can be used in sites with murky water as light does not need to penetrate the water column. Yet, all boat based surveys have difficulty mapping in shallow water, as well as require a high sampling effort (Vandermeulen 2014; Webster et al. 2016). Aerial photography, can capture eelgrass bed extent over large areas, but requires the use of aircraft (Hossain et al. 2015). Lidar, an active sensor based on laser pulses, also requires an aircraft, and can map both land, shallow and deep water habitats at large spatial scales (Webster et al. 2016).

Alternatively, satellite remote sensing (SRS) can be used to quantify the extent and density of eelgrass bed coverage over bay-wide and regional scales (Pettorelli et al. 2014; Hossain et al. 2015; Rose et al. 2015). SRS can be used over large areas, with less sampling effort then dive transects and boat based surveys, and doesn't necessarily require site access (Environment Canada 2002). New satellite imagery acquisition is not

as expensive as Lidar imagery (Kelly and Di Tommaso 2015), yet image quality is highly dependent on tidal cycle, water clarity, and atmospheric effects (Hossain et al. 2015). Furthermore, the strong attenuation of light by the water column decreases the depth range across which eelgrass can be classified, resulting in reduced confidence in mapping eelgrass along the deeper end of its depth range.

Eelgrass distribution has been successfully classified elsewhere in temperate waters using passive optical SRS (i.e. Ferguson and Korfmacher 1997; Macleod and Congalton 1998; Lathrop et al. 2006; O'Neill and Costa 2013; Hogrefe et al. 2014; Barrell et al. 2015). In Nova Scotia, there has been exploratory work conducted into the feasibility of using SRS to quantify eelgrass distribution (Milton et al. 2009), however as of yet there is no published work detailing eelgrass distribution with SRS in Nova Scotia.

This chapter used archived high-resolution multispectral satellite imagery to classify eelgrass distribution in three bays in southwestern Nova Scotia. Archived satellite imagery was used as new satellite imagery acquisition costs can be prohibitive to many research groups. Furthermore, the ability to obtain ground truth points may be limited in remote areas, and along exposed coastlines with high wave energy. As such we aimed to classify the satellite imagery, with reduced image acquisitions costs, and ground truth sampling effort. To do so, there were three objectives: (i) classify eelgrass presence with a traditional supervised classification approach using ground truthing points; (ii) classify eelgrass presence with an unsupervised classification approach without using ground truthing points; and (iii) compare the output of the two classifications. If the two methods provide similar results, then the unsupervised classification could be used to map future or archived satellite imagery. Therefore, SRS could provide a useful

management tool for monitoring past and potential future shifts in eelgrass distribution due to natural or anthropogenic impacts, which can be applied at bay-wide to regional scales, with minimal input data.

3.2 Methods

3.2.1 Study Area

Three separate bays in southwestern Nova Scotia were chosen for their known presence of eelgrass (*Zostera marina*) beds: Port Mouton, Jordan Bay, and Port Joli (Figure 3.1). Port Joli is bordered on the southwestern shore by the Thomas Raddall Provincial Park, the Port Joli migratory bird sanctuary at the head of the bay, and on the northeastern shore by the Kejimkujik Seaside National Park, and is thus little impacted by human activities. Port Joli is a shallow bay with a maximum depth within the inner portion of 8 m data (CHS Direct User Licence No. 2017-0515-1260-D), and is dominated by soft-sediment, and mixed substrate (Schumacher et al. In Press).

Port Mouton and Jordan Bay are much deeper bays, where water depths (25 m and 20 m, respectively) exceed the 12 m (CHS Direct User Licence No. 2017-0515-1260-D) published depth limit of eelgrass (DFO 2009), and bottom substrate ranged from rocky, mixed-substrate, and soft-sediment (Schumacher et al. In Press). Jordan Bay shoreline is mostly forested, with small fishing communities spread out along the coast. Port Mouton shoreline includes Carter's Beach, as well the Summerville Beach Provincial Park, with small fishing communities predominantly found along the northwestern shore.

Port Mouton and Jordan Bay also both contain open net-pen finfish farms which have been operating since 1994 and 2012, respectively, and both leases have been extended until 2020 (Loucks et al. 2012; Nova Scotia Department of Fisheries and

Aquaculture 2015). These finfish farms have been suspected to affect eelgrass distribution in Port Mouton (Friends of Port Mouton 2014), therefore it is possible that continual aquaculture operations in Jordan Bay may have the same impact on eelgrass beds.

3.2.2 Field Surveys and Ground Truthing Points

Two benthic ground truthing surveys were performed using a handheld GPS (Garmin, Canada; horizontal accuracy within 3 to 5m). One survey occurred from July 15-20, 2015, and a second survey occurred from July 8-12, 2016 to increase spatial coverage of survey points. Although these surveys occurred over two years, it was assumed that perennial vegetated habitat coverage would minimally change within one year. Ground truth points were collected via SCUBA and snorkeling, and substrate cover was marked as eelgrass, seaweed, rockweed, rock, sand, mud, or shallow water. In all three bays, coastal access was limited, and so ground cover points were obtained haphazardly whenever there was access to the water from the road. The exception to this was in Port Mouton in 2015 when some sampling occurred with the use of a boat. Ground truth points were haphazardly collected; however, if there was a known eelgrass beds then targeted points were taken within the bed.

In Port Joli, 79 field survey points were obtained (Figure 3.2) and comprised of sand (n=25), exposed rockweed band (n=25), submerged seaweed bed (n=12), and eelgrass (n=17). In Port Mouton, 102 field survey points were obtained (Figure 3.3) and comprised of sand (n=11), shallow water (<4m, n=20), exposed rockweed band (n=12), submerged seaweed bed (n=14), and eelgrass (n=45). In Jordan Bay, 41 field survey points were obtained (Figure 3.4) and comprised of sand (n=5), seaweed (n=19), eelgrass

(n=12), and mixed habitat including seaweed and seagrass (n=3). During the field surveys, it was noted that eelgrass and seaweed often co-occurred as mixed beds, therefore any field survey points that may be classified as mixed between seaweed and eelgrass, were denoted as eelgrass.

To supplement field survey points, visually identified points were added using colour composites of the satellite imagery, available benthic substrate data (Schumacher et al. In Press), local ecological knowledge in Port Mouton (Lee 2014) and previous seagrass mapping projects in Port Joli (Milton et al. 2009) providing further identification for mud, sand, shallow water, deep water, rockweed band, eelgrass and seaweed. This resulted in a total of 50 points across mud, sand, shallow water, deep water, rockweed band, and seaweed, as well as 75 points for eelgrass (Figure 3.2-3.4).

All ground truth points were buffered into circular polygons with a 10 m diameter to account for GPS inaccuracy. Furthermore, in order to have an independent data set to evaluate the accuracy of the classification, the ground truth data were split into training and testing groups at a ratio of 70% training and 30% testing for the satellite image classification (section 3.2.4 below).

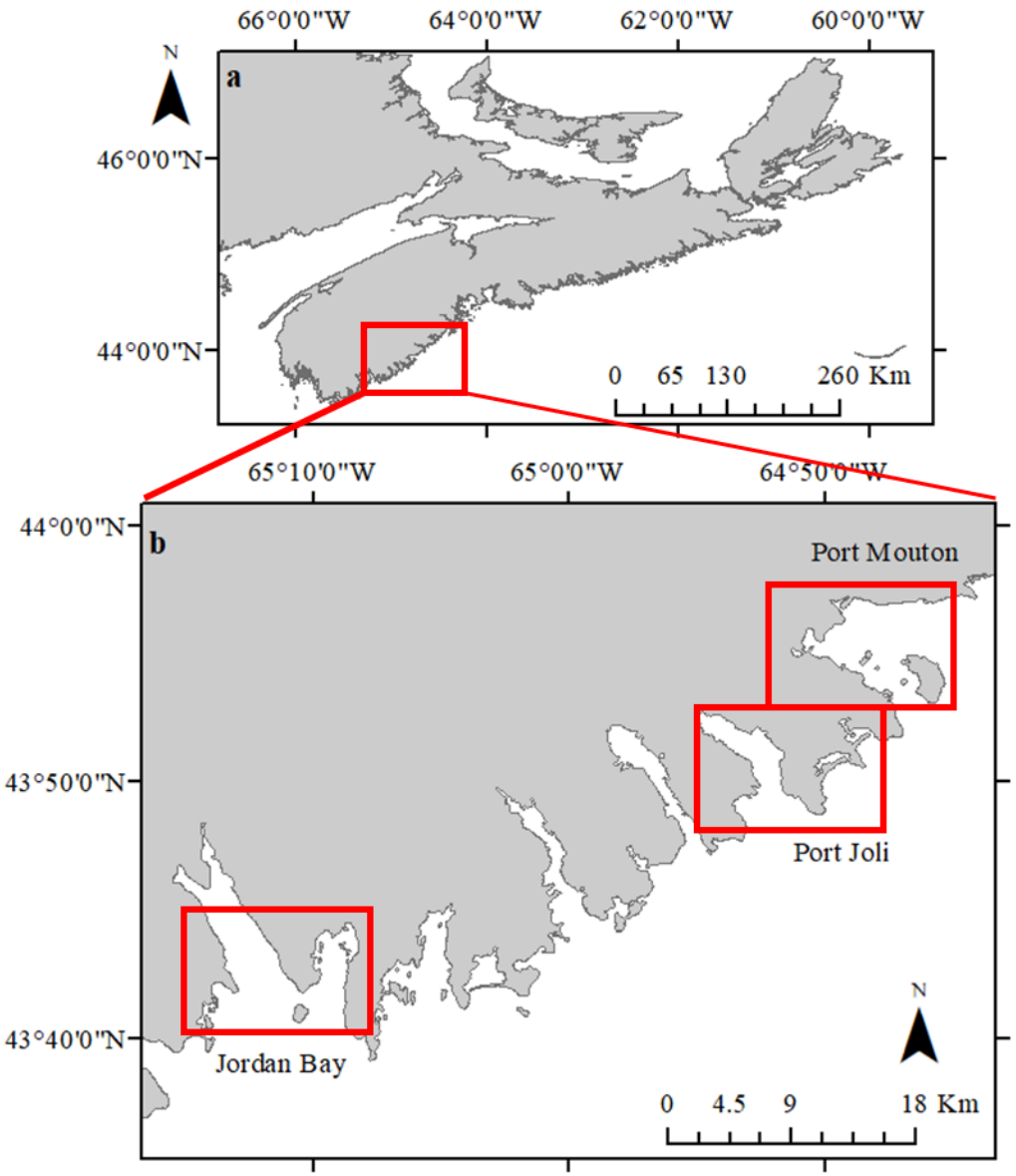

Figure 3.1 Map of Nova Scotia with red box outlining **a** general study area, and **b** showing location of three study sites: Port Mouton, Port Joli, and Jordan Bay.

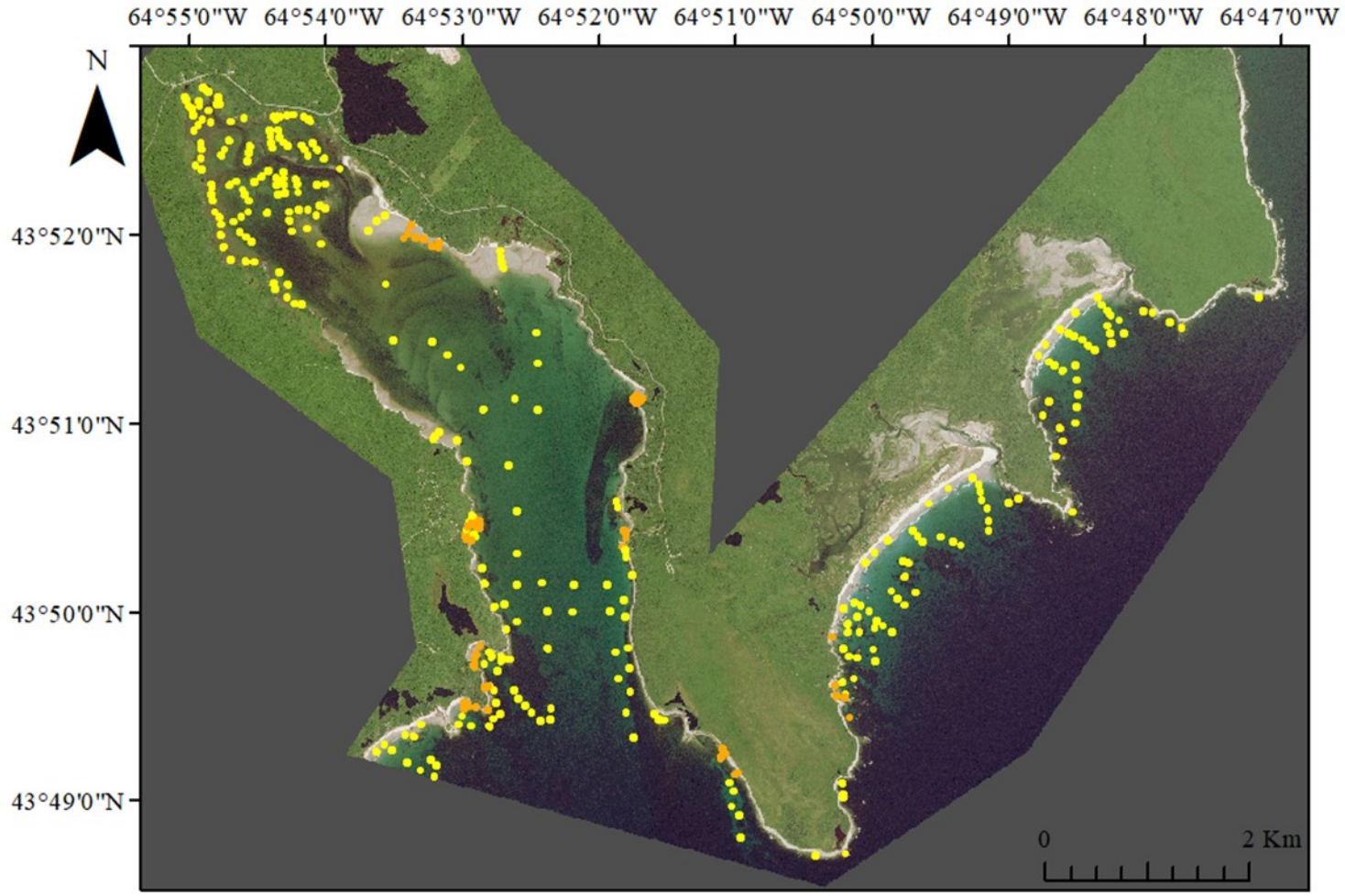

Figure 3.2 Ground truthing points collected in Port Joli over a true colour composite. Orange points were collected in the field, yellow points were added later (see section 3.2.2). Dark grey is background data outside the satellite imagery bounds.

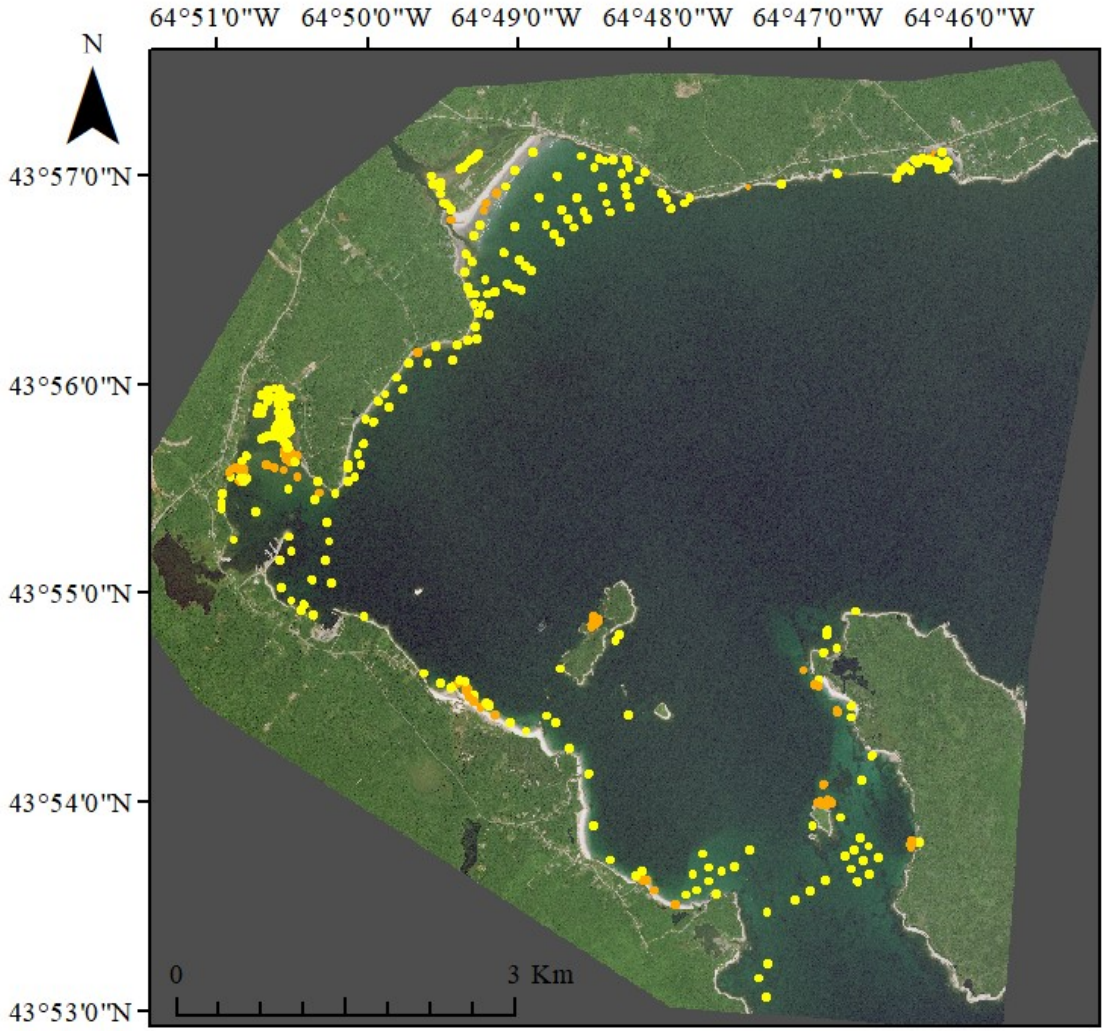

Figure 3.3 Ground truthing points collected in Port Mouton over a true colour composite. Orange points were collected in the field, yellow points were added later (see section 3.2.2). Dark grey is background data outside the satellite imagery bounds.

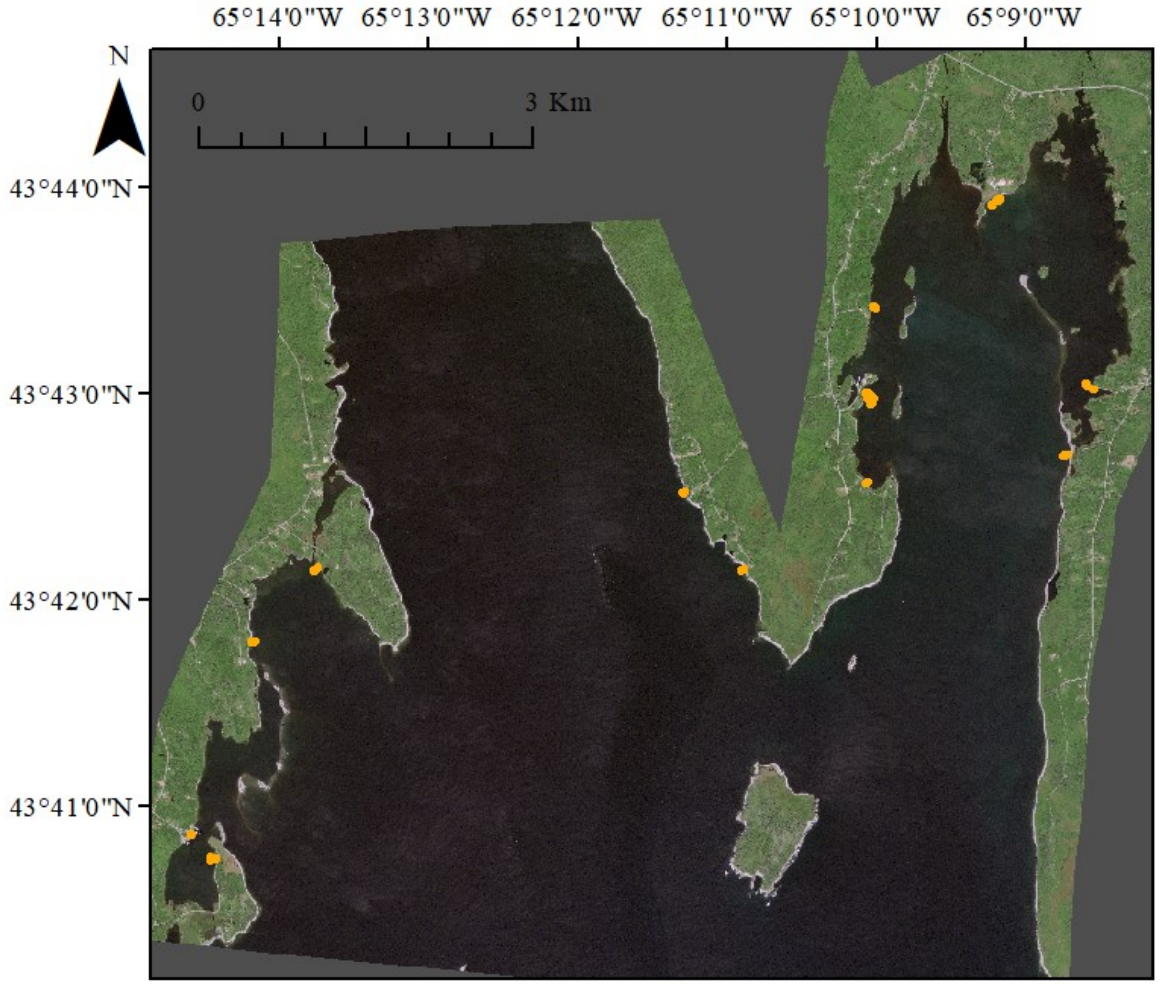

Figure 3.4 Ground truthing points collected in Jordan Bay over a true colour composite. Orange points were collected in the field and no additional points were added in due to poor image quality (see Appendix E). Dark grey is background data outside the satellite imagery bounds.

3.2.3 Satellite Image Collection and Preprocessing

An archived SPOT 6 image (BlackBridge Geomatics, Lethbridge, Alberta) of Jordan Bay was acquired on July 5, 2015, at 11:43 am local time, during falling tide, at a 16.18° viewing angle. An archived SPOT 7 image (BlackBridge Geomatics, Lethbridge, Alberta) of Port Mouton and Port Joli was acquired on July 11, 2015, at 11:47 am local time, during rising tide, at a 12.75° viewing angle. Imagery was obtained during the summer as this corresponds to increased density of eelgrass beds which peak in August/September (Wong et al. 2013). All images were free from cloud coverage. SPOT 6/7 have four multispectral bands: blue (450-520 nm), green (530-590 nm), red (625-695 nm), and near-infrared (NIR; 760-890 nm) at a spatial resolution of 6 x 6 m, and one panchromatic band (450-745 nm) at a spatial resolution of 1.5 x 1.5 m, all at a radiometric resolution of 16 bits (Astrium Services 2013). All images were pan-sharpened, orthorectified, and reduced to 8 bit by BlackBridge Geomatics to deliver a multispectral image at a spatial resolution of 1.5 x 1.5 m, a radiometric resolution of 8 bits, in UTM Zone 20N coordinates (Figure 3.5 Step 1).

All analyses were performed in the software program TerrSet® v. 18.31 (Clark University, Worcester, Massachusetts) and ArcGIS® v. 10.3 (ESRI, Redlands, USA) following the work flow outlined in Figure 3.5. An atmospheric and radiometric correction (Figure 3.5 Step 2) for all four multispectral bands (blue, green, red, and NIR) per bay was performed using the COST method (Chavez 1996). This method combines the dark object subtraction method (removes haze), with a cosine approximation of solar zenith angle to remove the impacts of Rayleigh scattering and atmospheric gases absorption. Haze was approximated in each image by examining each band's histogram

to determine the offset from zero. The removing of atmospheric effects allows for images across years to be compared in a future change detection study.

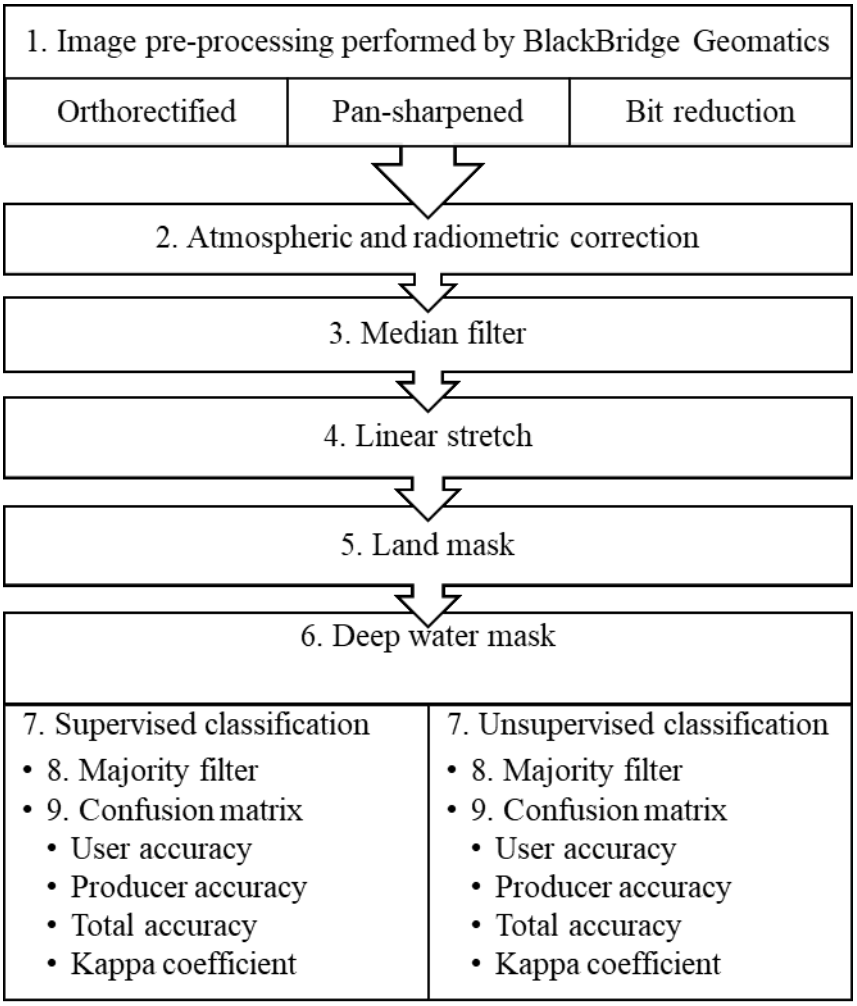

Figure 3.5 Outline of methods used to classify SPOT 6/7 satellite imagery in this study. Steps 1 through 6 are explained in section 3.2.3, Steps 7-8 are explained in section 3.2.4, and Step 9 is explained in section 3.2.5

To remove random noise in the images, all bands were filtered using a median filter with a 3 x 3 kernel (Figure 3.5 Step 3). A median filter was chosen as it performs well to generalize an image to remove random noise, while preserving edges (i.e. eelgrass bed edge; Carleer et al. 2005). Using a 3 x 3 kernel, the filter takes the median value of nine pixels, replaces only the central pixel with this median value, and continues through the imagery. Median filters are known to improve classification accuracy (Fauvel et al. 2012). Next the reflectance values were linearly stretched to 8 bits (values from 0 to 255; Figure 3.5 Step 4), and a land mask was created using the NIR band to mask out all land pixels (Figure 3.5 Step 5).

To create a deep water mask, an iterative self-organizing unsupervised classifier (ISOCLUST) analysis was performed using all four bands with land masked out (Figure 3.5 Step 6). This was an exploratory analysis to qualitatively determine the water depth that was spectrally close to the vegetation signal. Canadian Hydrographic Service single beam lowest mean tide bathymetric data (CHS Direct User Licence No. 2017-0515-1260-D) were used, in conjunction with true and false colour composites, to determine the deepest depth to be used in the analysis. The cluster associated with deep water, and spectrally confused with vegetation, was visually inspected to determine a depth where the algorithm could no longer differentiate vegetation from deep water.

3.2.4 Image Classification

Each bay was classified separately using both an unsupervised and supervised classification algorithm (Figure 3.5 Step 7). To create the supervised classification, training sites were created to run a maximum likelihood classification (Richards 1986) on all four bands with land and deep water masked out. Each class was assigned an equal

prior probability to occur, and each pixel was considered to occur as each class type, but was assigned to the class it had the highest probability of occurring as. Training sites were based on seven true ground cover types: mud, sand, shallow water, deep water, rockweed, seaweed, and eelgrass. Training sites were built using the 70% of ground truth points allocated to model building, and excluded the test points. The maximum likelihood classification was run through a 3 x 3 majority filter to reduce speckling (Macleod and Congalton 1998; Figure 3.5 Step 8).

The unsupervised classification was a two-step process where all four bands with land and deep water masked out were first run through an iterative self-organizing unsupervised classifier (ISOCLUST) with 3 iterations, up to 50 clusters, and a minimum training size of 40 pixels (Figure 3.5 Step 7). ISOCLUST works by: (1) determining a maximum number of clusters in the data based on examining peaks in the bands histograms (Richards 1986); (2) then the user chooses how many clusters to keep; (3) each pixel is assigned to the closest cluster; and (4) a new cluster mean is determined. Then in an iterative process Steps 3 and 4 are repeated three times to determine stable clusters (Ball and Hall 1965). In Step 2 the number of clusters was decided based on examining a histogram showing the frequency in which the cluster occurred. Areas with significant changes in the histogram peaks, are where major changes happened to the generality of the clusters. Based on these breaks, the user chooses the number of clusters to keep.

The first ISOCLUST was used to determine vegetated habitat from unvegetated habitat. To determine how a cluster should be labelled, each cluster's spectral signature was examined in conjunction with visual interpretation of the colour composites. Clusters

that corresponded to unvegetated pixels were assigned to groups for sand, mud, shallow water, and deep water. As this first iteration was spectrally confused between seaweed and eelgrass, vegetated pixels were classified into groups for the exposed rockweed band, and then by the strength of the NIR signal relative to the red signal into strong, moderate, weak (all NIR>Red), and negative NIR (Red<NIR; Hogrefe et al. 2014). These groupings were based on the spectral response of vegetation where visible light (i.e. blue, green, and red) is strongly absorbed by vegetation (i.e. eelgrass) but NIR light is strongly reflected. Therefore, a decrease in the NIR signal either corresponds to increased water depth due to the water absorbing NIR light or decreased vegetation coverage resulting in reduced NIR reflectance. All remaining clusters were specified as unknown. These clusters were used to create training sites to run a maximum likelihood classification to determine vegetated habitat from non-vegetated habitat. This classification was used to create a non-vegetated mask. This was the first iteration of the unsupervised classification (Table 3.1).

A second ISOCLUST was run with land, deep water, and unvegetated pixels masked out to differentiate between seaweed and eelgrass with 3 iterations, up to 50 clusters, and a minimum training size of 40 pixels. The resulting clusters were examined by looking at both their spectral signatures and visual inspection of colour composites to assign clusters to eight different ground cover types: mud, sand, shallow water, deep water, rockweed, seaweed, eelgrass, and unknown. These clusters were used to create training sites to run a second maximum likelihood classification to differentiate seaweed from seagrass. This final maximum likelihood classification was run through a 3 x 3 majority filter to reduce speckling (Macleod and Congalton 1998; Figure 3.5 Step 8).

This was the second iteration of the unsupervised classification (Table 3.1). To produce the final map for the unsupervised classification, all non-vegetated (bare ground) pixels from the first iteration, were overlaid over the classification for the second iteration (Table 3.1).

In addition to the methods described above, Port Mouton was further classified by breaking up the bay into segments to analyze separately as there were differences in objects spectral signatures across the imagery. To do so, the spectral curve of each training site established during the supervised classification was individually analyzed to determine areas where the spectral curve differed. As well, exploratory unsupervised classifications were performed to determine areas of the bay that tended to cluster together. Once the bay was segmented into four segments (Table 3.1; Figure 3.6) a new set of ground truth points was established. To start, the ground survey points collected in an area were used, and visually identified points were added to bring the categories if present in that section, i.e. mud was not present in all segments, up to a total of 20 points, using the same points established in section 3.2.1 if possible (Figure 3.6). These categories were for: sand, mud, shallow water, deeper water, exposed rockweed, shallow vegetation, and deeper vegetation. These points were split 70/30% for training and testing, as explained in section 3.2.2. Due to having a weak vegetation signal, seaweed and eelgrass were combined into one category, separated by the strength of the vegetation signal (i.e. shallow and deep vegetation). Each segment was then classified using the methods described earlier in this section. As this classification only determined vegetation from non-vegetated pixels, the resulting maps were compared to bottom

substrate (Schumacher et al. In Press), and local ecological knowledge (Lee 2014) to qualitatively determine areas that were more or less likely to be eelgrass or seaweed.

3.2.5 Image Evaluation

Each classification was evaluated using a confusion matrix (Figure 3.5 Step 9). A confusion matrix compares how the ground truth points relate to the image classification to determine user, producer, and total accuracy values (Story and Congalton 1986). Total accuracy examines the percentage of correctly classified points for the entire classification. It is calculated by dividing the number of correctly classified ground truth points, by the total number of ground truth points. To identify the accuracy of each ground cover category, user and producer accuracies are calculated. Producer accuracy assesses the proportion of times the ground truth data for a one ground cover category (i.e. eelgrass), is correctly portrayed in the map classification. It is calculated by dividing the total number of correctly classified ground truth points for one ground cover type, by the total number of points classified as that ground cover type. For instance, a value of 100% would indicate that all eelgrass ground truth points, were classified as eelgrass on the map. A value <100% indicates some eelgrass ground truth points, were classified as a different ground cover type on the map. User accuracy assesses how the ground truth points agree with the map, and indicates the confidence a user should have when using the map. It is calculated by dividing the number of examined pixels classified as one ground cover type, by the total number of examined pixels classified as that ground cover type. For instance, a value of 100% would indicate that all examined pixels classified on the map, corresponded to eelgrass ground truth points. A value <100% would indicate

that some pixels classified as eelgrass on the map, correspond to ground truth points for a different ground cover type.

Cohen's kappa coefficient of agreement, with z-tests for significance from zero, were also calculated to account for the chance agreement of the ground truth points and map classification (Foody 2002) using the "irr" package (Gamer 2012) in the statistical environment R (R Core Team 2014). Cohen's kappa ranges from -1 to 1, where values -1 to 0 indicate lower agreement then due to chance, 0 to 0.4 indicate very poor agreement, 0.4 to 0.8 indicate moderate agreement, and values >0.8 indicating very good agreement between datasets that is unlikely due to chance (Cohen 1960).

To evaluate the supervised classification, sand, mud, shallow water, and deep water test ground truth points, and classified pixels were respectively merged to create a non-vegetated class (labelled as bare ground in confusion matrixes; Table 3.1) as the goal of this study was to differentiate between types of vegetated habitat. Seaweed and rockweed classes and testing points were merged together to create one seaweed class set of test points (labelled as seaweed in confusion matrixes; Table 3.1). Then the confusion matrix was built. A test point was positive if any pixel within the 10 m diameter corresponded to the ground cover. A test point was negative if no pixel within the 10 m diameter corresponded to the ground cover. From this, user, producer, and total accuracies were calculated as well as a kappa coefficient.

For the first iteration of the unsupervised classification, the four NIR groups, as well as the rockweed group were merged into one vegetated class, and the test ground truth points for eelgrass, seaweed, and rockweed were merged into one vegetated class (Table 3.1). A bare ground class was also built as explained above to create a confusion

matrix examining vegetated from bare ground. The confusion matrix was built on both the test ground truth data set used for the supervised classification, and the entire data set. The second iteration of the unsupervised classification was evaluated in the same way as the supervised classification.; however, the image was evaluated using both the test data set, and the full data set.

In the case of Port Mouton, rockweed, shallow vegetation, and deep vegetation were merged into one vegetation group for both the supervised classification, and the second iteration of the unsupervised classification (Table 3.1). The bare ground group was merged as explained above.

The similarity of the final products for the supervised and unsupervised classifications were compared. In Port Joli and Port Mouton, all ground cover pixels associated with bare ground (Table 3.1) were reclassified into one bare ground group. In Port Joli, all pixels associated with seaweed and rockweed were reclassified into one seaweed group (Table 3.1). In Port Joli, this meant that a pixel could be defined as bare ground, seaweed, or eelgrass. In Port Mouton, all pixels associated with rockweed, shallow and deep vegetation were reclassified into one vegetation group (Table 3.1). In Port Mouton, this meant that a pixel could be defined as bare ground or vegetation. Then the supervised classification was overlaid over the unsupervised classification. The number of pixels that were classified the same by the two classifications (i.e. both bare ground), was divided by the total number of pixels in the imagery, to determine the percent similarity between the two classifications. Furthermore, the overall, producer and user accuracies were compared between the test data set for the final products for the supervised and unsupervised classification.

Table 3.1 Terminology used to refer to specific methods.

Name used in text	Definition
Bare Ground	In confusion matrix, refers to the merging of sand, mud, shallow water, and deep water
First iteration	Classification created by running an ISOCLUST, assigning clusters to groups based on the strength of NIR signal, using these clusters as training sites for a maximum likelihood classification to determine vegetation from not. This created a bare substrate mask
Rockweed	In figures, refers to rockweed band in the intertidal zone with a very strong vegetation signal
Seaweed	In confusion matrix, refers to the merging of seaweed and rockweed In figures, refers to all submerged seaweed species including kelp, fucoids etc.
Second iteration	Classification created by running an ISOCLUST, using the mask created in the first iteration, and assigning clusters to training sites for eelgrass, seaweed, and rockweed, for a maximum likelihood classification to eelgrass presence from absence
Segment one	Part of Port Mouton referring to area around Jackie and Port Mouton Island
Segment two	Part of Port Mouton from Clam Pond to Carter's Beach
Segment three	Part of Port Mouton from Carters' Beach until Jone's Cove
Segment four	Part of Port Mouton from Jone's Cove to Hunts Point
Supervised classification	Classification created by using training points (explained in section 3.2.2) to create training sites to run a maximum likelihood classification
Unsupervised classification	Classification created by using ISOCLUST to assign clusters to training sites to run a maximum likelihood classification. This was a two-step process and refers to the final product which merges the two iterations
Vegetated	In confusion matrix, refers to the merging of all NIR groupings, and the rockweed group
Vegetation	In confusion matrix, refers to the merging of rockweed, and shallow and deep water vegetation

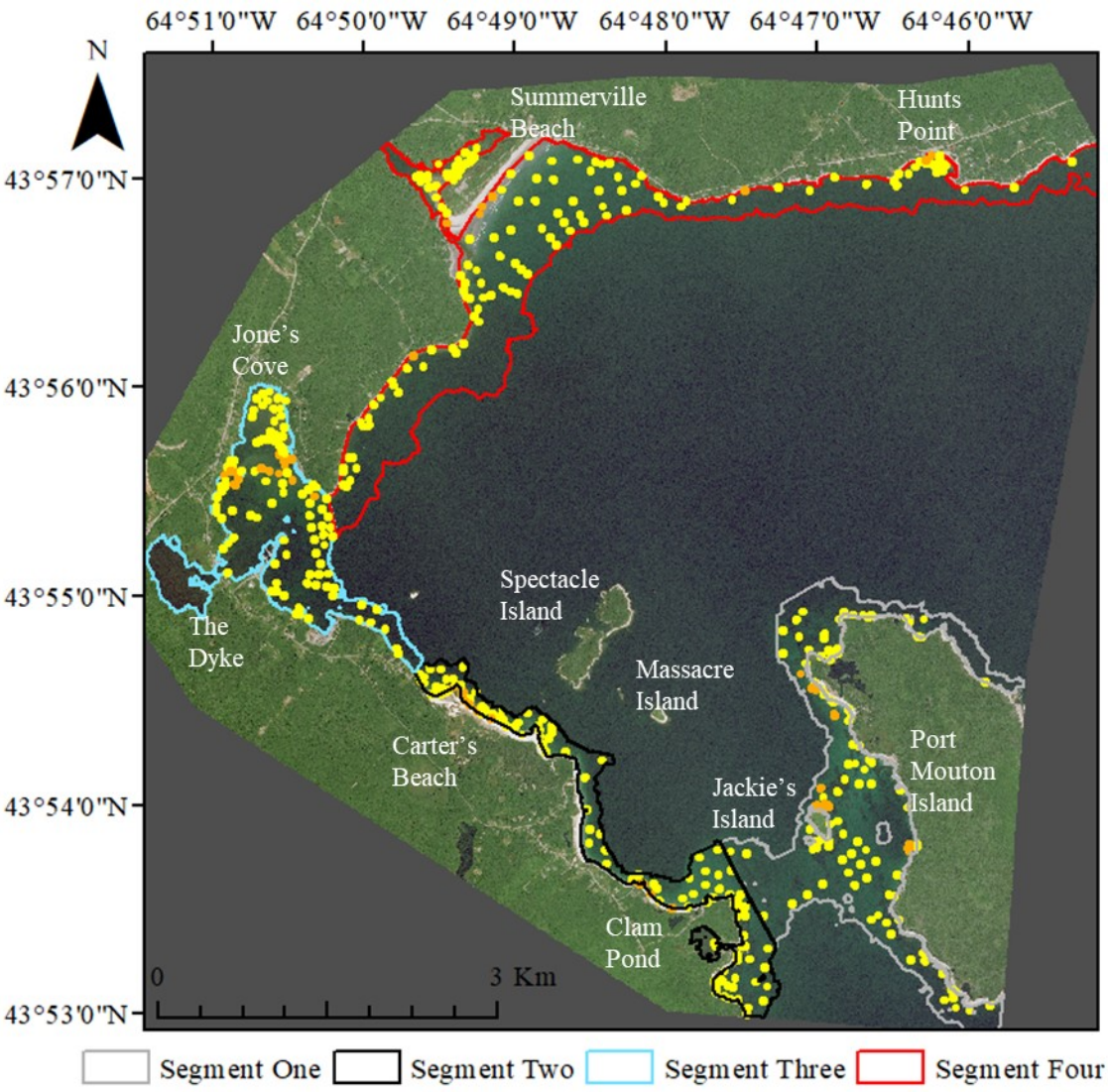

Figure 3.6 Breakdown of Port Mouton into the four segments, showing the names of landmarks throughout the bay, over a true colour composite, with dark grey as background data. Within each segment green dots indicate visually added points where orange dots indicate points collected in the field.

3.3 Results

3.3.1 Port Joli

Port Joli was successfully mapped using both classification techniques. First, the supervised classification, based on seven different ground cover types (Appendix E: Figure E.1a), classified 2.02 km^2 (11.11%) of Port Joli bay as having eelgrass present, and 5.71 km^2 (31.39%) as having seaweed present (Appendix E: Figure E.2). Seaweed presence was classified in areas of greater water depth, and both seaweed and eelgrass artifacts were noted in the middle of the bay. It is unknown if these artifacts are seaweed/eelgrass, floating wrack, or spectrally confused pixels. Substrate data is not shown in Port Joli as no area within the bay contained benthic substrate that eelgrass could not attach to (i.e. continuous bedrock).

The first iteration for the unsupervised classification, based on eight different ground cover types (Appendix E: Figure E.1b), classified 9.05 km^2 (49.74%) of Port Joli bay as having some degree of a vegetation signal (Appendix E: Figure E.3). The resulting map classified sand and water from shallow to moderate depths well, as well as shallow to mid-depth vegetation, with still some misclassification of deeper water and deeper vegetation, and mud from sparse vegetation. The second iteration for the unsupervised classification, based on six ground cover types (Appendix E: Figure E.1c), classified 1.57 km^2 (8.61%) of Port Joli bay as having eelgrass present, and 5.48 km^2 (30.12%) as having seaweed present (Appendix E: Figure E.4). The resulting map improved classification for mud from sparse vegetation, and deeper vegetation from deep water.

When the final products for the supervised and unsupervised classifications were compared, the two classifications were 86.91% similar to one another (Figure 3.7). The supervised classification, found the total area with eelgrass presence to be 2.50% greater,

and overall presence of vegetation to be 3.77% greater, than the unsupervised classification. Both classifications found a large eelgrass bed in the northwest of the bay bordered by muddy substrate in the shallow intertidal. Both also classified a narrow fringe of eelgrass in the shallow subtidal throughout Port Joli, with some vegetation artifacts in the middle of the bay. The largest differences between the two classifications existed in the eastern, outer portion of Port Joli where the supervised classification classified more of the pixels as seaweed, and the unsupervised classification classified more of the pixels as water. In the narrowing of the bay into Port Joli, the supervised classification classified more pixels as water, where the unsupervised classification classified it as seaweed. Along the border of the large eelgrass bed at the northwestern corner at the head of the bay, there were minor differences between the two classifications in delineating bed extent.

The final product for the supervised and unsupervised classification had similar accuracy values, as well as high kappa coefficients (Table 3.2a, d). To compare the two final products using the test data set, both the supervised and unsupervised classifications had similar producer (100.00%; 95.45%) and user accuracies (95.65%; 100.00%) for eelgrass presence, total map accuracies (97.32%, 96.42%), and significant kappa coefficients (0.94; 0.94), respectively (Table 3.2a, d). Furthermore, there was an improvement for total map accuracy and kappa coefficients from the first iteration of the unsupervised classification, to the second iteration of the unsupervised classification for the test (Table 3.2b, d) and full data set (Table 3.2c, e).

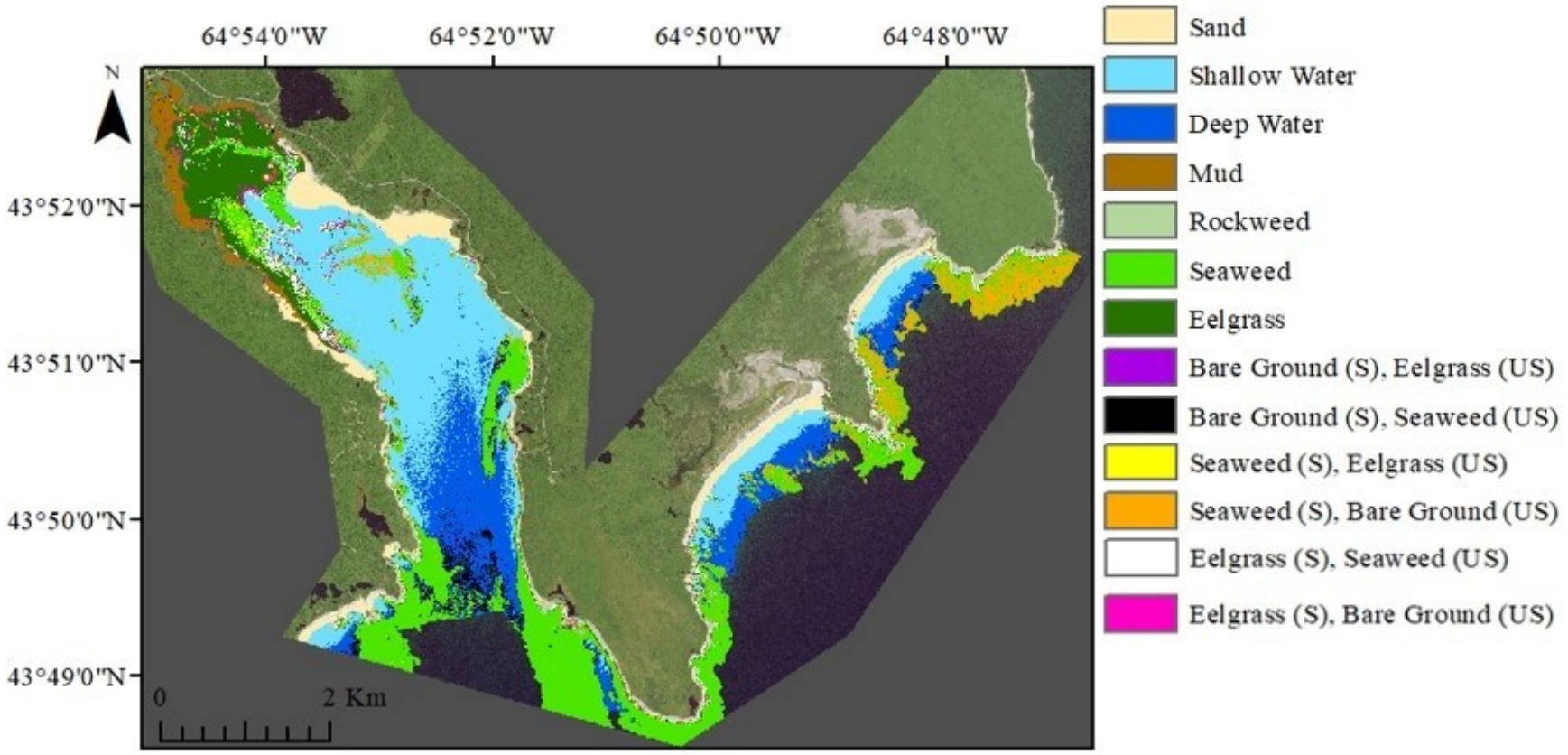

Figure 3.7 Vegetation coverage of Port Joli, based on the average response of the supervised and unsupervised classification. Where the two classifications disagree, the results from the supervised classification is denoted (S), and the unsupervised classification is denoted (US). These disagreements are denoted at the same level as the confusion matrix (see Table 3.1). The classification was overlaid over a true colour composite. Dark grey is background data outside the satellite imagery bounds.

Table 3.2 Confusion matrix for the classification in Port Joli based on **a** supervised classification on test points only; **b** the first iteration of the unsupervised classification for the test data set; and **c** the first iteration of the unsupervised classification for the full data set; and **d** the second iteration of the unsupervised classification for the test data set; and **e** the second iteration of the unsupervised classification for the full data set. For each confusion matrix mud, sand, shallow and deep water are merged into one bare ground group. Vegetated includes all NIR groups as well as rockweed group. Seaweed includes seaweed and rockweed. Total map accuracy (%) indicated in bold. Significant z-test ($p<0.05$) on kappa indicated by asterisk (*).

		Field Survey Reference Data			Total Correct	Total Points	User Accuracy (%)	Kappa coefficient
	Map Data	*Eelgrass*	*Seaweed*	*Bare Ground*				
	Eelgrass	22	1	0	22	23	95.65	
	Seaweed	0	27	0	27	27	100.00	
a	**Bare Ground**	0	2	60	60	62	96.77	0.94*
	Total Correct	22	27	60	109			
	Total Points	22	30	60		112		
	Producer Accuracy (%)	100.00	90.00	100.00			**97.32**	
	Map Data	*Vegetated*	*Bare Ground*					
	Vegetated	50	18		50	68	73.53	
b	**Bare Ground**	2	42		42	44	95.45	0.69*
	Total Correct	50	42		92			
	Total Points	52	60			112		
	Producer Accuracy (%)	96.15	70.00				**82.14**	
	Map Data	*Vegetated*	*Bare Ground*					
	Vegetated	166	59		166	225	73.78	
c	**Bare Ground**	7	141		141	148	95.27	0.66*
	Total Correct	166	141		307			
	Total Points	173	200			373		
	Producer Accuracy (%)	95.95	70.50				**82.31**	

		Field Survey Reference Data			Total Correct	Total Points	User Accuracy (%)	Kappa coefficient
	Map Data	*Eelgrass*	*Seaweed*	*Bare Ground*				
	Eelgrass	21	0	0	21	21	100.00	
	Seaweed	1	27	0	27	28	96.43	
d	**Bare Ground**	0	3	60	60	63	95.24	0.94*
	Total Correct	21	27	60	108			
	Total Points	22	30	60		112		
	Producer Accuracy (%)	95.45	90.00	100.00			**96.42**	
	Map Data	*Eelgrass*	*Seaweed*	*Bare Ground*				
	Eelgrass	65	0	0	65	65	100.00	
	Seaweed	8	92	1	92	101	91.09	
e	**Bare Ground**	2	6	199	199	207	96.14	0.92*
	Total Correct	65	92	199	356			
	Total Points	75	98	200		373		
	Producer Accuracy (%)	86.67	93.88	99.50			**95.44**	

3.3.4 Port Mouton

The supervised classification of Port Mouton, based on seven ground cover types (Appendix E: Figure E.5a), had poor discriminatory ability between eelgrass, seaweed, and deep water (Appendix E: Figure E.6). In some portions of the imagery, it was seemingly random assignment of pixels to one of these three groups, likely due to the high degree of similarity between the spectral curves for eelgrass, seaweed, and deep water (Appendix E: Figure E.5a). The first iteration of the unsupervised classification, based on nine ground cover types (Appendix E: Figure E.5b), had low discriminatory power in differentiating vegetation from non-vegetation, with most of the bay being classified with some degree of a vegetation signal (Appendix E: Figure E.7). The second iteration of the unsupervised classification, was unable to differentiate eelgrass from non-eelgrass and was therefore excluded from the results. Both the supervised classification (Appendix E: Table E.1a), and first iteration of the unsupervised classification (Appendix E: Table E.1b-c) had high accuracy values and kappa coefficients. The results shown in the confusion matrix are likely due to the good classification of rockweed, sand, mud, and shallow water for both the supervised classification and first iteration of the unsupervised classification, driving up the overall accuracy values.

To improve the classification of Port Mouton, the bay was broken up into four segments to analyze individually (Figure 3.6). This resulted in an improvement in Segments three (Jone's Cove and the Dyke) and four (Summerville Beach and Hunts Point). However, there is still some misclassification, particularly over deeper water, therefore the percentage of vegetated coverage within Port Mouton was not calculated like it was for Port Joli. These segments excluded Spectacle and Massacre Island's as the vegetation signature was the same as the deep water signature.

For all four segments, the final product for the supervised and unsupervised classifications produced similar user, producer, and total map accuracy values (>90%) as well as significant kappa coefficients (>0.90; Tables 3.3-3.6). In addition, there were improvements in user, producer, and total map accuracies, and kappa coefficients, from the first iteration of the unsupervised classification to the second iteration of the unsupervised classification, and these values were comparable between the training and test data sets.

Segment one consisted of the area surrounding Jackie's and Port Mouton Islands (Figure 3.6), and the final product for the supervised and unsupervised classifications were 86.27% similar to one another (Figure 3.8). Vegetated habitat was classified in the sandy shallows between Jackie's Island and Port Mouton Island. Throughout this segment, only a very small portion of benthic substrate was made up of continuous bedrock where eelgrass cannot attach (Figure 3.8a), with local ecological knowledge indicating the vegetation patches in the shallows between the two islands, as well as the vegetation in the small bay on the northwest shore of Port Mouton Island may contain eelgrass beds (Figure 3.8b). See Appendix E: Figures E.8, E.12a, E.13, E.17a, E.18, E.22a for the results of the individual classifications.

Segment two consisted of the southern shore of Port Mouton from Carter's Beach to Clam Pond (Figure 3.6). The final products for the supervised and unsupervised classifications were 85.74% similar to one another; however, this segment had the poorest agreement. Near Clam Pond, there was strong agreement between the two classifications for determining vegetated from non-vegetated (Figure 3.9). As the classification moves west towards Carter's Beach, there is strong disagreement between

the two datasets, particularly over deeper water. Only a very small portion of this segment contains unsuitable bottom substrate for eelgrass (Figure 3.9a), with local ecological knowledge suggesting the vegetated pixels in Clam Pond, as well as vegetation pixels along Carter's Beach may be eelgrass beds (Figure 3.9b). See Appendix E: Figures E.9, E.12b, E.14, E.17b, E.19, E.22b for the results of the individual classifications.

Segment three consisted of the Dyke and Jone's Cove (Figure 3.6). The final products for the supervised and unsupervised classifications produced a map with 86.62% similarity to one another (Figure 3.10), and decreased the amount of misclassification of deeper water as eelgrass relative to the supervised classification on the whole bay (Appendix E: Figure E.6). Large vegetated beds were classified throughout Jone's Cove and the Dyke over muddy substrate (Figure 3.10a), with local ecological knowledge suggesting these vegetated pixels may contain eelgrass beds (Figure 3.10b). See Appendix E: Figures E.10, E.12c, E.15, E.17b, E.20, E.22c for the results of the individual classifications.

Segment four consisted of the area outside of Jone's Cove, to Hunt's Point, including Summerville Beach (Figure 3.6), and had the highest similarity between the supervised and unsupervised classification at 95.55% (Figure 3.11). Furthermore, there was an improvement for the classification around Summerville Beach from the supervised classification on the whole bay (Appendix E: Figure E.6). Summerville and Hunt's Beach classified as non-vegetated and the rest of the segment classified as vegetated habitat (Figure 3.11). Large portions of this segment contained purely rocky bedrock bottom substrate (Figure 3.11a), and local ecological knowledge suggests only

two areas which may contain eelgrass (Figure 3.11b). See Appendix E: Figures E.11, E.12d, E.16, E.17d, E.21, E.22d for the results of the individual classifications.

3.3.5 Jordan Bay

The classification of Jordan Bay was unsuccessful due to the poor quality of the satellite imagery data. Similar results were obtained for both the supervised and unsupervised classification, across varying steps of images preprocessing. Furthermore, dividing the bay into smaller segments, as was performed in Port Mouton, did not help to improve the classification. Results for Jordan Bay were therefore excluded from the results section but see Appendix F for further details.

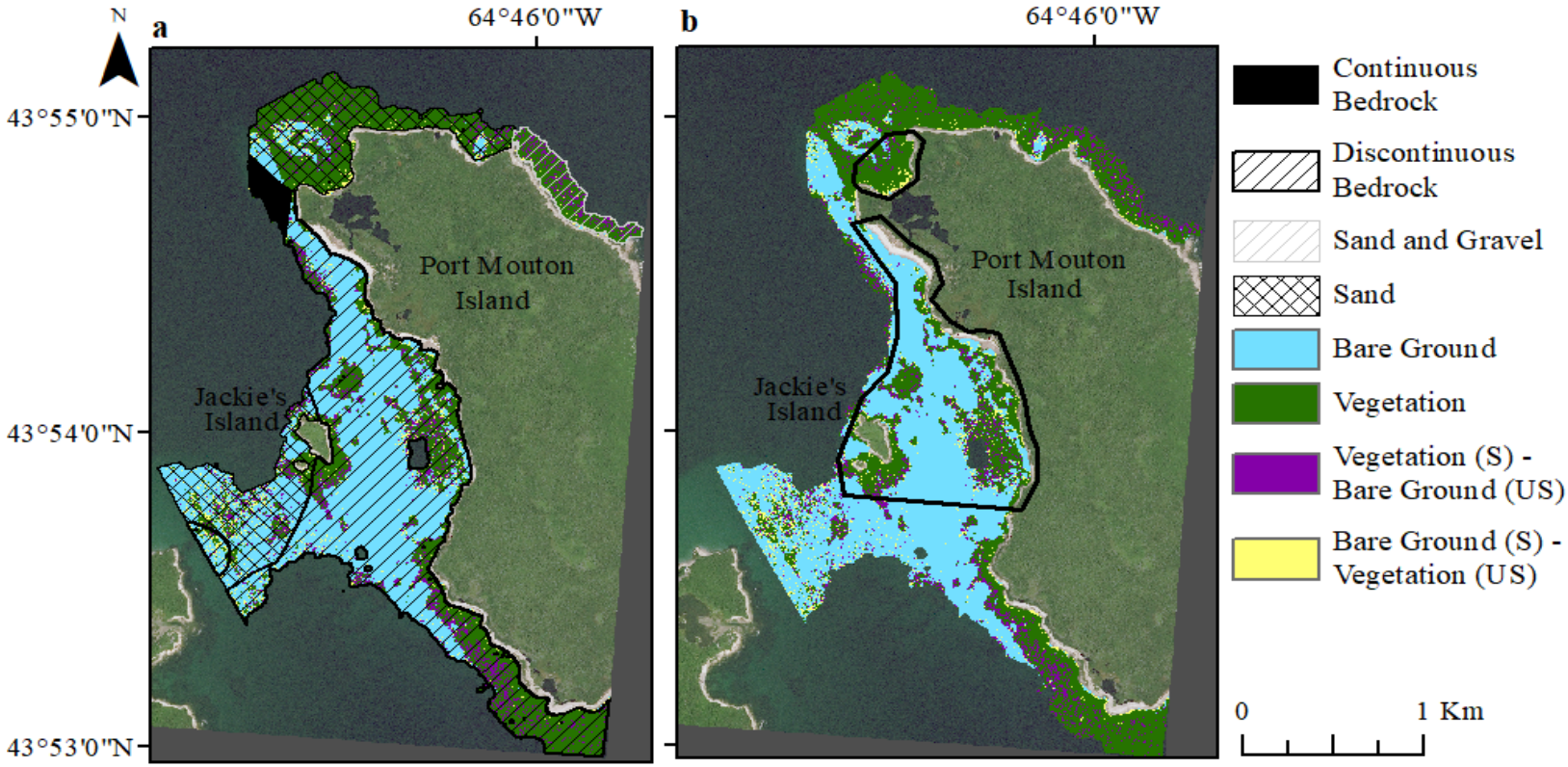

Figure 3.8 Average response of the supervised and unsupervised classification for Segment One in Port Mouton showing the location of vegetation in the bay, **a** has substrate data overlaid, and **b** shows a rough outline where local ecological knowledge (Lee 2014) suggests eelgrass beds may occur. Purple pixels indicate where the supervised classification (S) denoted vegetated and the unsupervised classification (US) denoted bare ground. Yellow pixels indicate where the supervised classification (S) denoted bare ground and the unsupervised classification (US) denoted vegetated. Hashed substrate areas indicate bottom substrates capable of containing eelgrass, while black substrate areas indicate bottom substrates not capable of containing eelgrass. The classification was overlaid over a true colour composite. Dark grey is background data outside the satellite imagery bounds.

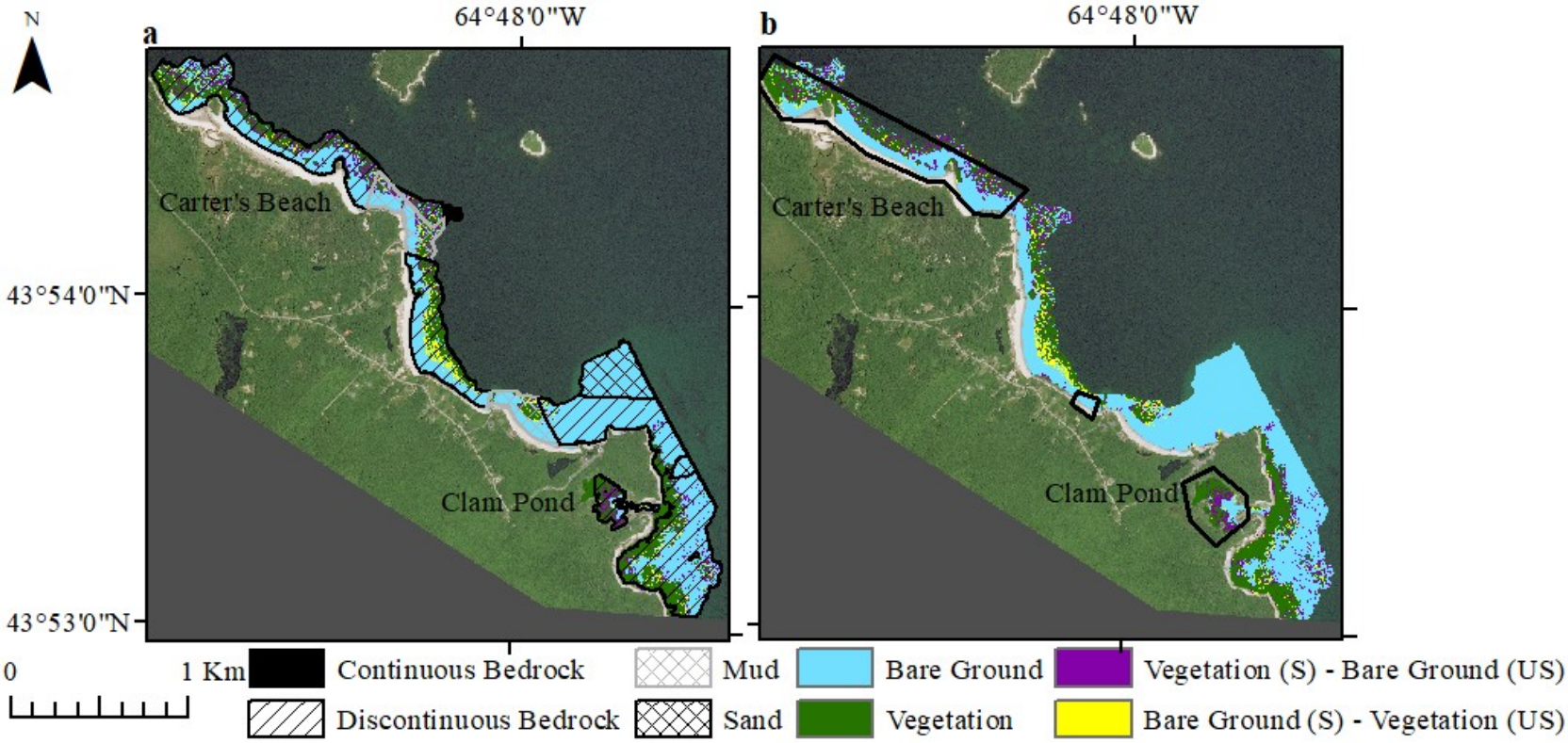

Figure 3.9 Average response of the supervised and unsupervised classification for Segment Two in Port Mouton showing the location of vegetation in the bay, **a** has substrate data overlaid, and **b** shows a rough outline where local ecological knowledge (Lee 2014) suggests eelgrass beds may occur. Purple pixels indicate where the supervised classification (S) denoted vegetated and the unsupervised classification (US) denoted bare ground. Yellow pixels indicate where the supervised classification (S) denoted bare ground and the unsupervised classification (US) denoted vegetated. Hashed substrate areas indicate bottom substrates capable of containing eelgrass, while black substrate areas indicate bottom substrates not capable of containing eelgrass. The classification was overlaid over a true colour composite. Dark grey is background data outside the satellite imagery bounds.

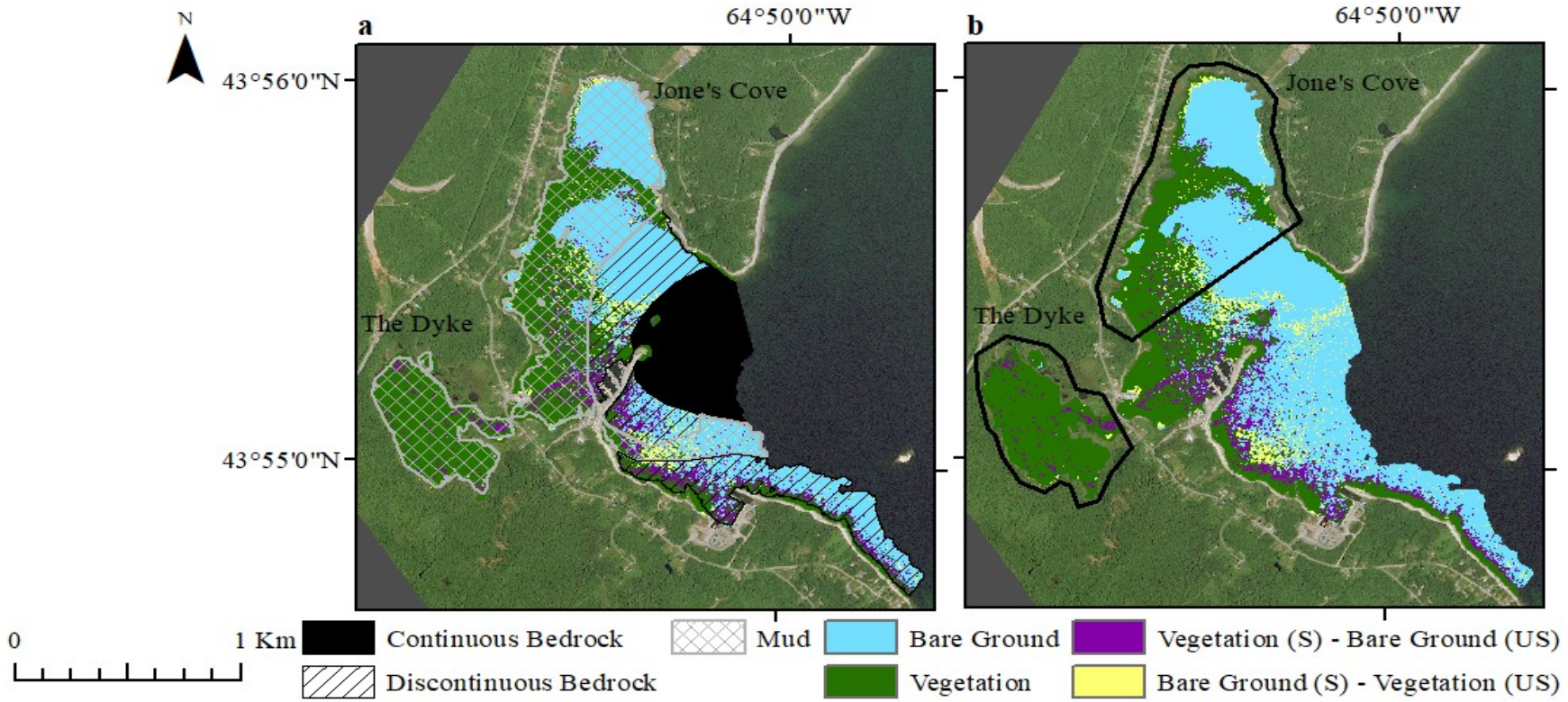

Figure 3.10 Average response of the supervised and unsupervised classification for Segment Three in Port Mouton showing the location of vegetation in the bay, **a** has substrate data overlaid, and **b** shows a rough outline where local ecological knowledge (Lee 2014) suggests eelgrass beds may occur. Purple pixels indicate where the supervised classification (S) denoted vegetated and the unsupervised classification (US) denoted bare ground. Yellow pixels indicate where the supervised classification (S) denoted bare ground and the unsupervised classification (US) denoted vegetated. Hashed substrate areas indicate bottom substrates capable of containing eelgrass, while black substrate areas indicate bottom substrates not capable of containing eelgrass. The classification was overlaid over a true colour composite. Dark grey is background data outside the satellite imagery bounds.

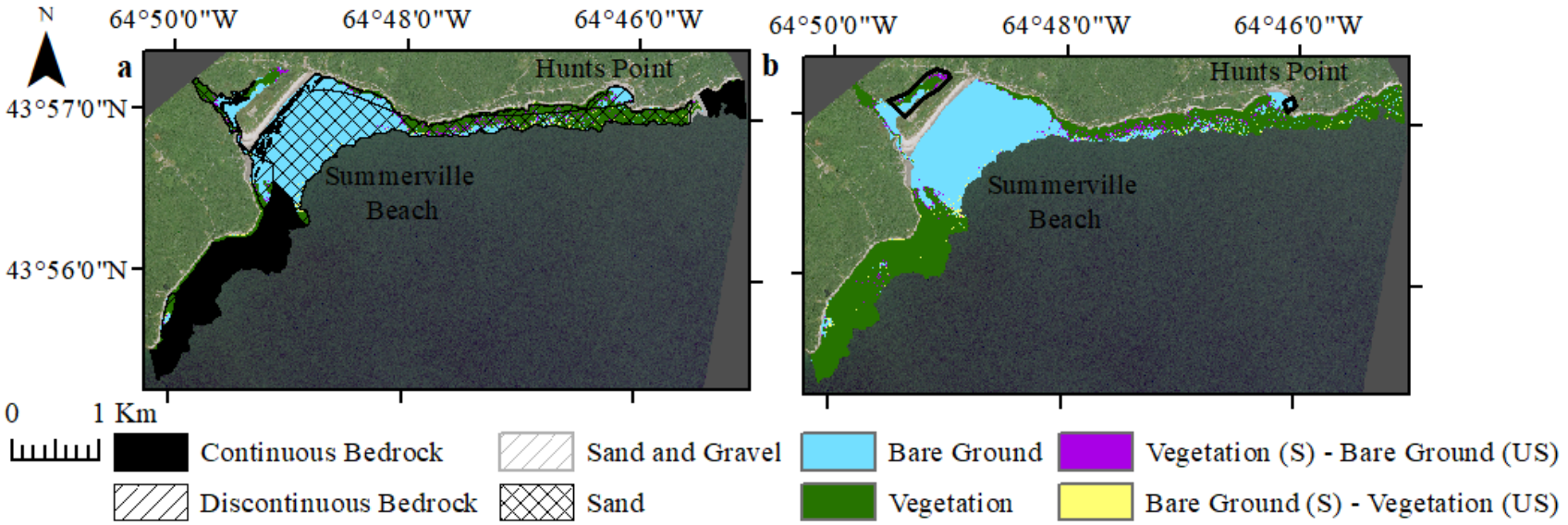

Figure 3.11 Average response of the supervised and unsupervised classification for Segment Four in Port Mouton showing the location of vegetation in the bay, **a** has substrate data overlaid, and **b** shows a rough outline where local ecological knowledge (Lee 2014) suggests eelgrass beds may occur. Purple pixels indicate where the supervised classification (S) denoted vegetated and the unsupervised classification (US) denoted bare ground. Yellow pixels indicate where the supervised classification (S) denoted bare ground and the unsupervised classification (US) denoted vegetated. Hashed substrate areas indicate bottom substrates capable of containing eelgrass, whileere black substrate areas indicate bottom substrates not capable of containing eelgrass. The classification was overlaid over a true colour composite. Dark grey is background data outside the satellite imagery bounds.

Table 3.3 Confusion matrix for the classification in Port Mouton Segment One based on **a** supervised classification on test points only; **b** the first iteration of the unsupervised classification for the test data set; and **c** the first iteration of the unsupervised classification for the full data set; and **d** the second iteration of the unsupervised classification for the test data set; and **e** the second iteration of the unsupervised classification for the full data set. For each confusion matrix mud, sand, shallow and deep water were merged into one bare ground group. Vegetated includes all NIR groups as well as rockweed group. Vegetation includes shallow and deep vegetation. Total map accuracy (%) indicated in bold. Significant z-test ($p<0.05$) on kappa indicated by asterisk (*).

		Field Survey Reference Data		Total Correct	Total Points	User Accuracy (%)	Kappa coefficient
	Map Data	*Vegetation*	*Bare Ground*				
	Vegetation	17	0	17	17	100.00	
	Bare Ground	1	18	18	19	94.74	
a	Total Correct	17	18	35			0.94*
	Total Points	18	18		36		
	Producer Accuracy (%)	94.44	100.00			**97.22**	
	Map Data	*Vegetated*	*Bare Ground*				
	Vegetated	17	6	17	23	73.91	
	Bare Ground	1	12	12	13	92.31	
b	Total Correct	17	12	29			0.61*
	Total Points	18	18		36		
	Producer Accuracy (%)	94.44	66.67			**80.56**	
	Map Data	*Vegetated*	*Bare Ground*				
	Vegetated	58	15	58	73	79.45	
	Bare Ground	2	45	45	47	95.74	
c	Total Correct	58	45	103			0.72*
	Total Points	60	60		120		
	Producer Accuracy (%)	96.67	75.00			**85.83**	

		Field Survey Reference Data		Total Correct	Total Points	User Accuracy (%)	Kappa coefficient
	Map Data	*Vegetation*	*Bare Ground*				
	Vegetation	17	0	17	17	100.00	
	Bare Ground	1	18	18	19	94.74	0.94*
d	Total Correct	17	18	35			
	Total Points	18	18		36		
	Producer Accuracy (%)	94.44	100.00			**97.22**	
	Map Data	*Vegetation*	*Bare Ground*				
	Vegetation	58	1	58	59	98.31	
	Bare Ground	2	59	59	61	96.72	0.95*
e	Total Correct	58	59	117			
	Total Points	60	60		120		
	Producer Accuracy (%)	96.67	98.33			**97.5**	

Table 3.4 Confusion matrix for the classification in Port Mouton Segment Two based on **a** supervised classification on test points only; **b** the first iteration of the unsupervised classification for the test data set; and **c** the first iteration of the unsupervised classification for the full data set; and **d** the second iteration of the unsupervised classification for the test data set; and **e** the second iteration of the unsupervised classification for the full data set. For each confusion matrix mud, sand, shallow and deep water were merged into one bare ground group. Vegetated includes all NIR groups as well as rockweed group. Vegetation includes rockweed, shallow and deep vegetation. Total map accuracy (%) indicated in bold. Significant z-test ($p<0.05$) on kappa indicated by asterisk (*).

		Field Survey Reference Data		Total Correct	Total Points	User Accuracy (%)	Kappa coefficient
	Map Data	*Vegetation*	*Bare Ground*				
	Vegetation	18	1	18	19	94.74	
	Bare Ground	0	17	17	17	100.00	
a	Total Correct	18	17	35			0.94*
	Total Points	18	18		36		
	Producer Accuracy (%)	100.00	94.44			**97.22**	
	Map Data	*Vegetated*	*Bare Ground*				
	Vegetated	18	3	18	21	85.71	
	Bare Ground	0	15	15	15	100.00	
b	Total Correct	18	15	33			0.83*
	Total Points	18	18		36		
	Producer Accuracy (%)	100.00	83.33			**91.67**	
	Map Data	*Vegetated*	*Bare Ground*				
	Vegetated	60	12	60	72	83.33	
	Bare Ground	0	48	48	48	100.00	
c	Total Correct	60	48	108			0.80*
	Total Points	60	60		120		
	Producer Accuracy (%)	100.00	80.00			**90.00**	

		Field Survey Reference Data		Total Correct	Total Points	User Accuracy (%)	Kappa coefficient
	Map Data	*Vegetation*	*Bare Ground*				
	Vegetation	17	0	17	17	100.00	
	Bare Ground	1	18	18	19	94.74	0.94*
d	Total Correct	17	18	35			
	Total Points	18	18		36		
	Producer Accuracy (%)	94.44	100.00			**97.22**	
	Map Data	*Vegetation*	*Bare Ground*				
	Vegetation	58	1	58	59	98.31	
	Bare Ground	2	59	59	61	96.72	0.95*
e	Total Correct	58	59	117			
	Total Points	60	60		120		
	Producer Accuracy (%)	96.67	98.33			**97.5**	

Table 3.5 Confusion matrix for the classification in Port Mouton Segment Three based on **a** supervised classification on test points only; **b** the first iteration of the unsupervised classification for the test data set; and **c** the first iteration of the unsupervised classification for the full data set; and **d** the second iteration of the unsupervised classification for the test data set; and **e** the second iteration of the unsupervised classification for the full data set. For each confusion matrix mud, sand, shallow and deep water were merged into one bare ground group. Vegetated includes all NIR groups as well as rockweed group. Vegetation includes shallow and deep vegetation. Total map accuracy (%) indicated in bold. Significant z-test ($p<0.05$) on kappa indicated by asterisk (*).

		Field Survey Reference Data		Total Correct	Total Points	User Accuracy (%)	Kappa coefficient
	Map Data	*Vegetation*	*Bare Ground*				
	Vegetation	18	0	18	18	100.00	
	Bare Ground	0	18	18	18	100.00	
a	Total Correct	18	18	36			1.00*
	Total Points	18	18		36		
	Producer Accuracy (%)	100.00	100.00			**100.00**	
	Map Data	*Vegetated*	*Bare Ground*				
	Vegetated	18	1	18	19	94.74	
	Bare Ground	0	17	17	17	100.00	
b	Total Correct	18	17	35			0.94*
	Total Points	18	18		36		
	Producer Accuracy (%)	100.00	94.44			**97.22**	
	Map Data	*Vegetated*	*Bare Ground*				
	Vegetated	58	3	58	61	95.08	
	Bare Ground	2	57	57	59	96.61	
c	Total Correct	58	57	115			0.92*
	Total Points	60	60		120		
	Producer Accuracy (%)	96.67	95.00			**95.83**	

		Field Survey Reference Data		Total Correct	Total Points	User Accuracy (%)	Kappa coefficient
	Map Data	*Vegetation*	*Bare Ground*				
	Vegetation	18	0	18	18	100.00	
	Bare Ground	0	18	18	18	100.00	1.00*
d	Total Correct	18	18	36			
	Total Points	18	18		36		
	Producer Accuracy (%)	100.00	100.00			**100.00**	
	Map Data	*Vegetation*	*Bare Ground*				
	Vegetation	58	1	58	59	98.31	
	Bare Ground	2	59	59	61	96.72	0.95*
e	Total Correct	58	59	117			
	Total Points	60	60		120		
	Producer Accuracy (%)	96.67	98.33			**97.50**	

Table 3.6 Confusion matrix for the classification in Port Mouton Segment Four based on **a** supervised classification on test points only; **b** the first iteration of the unsupervised classification for the test data set; and **c** the first iteration of the unsupervised classification for the full data set; and **d** the second iteration of the unsupervised classification for the test data set; and **e** the second iteration of the unsupervised classification for the full data set. For each confusion matrix mud, sand, shallow and deep water were merged into one bare ground group. Vegetated includes all NIR groups as well as rockweed group. Vegetation includes shallow and deep vegetation. Total map accuracy (%) indicated in bold.

		Field Survey Reference Data		Total Correct	Total Points	User Accuracy (%)	Kappa coefficient
	Map Data	*Vegetation*	*Bare Ground*				
	Vegetation	17	0	17	17	100.00	
	Bare Ground	1	24	24	25	96.00	
a	Total Correct	17	24	41			0.95*
	Total Points	18	24		42		
	Producer Accuracy (%)	94.44	100.00			**97.62**	
	Map Data	*Vegetated*	*Bare Ground*				
	Vegetated	18	0	18	18	100.00	
	Bare Ground	0	24	24	24	100.00	
b	Total Correct	18	24	42			1.00*
	Total Points	18	24		42		
	Producer Accuracy (%)	100.00	100.00			**100.00**	
	Map Data	*Vegetated*	*Bare Ground*				
	Vegetated	60	2	60	62	96.77	
	Bare Ground	0	78	78	78	100.00	
c	Total Correct	60	78	138			0.97*
	Total Points	60	80		140		
	Producer Accuracy (%)	100.00	97.50			**98.57**	

		Field Survey Reference Data		Total Correct	Total Points	User Accuracy (%)	Kappa coefficient
	Map Data	*Vegetation*	*Bare Ground*				
	Vegetation	17	0	17	17	100.00	
	Bare Ground	1	24	24	25	96.00	0.95*
d	Total Correct	17	24	41			
	Total Points	18	24		42		
	Producer Accuracy (%)	94.44	100.00			**97.62**	
	Map Data	*Vegetation*	*Bare Ground*				
	Vegetation	59	0	59	59	100.00	
	Bare Ground	1	80	80	81	98.77	0.99*
e	Total Correct	59	80	139			
	Total Points	60	80		140		
	Producer Accuracy (%)	98.33	100.00			**99.29**	

3.4 Discussion

Using satellite remote sensing (SRS), we successfully classified *Zostera marina* (eelgrass) distribution in Port Joli, whereas Port Mouton and Jordan Bay proved much more difficult to map. Yet, the methods used to produce an unsupervised classification yielded similar results to a supervised maximum likelihood classification. This suggests that the statistical methods used in this chapter are successful at mapping eelgrass distribution, and could be used for eelgrass monitoring and the detection of distribution changes, significantly reducing the cost and effort required to collect ground truth points through extensive field studies. However, this technique is highly dependent on the quality of satellite imagery, and the biophysical characteristics of the study area, including water depth and clarity.

3.4.1 Port Joli

The successful classification of eelgrass presence in Port Joli demonstrated that the unsupervised classification technique was capable of classifying eelgrass distribution. Overall, our results suggest that 2.02-5.71 km^2 or 8.61-11.10% of the bay is covered by eelgrass, and 30.12-31.39% by seaweed, with a total 40-41% of vegetated habitat, which is essential information needed by conservation and management agencies (Environment Canada 2002). Furthermore, the final classification for the eelgrass bed at the head of Port Joli was similar in terms of bed boundaries to an exploratory 2009 segmented supervised GeoEye-1 image classification (Milton et al. 2009). The GeoEye-1 image only classified the eelgrass bed at the northwestern head of the bay, at different eelgrass densities (sparse and dense), opposed to this study's presence-absence classification across the entire imagery. The GeoEye-1 image has a more refined spatial resolution, but

similar spectral resolution as the SPOT 6/7 images used in this study. Despite having similar bed boundaries, the 2009 classification suggests a larger bed than identified in 2015. There are three possibilities to explain the differences between the two images. The first is due to the seasonal variation of eelgrass shoot density, where density in Port Joli peaks in August/September (Wong et al. 2013). Our imagery was collected in early July, compared to the GeoEye-1 image collected in late August, therefore some areas with lower eelgrass density may not be detectable within the SPOT 6/7 imagery. The second possibility is that there has been a reduction of eelgrass coverage in Port Joli since 2009, as experienced elsewhere in Nova Scotia (Hanson 2004) and globally (Orth et al. 2006; Waycott et al. 2009). Lastly, the third possibility may be due to the inherent differences between satellite imagery where differences in the spectral resolution, or weather conditions (i.e. cloud cover, water column properties), resulted in different classifications of eelgrass bed extent.

The Port Joli classification described seaweed and eelgrass vegetation artifacts in the middle of the bay. While in the 2015 imagery this area appeared to be bare substrate based on examining colour composites, a drop camera survey which occurred in 2016 in Port Joli found patchy eelgrass and seaweed throughout this area (Vandermeulen 2017). It is unknown if these artifacts indicated vegetation coverage in 2015, or if it is misclassification of vegetation with deeper water. Furthermore, the presence of patchy vegetation in this deeper portion (Vandermeulen 2017) may be too deep and/or at to sparse of a density to be able to be picked up by the satellite imagery. Therefore, we may be underestimating eelgrass and seaweed coverage in Port Joli.

3.4.2 Port Mouton

In Port Mouton, the supervised and unsupervised classification per segment yielded similar results. However, the classification was only to the level of vegetated versus non-vegetated as there was a very weak vegetation signal. For future work, a higher sampling effort in areas of greater water depth would help to differentiate deeper bare ground from deeper vegetation, and would likely have improved the classification across all segments. Lastly, as there were many classification artifacts in deeper water, vegetation was not given as percent cover of Port Mouton.

Each segments classification was qualitatively examined using substrate data (Schumacher et al. In Press) and local ecological knowledge (Lee 2014) to provide insight into which areas may include eelgrass versus seaweed coverage (Roelfsema et al. 2009). Segment one, including Jackie's and Port Mouton Island classified several patches of vegetation between the two islands. This area traditionally has had continuous eelgrass beds up to the 1980s, with patchy beds observed into the 2010s (Lee 2014). During the 2015 ground truthing surveys, this area had only very patchy vegetation remaining, with eelgrass and seaweeds occurring together. Therefore, the results suggest a decrease in eelgrass coverage around Jackie and Port Mouton Islands between 1980 and 2015. The vegetation classified around the outer, exposed portions of Port Mouton Island are more likely to be seaweed coverage, although this persists to the edge of the classification bounds suggesting the algorithm has difficulty determining vegetation from deeper water.

Segment two, from Clam Pond west to Carter's Beach had the poorest classification and should be interpreted with caution. Notably the high degree of misclassification between deeper vegetation and deeper water around Carter's Beach made it impossible to determine if vegetation extents in that area. Incorporating side-scan

sonar data from this area (Skinner et al. unpublished data), would likely help to improve the classification. In Clam Pond, and the surrounding cove, the algorithms did a much better job. Based on local ecological knowledge (Lee 2014) it is possible the classified vegetation within Clam Pond contained eelgrass, whereas the outer cove more likely to contained seaweed beds. If this is correct, it would be the first known existence of eelgrass within Clam Pond since the 1980s (Lee 2014).

Segment three, containing the Dyke and Jone's Cove, was classified well within Jone's Cove. Based on local ecological knowledge (Lee 2014), the distribution and extent of eelgrass coverage appears to have decreased since 2010 in Jone's Cove. The extent of this areas eelgrass beds has been highly variable since 1930 (Lee 2014), so this recent change should be interpreted with caution. The Dyke is another area that has traditionally had eelgrass beds up until the 1980s, with an unknown distribution to the 2010s (Lee 2014). It is unlikely that the classified vegetation pixels within the Dyke were eelgrass, as visual examination of colour composites did not indicate vegetation coverage, and the spectral signature of pixels within the Dyke differed from vegetated pixels outside the Dyke. This suggests that floating wrack, or something in the water column such as tannins, microalgae, coloured dissolved organic matter (CDOM), or suspended inorganic particular matter, has cause spectral confusion in the satellite image (Hossain et al. 2015).

Segment four, from outside of Jone's Cove to Hunts Point, has predominantly rocky, exposed shores. Similar to the first segment around Port Mouton Island, the classification of vegetation extended to the edge of the study bounds suggesting it is difficult for the imagery to classify deeper vegetation, which is likely seaweed, from deeper water. The landward inlet behind Summerville Beach has contained an eelgrass

bed yet local knowledge is unsure of its distribution post 1990 (Lee 2014). It is possible that the pixels classified within this landward inlet were an eelgrass bed in 2015.

3.4.3 Differences Between the Supervised and Unsupervised Algorithms

The end goal with all remote sensing studies is to be able to quickly classify an image, as autonomously as possible. Traditionally, this includes field work to sample a predetermined set of points, and using this data to classify an image (Horning et al. 2010). However, the collection of enough input points is time consuming, expensive work, which often requires the use of differential high-precision GPS units. Eelgrass and other seagrass species have been successfully mapped using traditional remote sensing approaches at moderate and high spatial resolutions (i.e. Ferguson and Korfmacher 1997; Macleod and Congalton 1998; Lathrop et al. 2006; O'Neill and Costa 2013; Hogrefe et al. 2014; Barrell et al. 2015). This study builds on work by Hogrefe et al. (2014) and Roelfsema et al. (2009) to provide a framework for eelgrass classification with minimal ground truth points for ecologists studying eelgrass distribution, to aid local and regional monitoring programs.

For the two bays that could be classified, accuracy values as well as kappa coefficients were almost identical between the supervised and unsupervised approaches. Furthermore, the percentage of pixels differing between the two classifications ranged from 4.5-14.5%, median ~13.5%; therefore, more than 85% of the image was classified the same by the two algorithms. Based on these results, this study makes two main suggestions for classifying eelgrass presence with minimal ground truth points: (i) the unsupervised classification approach can be used as a first step in image classification where an image is classified using this technique and then based on the results, targeted ground truth points are collected within areas classified as eelgrass versus not classified

as eelgrass, thus reducing the sampling effort required, or (ii) the unsupervised classification approach can be used to classify imagery without ground truth points but should rely on previous mapping projects, local ecological knowledge, and available depth and substrate data to aid in assigning clusters to ground cover types. This second suggestion will only be able to map to the level of vegetated versus non-vegetated pixels, and would be unable to the evaluated using traditional error evaluation methods.

3.4.4 Eelgrass Monitoring Programs in Nova Scotia

Eelgrass is an indicator of ecosystem health (Environment Canada 2002), as well as being an important ecosystem engineer in coastal ecosystems (Jones et al. 1994). As such, the Nova Scotia Department of Natural Resources (NS DNR), Fisheries and Oceans Canada (DFO), as well as local non-governmental organizations are attempting to understand eelgrass bed distribution and density, and quantify any changes in Nova Scotia. In 2009 the eelgrass bed at the head of Port Joli was classified as part of an exploratory analysis to examine the potential use of high-resolution satellite imagery for eelgrass monitoring with a joint project through NS DNR and DFO (Milton et al. 2009). In Port Mouton, the Friends of Port Mouton have been monitoring select eelgrass sites since 2010 using underwater photography and dive quadrats (Friends of Port Mouton 2014), in response to the fallowing of the nearby finfish aquaculture site. Furthermore, in 2015 the Atlantic Eelgrass Monitoring Consortium, partnered with SeagrassNet Monitoring, established a monitoring site in Jone's Cove to understand the present state of the eelgrass bed and monitor for future declines using traditional dive transects and remote sensing (COINAtlantic 2015). Ideally, a Nova Scotia wide habitat monitoring should be established to inform the conservation and management of eelgrass and other

vegetated or non-vegetated coastal habitats (Hanson 2004). Such a large-scale effort likely would have to rely on remote sensing as the primary tool for eelgrass monitoring. If changes are noted in eelgrass bed extent, then this may warrant further field work to examine more specific changes with dive transects or boat based surveys.

Our results from the classifications for both Port Mouton and Port Joli contribute to our current understanding of eelgrass bed extents in these two, well-studied bays. Furthermore, the methods developed with this current study can be used to map eelgrass extent elsewhere in the province, particularly those that are less well studied, to create baseline knowledge. These methods also provide a framework to perform change detection studies in eelgrass beds based on older imagery, as the unsupervised classification requires little input ground truth data. This may be particularly important for helping to determine historical baseline knowledge of eelgrass extent throughout Nova Scotia. It may be possible to examine eelgrass distribution since the early 2000s, corresponding to the launch of medium and high resolution commercial satellites, and at a much lower spatial resolution, back until the early 1970s with Landsat imagery (Hossain et al. 2015).

3.4.5 Limitations and Considerations for Eelgrass SRS Studies

SRS can be used to classify eelgrass presence/absence, percent cover, and density, as well as differentiate between different seagrass and seaweed species (Hossain et al. 2015). The successful classification of any satellite imagery depends on a study's objectives, whether the goal was to map to the level of vegetated versus non-vegetated, or to obtain more detailed measures of eelgrass coverage. A successful classification is also constrained by abiotic limitations including water clarity, which can limit the depth range

eelgrass can be classified within (Hossain et al. 2015). In addition, wave action, as well as cloud cover and fog may also obscure the satellite imagery. This study demonstrated, that while SRS can be a useful tool to map eelgrass distribution, it is not always successful at classifying eelgrass versus seaweed distribution. As such, there are several limitations that should be considered when planning to remotely sense eelgrass distribution with multispectral imagery.

The unsupervised classification is susceptible to the same limitations presently faced when classifying eelgrass distribution using traditional supervised classification methods. First and foremost is the strong absorption of visible and NIR light by water (Hossain et al. 2015). Land-based vegetation classifications heavily rely on vegetation indices which use the ratio of reflected red to NIR light, such as normalized difference vegetation index (NDVI), which is very good at differentiating vegetation from non-vegetation (Myneni et al. 1995). However, NIR light is completely absorbed by water in depths of a few centimetres making vegetation indices impractical to use in a submerged environment (Hossain et al. 2015). Therefore, it is important to acquire imagery as close to low tide as possible to minimize impacts of water absorption across all wavelengths. As SPOT 6/7, and other similar commercial satellites cross over a point on the ground at the same time every day (near noon in southern Nova Scotia), this can limit the use of archived satellite imagery as the imagery not only needs to exist, and be of good quality, it also needs to match the tidal cycle. This can be circumvented by acquiring new tasks on a day known to have a low tide at the time of image acquisition at a specific site. New satellite image tasking has a much higher cost per squared kilometre ($29 USD versus $19 USD for WorldView-2), as well as requiring a larger minimum order area (100km^2

versus 25km^2) therefore costing $475 USD for archived WorldView-2 imagery versus $2900 USD for new tasks (LANDinfo 2016). This cost may be prohibitive for monitoring programs who often operate with very small budgets.

Determining which sensor to use also has a cost factor, which ranges from freely available Landsat data, to thousands of dollars for new acquisition of commercial satellites (i.e. SPOT, WorldView). Eelgrass distribution has been mapped with both Landsat and commercial satellites (Hossain et al. 2015). The newest Landsat 8 has a high spectral resolution covering eleven different bands; however, the smallest spatial scale available is at most 15 m pixels (Department of the Interior U. S. Geological Survey 2016). This broad spatial scale may miss eelgrass, intermixed with seaweed, or at very low density, as was commonly observed throughout Port Mouton and Port Joli (Hossain et al. 2015). SPOT 6/7 data, used in this study, is mid-range in cost, at a very high spatial resolution of 1.5m, but has limited spectral resolution at four bands (Astrium Services 2013). This classification may have improved with products such as WorldView-2, with both a high spatial resolution (0.5m) and high spectral resolution (8 bands), at a slight increase in price from SPOT 6/7 imagery (Digital Globe 2009). However, no suitable, archived WorldView-2 imagery was available for 2015 in the three study areas, at a suitable low tide.

Once an image has been deemed appropriate to use based on the tidal cycle, prior screening of satellite imagery for water clarity and cloud coverage should be performed prior to purchasing. In the case of a change detection study, the date the imagery was collected should also be noted as there are seasonal and inter-annual differences within an eelgrass bed (Wong et al. 2013). Therefore, it is important to acquire imagery from the

same season. Furthermore, once the imagery has been acquired, and pre-processing completed, spectral signatures across the entire image should be examined. The spectral signatures may vary across large areas, and therefore have negative impacts on the classification.

3.5 Conclusion

This chapter used archived high-resolution multispectral satellite imagery to classify eelgrass (*Zostera marina*) distribution in Port Mouton, Port Joli, and Jordan Bay. Each bay was run through a supervised classification with ground truth data to determine eelgrass presence from absence. As ground truth points are time consuming and require extensive field studies, an unsupervised classification was also performed without using ground truth points. While eelgrass presence could only be successfully classified within one bay due to satellite image quality, our methods were appropriate to determine eelgrass distribution, with the two classification approaches having more than 85% classification similarity. Based on these results, the unsupervised classification approach could be used as a first step in image classification, where targeted ground truth points are collected afterwards, or should rely on local ecological knowledge, previous mapping projects, depth, and substrate data to assign clusters to classify the imagery without the use of known ground truth points to map to the level of vegetated versus non-vegetated. These methods can be used on previous or current-years satellite imagery, on a variety of government or commercial optical remote sensing imagery, and can be used to classify imagery to be later used in a change detection study. With the recent declines in eelgrass (Orth et al. 2006; Garbary et al. 2014), tools that help to quantify eelgrass distribution, are becoming increasingly important management tools to monitor changes in eelgrass

beds. Any observed changes in distributions can promote future work, examining why the eelgrass beds are changing, and what impact this may have on the species that depend on them.

Chapter 4 Conclusion

4.1 Use of Remote Sensing and Species Distribution Models

This thesis examined how satellite remote sensing (SRS) and species distribution models (SDM) can be used to estimate or project marine macrophyte distribution. In chapter two, I used correlative SDMs, in conjunction with physiological thresholds, to project how the distribution of fucoids (*Ascophyllum nodosum, Fucus vesiculosus*), Irish moss (*Chondrus crispus*), *Codium fragile,* and kelps (*Laminaria digitata,* and *Saccharina latissima*) may change by 2100 under projected climate warming. I found that distribution shifts are species-specific and depend on the choice of climate model and RCP scenario. Kelp and fucoids are expected to have an overall net loss of latitudinal habitat range due to a northward range shift and latitudinal range contraction. In contrast *C. crispus* and *C. fragile* are projected to experience lattitudinal range expansions due to only small distribution shifts at the southern edge yet large shifts at the northern edge. Furthermore, if emission levels continue to correspond with the RCP 8.5 scenario, south of Newfoundland, the mid-intertidal zone may see a transition from *A. nodosum* to *F. vesiculosus* dominance and the subtidal zone may see a transition from kelp to *C. fragile* dominance. Along each species northern boundary there will be northward shifts as well as increases in abundance.

Climate warming impacts aren't limited to seaweeds; eelgrass (*Zostera marina*) is also expected to experience range shifts, as well as benefit from Arctic warming (Olesen et al. 2015). Thus, marine macrophyte coverage is projected to increase along both rocky and sandy shores within the Arctic, with potential benefits to associated species and the ecosystem functions and services these vegetated habitats provide (Krause-Jensen and Duarte 2014).

In chapter three I compared a supervised and unsupervised classification technique to classify eelgrass distribution with archived high-resolution multispectral satellite imagery in three bays in southwestern Nova Scotia. I found that both the supervised and the unsupervised classification techniques, produced similar classifications (>85% similarity), and at similarly high accuracy values (>90%). Therefore, the unsupervised classification technique could be used to classify satellite imagery with minimal input ground truth points. However, this technique depends on high-quality satellite imagery, and on the biophysical properties of the study area, to successfully map eelgrass presence and absence.

The use of SRS is not limited to eelgrass distribution mapping. Multispectral satellite imagery can be used to quantify the distribution of other marine macrophytes including seaweeds (Taylor et al. 2001; Kutser et al. 2006; Vahtmae and Kutser 2007). Intertidal species such as fucoids and *C. crispus* would be ideal for this type of monitoring as they are minimally obscured by effects from the water column. Subtidal species such as kelps or *C. fragile* would be more difficult to map as they occur in much deeper waters.

4.2 Management Applications

As canopy-forming marine macrophytes provide critical ecosystem services, understanding their past, present and future distributions will provide insight into how these services have changed, or may continue to change in the future. If the seaweed species examined in this thesis shift north as projected by 2100, there may be impacts on the commercial fish and invertebrate species that depend on them. Understanding how fish habitat may be impacted by climate warming, will be useful to inform policy makers

and management agencies in charge of managing commercial stocks. Furthermore, as *A. nodosum* is commercially harvested throughout Maine (Arbuckle et al. 2014) and the Canadian Maritimes (Vandermeulen 2013), knowing the impacts of projected climate warming will help to inform managers when determining harvest allowances.

In addition to the threats facing eelgrass communities presently, continued climate warming will also impact eelgrass throughout Nova Scotia and the NW Atlantic (Orth et al. 2006). This thesis provides a methods framework for quantifying eelgrass distribution, which can be used for long-term monitoring throughout Nova Scotia. This framework is unique as it requires minimal ground truth points, and can use archived satellite imagery, both of which greatly reduce the cost for implementing monitoring programs.

4.3 Future Research

The results of this thesis spur several future research questions. Firstly, the SDMs created are at a very broad range in scale. Therefore, they can only capture broad, latitudinal range shifts in seaweed distributions. Regional species distribution models are better adapted for determining more specific shifts in distributions and identifying potential local refugia from climate warming (Lowen and DiBacco 2017). Cold-water upwelling along the exposed Atlantic Coast may allow *A. nodosum, L. digitata,* and *S. latissima* to persist in Nova Scotia in 2100. Therefore, it would be interesting to see what regional models project for seaweed distribution by 2100 in the Canadian Maritimes. Furthermore, currently no SDMs and, associated projections into future climate exist for eelgrass distribution for the entire NW Atlantic, or at regional scales. As an ecologically significant species (DFO 2009), both a present-day SDM and future projections would be highly valuable to inform eelgrass conservation and management. With these

suggestions, the results from the future projections from this thesis, and the two suggestions above, can also be compared to climate velocities, another tool used to project how species may respond to continued warming (Pinsky et al. 2013). Climate velocities complement SDM as they do not incorporate the biological response, or any occurrence records (Hamann et al. 2015). Lastly, while the methods for the eelgrass remote sensing study were successful at classifying eelgrass distribution in Port Joli, next steps would include using these methods in a change detection study based on past satellite images or images of future years, to determine its effectiveness as a long-term monitoring tool.

Literature Cited

Aberg P (1992) A demographic study of two populations of the seaweed *Ascophyllum nodosum*. Ecology 73:1473–1487. doi: 10.2307/1940691

Adey WH, Hayek LC (2011) Elucidating marine biogeography with macrophytes: quantitative analysis of the North Atlantic supports the thermogeographic model and demonstrates a distinct subarctic region in the Northwestern Atlantic. Northeast Nat 18:1–128. doi: 10.1656/045.018.m801

Arbuckle J, Beal B, Brawley S, Domizi S, Mercer L, Preston D, Seaver G, Sferra N, Thayer P, Ugarte R, Vonderweidt C (2014) Fishery management plan for rockweed (*Ascophyllum nodosum*). Maine Department of Marine Resources: iv + 55pp.

Arrigo KR, van Dijken G, Pabi S (2008) Impact of a shrinking Arctic ice cover on marine primary production. Geophys Res Lett 35:1–6. doi: 10.1029/2008GL035028

Assis J, Serrão EA, Claro B, Perrin C, Pearson GA (2014) Climate-driven range shifts explain the distribution of extant gene pools and predict future loss of unique lineages in a marine brown alga. Mol Ecol 23:2797–2810. doi: 10.1111/mec.12772

Assis J, Araújo MB, Serrão EA (2017) Projected climate changes threaten ancient refugia of kelp forests in the North Atlantic. Glob Chang Biol 1–12. doi: 10.1111/ijlh.12426

Astrium Services (2013) SPOT 6 & SPOT 7 imagery user guide. France

Ball GH, Hall DJ (1965) ISODATA, a novel method of data analysis and pattern classification. Analysis 1–79.

Barnett TP, Pierce DW, Schnur R (2001) Detection of anthropogenic climate change in the world's cceans. Science 292:270–274.

Barrell J, Grant J, Hanson A, Mahoney M (2015) Evaluating the complementarity of acoustic and satellite remote sensing for seagrass landscape mapping. Int J Remote Sens 36:4069–4094. doi: 10.1080/01431161.2015.1076208

Baumann H, Doherty O (2013) Decadal changes in the world's coastal latitudinal temperature gradients. PLoS One 8:e67596. doi: 10.1371/journal.pone.0067596

Bolton JJ, Lüning K (1982) Optimal growth and maximal survival temperatures of Atlantic Laminaria species (Phaeophyta) in culture. Mar Biol 66:89–94. doi: 10.1007/BF00397259

Bopp L, Resplandy L, Orr JC, Doney SC, Dunne JP, Gehlen M, Halloran P, Heinze C, Ilyina T, Séférian R, Tjiputra J, Vichi M (2013) Multiple stressors of ocean ecosystems in the 21st century: Projections with CMIP5 models. Biogeosciences 10:6225–6245. doi: 10.5194/bg-10-6225-2013

Bos AR, Bouma TJ, de Kort GLJ, van Katwijk MM (2007) Ecosystem engineering by annual intertidal seagrass beds: Sediment accretion and modification. Estuar Coast Shelf Sci 74:344–348. doi: 10.1016/j.ecss.2007.04.006

Boscutti F, Marcorin I, Sigura M, Bressan E, Tamberlich F, Vianello A, Casolo V (2015) Distribution modeling of seagrasses in brackish waters of Grado-Marano lagoon (Northern Adriatic Sea). Estuar Coast Shelf Sci 164:183–193. doi: 10.1016/j.ecss.2015.07.035

Brickman D, Wang Z, Detracey B (2016) High resolution future climate ocean model simulations for the Northwest Atlantic Shelf region. Can Tech Rep Hydrogr Ocean Sci 315:xiv + 143 pp.

Carleer AP, Debeir O, Wolff E (2005) Assessment of very high spatial resolution satellite image segmentations. Photogramm Eng Remote Sensing 71:1285–1294. doi: 10.1117/12.511027

Carlton J, Scanlon J (1985) Progression and dispersal of an introduced alga: *Codium fragile* ssp . *tomentosoides* (Chlorophyta) on the Atlantic coast of North America. Bot Mar 28:155–165.

Carman MR, Colarusso PD, Nelson EP, Grunden DW, Wong MC, Mckenzie C, Matheson K, Davidson J, Fox S, Neckles HA, Bayley H, Schott S, Dijkstra JA, Stewart-Clark S, Bullard S (2016) Distribution and diversity of tunicates utilizing eelgrass as substrate in the western North Atlantic between 39° and 47° north latitude (New Jersey to Newfoundland). Manag Biol Invasions 7:51–57. doi: 10.3391/mbi.2016.7.1.07

Casal G, Sánchez-Carnero N, Sánchez-Rodríguez E, Freire J (2011) Remote sensing with SPOT-4 for mapping kelp forests in turbid waters on the south European Atlantic shelf. Estuar Coast Shelf Sci 91:371–378. doi: 10.1016/j.ecss.2010.10.024

Chapman ARO, Lindley JE (1980) Seasonal growth of *Laminaria solidungula* in the Canadian High Arctic in relation to irradiance and dissolved nutrient concentrations. Mar Biol 57:1–5. doi: 10.1007/BF00420961

Chavez PSJ (1996) Image-based atmospheric corrections-revisited and improved. Photogramm. Eng. Remote Sens. 62:1025–1035.

Clark Labs (2015) TerrSet. Worcester, MA: Clark Univeristy.

Cohen J (1960) A coefficient of agreement for nominal sclaes. Educ Psychol Meas XX:37–46.

COINAtlantic (2015) Atlantic eelgrass monitoring consortium. http://dev.coinatlantic.ca/index.php/partnerships/atlantic-eelgrass-monitoring-consortium. Accessed 17 Oct 2017

Department of Fisheries and Aquaculture (2015) Public information: 2015 lease renewal. http://novascotia.ca/fish/aquaculture/public-information/. Accessed 26 Nov 2015

Department of the Interior U. S. Geological Survey (2016) Landsat 8 (L8) Data Users Handbook. Sioux Falls, South Dakota

DFO (2009) Does eelgrass (*Zostera marina*) meet the criteria as an ecologically significant species? Can Sci Advis Secr 2009/018:1–11.

Digital Globe (2009) WorldView-2 product overview. http://www.blackbridge.com/geomatics/about/resources.html. Accessed 1 Nov 2015

Dijkstra JA, Harris LG, Mello K, Litterer A, Wells C, Ware C (2017) Invasive seaweeds transform habitat structure and increase biodiversity of associated species. J Ecol 105:1668–1678. doi: 10.1111/1365-2745.12775

Duarte CM, Cebrián J (1996) The fate of marine autotrophic production. Limnol Oceanogr 41:1758–1766. doi: 10.4319/lo.1996.41.8.1758

Duarte CM, Losada IJ, Hendriks IE, Mazarrasa I, Marbà N (2013a) The role of coastal plant communities for climate change mitigation and adaptation. Nat Clim Chang 3:961–968. doi: 10.1038/nclimate1970

Duarte L, Viejo RM, Martínez B, deCastro M, Gómez-Gesteira M, Gallardo T (2013b) Recent and historical range shifts of two canopy-forming seaweeds in North Spain and the link with trends in sea surface temperature. Acta Oecologica 51:1–10. doi: 10.1016/j.actao.2013.05.002

Dufresne JL, Foujols MA, Denvil S, Caubel A, Marti O, Aumont O, Balkanski Y, Bekki S, Bellenger H, Benshila R, Bony S, Bopp L, Braconnot P, Brockmann P, Cadule P, Cheruy F, Codron F, Cozic A, Cugnet D, de Noblet N, Duvel JP, Ethé C, Fairhead L, Fichefet T, Flavoni S, Friedlingstein P, Grandpeix JY, Guez L, Guilyardi E, Hauglustaine D, Hourdin F, Idelkadi A, Ghattas J, Joussaume S, Kageyama M, Krinner G, Labetoulle S, Lahellec A, Lefebvre MP, Lefevre F, Levy C, Li ZX, Lloyd J, Lott F, Madec G, Mancip M, Marchand M, Masson S, Meurdesoif Y, Mignot J, Musat I, Parouty S, Polcher J, Rio C, Schulz M, Swingedouw D, Szopa S, Talandier C, Terray P, Viovy N, Vuichard N (2013) Climate change projections using the IPSL-CM5 Earth System Model: From CMIP3 to CMIP5. Clim Dyn 40:2123–2165. doi: 10.1007/s00382-012-1636-1

Dunne JP, John JG, Adcroft A, Griffies SM, Hallberg RW, Shevliakova E, Stouffer RJ, SL M, Milly P (2012) GFDL's ESM2 global coupled climate-carbon earth system models. Part I: Physical formulation and baseline simulation characteristics. J Clim 25:6646–6665. doi: http://dx.doi.org/10.1175/JCLI-D-11-00560.1

Elith J, Leathwick JR (2009) Species distribution models: Ecological explanation and prediction across space and time. Annu Rev Ecol Evol Syst 40:677–697. doi: 10.1146/annurev.ecolsys.110308.120159

Elith J, Graham CH, Anderson RP, Dudik M, Ferrier S, Guisan A, Hijmans RJ, Huettmann F, Leathwick JR, Lehmann A, Li J, Lohmann LG, Loiselle B a., Manion G, Moritz C, Nakamura M, Nakazawa Y, Overton JMC, Peterson AT, Phillips SJ, Richardson K, Scachetti-Pereira R, Schapire RE, Soberon J, Williams S, Wisz MS, Zimmermann NE (2006) Novel methods improve prediction of species' distributions from occurrence data. Ecography (Cop) 29:129–151.

Elith J, Kearney M, Phillips S (2010) The art of modelling range-shifting species. Methods Ecol Evol 1:330–342. doi: 10.1111/j.2041-210X.2010.00036.x

Elith J, Phillips SJ, Hastie T, Dudík M, Chee YE, Yates CJ (2011) A statistical explanation of MaxEnt for ecologists. Divers Distrib 17:43–57. doi: 10.1111/j.1472-4642.2010.00725.x

Environment Canada (2002) Methods for mapping and monitoring eelgrass habitat in British Columbia. Environment Canada Internal Report: ii + 38pp.

ESRI (2011) ArcGIS Desktop: Release 10. Redlands, CA: Environmental Systems Research Institute.

Fan Y, van den Dool H (2008) A global monthly land surface air temperature analysis for 1948-present. J Geophys Res 113:D01103. doi: 10.1029/2007JD008470

Fauvel M, Chanussot J, Benediktsson JA (2012) A spatial-spectral kernel-based approach for the classification of remote-sensing images. Pattern Recognit 45:381–392. doi: 10.1016/j.patcog.2011.03.035

Ferguson RL, Korfmacher K (1997) Remote sensing and GIS analysis of seagrass meadows in North Carolina, USA. Aquat Bot 58:241–258. doi: 10.1016/S0304-3770(97)00038-7

Field C, Behrenfeld M, Randerson J, Falkowski P (1998) Primary production of the biosphere: integrating terrestrial and oceanic components. Science 281:237–240. doi: 10.1126/science.281.5374.237

Filbee-Dexter K, Feehan CJ, Scheibling RE (2016) Large-scale degradation of a kelp ecosystem in an ocean warming hotspot. Mar Ecol Prog Ser 543:141–152.

Foody GM (2002) Status of land cover classification accuracy assessment. Remote Sens Environ 80:185–201. doi: 10.1016/S0034-4257(01)00295-4

Franco JN, Tuya F, Bertocci I, Rodríguez L, Martinez B, Sousa-Pinto I, Arenas F (2017) The "golden kelp" *Laminaria ochroleuca* under global change: integrating multiple eco- physiological responses with species distribution models. J Ecol. doi: 10.1111/1365-2745.12810

Franklin J (2009) Mapping species distributions: spatial inference and prediction. Cambridge University Press, New York

Friends of Port Mouton (2014) Eelgrass Monitoring in Port Mouton Bay. Port Mouton: 8pp

Gallon RK, Robuchon M, Leroy B, Le Gall L, Valero M, Feunteun E (2014) Twenty years of observed and predicted changes in subtidal red seaweed assemblages along a biogeographical transition zone: Inferring potential causes from environmental data. J Biogeogr 41:2293–2306. doi: 10.1111/jbi.12380

Gamer M (2012) Various coefficients of interrater reliability and agreement. v 0.84. R Package.

Garbary D, Miller A (2006) Green crabs (*Carcinus maenas*) as the grim reaper: destruction of eelgrass beds in Nova Scotia. J Shellfish Res 25:728.

Garbary DJ, Miller AG, Williams J, Seymour NR (2014) Drastic decline of an extensive eelgrass bed in Nova Scotia due to the activity of the invasive green crab (*Carcinus maenas*). Mar Biol 161:3–15. doi: 10.1007/s00227-013-2323-4

Gosner KL (1978) A field guide to the Atlantic seashore. Houghton Mifflin Company, New York

Hamann A, Roberts DR, Barber QE, Carroll C, Nielsen SE (2015) Velocity of climate change algorithms for guiding conservation and management. Glob Chang Biol 21:997–1004. doi: 10.1111/gcb.12736

Hanisak MD (1979) Growth patterns of *Codium fragile* ssp. *tomentosoides* in response to temperature, irradiance, salinity, and nitrogen source. Mar Biol 50:319–332. doi: 10.1007/BF00387009

Hansen J, Sato M, Ruedy R, Lo K, Lea DW, Medina-Elizade M (2006) Global temperature change. Proc Natl Acad Sci U S A 103:14288–14293. doi: 10.1073/pnas.0606291103

Hanson A, Swanson L, Ewing D, Grabas G, Meyer S, Ross L, Watmough M, Kirkby J (2008) Wetland ecological functions assessment: An overview of approaches. Canadian Wildlife Service Technical Report Series No. 497. Atlantic Region. 59 pp.

Hanson AR (2004) Status and conservation of eelgrass (*Zostera marina*) in eastern Canada. Technical Report Series No. 412. Canadian Wildlife Service, Atlantic Region. viii. + 40 pp.

Harley CDG, Randall Hughes A, Hultgren KM, Miner BG, Sorte CJB, Thornber CS, Rodriguez LF, Tomanek L, Williams SL (2006) The impacts of climate change in coastal marine systems. Ecol Lett 9:228–241. doi: 10.1111/j.1461-0248.2005.00871.x

Harley CDG, Anderson KM, Demes KW, Jorve JP, Kordas RL, Coyle T a., Graham MH (2012) Effects of climate change on global seaweed communities. J Phycol 48:1064–1078. doi: 10.1111/j.1529-8817.2012.01224.x

Hauxwell J, Cebrian J, Furlong C, Valiela I (2001) Macroalgal canopies contribute to Eelgrass (*Zostera marina*) decline in temperate estuarine ecosystems. Ecology 82:1007–1022.

Hauxwell J, Cebrián J, Valiela I (2003) Eelgrass *Zostera marina* loss in temperate estuaries: Relationship to land-derived nitrogen loads and effect of light limitation imposed by algae. Mar Ecol Prog Ser 247:59–73. doi: 10.3354/meps247059

Heck KL, Hays G, Orth RJ (2003) Critical evaluation of the nursery role hypothesis for seagrass meadows. Mar Ecol Prog Ser 253:123–136. doi: 10.3354/meps253123

Hedley JD, Harborne a. R, Mumby PJ (2005) Technical note: Simple and robust removal of sun glint for mapping shallow-water benthos. Int J Remote Sens 26:2107–2112. doi: 10.1080/01431160500034086

Hogrefe KR, Ward DH, Donnelly TF, Dau N (2014) Establishing a baseline for regional scale monitoring of eelgrass (*Zostera marina*) habitat on the lower Alaska Peninsula. Remote Sens 6:12447–12477. doi: 10.3390/rs61212447

Høgslund S, Sejr MK, Wiktor J, Blicher ME, Wegeberg S (2014) Intertidal community composition along rocky shores in Southwest Greenland: a quantitative approach. Polar Biol 37:1549–1561. doi: 10.1007/s00300-014-1541-7

Holmer M, Argyrou M, Dalsgaard T, Danovaro R, Diaz-Almela E, Duarte CM, Frederiksen M, Grau A, Karakassis I, Marbà N, Mirto S, Pérez M, Pusceddu A, Tsapakis M (2008) Effects of fish farm waste on *Posidonia oceanica* meadows: synthesis and provision of monitoring and management tools. Mar Pollut Bull 56:1618–1629. doi: 10.1016/j.marpolbul.2008.05.020

Horning N, Robinson JA, Sterling EJ, Turner W, Spector S (2010) Remote sensing for ecology and conservation: A handbook of techniques. Oxford University Press, New York

Hossain MS, Bujang JS, Zakaria MH, Hashim M (2015) The application of remote sensing to seagrass ecosystems: an overview and future research prospects. Int J Remote Sens 36:61–114. doi: 10.1080/01431161.2014.990649

Hutchinson G (1957) Concluding remarks. In: Cold Spring Harbor smposia on quantitative biology. Cold Spring Harbor Labratory Press,

IPCC (2013) Climate change 2013: the physical science basis. Contribution of working group I to the fifth assessment report of the Intergovernmental Panel on Climate Change. Cambridge University Press, Cambridge and New York

Jones CG, Lawton JH, Shachak M (1994) Organisms as ecosystem engineers. Oikos 69:373–386. doi: 10.2307/3545850

Jueterbock A, Tyberghein L, Verbruggen H, Coyer JA, Olsen JL, Hoarau G (2013) Climate change impact on seaweed meadow distribution in the North Atlantic rocky intertidal. Ecol Evol 3:1356–1373.

Kalvas A, Kautsky L (1998) Morphological variation in *Fucus vesiculosus* populations along temperature and salinity gradients in Iceland. J Mar Biol Assoc United Kingdom 78:985–1001. doi: 10.1017/S0025315400044921

Kay LM, Schmidt AL, Wilson KL, Lotze HK (2016) Interactive effects of increasing temperature and nutrient loading on the habitat-forming rockweed *Ascophyllum nodosum*. Aquat Bot 133:70–78. doi: 10.1016/j.aquabot.2016.06.002

Kearney M, Porter W (2009) Mechanistic niche modelling: combining physiological and spatial data to predict species' ranges. Ecol Lett 12:334–350. doi: 10.1111/j.1461-0248.2008.01277.x

Kelly M, Di Tommaso S (2015) Mapping forests with Lidar provides flexible, accurate data with many uses. Calif Agric 69:14–20. doi: 10.3733/ca.v069n01p14

Keser M, Swenarton JT, Foertch JF (2005) Effects of thermal input and climate change on growth of *Ascophyllum nodosum* (Fucales, Phaeophyceae) in eastern Long Island Sound (USA). J Sea Res 54:211–220. doi: 10.1016/j.seares.2005.05.001

Kingsbury M, Prince JS, Kingsbury JM (1973) The ecology of *Chondrus crispus* at Plymouth, Massachusetts. III. Effect of elevated temperature on growth and survival. Biol Bull 145:580–588.

Klemas V (2011) Remote sensing techniques for studying coastal ecosystems: An overview. J Coast Res 27:2–17. doi: 10.2112/JCOASTRES-D-10-00103.1

Kohavi R (1995) A study of cross-validation and bootstrap for accuracy estimation and model selection. Int Jt Conf Artif Intell 14:1137–1143. doi: 10.1067/mod.2000.109031

Kortsch S, Primicerio R, Beuchel F, Renaud PE, Rodrigues J, Lonne OJ, Gulliksen B (2012) Climate-driven regime shifts in Arctic marine benthos. Proc Natl Acad Sci U S A 109:14052–14057. doi: 10.1073/pnas.1207509109

Kraemer G, Yarish C, Kim JK, Zhang H, Lin S (2017) Life history interactions between the red algae *Chondrus crispus* (Gigartinales) and *Grateloupia turuturu* (Halymeniales) in a changing global environment. Phycologia 56:176–185.

Krause-Jensen D, Duarte CM (2014) Expansion of vegetated coastal ecosystems in the future Arctic. Front Mar Sci 1:1–10. doi: 10.3389/fmars.2014.00077

Krause-Jensen D, Marbà N, Olesen B, Sejr MK, Christensen PB, Rodrigues J, Renaud PE, Balsby TJS, Rysgaard S (2012) Seasonal sea ice cover as principal driver of spatial and temporal variation in depth extension and annual production of kelp in Greenland. Glob Chang Biol 18:2981–2994. doi: 10.1111/j.1365-2486.2012.02765.x

Krumhansl KA, Scheibling RE (2012) Production and fate of kelp detritus. Mar Ecol Prog Ser 467:281–302. doi: 10.3354/meps09940

Krumhansl KA, Okamoto DK, Rassweiler A, Novak M, Bolton JJ, Cavanaugh KC, Connell SD, Johnson CR, Konar B, Ling SD, Micheli F, Norderhaug KM, Pérez-Matus A, Sousa-Pinto I, Reed DC, Salomon AK, Shears NT, Wernberg T, Anderson RJ, Barrett NS, Buschmann AH, Carr MH, Caselle JE, Derrien-Courtel S, Edgar GJ, Edwards M, Estes JA, Goodwin C, Kenner MC, Kushner DJ, Moy FE, Nunn J, Steneck RS, Vásquez J, Watson J, Witman JD, Byrnes JEK, Conceptualized Research JEKB (2016) Global patterns of kelp forest change over the past half-century. PNAS 113:13785–13790. doi: 10.1073/pnas.1606102113

Küpper FC, Peters AF, Shewring DM, Sayer MDJ, Mystikou A, Brown H, Azzopardi E, Dargent O, Strittmatter M, Brennan D, Asensi AO, van West P, Wilce RT (2016) Arctic marine phytobenthos of northern Baffin Island. J Phycol 52:532–549. doi: 10.1111/jpy.12417

Kutser T, Vahtmäe E, Martin G (2006) Assessing suitability of multispectral satellites for mapping benthic macroalgal cover in turbid coastal waters by means of model simulations. Estuar Coast Shelf Sci 67:521–529. doi: 10.1016/j.ecss.2005.12.004

LANDinfo (2016) Buying satellite imagery: pricing information for high resolution satellite imagery. http://www.landinfo.com/satellite-imagery-pricing.html. Accessed 11 Nov 2017

Lathrop RG, Montesano P, Haag S (2006) A multi-scale segmentation approach to mapping seagrass habitats using airborne digital camera imagery. Photogramm Eng Remote Sens 72:665–675. doi: 10.14358/PERS.72.6.665

Lee J-A, Brinkhuis BH (1986) Reproductive phenology of *Laminaria Saccharina* (L.) Lamour. (Phaeophyta) at the southern limit of its distribution in the Nothwestern Atlantic Ocean. J Phycol 22:276–285. doi: 10.1111/j.1529-8817.1986.tb00024.x

Lee RKS (1980) A catalogue of the marine algae of the Canadian Arctic. National Museum of Natural Sciences, Ottawa Canada

Lee SK, Park W, Van Sebille E, Baringer MO, Wang C, Enfield DB, Yeager SG, Kirtman BP (2011) What caused the significant increase in Atlantic Ocean heat content since the mid-20th century? Geophys Res Lett 38:L17607. doi: 10.1029/2011GL048856

Lee SS (2014) Combining local ecological knowledge and conventional science to assess the dynamics of eelgrass (Zostera marina) in relation to finfish aquaculture operation in Port Mouton Bay, Nova Scotia. Honour's Thesis. Dalhousie University

Lima FP, Ribeiro P a., Queiroz N, Hawkins SJ, Santos AM (2007) Do distributional shifts of northern and southern species of algae match the warming pattern? Glob Chang Biol 13:2592–2604. doi: 10.1111/j.1365-2486.2007.01451.x

Liu C, Newell G, White M (2016) On the selection of thresholds for predicting species occurrence with presence-only data. Ecol Evol 6:337–348. doi: 10.1002/ece3.1878

Loucks RH, Smith RE, Fisher C V., Brian Fisher E (2012) Copper in the sediment and sea surface microlayer near a fallowed, open-net fish farm. Mar Pollut Bull 64:1970–1973. doi: 10.1016/j.marpolbul.2012.05.025

Lowen J, McKindsey C, Therriault T, DiBacco C (2016) Effects of spatial resolution on predicting the distribution of aquatic invasive species in nearshore marine environments. Mar Ecol Prog Ser 556:17–30. doi: 10.3354/meps11765

Lowen JB, DiBacco C (2017) Distributional changes in a guild of non-indigenous tunicates in the NW Atlantic under high resolution climate projections. Mar Ecol Prog Ser 570:173–186.

Lüning K (1990) Seaweeds their environment, biogeography, and ecophysiology. John Wiley & Sons Inc, New York

Lüning K, Guiry MD, Masuda M (1986) Upper temperature tolerance of North Atlantic and North Pacific geographical isolates of Chondrus species (Rhodophyta). Helgoländer Meeresuntersuchungen 41:297–306. doi: 10.1007/BF02366194

Macleod RD, Congalton RG (1998) Quantitative comparison of change-detection algorithms for monitoring eelgrass from remotely sensed data. Photogramm Eng Remote Sensing 64:207–216.

Marbà N, Krause-Jensen D, Olesen B, Christensen PB, Merzouk A, Rodrigues J, Wegeberg S, Wilce RT (2017) Climate change stimulates the growth of the intertidal macroalgae *Ascophyllum nodosum* near the northern distribution limit. Ambio 46:119–131. doi: 10.1007/s13280-016-0873-7

Marcelino VR, Verbruggen H (2015) Ecological niche models of invasive seaweeds. J Phycol 51:606–620. doi: 10.1111/jpy.12322

Martínez B, Arenas F, Trilla A, Viejo RM, Carreño F (2014) Combining physiological threshold knowledge to species distribution models is key to improving forecasts of the future niche for macroalgae. Glob Chang Biol Biol 21:1422–1433. doi: 10.1111/gcb.12655

Matheson K, Mckenzie CH, Sargent P, Hurley M, Wells T (2014) Northward expansion of the invasive green algae *Codium fragile* spp. *fragile* (Suringar) Hariot, 1889 into coastal waters of Newfoundland, Canada. BioInvasions Rec 3:151–158.

Mathieson AC, Dawes CJ, Pederson J, Gladych RA, Carlton JT (2008) The Asian red seaweed *Grateloupia turuturu* (Rhodophyta) invades the Gulf of Maine. Biol Invasions 10:985–988. doi: 10.1007/s10530-007-9176-z

Mattila J, Chaplin G, Eilers MR, Heck KL, O'Neal JP, Valentine JF (1999) Spatial and diurnal distribution of invertebrate and fish fauna of a *Zostera marina* bed and nearby unvegetated sediments in Damariscotta River, Maine (USA). J Sea Res 41:321–332. doi: 10.1016/S1385-1101(99)00006-4

Merow C, Smith MJ, Silander JA (2013) A practical guide to MaxEnt for modeling species' distributions: What it does, and why inputs and settings matter. Ecography (Cop) 36:1058–1069. doi: 10.1111/j.1600-0587.2013.07872.x

Merzouk A, Johnson LE (2011) Kelp distribution in the Northwest Atlantic Ocean under a changing climate. J Exp Mar Bio Ecol 400:90–98. doi: 10.1016/j.jembe.2011.02.020

Milton GR, Parsons FMG, McIntyre LBJHC (2009) Interim report of eelgrass classification project. Nova Scotia Department of Natural Resources: 32pp.

Moss RH, Edmonds JA, Hibbard KA, Manning MR, Rose SK, van Vuuren DP, Carter TR, Emori S, Kainuma M, Kram T, Meehl G a, Mitchell JFB, Nakicenovic N, Riahi K, Smith SJ, Stouffer RJ, Thomson AM, Weyant JP, Wilbanks TJ (2010) The next generation of scenarios for climate change research and assessment. Nature 463:747–756. doi: 10.1038/nature08823

Müller R, Laepple T, Bartsch I, Wiencke C (2009) Impact of oceanic warming on the distribution of seaweeds in polar and cold-temperate waters. Bot Mar 52:617–638. doi: 10.1515/BOT.2009.080

Myneni RB, Hall FG, Sellers PJ, Marshak AL (1995) The interpretation of spectral vegetation indexes. IEEE Trans Geosci Remote Sens 33:481–486.

Naimi B, Araújo MB (2016) SDM: A reproducible and extensible R platform for species distribution modelling. Ecography (Cop) 39:368–375. doi: 10.1111/ecog.01881

Nelson W (2009) Seagrasses and protective criteria: A review and assessment of research status. Office of Research and Development, National Health and Environmental Effects Research Laboratory, EPA/600/R-09/050.

O'Neill JD, Costa M (2013) Mapping eelgrass (*Zostera marina*) in the Gulf Islands National Park Reserve of Canada using high spatial resolution satellite and airborne imagery. Remote Sens Environ 133:152–167. doi: 10.1016/j.rse.2013.02.010

Olesen B, Krause-Jensen D, Marbà N, Christensen PB (2015) Eelgrass *Zostera marina* in subarctic Greenland: Dense meadows with slow biomass turnover in cold waters. Mar Ecol Prog Ser 518:107–121. doi: 10.3354/meps11087

Olsen JL, Zechman FW, Hoarau G, Coyer JA, Stam WT, Valero M, Åberg P (2010) The phylogeographic architecture of the fucoid seaweed *Ascophyllum nodosum*: An intertidal "marine tree" and survivor of more than one glacial-interglacial cycle. J Biogeogr 37:842–856. doi: 10.1111/j.1365-2699.2009.02262.x

Orth RJ, Carruthers TJB, Denntson WC, Duarte JW, Fourqurean KL, Heck J, Randall Hughes A (2006) A global crisis for seagrass ecosystems. Bioscience 56:987–997.

Pearson RG, Dawson TP (2003) Predicting the impacts of climate change on the distribution of speces: are bioclimate envelope models useful? Glob Ecol Biogeogr 12:361–371.

Pershing AJ, Alexander MA, Hernandez CM, Kerr LA, Le Bris A, Mills KE, Nye JA, Record NR, Scannell HA, Scott JD, Sherwood GD, Thomas AC (2015) Slow adaptation in the face of rapid warming leads to collapse of the Gulf of Maine cod fishery. Science 350:809–812. doi: 10.1126/science.aac9819

Pettorelli N, Laurance WF, O'Brien TG, Wegmann M, Nagendra H, Turner W (2014) Satellite remote sensing for applied ecologists: opportunities and challenges. J Appl Ecol 51:839–848. doi: 10.1111/1365-2664.12261

Phillips SJ, Dudík M, Schapire RE (2004) A maximum entropy approach to species distribution modeling. Proc Twenty-First Intenational Conf Mach Learn 21:655–662. doi: 10.1145/1015330.1015412

Phillips SJ, Anderson RP, Schapire RE (2006) Maximum entropy modeling of species geographic distributions. Ecol Modell 190:231–259. doi: 10.1016/j.ecolmodel.2005.03.026

Piñeiro-Corbeira C, Barreiro R, Cremades J (2016) Decadal changes in the distribution of common intertidal seaweeds in Galicia (NW Iberia). Mar Environ Res 113:106–115. doi: 10.1016/j.marenvres.2015.11.012

Pinsky ML, Worm B, Fogarty MJ, Sarmiento JL, Levin SA (2013) Marine taxa track local climate velocities. Science 341:1239–1242.

Poloczanska ES, Brown CJ, Sydeman WJ, Kiessling W, Schoeman DS, Moore PJ, Brander K, Bruno JF, Buckley LB, Burrows MT, Duarte CM, Halpern BS, Holding J, Kappel C V, O/'Connor MI, Pandolfi JM, Parmesan C, Schwing F, Thompson SA, Richardson AJ (2013) Global imprint of climate change on marine life. Nat Clim Chang 3:919–925. doi: 10.1038/nclimate1958

Provan J, Booth D, Todd NP, Beatty GE, Maggs CA (2008) Tracking biological invasions in space and time: Elucidating the invasive history of the green alga *Codium fragile* using old DNA. Divers Distrib 14:343–354. doi: 10.1111/j.1472-4642.2007.00420.x

Raybaud V, Beaugrand G, Goberville E, Delebecq G, Destombe C, Valero M, Davoult D, Morin P, Gevaert F (2013) Decline in kelp in West Europe and climate. PLoS One 8:e66044. doi: 10.1371/journal.pone.0066044

Redmond S (2013) Effects of increasing temperature and ocean acidification on the microstages of two populations of *Saccharina latissima* in the Northwest Atlantic. University of Connecticut

Reed DC, Laur DR, Ebeling AW (1988) Variation in algal dispersal and recruitment: The importance of episodic events. Ecol Monogr 58:321–335.

Reynolds RW, Smith TM, Liu C, Chelton DB, Casey KS, Schlax MG (2007) Daily high-resolution-blended analyses for sea surface temperature. J Clim 20:5473–5496. doi: 10.1175/2007JCLI1824.1

Richards JA (1986) Remote sensing digital image analysis. Springer-Verlag, Berlin

Roelfsema CM, Phinn SR, Udy N, Maxwell P (2009) An integrated field and remote sensing approach for mapping seagrass cover, Moretón bay, Australia. J Spat Sci 54:45–62. doi: 10.1080/14498596.2009.9635166

Rose RA, Byler D, Eastman JR, Fleishman E, Geller G, Goetz S, Guild L, Hamilton H, Hansen M, Headley R, Hewson J, Horning N, Kaplin B a, Laporte N, Leidner A, Leimgruber P, Morisette J, Musinsky J, Pintea L, Prados A, Radeloff VC, Rowen M, Saatchi S, Schill S, Tabor K, Turner W, Vodacek A, Vogelmann J, Wegmann M, Wilkie D, Wilson C (2015) Ten ways remote sensing can contribute to conservation. Conserv Biol 29:350–359. doi: 10.1111/cobi.12397

Saba VS, Griffies SM, Anderson WG, Winton M, Alexander MA, Delworth TL, Hare JA, Harrison MJ, Rosati A, Vecchi GA (2015) Enhanced warming of the Northwest Atlantic Ocean under climate change. J Geophys Res Ocean 121:118–132. doi: 10.1002/2015JC011346.Received

Sanford T, Frumhoff PC, Luers A, Gulledge J (2014) The climate policy narrative for a dangerously warming world. Nat Clim Chang 4:164–166. doi: 10.1038/nclimate2148

Scheibling RE, Gagnon P (2006) Competitive interactions between the invasive green alga *Codium fragile* ssp . *tomentosoides* and native canopy-forming seaweeds in Nova Scotia (Canada). Mar Ecol Prog Ser 325:1–14.

Schmidt AL, Scheibling RE (2006) A comparison of epifauna and epiphytes on native kelps (Laminaria species) and an invasive alga (*Codium fragile ssp. tomentosoides*) in Nova Scotia, Canada. Bot Mar 49:315–330. doi: 10.1515/BOT.2006.039

Schmidt AL, Scheibling RE (2007) Effects of native and invasive macroalgal canopies on composition and abundance of mobile benthic macrofauna and turf-forming algae. J Exp Mar Bio Ecol 341:110–130. doi: 10.1016/j.jembe.2006.10.003

Schmidt AL, Coll M, Romanuk TN, Lotze HK (2011) Ecosystem structure and services in eelgrass *Zostera marina* and rockweed *Ascophyllum nodosum* habitats. Mar Ecol Prog Ser 437:51–68. doi: 10.3354/meps09276

Schmidt AL, Wysmyk JKC, Craig SE, Lotze HK (2012) Regional-scale effects of eutrophication on ecosystem structure and services of seagrass beds. Limnol Oceanogr 57:1389–1402. doi: 10.4319/lo.2012.57.5.1389

Schmidt AL, Coll M, Lotze HK (2017) Regional-scale differences in eutrophication effects on eelgrass-associated (Zostera marina) macrofauna. Estuaries and Coasts 40:1096–1112. doi: 10.1007/s12237-016-0204-z

Schneider CW, Searles RB (1991) Seaweeds of the southeastern United States. Cape Hatteras to Cape Canaveral. Duke University Press, London

Schneider FI, Mann KH (1991) Rapid recovery of fauna following simulated ice rafting in a Nova Scotian seagrass bed. Mar Ecol Prog Ser 78:57–70. doi: 10.3354/meps078057

Schumacher M, Greenlaw ME, King E, McCurdy Q, Smith K, Doon M, Page F, Kostylev V (In. Press) A knowledge-based approach for the determination of surficial substrate using surficial geology and geomorphology in the coastal western Maritimes Region. DFO Can Sci Advis Sec Res Doc.

Seeley RH, Schlesinger WH (2012) Sustainable seaweed cutting? The rockweed (*Ascophyllum nodosum*) industry of Maine and the Maritime Provinces. Ann N Y Acad Sci 1249:84–103. doi: 10.1111/j.1749-6632.2012.06443.x

Simonson E, Scheibling R, Metaxas A (2015) Kelp in hot water: I. Warming seawater temperature induces weakening and loss of kelp tissue. Mar Ecol Prog Ser 537:89–104. doi: 10.3354/meps11438

Skinner MA, Courtenay SC, McKindsey CW (2013) Reductions in distribution, photosynthesis, and productivity of eelgrass *Zostera marina* associated with oyster *Crassostrea virginica* aquaculture. Mar Ecol Prog Ser 486:105–119. doi: 10.3354/meps10345

Smith S V (1981) Marine macrophytes as a global carbon sink. Science 211:838–840. doi: 10.1126/science.211.4484.838

Steneck RS, Graham MH, Bourque BJ, Corbett D, Erlandson JM, Estes J a., Tegner MJ (2002) Kelp forest ecosystems: biodiversity, stability, resilience and future. Environ Conserv 29:436–459. doi: 10.1017/S0376892902000322

Stock CA, Alexander MA, Bond NA, Brander KM, Cheung WWL, Curchitser EN, Delworth TL, Dunne JP, Griffies SM, Haltuch MA, Hare JA, Hollowed AB, Lehodey P, Levin SA, Link JS, Rose KA, Rykaczewski RR, Sarmiento JL, Stouffer RJ, Schwing FB, Vecchi GA, Werner FE (2011) On the use of IPCC-class models to assess the impact of climate on Living Marine Resources. Prog Oceanogr 88:1–27. doi: 10.1016/j.pocean.2010.09.001

Story M, Congalton RG (1986) Accuracy assessment: a user's perspective. Photogramm Eng Remote Sens 52:397–399. doi: 10.1111/j.1530-9290.2010.00257.x

Sunday JM, Bates AE, Dulvy NK (2012) Thermal tolerance and the global redistribution of animals. Nat Clim Chang 2:686–690. doi: 10.1038/nclimate1539

Takao S, Kumagai NH, Yamano H, Fujii M, Yamanaka Y (2015) Projecting the impacts of rising seawater temperatures on the distribution of seaweeds around Japan under multiple climate change scenarios. Ecol Evol 5:213–223. doi: 10.1002/ece3.1358

Tanaka K, Taino S, Haraguchi H, Prendergast G, Hiraoka M (2012) Warming off southwestern Japan linked to distributional shifts of subtidal canopy-forming seaweeds. Ecol Evol 2:2854–2865. doi: 10.1002/ece3.391

Taylor KE, Stouffer RJ, Meehl GA (2012) An overview of CMIP5 and the experiment design. Bull Am Meteorol Soc 93:485–498. doi: 10.1175/BAMS-D-11-00094.1

Taylor P, Simms ÉL, Dubois JM (2001) Satellite remote sensing of submerged kelp beds on the Atlantic coast of Canada. Int J Remote Sens 22:2083–2094.

Taylor W. (1957) Marine algae of the northeastern coast of North America, 2nd edn. The University of Michigan Press, Ann Arbor

Team RC (2014) R: A language and environment for statistical computing. R Foundation for Statistical Computing, Vienna, Austria. http://www.r-project.org/.

Thomas MLH (1994) Littoral communities and zonation on rocky shores in the Bay of Fundy, Canada: An area of high tidal range. Biol J Linn Soc 51:149–168.

Thomsen HA, Brandt A (1999) The 1998 Danish-German excursion to Disko Island, West Greenland. Berichte zur Polarforsch 330:1–10.

Trowbridge CD, Todd CD (1999) The familiar is exotic: I. *Codium fragile* ssp. *atlanticum* on Scottish rocky intertidal shores. Bot J Scotl 51:161–179. doi: 10.1080/03746609908684932

Ugarte RA, Craigie JS, T. CA (2010) Fucoid flora of the rocky intertidal of the Canadian Maritimes: Implications for the future with rapid climate change. In: Seckbach J, Einav R, Israel A (eds) Seaweeds and their Role in Globally Changing Environments. Springer Netherlands, Dordrecht, Netherland,

Uhl F, Bartsch I, Oppelt N (2016) Submerged kelp detection with hyperspectral data. Remote Sens 8:487. doi: 10.3390/rs8060487

Vadas RL, Wright WA, Miller SL (1990) Recruitment of *Ascophyllum nodosum*: wave action as a source of mortality. Mar Ecol Prog Ser 61:263–272. doi: 10.3354/meps061263

Vahtmae E, Kutser T (2007) Mapping bottom type and water depth in shallow coastal waters with satellite remote sensing. J Coast Res SI 50:185–189.

Valle M, Chust G, del Campo A, Wisz MS, Olsen SM, Garmendia JM, Borja Á (2014) Projecting future distribution of the seagrass *Zostera noltii* under global warming and sea level rise. Biol Conserv 170:74–85. doi: 10.1016/j.biocon.2013.12.017

van den Hoek C (1975) Phytogeographic provinces along the coasts of the northern Atlantic Ocean. Phycologia 14:317–330.

Vandermeulen H (2013) Information to support assessment of stock status of commercially harvested species of marine plants in Nova Scotia: Irish moss, rockweed and kelp. DFO Can Sci Advis Sec Res Doc 2013/042.:vi +50.

Vandermeulen H (2014) Nearshore habitat mapping in Atlantic Canada: early results with high frequency side-scan sonar, drop and towed cameras. Can Tech Rep Fish Aquat Sci 3092:vi + 16 p.

Vandermeulen H (2017) A drop camera survey of Port Joli, Nova Scotia. Can Tech Rep Fish Aquat Sci 3215:viii + 59 p.

Wassmann P, Duarte CM, Agustí S, Sejr MK (2011) Footprints of climate change in the Arctic marine ecosystem. Glob Chang Biol 17:1235–1249. doi: 10.1111/j.1365-2486.2010.02311.x

Watanabe S, Scheibling RE, Metaxas A (2010) Contrasting patterns of spread in interacting invasive species: *Membranipora membranacea* and *Codium fragile* off Nova Scotia. Biol Invasions 12:2329–2342. doi: 10.1007/s10530-009-9647-5

Waycott M, Duarte CM, Carruthers TJB, Orth RJ, Dennison WC, Olyarnik S, Calladine A, Fourqurean JW, Heck KL, Hughes Ar, Kendrick GA, Kenworthy Wj, Short FT, Williams SL (2009) Accelerating loss of seagrasses across the globe threatens coastal ecosystems. Proc Natl Acad Sci USA 106:12377–12381. doi: 10.1073/pnas.0905620106

Webster T, McGuigan K, Crowell N, Collins K, MacDonald C (2016) Optimization of data collection and refinement of post-processing techniques for Maritime Canada's first shallow water topographic-bathymetric Lidar survey. J Coast Res 76:31–43. doi: 10.2112/SI76-004

Wernberg T, Russell BD, Thomsen MS, Gurgel CFD, Bradshaw CJA, Poloczanska ES, Connell SD (2011) Seaweed communities in retreat from ocean warming. Curr Biol 21:1828–1832. doi: 10.1016/j.cub.2011.09.028

Wilce RT (1959) The marine algae of the Labrador Peninsula and Northwest Newfoundland (Ecology and Distribution). National Musuem of Canada, Ottawa

Wilce RT, Dunton KH (2014) The Boulder Patch (North Alaska, Beaufort Sea) and its benthic algal flora. Arctic 67:43–56. doi: 10.14430/arctic4360

Wilson KL, Kay LM, Schmidt AL, Lotze HK (2015) Effects of increasing water temperatures on survival and growth of ecologically and economically important seaweeds in Atlantic Canada: implications for climate change. Mar Biol 162:2431–2444. doi: 10.1007/s00227-015-2769-7

Wong MC, Bravo MA, Dowd M (2013) Ecological dynamics of *Zostera marina* (eelgrass) in three adjacent bays in Atlantic Canada. Bot Mar 56:413–424. doi: 10.1515/bot-2013-0068

Worm B, Lotze HK (2006) Effects of eutrophication, grazing, and algal blooms on rocky shores. Limnol Oceanogr 51:569–579. doi: 10.4319/lo.2006.51.1_part_2.0569

Yackulic CB, Chandler R, Zipkin EF, Royle JA, Nichols JD, Campbell Grant EH, Veran S (2013) Presence-only modelling using MAXENT: When can we trust the inferences? Methods Ecol Evol 4:236–243. doi: 10.1111/2041-210x.12004

Yesson C, Bush LE, Davies AJ, Maggs C a, Brodie J (2015) Large brown seaweeds of the British Isles: Evidence of changes in abundance over four decades. Estuar Coast Shelf Sci 155:167–175. doi: 10.1016/j.ecss.2015.01.008

Yost AC, Petersen SL, Gregg M, Miller R (2008) Predictive modeling and mapping sage grouse (*Centrocercus urophasianus*) nesting habitat using Maximum Entropy and a long-term dataset from Southern Oregon. Ecol Inform 3:375–386. doi: 10.1016/j.ecoinf.2008.08.004

Zweng MM, Reagan JR, Antonov JI, Locarnini RA, Mishonov AV, Boyer TP, Garcia HE, Baranova OK, Johnson DR, Seidov D, Bidlle MM (2013) World Ocean Atlas 2013 Volume 2: Salinity. S. Levitus, Ed.; A. Mishonov, Technical Ed.; NOAA Atlas NESDIS 74, 39 pp.

Appendix A: Occurrence Records

As well as the published records recorded below I would like to acknowledge Drs. Heike Lotze, Gary Saunders, and Marième Bouchard Marmen for providing unpublished occurrence records that were used in this study.

Ascophyllum nodosum

Archambault P, Bourget E (1996) Scales of coastal heterogeneity and benthic intertidal species richness, diversity and abundance. Mar Ecol Prog Ser 136: 111–121.

Aquatic Biodiversity Monitoring Network (n.d.) Egg wrack, *Ascophyllum nodosum* (Retrieved on: October 20, 2015). Retrieved from: http://www.rsba.ca/recherche_espece/fiche_espece.php?recordID=323&lan=en

Bates CR, Saunders GW, Chopin T (2009) Historical versus contemporary measures of seaweed biodiversity in the Bay of Fundy. Botany 87: 1066-1076.

E. C. Smith Herbarium (2016) Fucaceae *Ascophyllum nodosum* Scorpiodes (Retrieved on June, 9, 2016). Retrieved from: http://procyon.acadiau.ca/ecsmith/cgiin/results.cgi?acad,Fucaceae,Ascophyllum,nodosum,,species,

Garbary DJ, Brackenbury A, McLean AM, Morrison D (2006) Structure and development of air bladders in *Fucus* and *Ascophyllum* (Fucales, Phaeophyceae). Phycologia 45: 557–566.

http://data.gbif.org (2015), *Ascophyllum nodosum* and Northwest Atlantic, 292 records, accessed on 17 June 2015: 7:41:00 hrs, user doi:10.15468/dl.i6ayrg , contributed by 11 datasets. publishers identifiers: 10.15468/5uprth (49 records); 10.5886/ujwtvvs2 (8 records); 10.15468/bxmxx0 (68 records); 10.15468/w35jmd (38 records); 10.15468/8oxxmx (25 records); 10.15468/zc4csq (90 records); 10.15468/s6ctus (1 record); 10.15468/ab3s5x (2 records); 10.15468/pal1lb (1 record); 10.15468/dipjcr (8 records); 10.15468/nztqk6 (1 record)

Høgslund S, Sejr MK, Wiktor J, Blicher Mem Wegeberg S (2014) Intertidal community composition along rocky shores in South-west Greenland: a quantitative approach. Polar Biol 37: 1549–1561.

Hooper RG, Whittick A (1984) The benthic marine algae of the Kaipokok Bay, Makkovik Bay, and Big River Bay region of the central Labrador coast. Natur Can 111: 131–138.

Kim K, Seasonal variation of seaweed components and novel biological function of fucoidon extracted from brown algae in Quebec. PhD diss., Laval University, 2012.

Krause-Jensen D, Duarte CM, Hendriks IE, Meire, L, Blcher ME, Marbà N, Sejr MK (2015) Macroalgae contribute to nested mosaics of pH variability in a subarctic fjord. Biogeosciences Discuss 12: 4907–4945.

Lamote M, Johnson LE, Lemoine Y (2007) Interspecific differences in the response of juvenile stages to physical stress: Fluorometric responses of fucoid embryos to variation in meteorological conditions. J Phycol 43:1164–1176

Longtin CM, Scrosati R a., Whalen GB, Garbary DJ (2009) Distribution of algal epiphytes across environmental gradients at different scales: Intertidal elevation, host canopies, and host fronds. J Phycol 45:820–827.

Mathieson AC, Dawes CJ (2011) A floristic comparison of benthic "marine" algae in Bras D'Or Lake, Nova Scotia with five other Northwest Atlantic embayments and the Baltic Sea in Northern Europe. Rhodora 113:300–350.

Metcalfe P (2013) An examination of the Barachois Pond ecosystems on the Northeast Avalon Peninsula of Newfoundland and Labrador. Northeast Avlon ACAP.

OBIS (2015). Data from the Ocean Biogeographic Information System. Intergovernmental Oceanographic Commission of UNESCO. Web. http://www.iobis.org (Retrieved on 2015/06/17).

Riget F, Johansen P, Asmund G (1997) Baseline levels and natural variability of elements in three seaweed species from West Greenland. Mar Pollut Bull 34:171–176.

Ryan S, An investigation into the biochemical effects of heavy metal exposure on seaweeds. PhD diss., Waterford Institute of Technology, 2010.

Schmidt AL, Wysmyk JKC, Craig SE, Lotze HK (2012) Regional-scale effects of eutrophication on ecosystem structure and services of seagrass beds. Limnol Oceanogr 57:1389–1402.

Scrosati RA, Genne B Van, Heaven CS, Watt CA (2011) Species richness and diversity in different functional groups across environmental stress gradients: a model for marine rocky shores. Ecography 34:151–161.

Veinott G, Sylvester P, Hamoutene D, Anderson MR, Meade J, Payne J (2003) State of the marine environment at Little Bay Arm, Newfoundland and Labrador, Canada, 10 years after a "do nothing" response to a mine tailings spill. J Environ Monit 5:626–634.

Wilce RT (1959) The marine algae of the Labrador Peninsula and Northwest Newfoundland (Ecology and Distribution). National Museum of Canada, Ottawa

Fucus vesiculosus

Aquatic Biodiversity Monitoring Network (n.d.) Bladder Wrack, *Fucus vesiculosus* (Retrieved on: October 20, 2015). Retrieved from: http://www.rsba.ca/recherche_espece/fiche_espece.php?recordID=90&lan=en

Archambault P, Bourget E (1996) Scales of coastal heterogeneity and benthic intertidal species richness, diversity and abundance. Mar Ecol Prog Ser 136:111–121.

Assis J, Serrão EA, Claro B, Perrin C, Pearson GA (2014) Climate-driven range shifts explain the distribution of extant gene pools and predict future loss of unique lineages in a marine brown alga. Mol Ecol 23:2797–2810.

Bird C, Greenwell M, J M (1983) Benthic marine algal flora of the north shore of Prince Edward Island (Gulf of St. Lawrence), Canada. Aquat Bot 16:315–335.

Chaudhuri A, Mitra M, Havrilla C, Waguespack Y, Schawrz J (2007) Heavy metal biomonitoring by seaweeds on the Delmarva Peninsula, east coast of the USA. Bot Mar 50:151–158.

Chavanich S, Wilson KA (2000) Rocky intertidal zonation of gammaridean amphipods in Long Island Sound, Connecticut. Crustaceana 73:835–846.

Deal MS, Hay ME, Wilson D, Fenical W (2003) Galactolipids rather than phlorotannins as herbivore deterrents in the brown seaweed *Fucus vesiculosus*. Oecologia 136:107–114.

E. C. Smith Herbarium (2015) Fucaceae *Fucus vesiculosus* Linnaeus, 1767 (Retrieved on November 1, 2016). Retrieved from: http://procyon.acadiau.ca/ecsmith/cgibin/results.cgi?acad,Fucaceae,Fucus,vesiculosus,,species

Heaven CS, Scrosati RA (2008) Benthic community composition across gradients of intertidal elevation, wave exposure, and ice scour in Atlantic Canada. Mar Ecol Prog Ser 369:13–23.

Hicks BJ (1990) Observations on the intertidal Staphylinid, *Micralymma marinum* (Stroem) (Coleoptera: Staphylinidae), from Newfoundland. Coleopt Bull 44:304–306.

Himmelman JH, Steele DH (1971) Foods and predators of the green sea urchin Strongylocentrotus droebachiensis in Newfoundland waters. Mar Biol 9:315–322.

Høgslund S, Sejr MK, Wiktor J, Blicher ME, Wegeberg S (2014) Intertidal community composition along rocky shores in South-west Greenland: a quantitative approach. Polar Biol 37:1549–1561.

Hooper RG, Whittick A (1984) The benthic marine algae of the Kaipokok Bay, Makkovik Bay, and Big River Bay region of the central Labrador coast. Natur Can 111:131–138.

http://data.gbif.org (2015), *Fucus vesiculosus* and Northwest Atlantic, 180 records, accessed on 29 November 2015: 23:12:00 hrs, user doi: 10.15468/dl.8c1e0x, contributed by 18 datasets. Publishers identifiers:
10.15468/pal1lb (1 record); 10.15468/ib5ypt (1 record); 10.15468/rhzrxw (2 records); 10.15468/ab3s5x (2 records); 10.15468/w35jmd (40 records); 10.15468/dipjcr (5 records); 10.15468/uc1apo (1 record); 10.15468/hja69f (2 records); 10.15468/8oxxmx (1 record); 10.15468/5uprth (36 records); 10.15468/nztqk6 (1 record); 10.15468/o3pvnh (1 record); 10.15468/bxmxx0 (58 records); 10.5886/ujwtvvs2 (4 records); 10.15468/cndomv (14 records); 10.15468/s6ctus (1 record); 10.15468/zc4csq (8 records) 10.15468/md6zcx (2 records)

Jones E, Thornber CS (2010) Effects of habitat-modifying invasive macroalgae on epiphytic algal communities. Mar Ecol Prog Ser 400:87–100.

Kawamitsu Y, Boyer JS (1999) Photosynthesis and carbon storage between tides in a brown alga, *Fucus vesiculosus*. Mar Biol 133:361–369.

Kawamitsu Y, Driscoll T, Boyer JS (2000) Photosynthesis during desiccation in an intertidal alga and a land plant. Plant Cell Physiol 41:344–353.

Krause-Jensen D, Duarte CM, Hendriks IE, Blicher ME, Marbà N, Sejr MK (2015) Macroalgae contribute to nested mosaics of pH variability in a subarctic fjord. Biogeosciences Discuss 12:4907–4945.

Kubanek J, Lester SE, Fenical W, Hay ME (2004) Ambiguous role of phlorotannins as chemical defenses in the brown alga *Fucus vesiculosus*. Mar Ecol Prog Ser 277:79–93.

Largaespada C, Guichard F, Archambault P (2012) Meta-ecosystem engineering: nutrient fluxes reveal intraspecific and interspecific feedbacks in fragmented mussel beds. Ecology 93:324–333.

Madden M, Mitra M, Ruby D, Schwarz J (2012) Seasonality of selected nutritional constituents of edible delmarva seaweeds. J Phycol 48:1289–1298. doi: 10.1111/j.1529-8817.2012.01207.x

Mathieson AC, Dawes CJ (2011) A floristic comparison of benthic “marine” algae in Bras D’Or Lake, Nova Scotia with five other Northwest Atlantic embayments and the Baltic Sea in Northern Europe. Rhodora 113:300–350.

Novaczek I, McLachlan J (1989) Investigations of the marine algae of Nova Scotia XVII: vertical and geographic distributions of marine algae on rocky shores of the Maritime Provinces. Proc NS Inst Sci 38:91–143.

OBIS (2015). Data from the Ocean Biogeographic Information System. Intergovernmental Oceanographic Commission of UNESCO. Web. http://www.iobis.org (consulted on 2015/06/17).

Pedersen A, Kraemer G, Yarish C (2008) Seaweed of the littoral zone at Cove Island in Long Island Sound: Annual variation and impact of environmental factors. J Appl Phycol 20:869–882.

Phaneuf D, Côté I, Dumas P, et al (1999) Evaluation of the contamination of marine algae (seaweed) from the St. Lawrence River and likely to be consumed by humans. Environ Res 80:S175–S182.

Riget F, Johansen P, Asmund G (1997) Baseline levels and natural variability of elements in three seaweed species from West Greenland. Mar Pollut Bull 34:171–176.

Thomsen HA, Brandt A (1999) The 1998 Danish-German excursion to Disko Island, West Greenland. Berichte zur Polarforsch 330:1–10.

Watt CA, Scrosati RA (2014) Experimental and mensurative data on the abundance of primary producers and consumers from intertidal habitats in Canada. Ecology 95:1429–1429.

Weber JC, Epifanio CE (1996) Response of mud crab (*Panopeus herbstii*) megalopae to cues from adult habitat. Mar Biol 126:655–661.

Yao S (2014) Silver biosorption study by using seaweed-based sorbents. Memorial University of Newfoundland

Chondrus crispus

Aquatic Biodiversity Monitoring Network (n.d.) Irish Moss, *Chondrus crispus* (Retrieved on: October 20, 2015). Retrieved from: http://www.rsba.ca/recherche_espece/fiche_espece.php?recordID=499&lan=en

Bird C, Greenwell M, JM (1983) Benthic marine algal flora of the north shore of Prince Edward Island (Gulf of St. Lawrence), Canada. Aquat Bot 16:315–335.

Chopin T, Sharp G, Belyea E, Semple R, Jones D (1999) Open-water aquaculture of the red alga *Chondrus crispus* in Prince Edward Island, Canada. Hydrobiologia 399:417–425.

Hu Z, Zeng X, Critchley AT, Morrell SL, Duan D (2007) Phylogeography of the Northern Atlantic species *Chondrus crispus* (Gigartinales, Rhodophyta) inferred from nuclear rDNA internal transcribed spacer sequences. Hydrobiologia 575:315–327.

http://data.gbif.org (2015), *Chondrus crispus* and Northwest Atlantic, 335 records, accessed on 21 October 2015: 18:48:00 hrs, user doi: 10.15468/dl.7j0ccv, contributed by 10 datasets. Publishers identifiers: 10.15468/rhzrxw (1 record); 10.15468/w35jmd (19 records); 10.15468/dipjcr (5 records); 10.15468/5uprth (40 records); 10.15468/nztqk6 (1 record); 10.15468/bxmxx0 (230 records); 10.5886/ujwtvvs2 (7 records); 10.15468/cndomv (2 records); 10.15468/zc4csq (28 records); 10.15468/md6zcx (2 records)

Mathieson AC, Dawes CJ (2011) A floristic comparison of benthic "marine" algae in Bras D'Or Lake, Nova Scotia with five other Northwest Atlantic embayments and the Baltic Sea in Northern Europe. Rhodora 113:300–350.

OBIS (2015). Data from the Ocean Biogeographic Information System. Intergovernmental Oceanographic Commission of UNESCO. Web. http://www.iobis.org (consulted on 2015/06/17).

Phaneuf D, Côté I, Dumas P, Ferron LA, LeBlanc A (1999) Evaluation of the contamination of marine algae (seaweed) from the St. Lawrence River and likely to be consumed by humans. Environ Res 80: S175–S182.

Watanabe S, Metaxas A, Scheibling RE (2009) Dispersal potential of the invasive green alga *Codium fragile* ssp. *fragile.* J Exp Mar Bio Ecol 381:114–125.

Watt CA, Scrosati RA (2014) Experimental and mensurative data on the abundance of primary producers and consumers from intertidal habitats in Canada. Ecology 95:1429–1429.

Codium fragile

Aquatic Biodiversity Monitoring Network (n.d.) Oyster thief, *Codium fragile* (Retrieved on: October 20, 2015). Retrieved from: http://www.rsba.ca/recherche_espece/fiche_espece.php?recordID=85&lan=en

Carroll JM, Peterson BJ (2013) Comparisons in demographic rates of bay scallops in eelgrass and the introduced alga, *Codium fragile*, in New York. Mar Biol 160:1451–1463.

Drouin A, McKindsey CW, Johnson LE (2011) Higher abundance and diversity in faunal assemblages with the invasion of *Codium fragile* ssp. *fragile* in eelgrass meadows. Mar Ecol Prog Ser 424:105–117.

E. C. Smith Herbarium (2015) Codiaceae Codium *fragile* (Suringar) Hariot. (Retrieved on October 20, 2015). Retrieved from: http://procyon.acadiau.ca/ecsmith/cgiin/results.cgi?acad,Codiaceae,Codium,fragile,,species

Filbee-Dexter K, Feehan C, Scheibling R (2016) Large-scale degradation of a kelp ecosystem in an ocean warming hotspot. Mar Ecol Prog Ser 543:141–152.

Fisheries and Oceans Canada (n.d.) Community aquatic monitoring program. Provided on 2015/10/23. http://www.glf.dfo-mpo.gc.ca/Gulf/CAMP

Gagnon K, McKindsey CW, Johnson LE (2011) Dispersal potential of invasive algae: the determinants of buoyancy in *Codium fragile* ssp. *fragile*. Mar Biol 158:2449–2458.

Garbary DJ, Fraser SJ, Hubbard C, Kim KY (2004) *Codium fragile*: rhizomatous growth in the Zostera thief of eastern Canada. Helgol Mar Res 58:141–146.

Gerard VA, Dunham SE, Rosenberg G (1990) Nitrogen-fixation by cyanobacteria associated with *Codium fragile* (Chlorophyta): Environmental effects and transfer of fixed nitrogen. Mar Biol 105:1–8.

Harris LG, Jones AC (2005) Temperature, herbivory and epibiont acquisition as factors controlling the distribution and ecological role of an invasive seaweed. Biol Invasions 7:913–924.

Hubbard CB, Garbary DJ (2002) Morphological Variation of *Codium fragile* (Chlorophyta) in Eastern Canada. Bot Mar 45:476–485.

http://data.gbif.org (2015), Codium fragile subsp. tomentosoides and Northwest Atlantic, 5 records, accessed on 21 October 2015: 19:01:00 hrs, user doi: 10.15468/dl.fcjdyu, contributed by 2 datasets. Publishers identifiers: 10.15468/ab3s5x (1 record); 10.15468/w35jmd (4 records)

Jones E, Thornber CS (2010) Effects of habitat-modifying invasive macroalgae on epiphytic algal communities. Mar Ecol Prog Ser 400:87–100.

Matheson K, Mckenzie CH, Sargent P, et al (2014) Northward expansion of the invasive green algae *Codium fragile* spp. *fragile* (Suringar) Hariot, 1889 into coastal waters of Newfoundland, Canada. BioInvasions Rec 3:151–158.

Mathieson AC, Dawes CJ (2011) A floristic comparison of benthic “marine” algae in Bras D’Or Lake, Nova Scotia with five other Northwest Atlantic embayments and the Baltic Sea in Northern Europe. Rhodora 113:300–350.

Mathieson AC, Hehre EJ, Dawes CJ, Neefus CD (2008) An historical comparison of seaweed populations from Casco Bay, Maine. Rhodora 110:1–102.

OBIS (2015). Data from the Ocean Biogeographic Information System. Intergovernmental Oceanographic Commission of UNESCO. Web. HTTP://WWW.IOBIS.ORG (consulted on 2015/06/17).

Provan J, Booth D, Todd NP, Beatty GE, Maggs CA (2008) Tracking biological invasions in space and time: Elucidating the invasive history of the green alga *Codium fragile* using old DNA. Divers Distrib 14:343–354.

Puckett BJ, Eggleston DB (2012) Oyster demographics in a network of no-take reserves: recruitment, growth, survival, and density dependence. Mar Coast Fish 4:605–627.

Raven JA, Osmond CB (1992) Inorganic C acquisition processes and their ecological significance in inter- and sub-tidal macroalgae of North Carolina. Funct Ecol 6:41–47.

Searles RB, Hommerstand MH, Amsler CD (1984). The occurrence of *Codium fragile* subsp. *tomentosoides* and *C. taylorii* (Chlorophyta) in North Carolina. Bot Mar 27: 185-187.

Stutz J, Pikelnaya O, Hurlock SC, Trick S, Pechtl S, von Glasow R (2007) Daytime OIO in the Gulf of Maine. Geophys Res Lett 34:3–7.

Thomsen MS (2004) Species, thallus size and substrate determine macroalgal break force and break location in a low-energy soft-bottom lagoon. Aquat Bot 80:153–161.

Watanabe S, Scheibling RE, Metaxas A (2010) Contrasting patterns of spread in interacting invasive species: *Membranipora membranacea* and *Codium fragile* off Nova Scotia. Biol Invasions 12:2329–2342.

Wyda JC, Deegan LA, Hughes JE, Weaver MJ (2002) The response of fishes to submerged aquatic vegetation complexity in two ecoregions of the Mid-Atlantic Bight: Buzzards Bay and Chesapeake Bay. Estuaries 25:86–100.

Laminaria digitata

Aquatic Biodiversity Monitoring Network (n.d.) Oarweed, *Laminaria digitata* (Retrieved on: October 20, 2015). Retrieved from: http://www.rsba.ca/recherche_espece/fiche_espece.php?recordID=396&lan=en

Adey WH, Hayek LC (2011) Elucidating marine biogeography with macrophytes: quantitative analysis of the North Atlantic supports the thermogeographic model and demonstrates a distinct subarctic region in the Northwestern Atlantic. Northeast Nat 18:1–128.

Archambault P, Bourget E (1996) Scales of coastal heterogeneity and benthic intertidal species richness, diversity and abundance. Mar Ecol Prog Ser 136:111–121.

Cardinal A, Villalard M (1971) Inventaire des algues marines benthiques de l'estuaire du Saint- Laurent (Québec). Natur Can 98:887–904.

E. C. Smith Herbarium (2015) Laminariaceae *Laminaria digitata* Kjellm (Retrieved on November 1, 2016). Retrieved from: http://procyon.acadiau.ca/ecsmith/cgibin/results.cgi?acad,Laminariaceae,Laminaria,digitata,,species

Filbee-Dexter K, Feehan C, Scheibling R (2016) Large-scale degradation of a kelp ecosystem in an ocean warming hotspot. Mar Ecol Prog Ser 543:141–152.

Frey DL, Gagnon P (2015) Thermal and hydrodynamic environments mediate individual and aggregative feeding of a functionally important omnivore in reef communities. PLoS One 10: e0118583.

Gregory RS, Anderson JT, Dalley EL (1997) Distribution of Juvenile Atlantic cod (*Gadus morhua*) relative to available habitat in Placentia Bay, Newfoundland. NAFO Sci Counc Stud 3–12.

http://data.gbif.org (2016), Laminaria digitata and Northwest Atlantic, 86 records, accessed on 2 October 2015: 18:38:00 hrs, user doi: 10.15468/dl.nsm0gk, contributed by 8 datasets. publishers identifiers: 10.15468/rhzrxw (2 records); 10.15468/w35jmd (15 records); 10.15468/5uprth (1 record); 10.15468/nztqk6 (1 record); 10.15468/bxmxx0 (16 records); 10.15468/cndomv (39 records); 10.15468/s6ctus (1 record); 10.15468/zc4csq (11 records)

Hooper RG, Whittick A (1984) The benthic marine algae of the Kaipokok Bay, Makkovik Bay, and Big River Bay region of the central Labrador coast. Natur Can 111:131–138.

Liddle LB, Abramson M (2011) Inventory of the seaweeds of Lake Montauk. Montauk, New York.

Mathieson AC, Dawes CJ (2011) A floristic comparison of benthic "marine" algae in Bras D'Or Lake, Nova Scotia with five other Northwest Atlantic embayments and the Baltic Sea in Northern Europe. Rhodora 113:300–350.

Mathieson AC, Dawes CJ, Hehre EJ (1998) Floristic and zonation studies of seaweeds from Mount Desert Island, Maine: An historical comparison. Rhodra 100:333–379.

McDevit DC, Saunders GW (2010) A DNA barcode examination of the Laminariaceae (Phaeophyceae) in Canada reveals novel biogeographical and evolutionary insights. Phycologia 49:235–248.

Nadon M, Himmelman JH (2010) The structure of subtidal food webs in the northern Gulf of St. Lawrence, Canada, as revealed by the analysis of stable isotopes. Aquat Living Resour 23:167–176.

Neefus CD, Allen BP, Baldwin HP, Mathieson AC, Eckert RT, Yarish C, Miller MA (1993) An examination of the population genetics of Laminaria and other brown algae in the laminariales using starch gel electrophoresis. Hydrobiologia 260-261:67–79.

OBIS (2015). Data from the Ocean Biogeographic Information System. Intergovernmental Oceanographic Commission of UNESCO. Web. http://www.iobis.org (consulted on 2015/06/17).

Schmidt AL, Scheibling RE (2006) A comparison of epifauna and epiphytes on native kelps (Laminaria species) and an invasive alga (*Codium fragile* ssp. *tomentosoides*) in Nova Scotia, Canada. Bot Mar 49:315–330.

Sharp G, Allard M, Lewis A (2008) The potential for seaweed resource development in subarctic Canada; Nunavik, Ungava Bay. J Appl Phycol 20:41–48.

Watt CA, Scrosati RA (2014) Experimental and mensurative data on the abundance of primary producers and consumers from intertidal habitats in Canada. Ecology 95:1429–1429.

Witman JD (1987) Subtidal coexistence: storms, grazing, mutualism, and the zonation of kelps and mussels. Ecol Monogr 57:167–187.

Saccharina latissima

Adey WH, Hayek LC (2011) Elucidating marine biogeography with macrophytes: quantitative analysis of the North Atlantic supports the thermogeographic model and demonstrates a distinct subarctic region in the Northwestern Atlantic. Northeast Nat 18:1–128.

Archambault P, Bourget E (1996) Scales of coastal heterogeneity and benthic intertidal species richness, diversity and abundance. Mar Ecol Prog Ser 136:111–121.

Bird C, Greenwell M, J M (1983) Benthic marine algal flora of the north shore of Prince Edward Island (Gulf of St. Lawrence), Canada. Aquat Bot 16:315–335.

Caines S, Gagnon P (2012) Population dynamics of the invasive bryozoan *Membranipora membranacea* along a 450-km latitudinal range in the subarctic northwestern Atlantic. Mar Biol 159:1817–1832.

Eastwood M, Quinby K, Seeley R, et al (2009) Borror's Species Checklist for the Isles of Shoals Archipelago. Cornell Univeristy, Ithaca, NY.

E. C. Smith Herbarium (2015) Laminariaceae *Laminaria saccharina* Setch. (Retrieved on November 1, 2016). Retrieved from: http://procyon.acadiau.ca/ecsmith/cgibin/results.cgi?acad,Laminariaceae,Laminaria,saccharina,,species

Filbee-Dexter K, Feehan C, Scheibling R (2016) Large-scale degradation of a kelp ecosystem in an ocean warming hotspot. Mar Ecol Prog Ser 543:141–152.

Gerard VA (1997) The role of nitrogen nutrition in high-temperature tolerance of the kelp *Laminaria saccharina* (Chromophyta). J Phycol 33:800–810.

Hooper RG, Whittick A (1984) The benthic marine algae of the Kaipokok Bay, Makkovik Bay, and Big River Bay region of the central Labrador coast. Natur Can 111:131–138.

http://data.gbif.org (2016), Saccharina latissima and Northwest Atlantic, 410 records, accessed on 7 November 2015: 17:26:00 hrs, user doi: 10.15468/dl.bqmdho, contributed by 2 datasets. Publishers identifiers: 10.15468/5uprth (14 records); 10.15468/cndomv (122 records)

Krause-Jensen D, Duarte CM, Hendriks IE, Meire L, Blicher ME, Marbà N, Sejr MK (2015) Macroalgae contribute to nested mosaics of pH variability in a subarctic fjord. Biogeosciences Discuss 12:4907–4945.

Küpper FC, Peters AF, Shewring DM, Sayer MDJ, Mystikou A, Brown H, Azzopardi E, Dargent O, Strittmatter M, Brennan D, Asensi AO, van West P, Wilce RT (2016) Arctic marine phytobenthos of northern Baffin Island. J Phycol 52: 532-549.

Lee J, Brinkhuis BH (1988) Seasonal light and temperature interaction effects on development of *Laminaria Saccharina* (Phaeophyta) gametophytes and juvenile sporophytes. J Phycol 24:181–191.

Liddle LB, Abramson M (2011) Inventory of the seaweeds of Lake Montauk. Montauk, New York.

Mathieson AC, Dawes CJ (2011) A floristic comparison of benthic “marine” algae in Bras D’Or Lake, Nova Scotia with five other Northwest Atlantic embayments and the Baltic Sea in Northern Europe. Rhodora 113:300–350.

McDevit DC, Saunders GW (2010) A DNA barcode examination of the Laminariaceae (Phaeophyceae) in Canada reveals novel biogeographical and evolutionary insights. Phycologia 49:235–248.

Neefus CD, Allen BP, Baldwin HP, Mathieson AC, Eckert RT, Yarish C, Miller MA (1993) An examination of the population genetics of Laminaria and other brown algae in the laminariales using starch gel electrophoresis. Hydrobiologia 260-261:67–79.

OBIS (2015). Data from the Ocean Biogeographic Information System. Intergovernmental Oceanographic Commission of UNESCO. Web. http://www.iobis.org (consulted on 2015/06/17).

Watanabe S, Metaxas A, Scheibling RE (2009) Dispersal potential of the invasive green alga *Codium fragile* ssp. *fragile*. J Exp Mar Bio Ecol 381:114–125.

Appendix B: Model Metrics

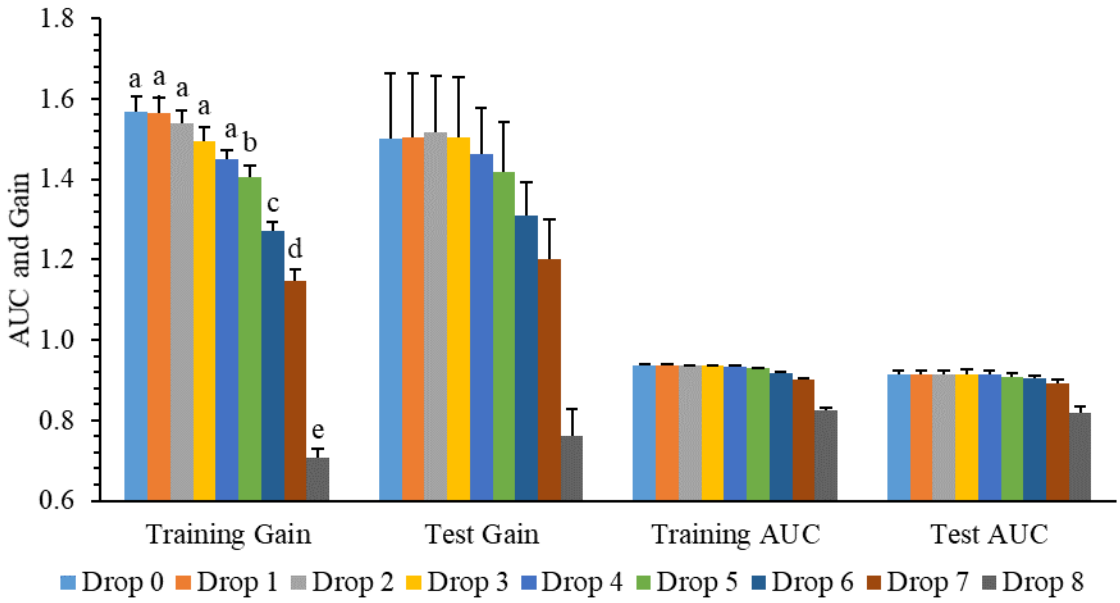

Figure B.1 Change in *Ascophyllum nodosum* average model regularized training and test gain (+SE) and AUC (area under the curve) when a variable is removed from the model (See text for detailed explanation). Letters indicate significant change in training gain based on whether 95% CI overlap or not.

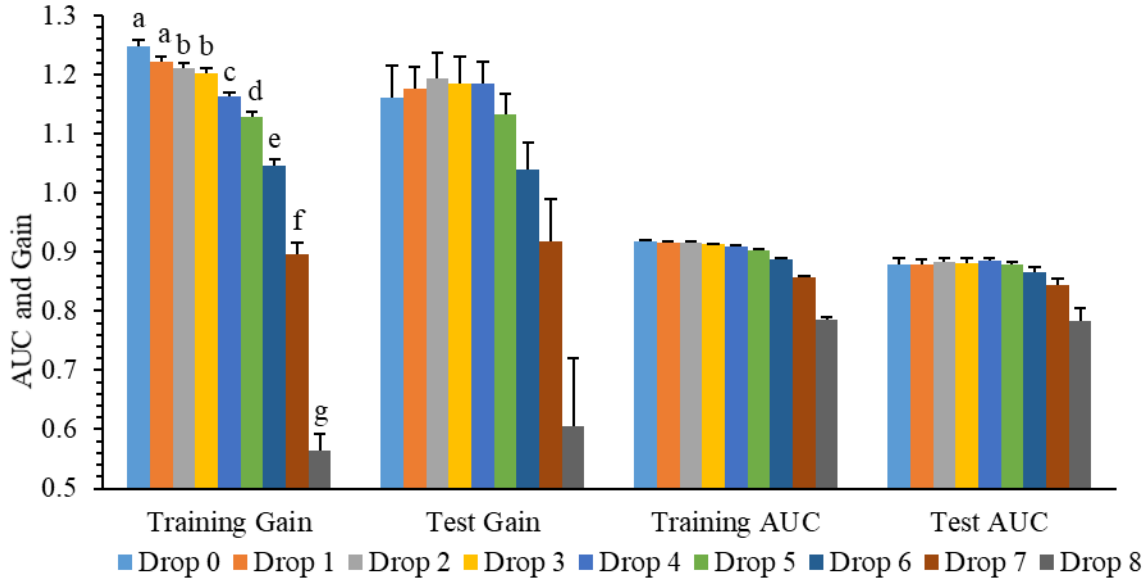

Figure B.2 Change in *Fucus vesiculosus* average model regularized training and test gain (+SE) and AUC (area under the curve) when a variable is removed from the model (See text for detailed explanation). Letters indicate significant change in training gain based on whether 95% CI overlap or not.

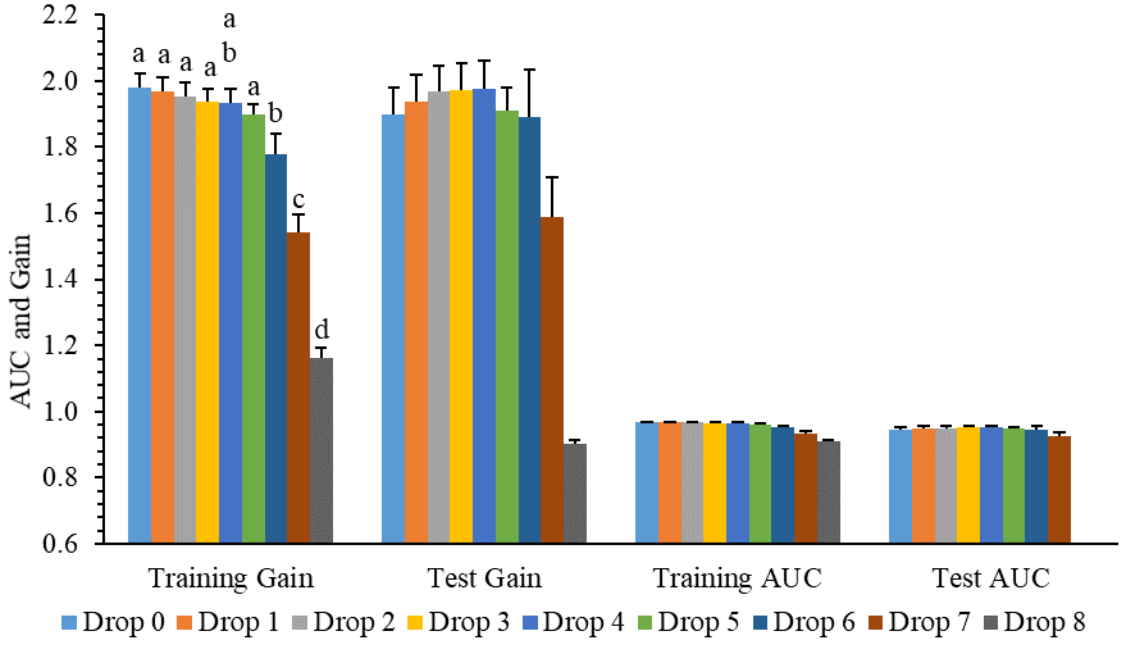

Figure B.3 Change in *Codium fragile* average model regularized training and test gain (+SE) and AUC (area under the curve) when a variable is removed from the model (See text for detailed explanation). Letters indicate significant change in training gain based on whether 95% CI overlap or not.

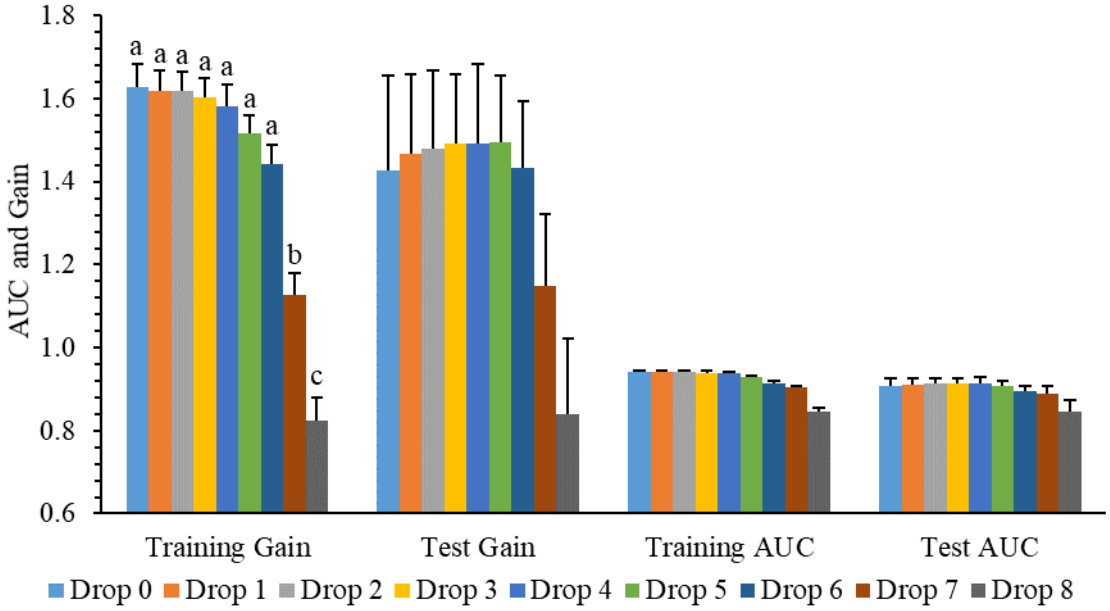

Figure B.4 Change in L*aminaria digitata* average model regularized training and test gain (+SE) and AUC (area under the curve) when a variable is removed from the model (See text for detailed explanation). Letters indicate significant change in training gain based on whether 95% CI overlap or not.

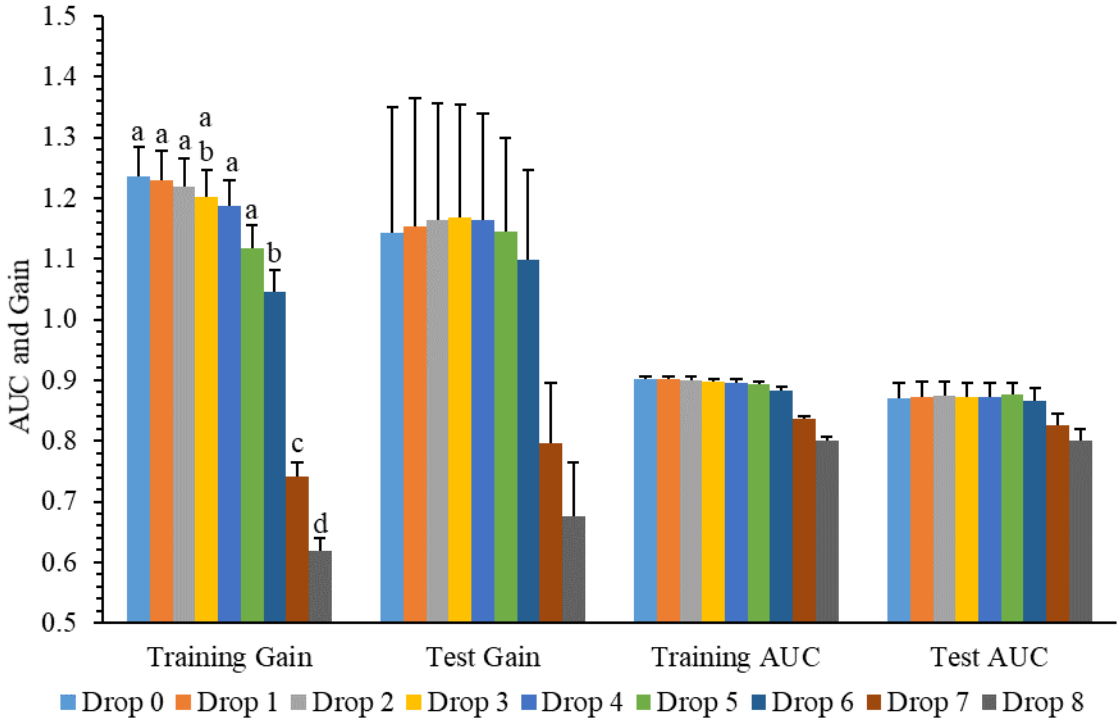

Figure B.5 Change in *Saccharina latissima* average model regularized training and test gain (+SE) and AUC (area under the curve) when a variable is removed from the model (See text for detailed explanation). Letters indicate significant change in training gain based on whether 95% CI overlap or not.

Table B.1 Order of variables removed from each model. The top variable is least important in developing the model, and the bottom variable was the most important for predicting the relative probability of species presence by the average test gain. Asterisk denotes that the variable was used in best model. See Table 2 for abbreviations.

A. nodosum	*F. vesiculosus*	*C. crispus*	*C. fragile*	*S. latissima*	*L. digitata*
AugMaxSAT	SmrMeaSSS	SmrMeaSIC	AugMaxSAT	SmrMeaSSS	SmrMinSST
SmrMinSIC	SmrMinSST*	SmrMinSIC	SmrMinSST	AugMaxSAT	WntMaxSAT
SmrMinSST	AugMaxSAT*	SmrMeaSSS	SmrMinSIC	SmrMinSST	WntMeaSSS
WntMeaSSS	SmrMinSIC*	AugMaxSAT	SmrMeaSSS	WntMaxSAT	AugMaxSAT
WntMaxSAT*	WntMaxSAT*	WntMaxSAT	WntMaxSAT	SmrMinSIC	SmrMeaSSS
AugMaxSST*	AugMaxSST*	WntMeaSSS*	WntMeaSSS*	WntMeaSSS*	SmrMeaSIC
SmrMeaSIC*	SmrMeaSIC*	SmrMinSST*	SmrMeaSIC*	AugMaxSST*	SmrMinSIC*
SmrMeaSSS*	WntMaxSIC*	WntMaxSIC*	WntMaxSIC*	SmrMeaSIC*	WntMaxSIC*
WntMaxSIC*	WntMeSSS*	AugMaxSST*	AugMaxSST*	WntMaxSIC*	AugMaxSST*

Appendix C: Physiological Thresholds

Table C.1 Physiological thresholds used in this study. Growth and survival of seaweeds from Atlantic Canada was monitored in a controlled laboratory experiment at water temperatures of 12 to 29°C over the course of 8 weeks. NA indicates growth type was not observed across these temperatures. Data from Wilson et al. (2015).

Species	Good growth	Reduced growth	Reduced growth/ partial mortality	Complete mortality
A. nodosum	12-22°C	23-25°C	26-28°C	≥29°C
F. vesiculosus	12-25°C	NA	26-28°C	≥29°C
C. crispus	12-28°C	≥29°C	NA	NA
Codium	12-25°C	≥26°C	NA	NA
L. digitata	12-19°C	NA	20-22°C	≥23°C
S. latissima	12-19°C	NA	20-22°C	≥23°C

Table C.2 Present-day (1980-2015), mid-century (2040-2050), and end-century (2090-2100) sea surface temperature isotherms (°N) denoting the six temperatures used as physiological thresholds. Mid-century and end-century are the average relative isotherm of GFDL and IPSL. Latitude rounded to nearest half degree in text.

Time	**RCP**	**12°C**	**20°C**	**23°C**	**26°C**	**29°C**
1980-2015	NA	55.72	47.76	41.92	41.25	35.58
2040-2050	2.6	56.09	47.82	43.21	42.81	38.45
	8.5	56.18	48.17	46.26	43.81	38.80
2090-2100	2.6	56.09	47.87	43.20	41.79	38.75
	8.5	66.21	48.48	48.37	48.13	40.86

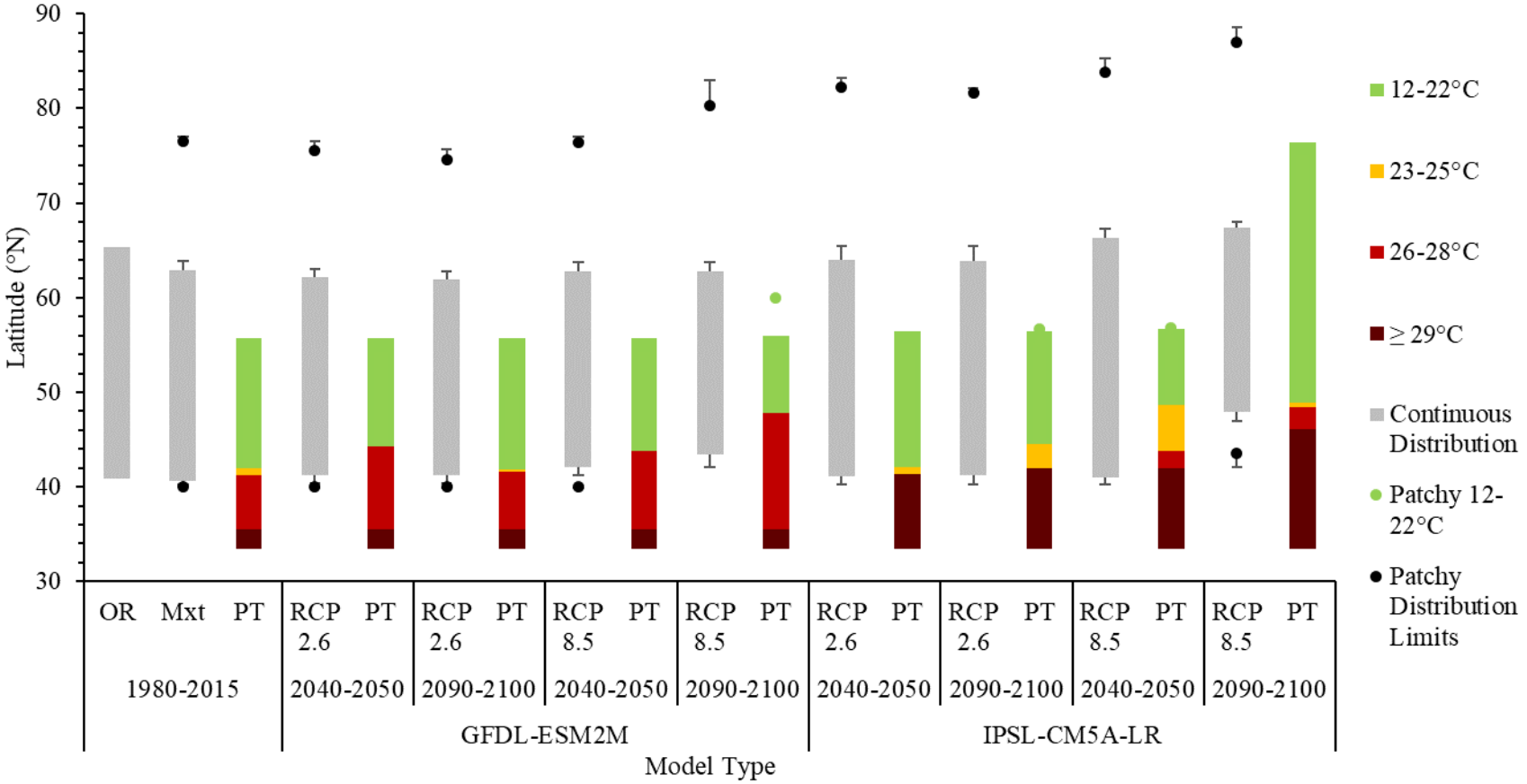

Figure D.1 *Ascophyllum nodosum* average relative northern and southern distribution limits (n=4, ±SE) over different time periods using occurrence records (OR), Maxent (Mxt), physiological thresholds (PT), and climate projections (RCP 2.6, 8.5 for two climate models). Grey bars show continuous distribution and black dots indicating patchy distribution. The PT colours indicate SST of 12-22°C (green, good growth), 23-25°C (yellow, reduced growth), 25-28°C (red, reduced growth and partial mortality), and ≥29°C (dark red, complete mortality.)

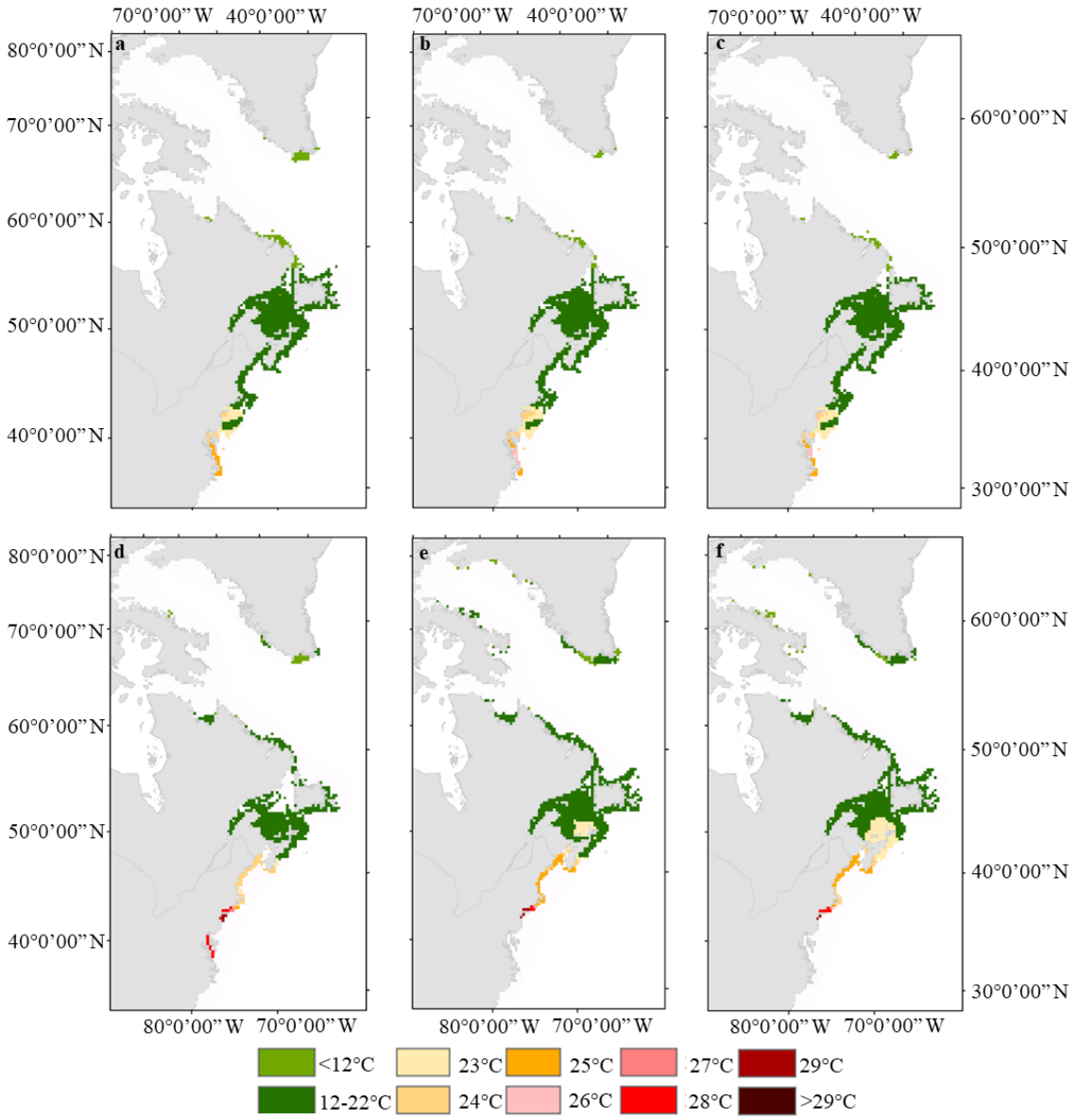

Figure D.2 Average Maxent model output (n=4) for *Ascophyllum nodosum* for GFDL RCP 2.6 over **a** 2006-2015, **b** 2040-2050, and **c** 2090-2100, and for IPSL RCP 2.6 over **d** 2006-2015, **e** 2040-2050, and **f** 2090-2100 with corresponding physiological thresholds (PT). PT were overlaid over the distribution to show areas of good growth (green), reduced growth (yellow-orange), reduced growth and partial mortality (pink-red,), and complete mortality (dark red). Data is in an equal-area projection.

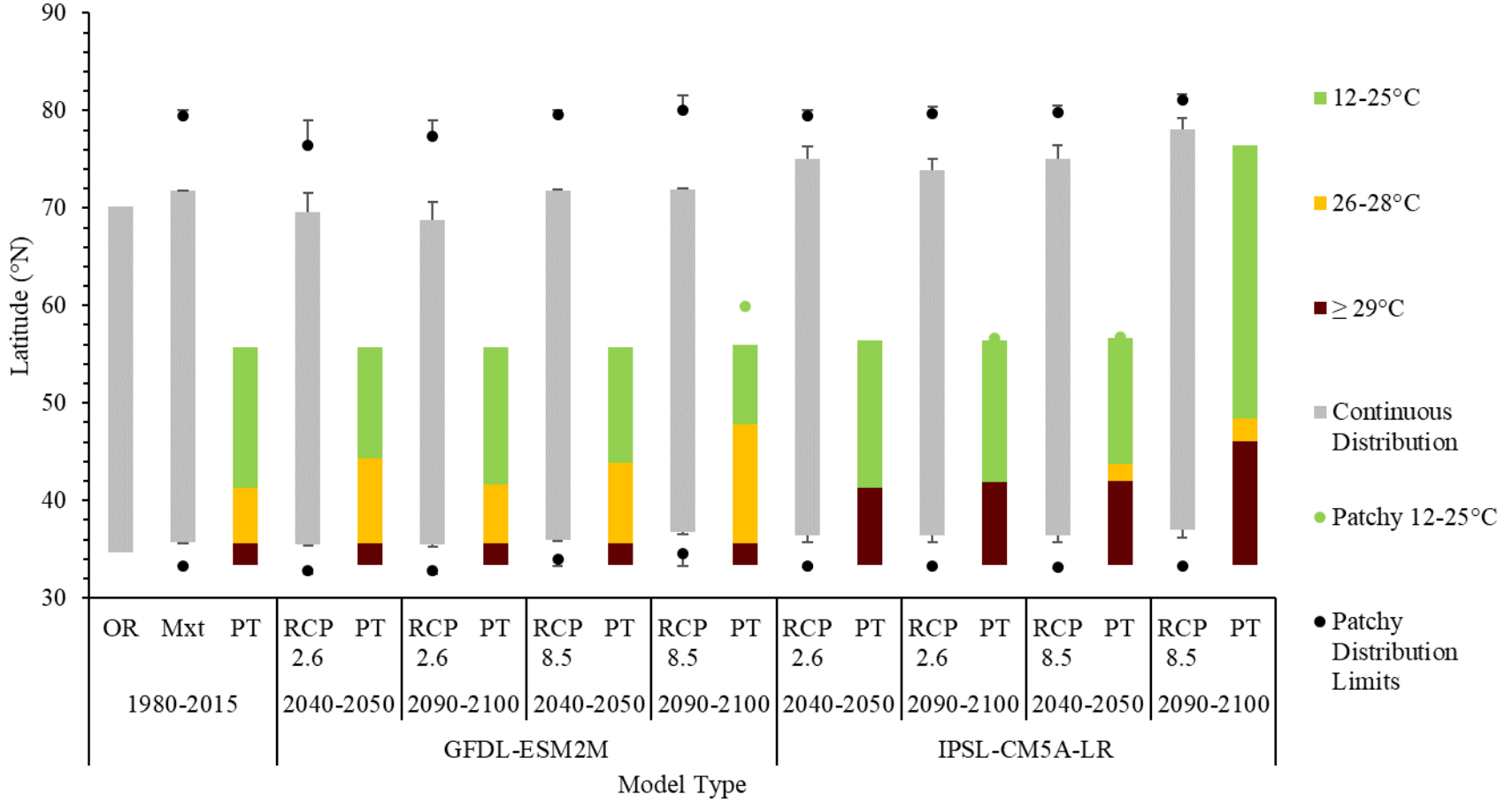

Figure D.3 *Fucus vesiculosus* average relative northern and southern distribution limits (n=5, ±SE) over different time periods using occurrence records (OR), Maxent (Mxt), physiological thresholds (PT), and climate projections (RCP 2.6, 8.5 for two climate models). Grey bars show continuous distribution and black dots indicating patchy distribution. The PT colours indicate SST of 12-25°C (green, good growth), 25-28°C (yellow, reduced growth and partial mortality), and ≥29°C (red, complete mortality).

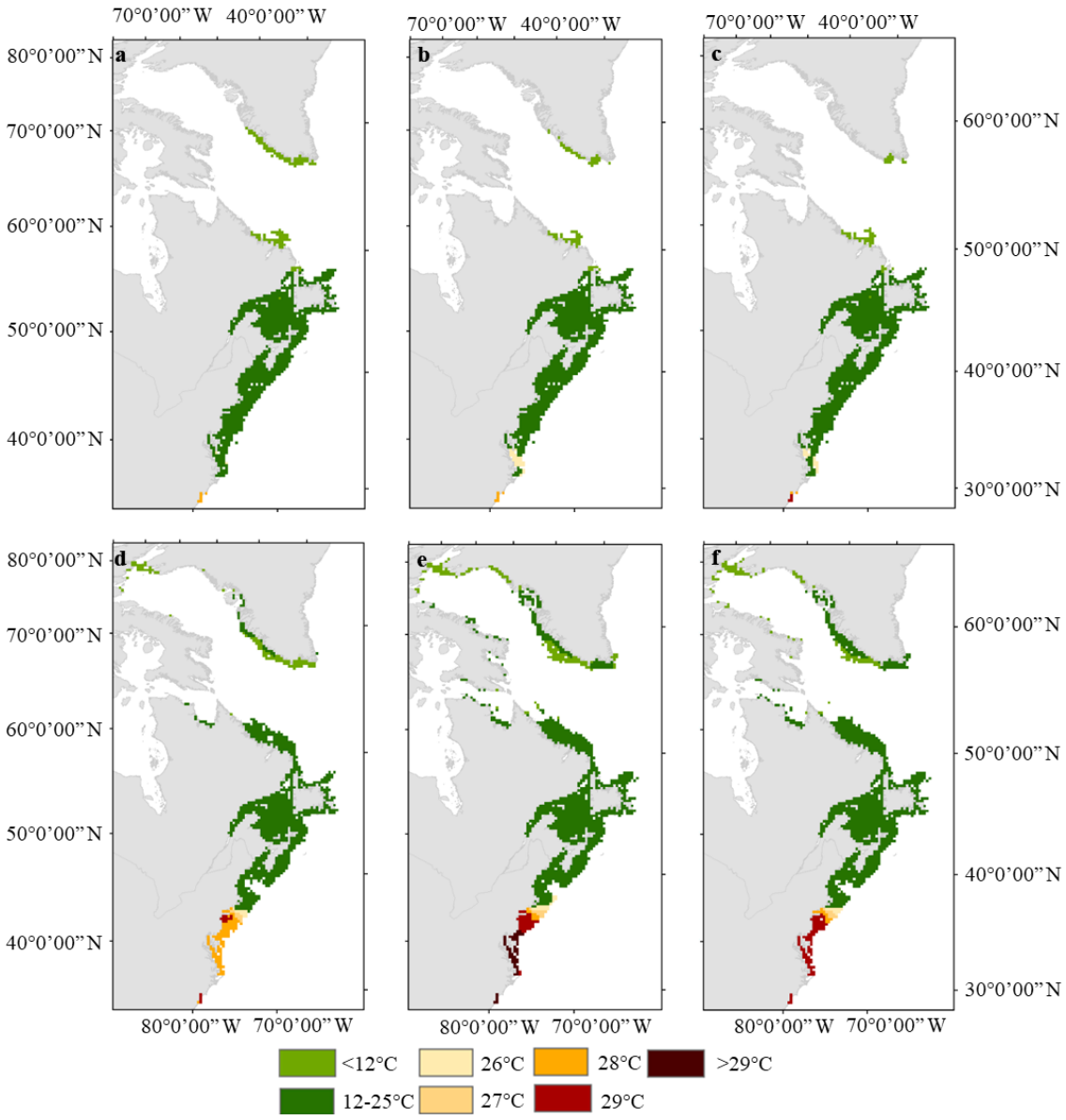

Figure D.4 Average Maxent model output (n=5) for *Fucus vesiculosus* for GFDL RCP 2.6 over **a** 2006-2015, **b** 2040-2050, and **c** 2090-2100, and for IPSL RCP 2.6 over **d** 2006-2015, **e** 2040-2050, and **f** 2090-2100 with corresponding physiological thresholds (PT). PT were overlaid over the distribution to show areas of good growth (green), reduced growth and partial mortality (orange), and complete mortality (red). Data is in an equal-area projection.

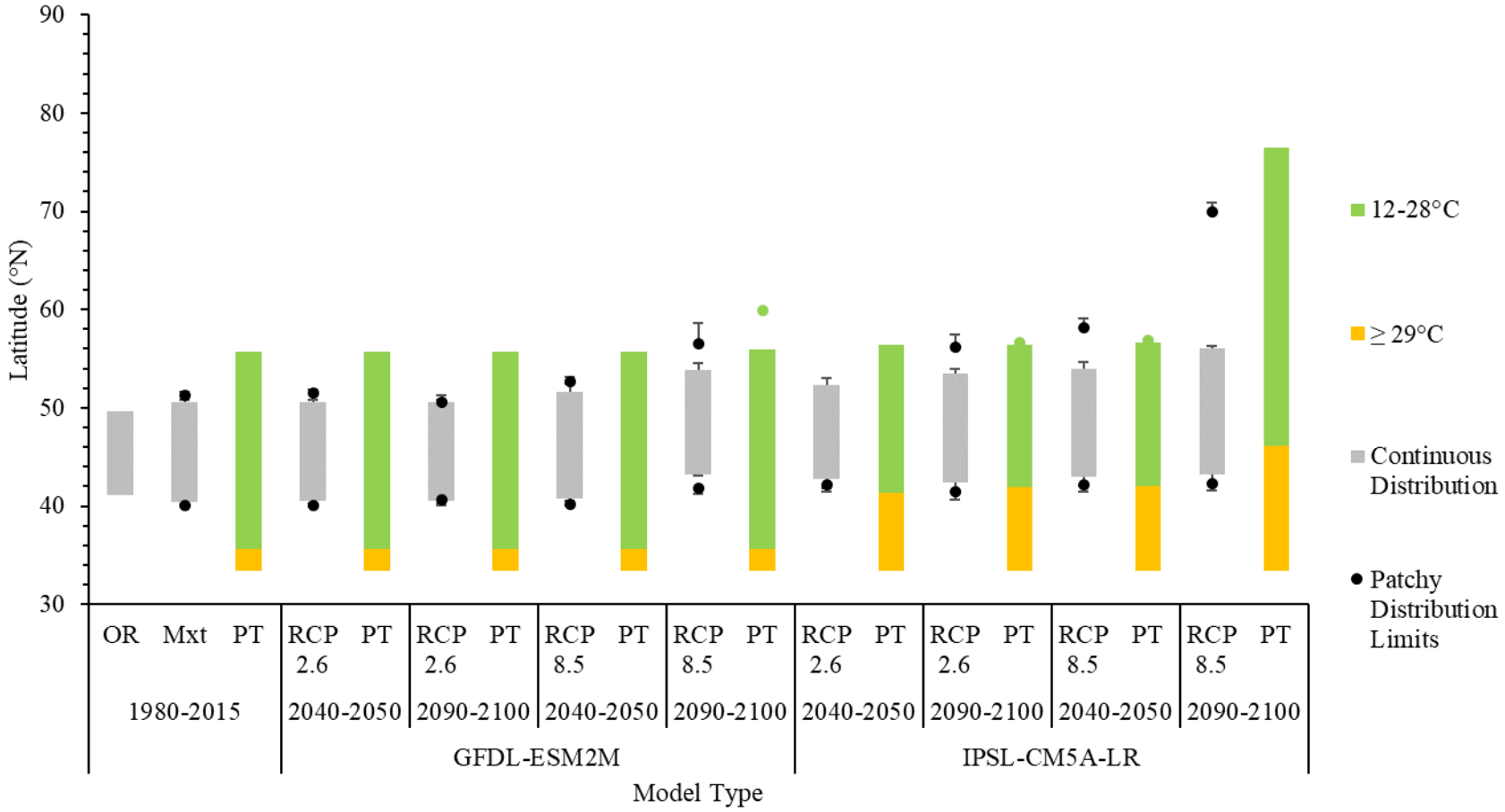

Figure D.5 *Chondrus crispus* average relative northern and southern distribution limits (n=4, ±SE) over different time periods using occurrence records (OR), Maxent (Mxt), physiological thresholds (PT), and climate projections (RCP 2.6, 8.5 for two climate models). Grey bars show continuous distribution and black dots indicating patchy distribution. The PT colours indicate SST of 12-28°C (green, good growth), and ≥29°C (yellow, poor growth).

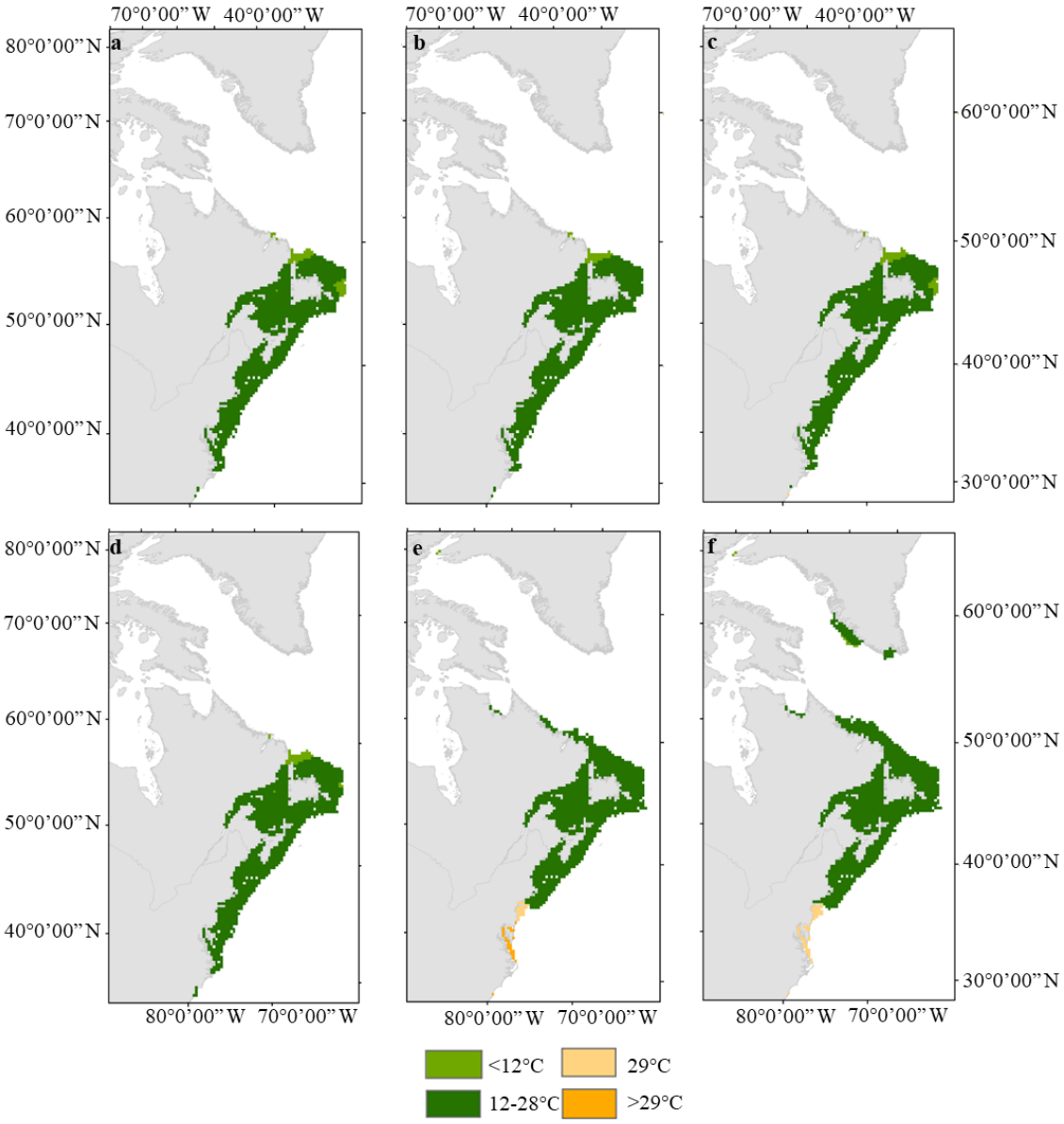

Figure D.6 Average Maxent model output (n=4) for *Chondrus crispus* for GFDL RCP 2.6 over **a** 2006-2015, **b** 2040-2050, and **c** 2090-2100, and for IPSL RCP 2.6 over **d** 2006-2015, **e** 2040-2050, and **f** 2090-2100 with corresponding physiological thresholds (PT). PT were overlaid over the distribution to show areas of good growth (green), and reduced growth (yellow-orange). Data is in an equal-area projection.

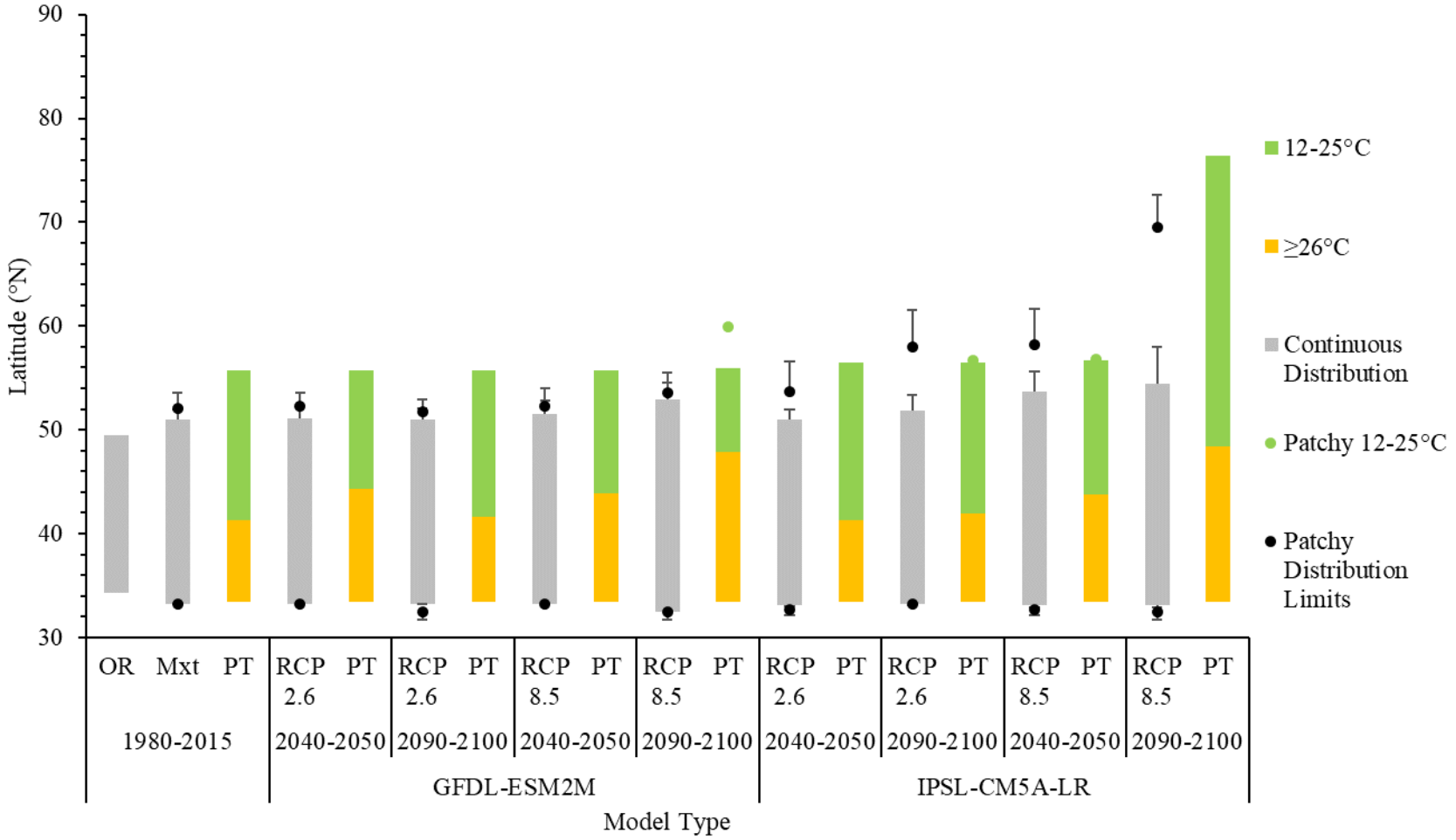

Figure D.d7 *Codium fragile* average relative northern and southern distribution limits (n=4, ±SE) over different time periods using occurrence records (OR), Maxent (Mxt), physiological thresholds (PT), and climate projections (RCP 2.6, 8.5 for two climate models). Grey bars show continuous distribution and black dots indicating patchy distribution. The PT colours indicate SST of 12-25°C (green, good growth) and >25°C (yellow, reduced growth).

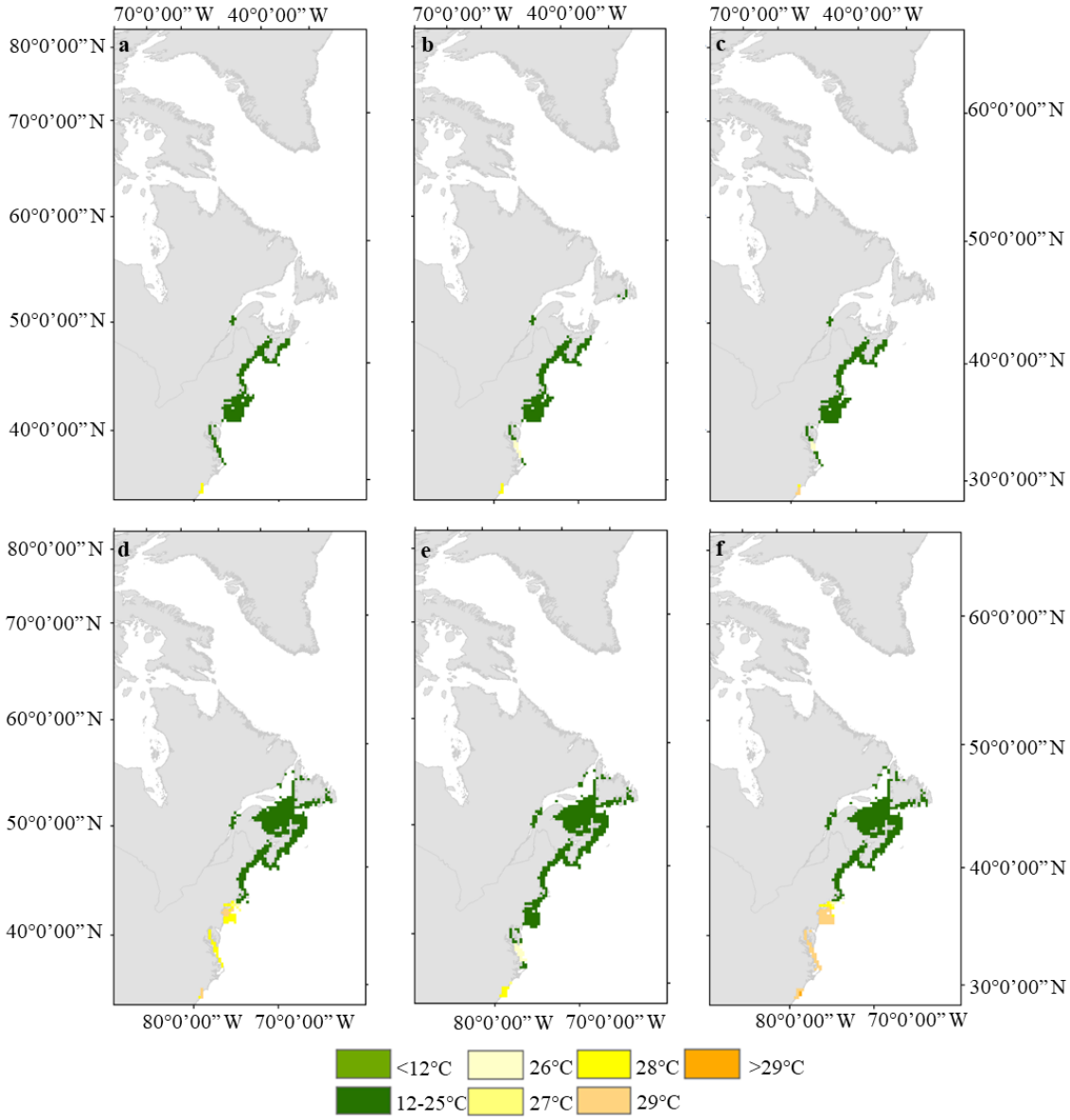

Figure D.8 Average Maxent model output (n=4) for *Codium fragile* for GFDL RCP 2.6 over **a** 2006-2015, **b** 2040-2050, and **c** 2090-2100, and for IPSL RCP 2.6 over **d** 2006-2015, **e** 2040-2050, and **f** 2090-2100 with corresponding physiological thresholds (PT). PT were overlaid over the distribution to show areas of good growth (green), and reduced growth (yellow-orange). Data is in an equal-area projection.

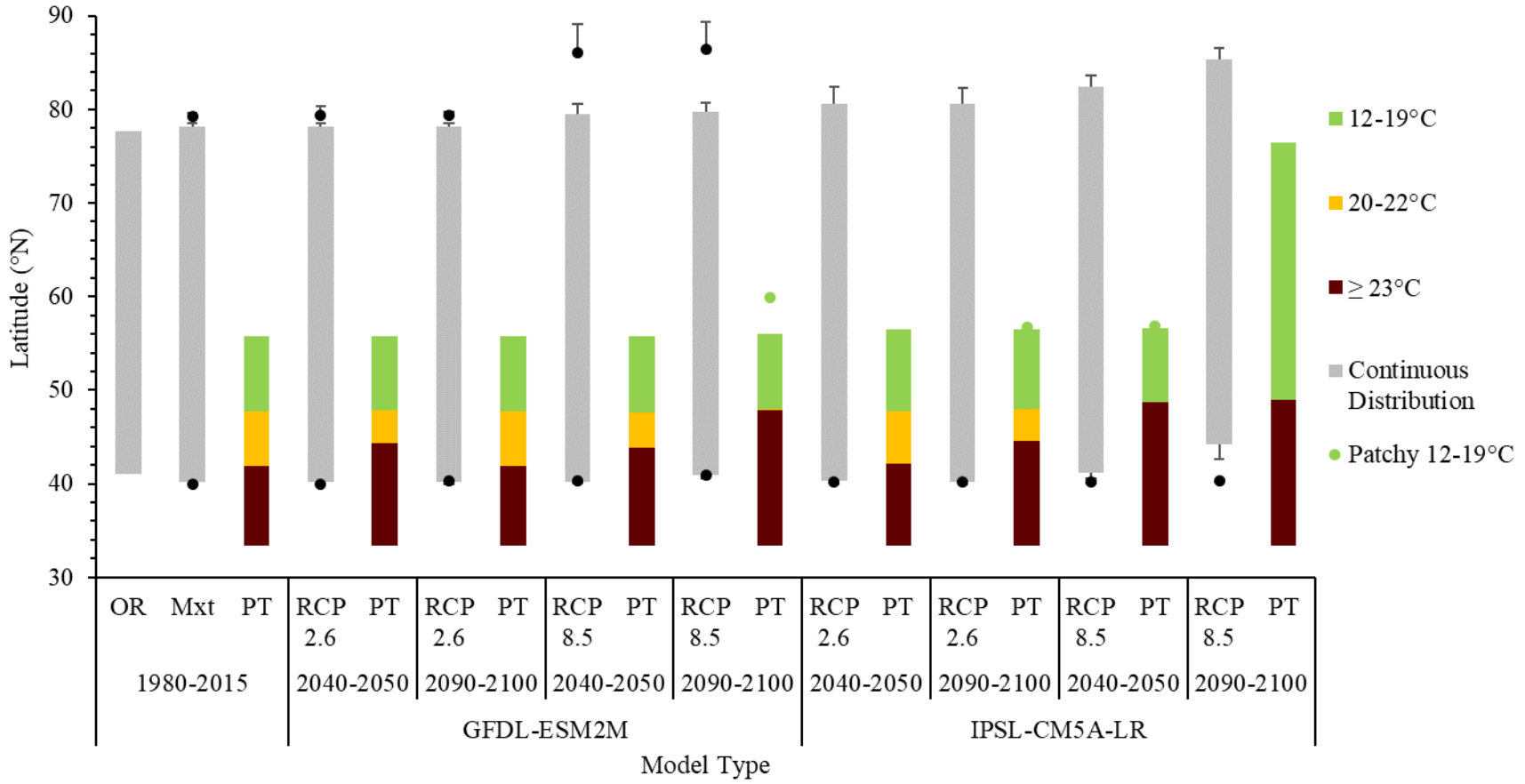

Figure D.9 *Saccharina latissima* average relative northern and southern distribution limits (n=5, ±SE) over different time periods using occurrence records (OR), Maxent (Mxt), physiological thresholds (PT), and climate projections (RCP 2.6, 8.5 for two climate models). Grey bars show continuous distribution and black dots indicating patchy distribution. The PT colours indicate SST of 12-19°C (green, good growth), 20-22°C (yellow, reduced growth and partial mortality), and >22°C (red, complete mortality).

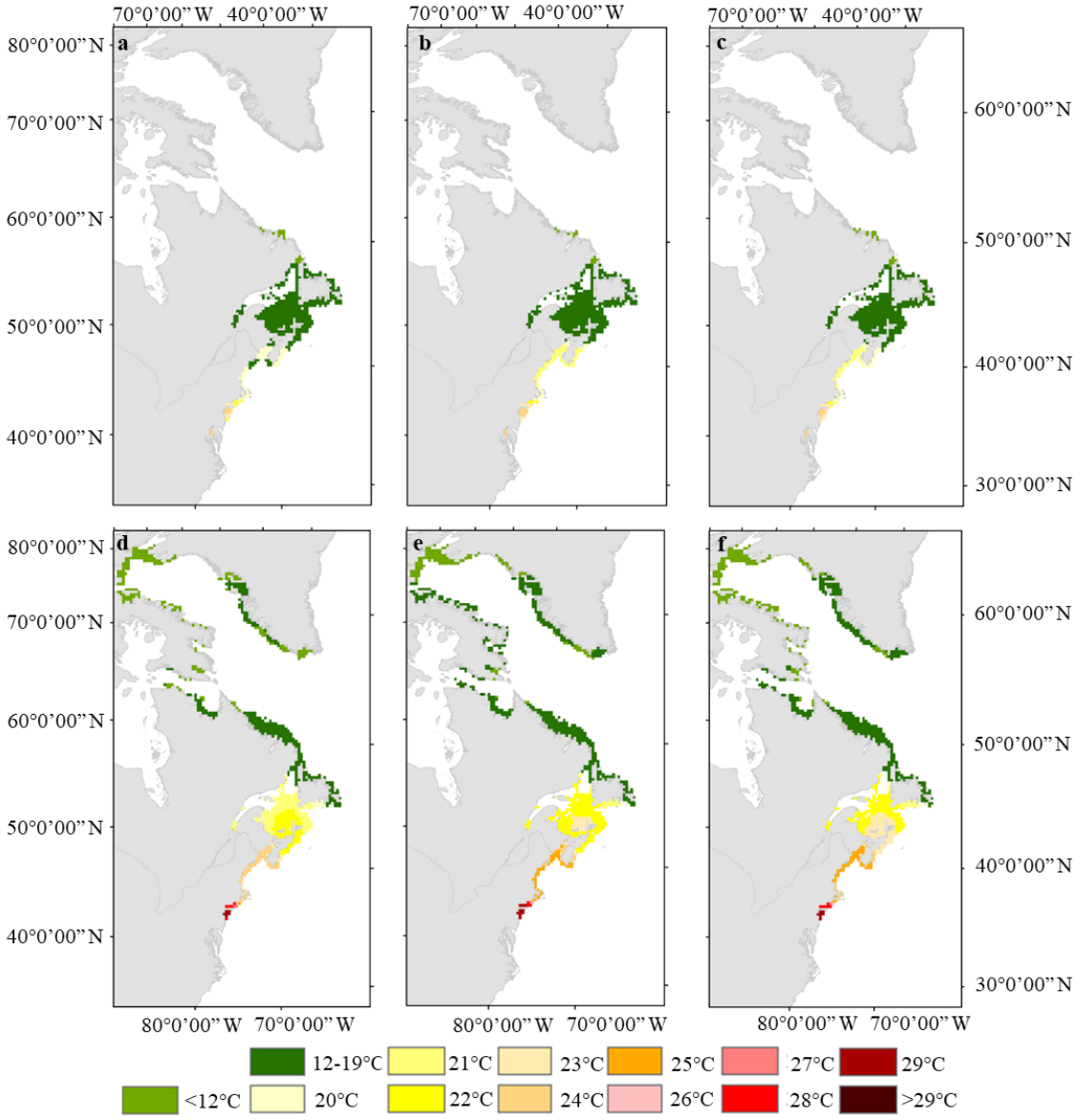

Figure D.10 Average Maxent model output (n=5) for *Saccharina latissima* for GFDL RCP 2.6 over **a** 2006-2015, **b** 2040-2050, and **c** 2090-2100, and for IPSL RCP 2.6 over **d** 2006-2015, **e** 2040-2050, and **f** 2090-2100 with corresponding physiological thresholds (PT). PT were overlaid over the distribution to show areas of good growth (green), reduced growth and partial mortality (yellow and complete mortality (orange-red). Data is in an equal-area projection.

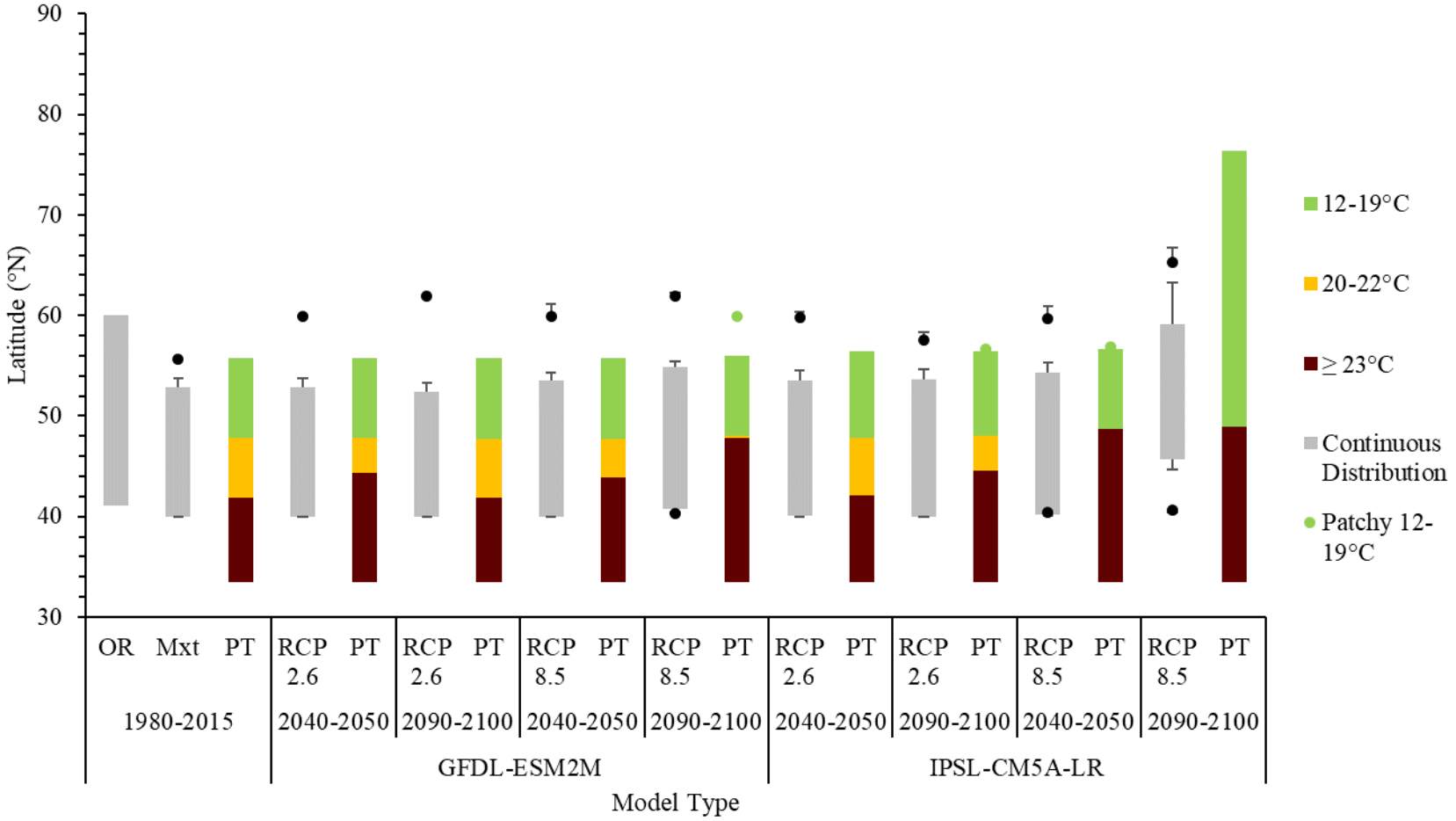

Figure D.11 *Laminaria digitata* average relative northern and southern distribution limits (n=4, ±SE) over different time periods using occurrence records (OR), Maxent (Mxt), physiological thresholds (PT), and climate projections (RCP 2.6, 8.5 for two climate models). Grey bars show continuous distribution and black dots indicating patchy distribution. The PT colours indicate SST of 12-19°C (green, good growth), 20-22°C (yellow, reduced growth and partial mortality), and >22°C (red, complete mortality).

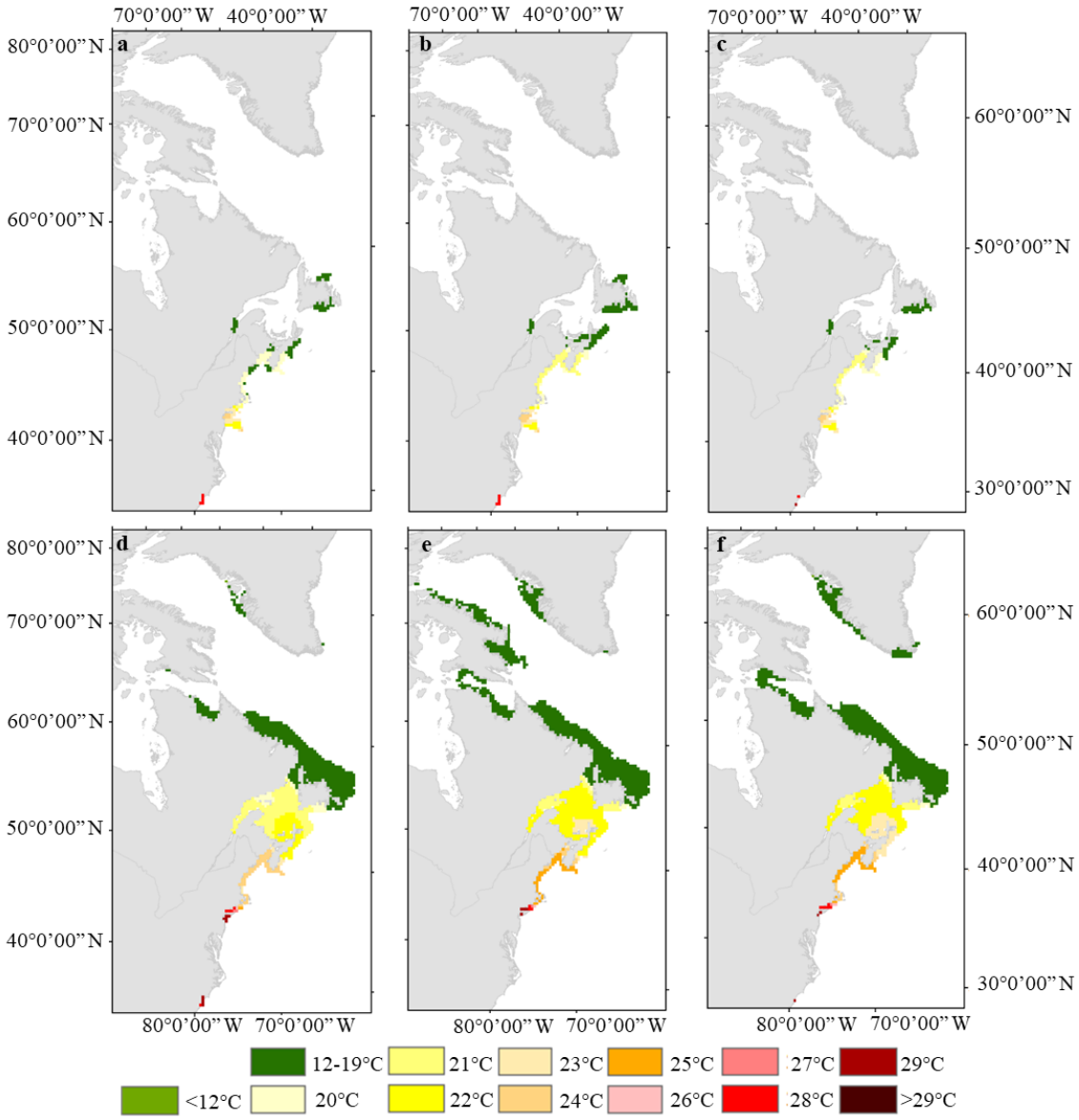

Figure D.12 Average Maxent model output (n=5) for *Laminaria digitata* for GFDL RCP 2.6 over **a** 2006-2015, **b** 2040-2050, and **c** 2090-2100, and for IPSL RCP 2.6 over **d** 2006-2015, **e** 2040-2050, and **f** 2090-2100 with corresponding physiological thresholds (PT). PT were overlaid over the distribution to show areas of good growth (green), reduced growth and partial mortality (yellow), and complete mortality (orange-red). Data is in an equal-area projection.

Appendix E: Port Mouton and Port Joli Classification

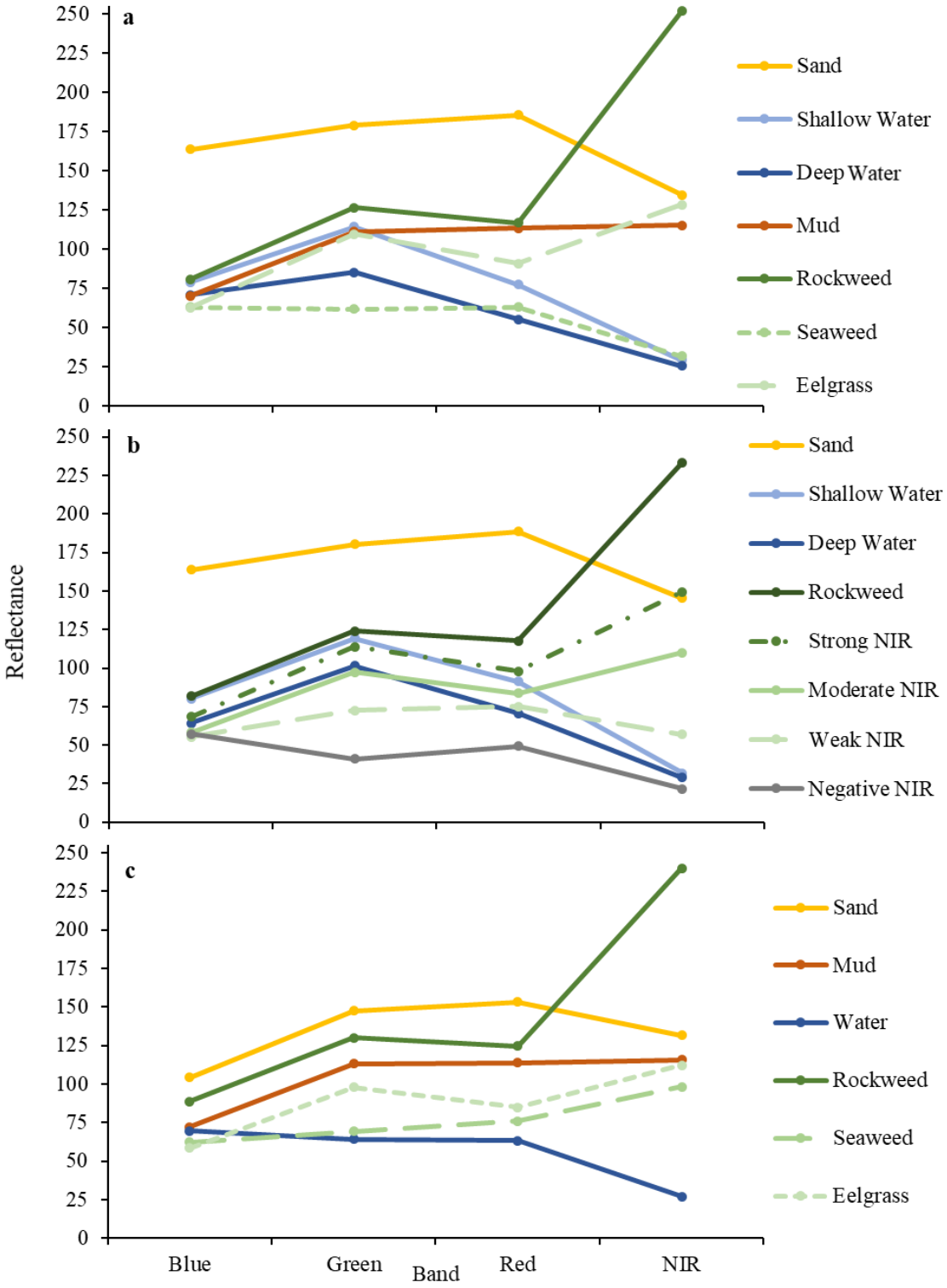

Figure E.1 Training sites spectral signature plots used to build **a** the supervised maximum likelihood classification, and **b** the unsupervised classification first iteration maximum likelihood and **c** second iteration maximum likelihood classification.

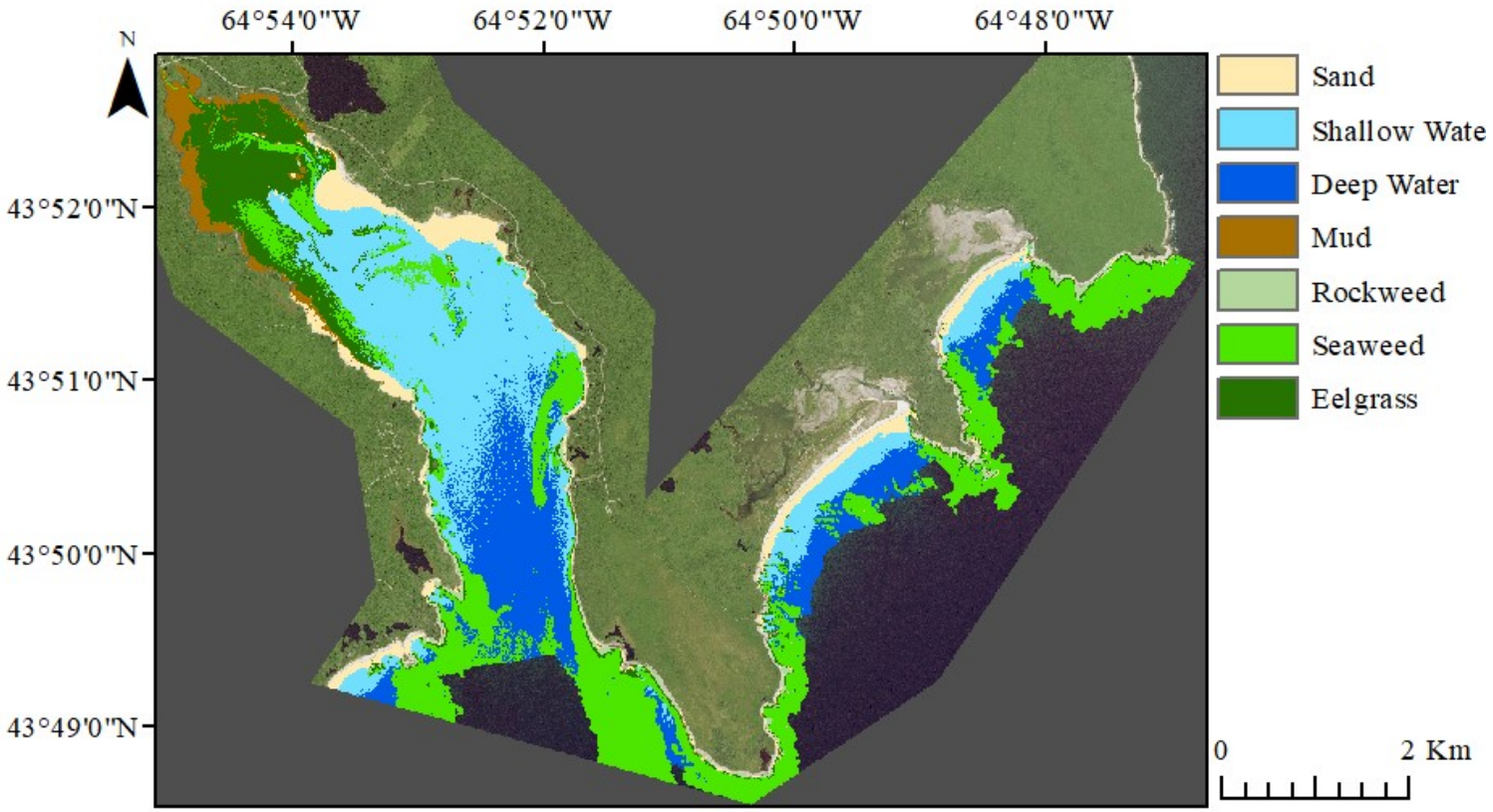

Figure E.2 Supervised maximum likelihood classification in Port Joli, on all four bands which were atmospherically corrected, run through a 3x3 majority filter, land and deep water (>8m) masked out run through a 3x3 majority filter. The classification was overlaid over a true colour composite. Dark grey is background data outside the satellite imagery bounds.

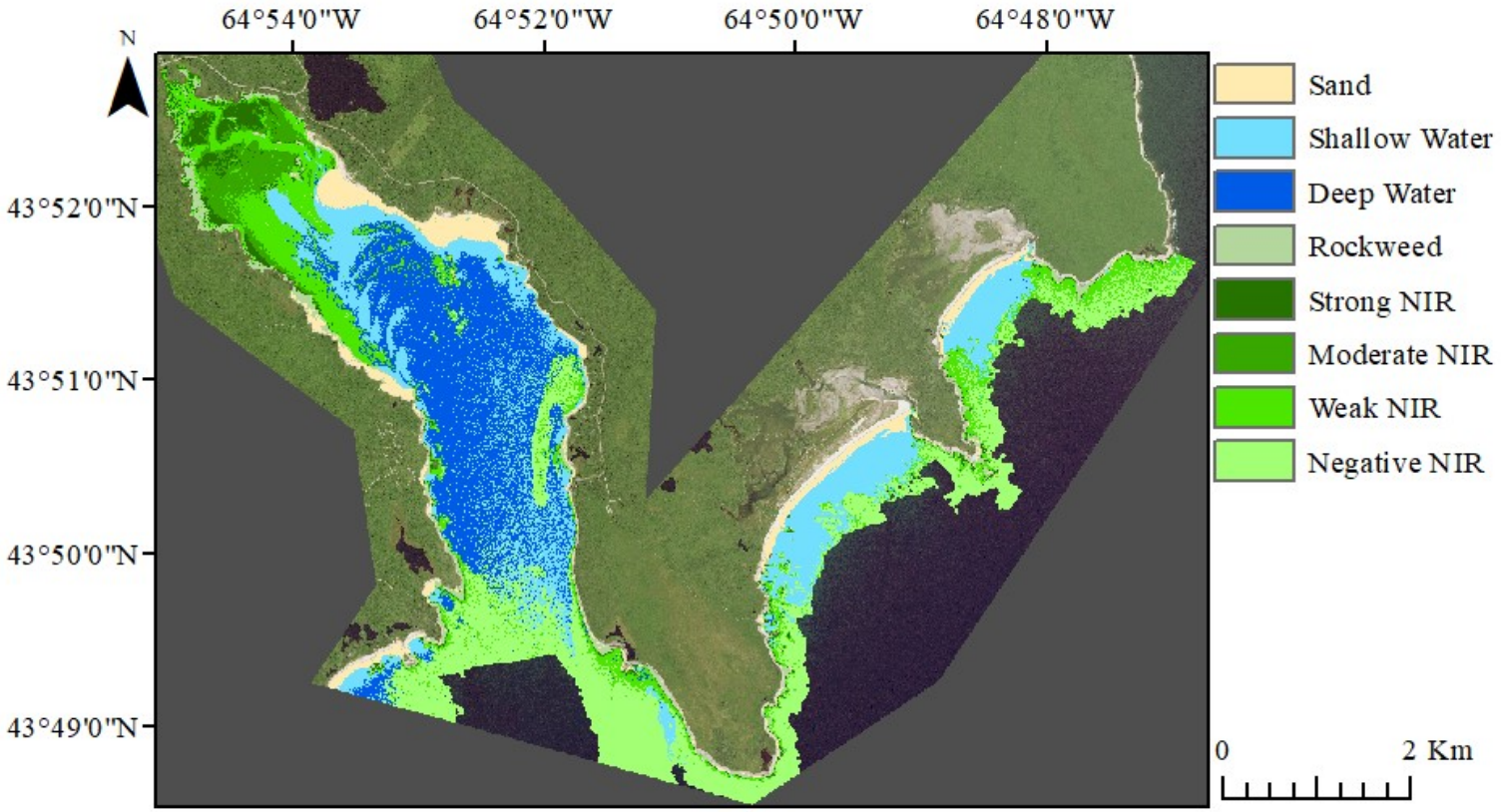

Figure E.3 First iteration of the unsupervised classification in Port Joli showing the results of a maximum likelihood classification, based on training sites created with ISOCLUST, on all four bands which were atmospherically corrected, run through a 3x3 majority filter, land and deep water (>8m) masked out run through a 3x3 majority filter. The classification was overlaid over a true colour composite. Dark grey is background data outside the satellite imagery bounds.

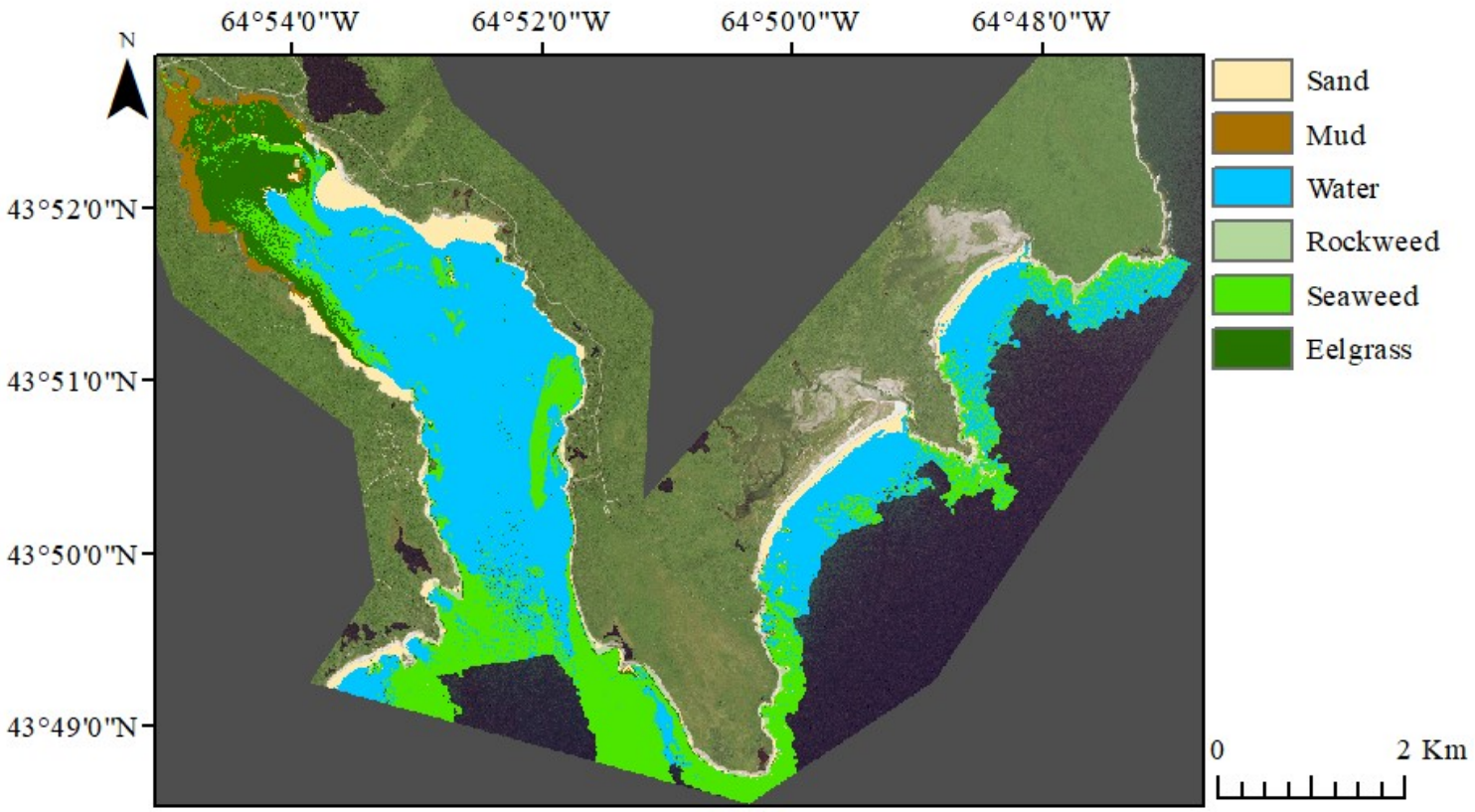

Figure E.4 Second iteration of the unsupervised classification in Port Joli showing the results of a maximum likelihood classification, based on training sites created with ISOCLUST, on all four bands which were atmospherically corrected, run through a 3x3 majority filter, land and deep water (>8m) masked out run through a 3x3 majority filter. The classification was overlaid over a true colour composite. Dark grey is background data outside the satellite imagery bounds.

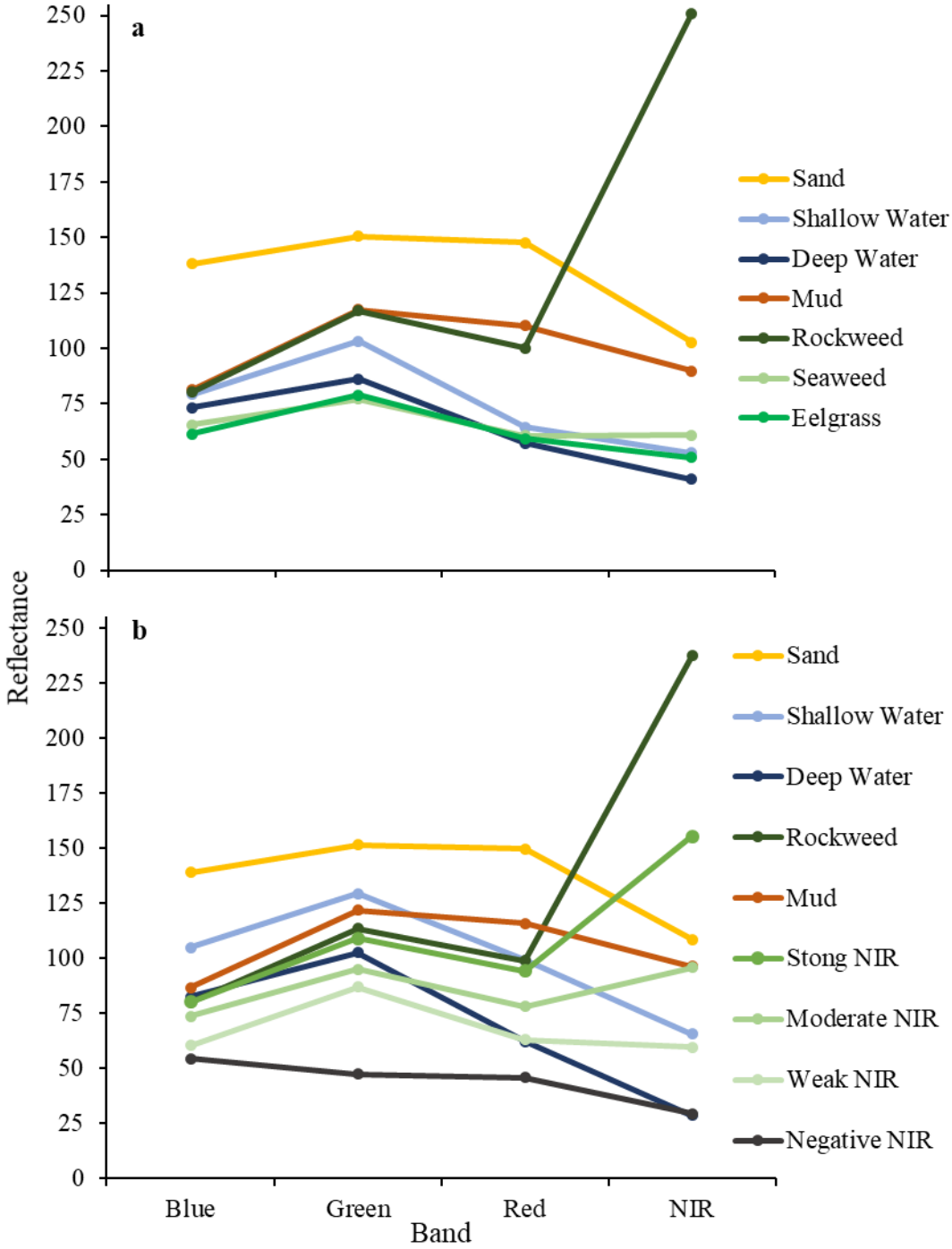

Figure E.5 Training sites spectral signature plots used to build **a** supervised maximum likelihood classification, **b** the first maximum likelihood classification from the first ISOCLUST run, for the whole of Port Mouton.

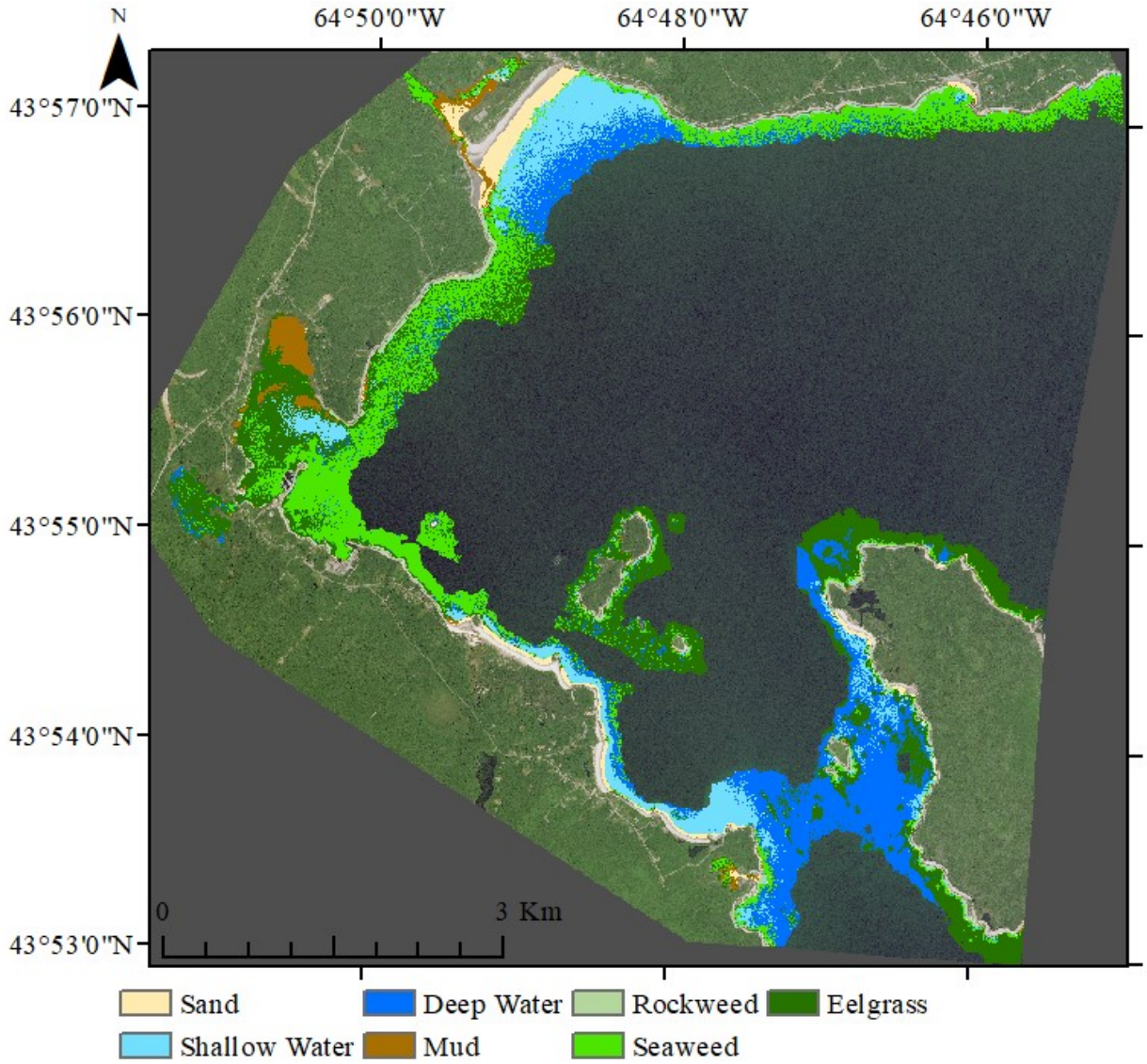

Figure E.6 Supervised maximum likelihood classification in Port Mouton, on all four bands which were atmospherically corrected, run through a 3x3 majority filter, land and deep water (>8m) masked out run through a 3x3 majority filter. The classification was overlaid over a true colour composite. Dark grey is background data outside the satellite imagery bounds.

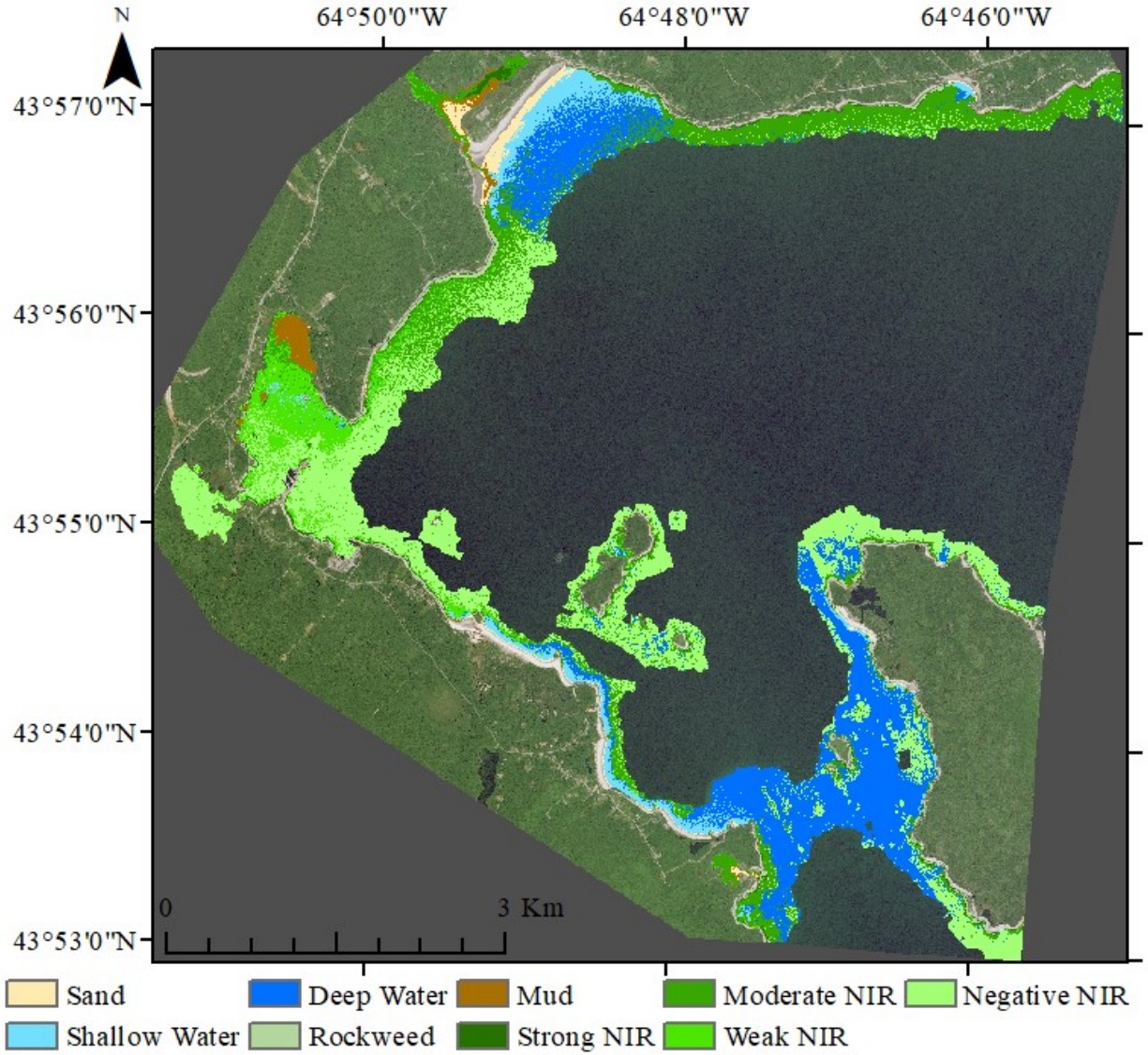

Figure E.7 First iteration of the unsupervised classification in Port Mouton showing the results of a maximum likelihood classification, based on training sites created with ISOCLUST, on all four bands which were atmospherically corrected, run through a 3x3 majority filter, land and deep water (>8m) masked out run through a 3x3 majority filter. The classification was overlaid over a true colour composite. Dark grey is background data outside the satellite imagery bounds.

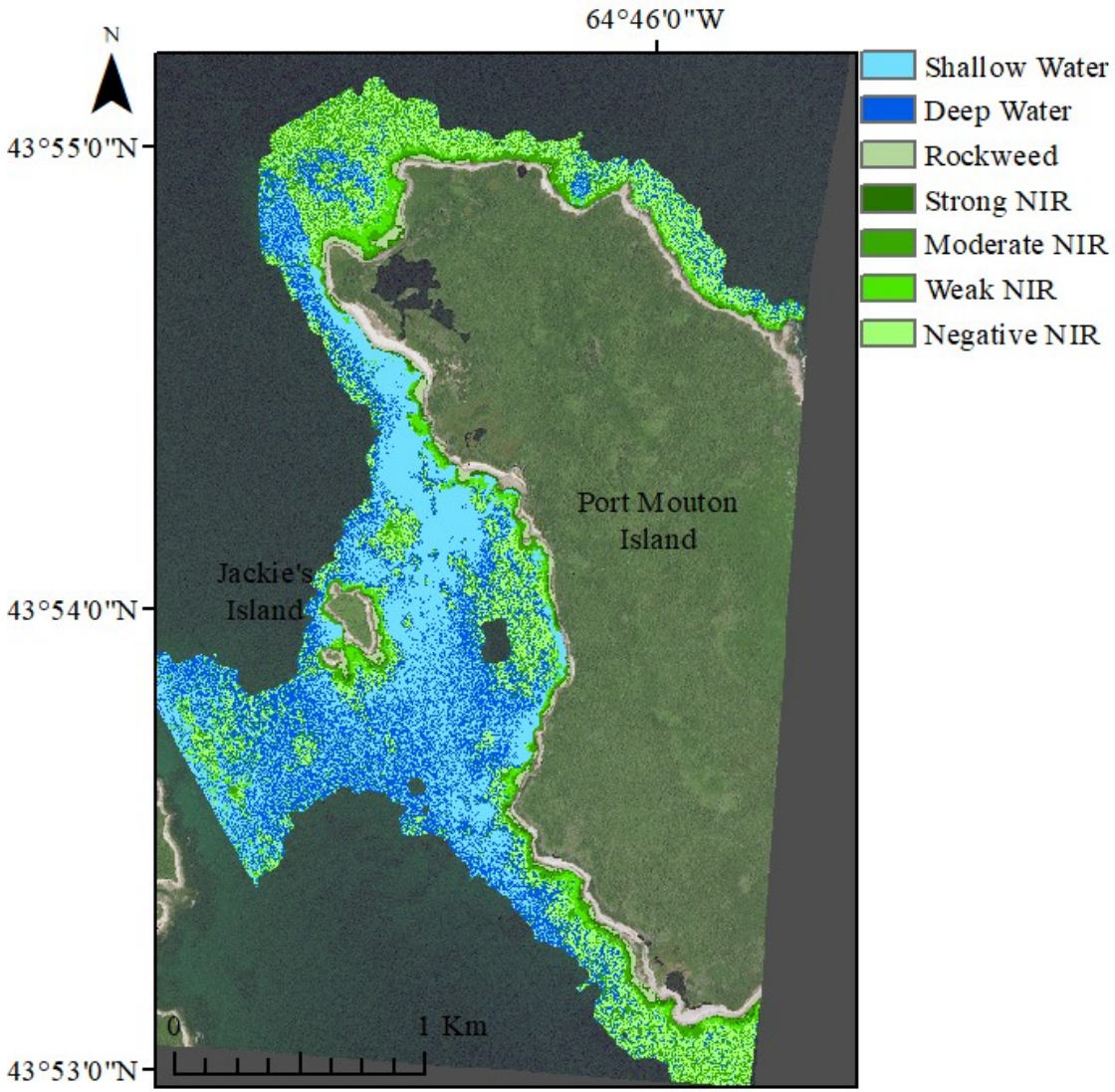

Figure E.8 First iteration of the unsupervised classification in Port Mouton showing the results of a maximum likelihood classification, based on training sites created with ISOCLUST for Segment one. The classification was run on all four bands which were atmospherically corrected, run through a 3x3 majority filter, land and deep water (>8m) masked out run through a 3x3 majority filter. The classification was overlaid over a true colour composite. Dark grey is background data outside the satellite imagery bounds.

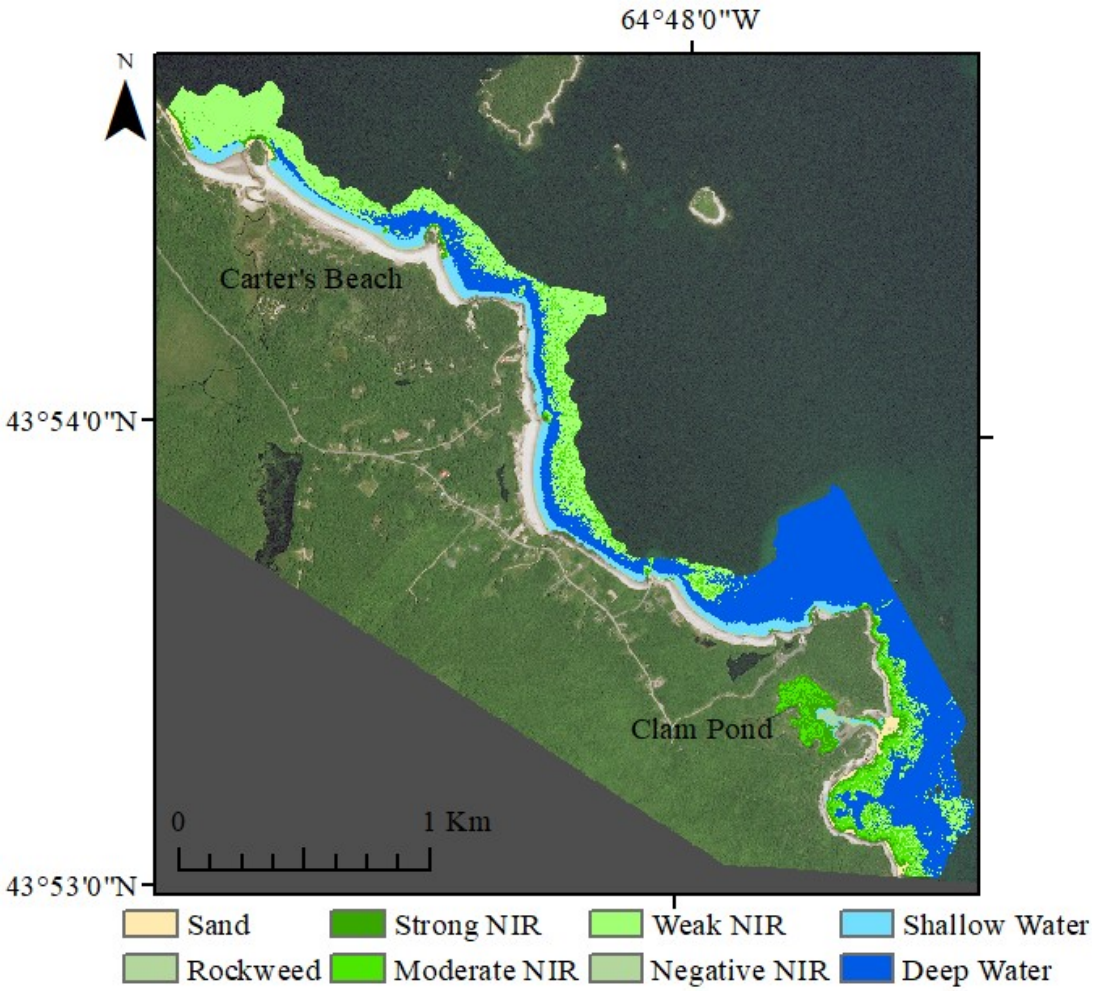

Figure E.9 First iteration of the unsupervised classification in Port Mouton showing the results of a maximum likelihood classification, based on training sites created with ISOCLUST for Segment two. The classification was run on all four bands which were atmospherically corrected, run through a 3x3 majority filter, land and deep water (>8m) masked out run through a 3x3 majority filter. The classification was overlaid over a true colour composite. Dark grey is background data outside the satellite imagery bounds.

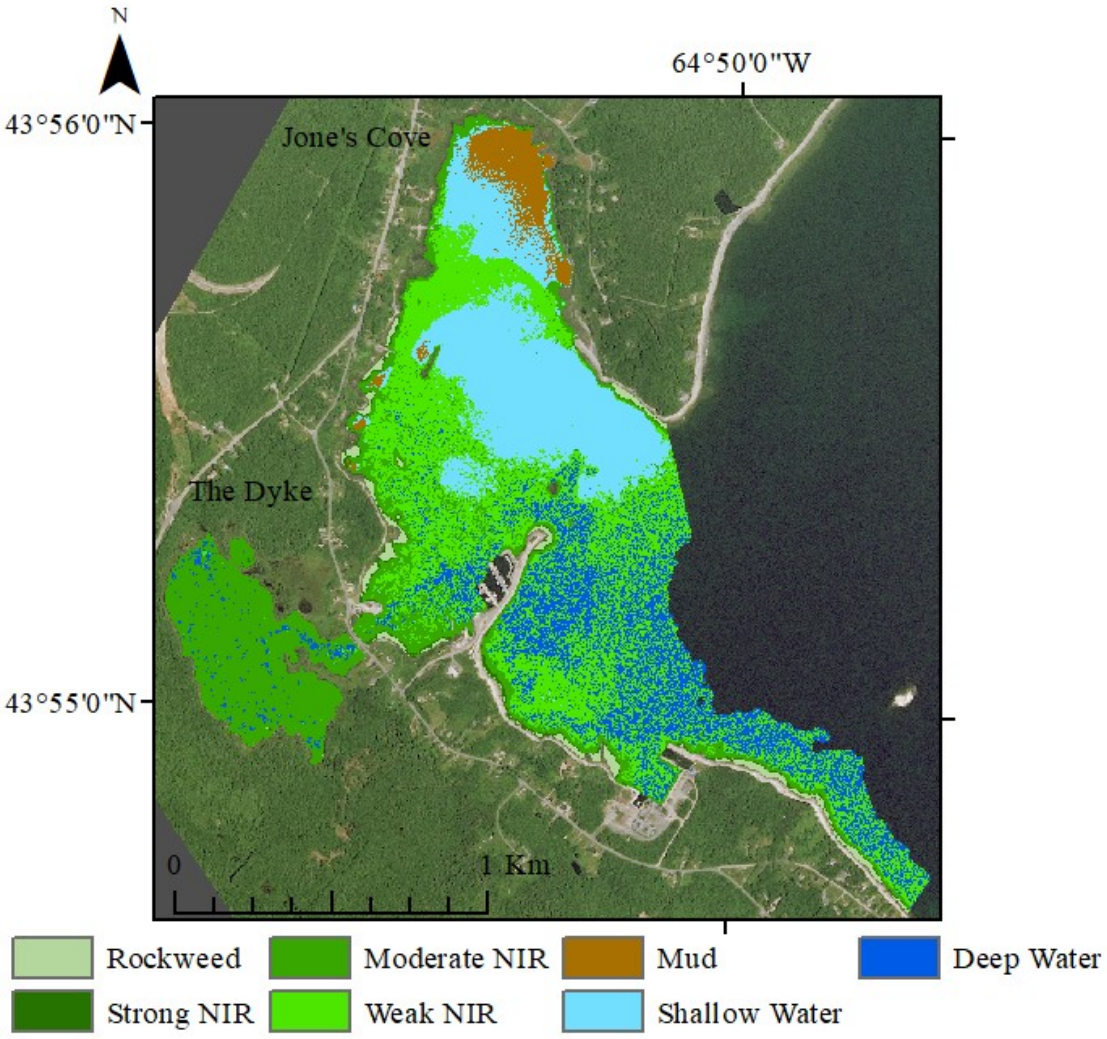

Figure E.10 First iteration of the unsupervised classification in Port Mouton showing the results of a maximum likelihood classification, based on training sites created with ISOCLUST for Segment three. The classification was run on all four bands which were atmospherically corrected, run through a 3x3 majority filter, land and deep water (>8m) masked out run through a 3x3 majority filter. The classification was overlaid over a true colour composite. Dark grey is background data outside the satellite imagery bounds.

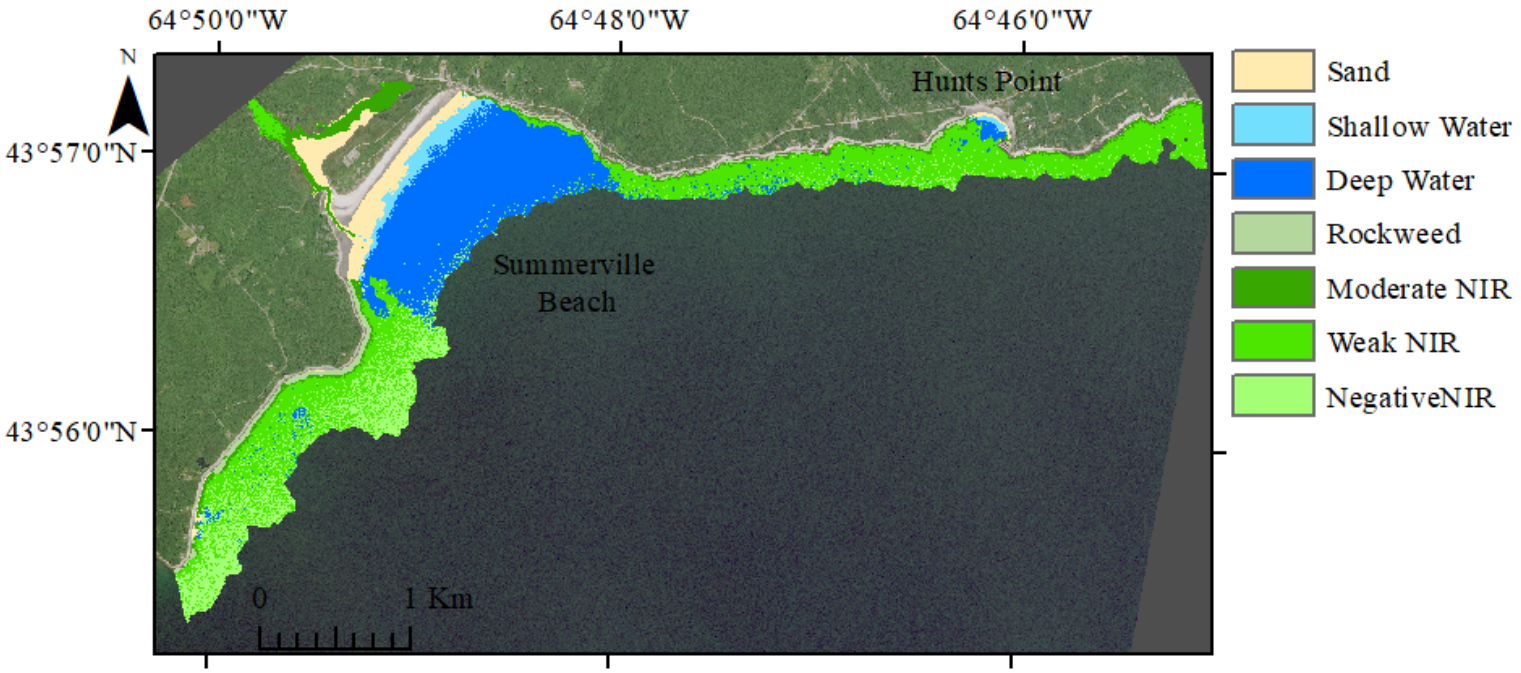

Figure E.11 First iteration of the unsupervised classification in Port Mouton showing the results of a maximum likelihood classification, based on training sites created with ISOCLUST for Segment four. The classification was run on all four bands which were atmospherically corrected, run through a 3x3 majority filter, land and deep water (>8m) masked out run through a 3x3 majority filter. The classification was overlaid over a true colour composite. Dark grey is background data outside the satellite imagery bounds.

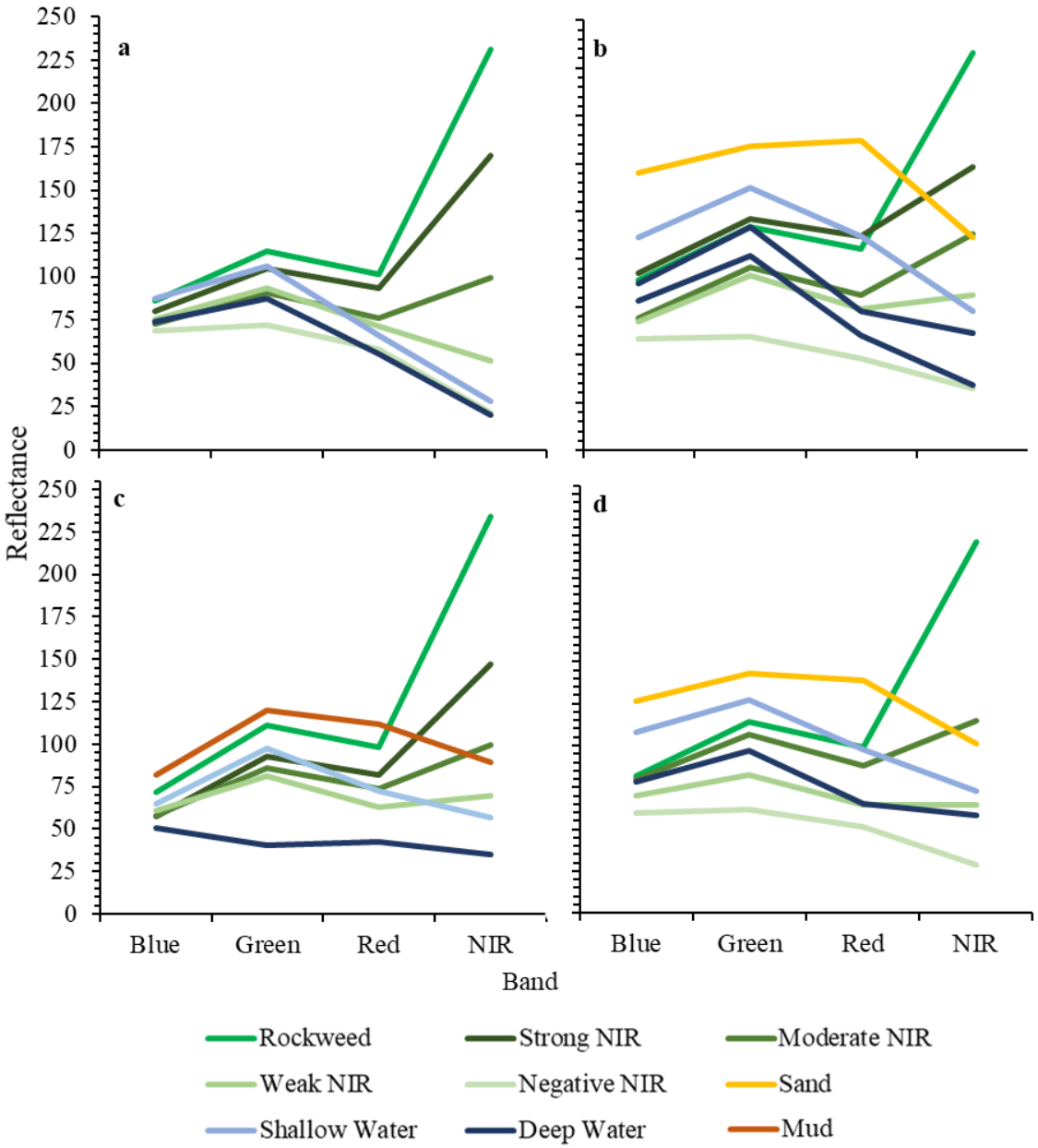

Figure E.12 Training sites spectral signature plots for the training sites created with ISOCLUST to be used in the maximum likelihood classification for the first iteration of the unsupervised classification for **a** Segment one, **b** two, **c** three, and **d** four in Port Mouton.

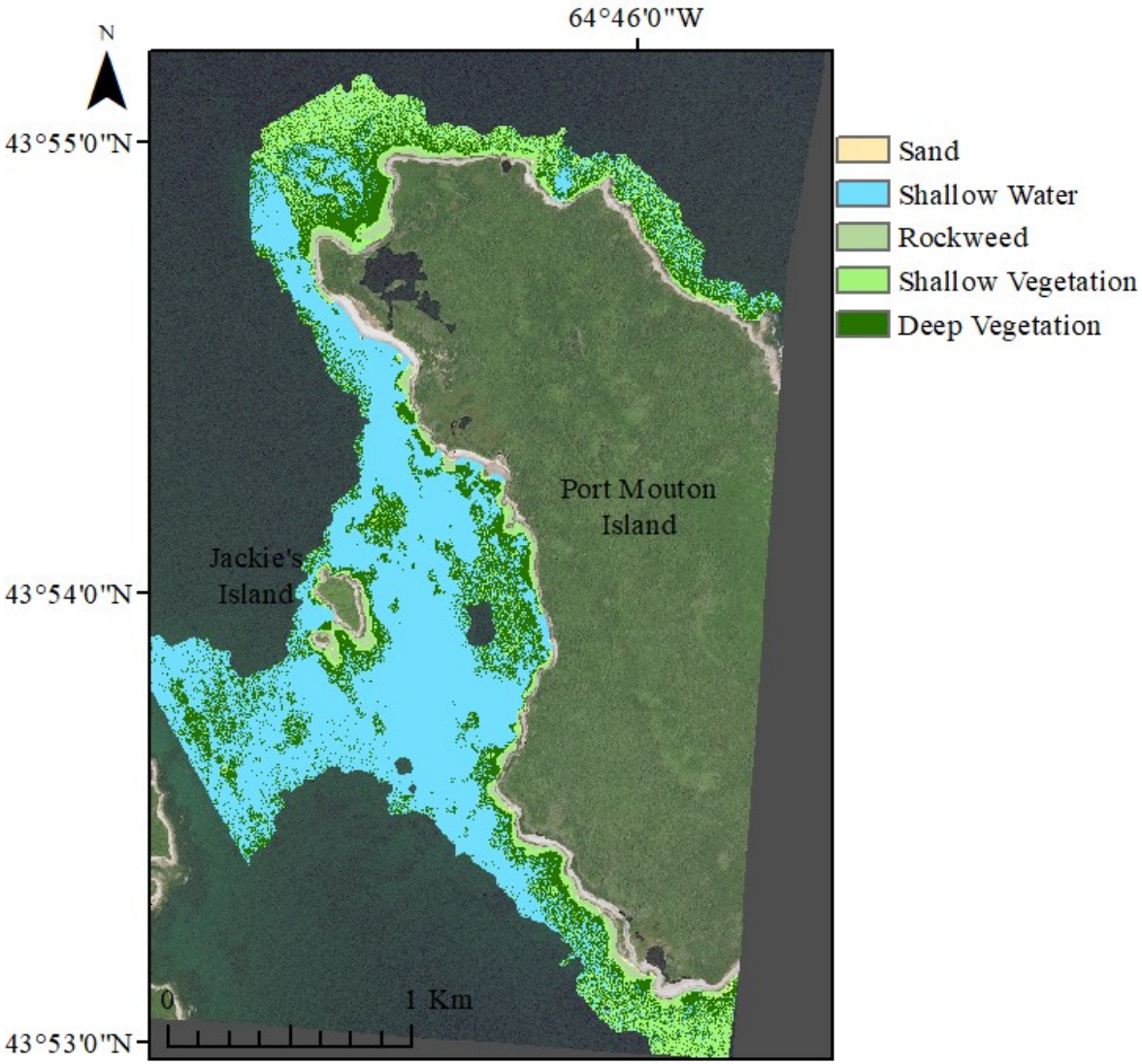

Figure E.13 Second iteration of the unsupervised classification in Port Mouton showing the results of a maximum likelihood classification, based on training sites created with ISOCLUST for Segment one. The classification was run on all four bands which were atmospherically corrected, run through a 3x3 majority filter, land and deep water (>8m) masked out run through a 3x3 majority filter. The classification was overlaid over a true colour composite. Dark grey is background data outside the satellite imagery bounds.

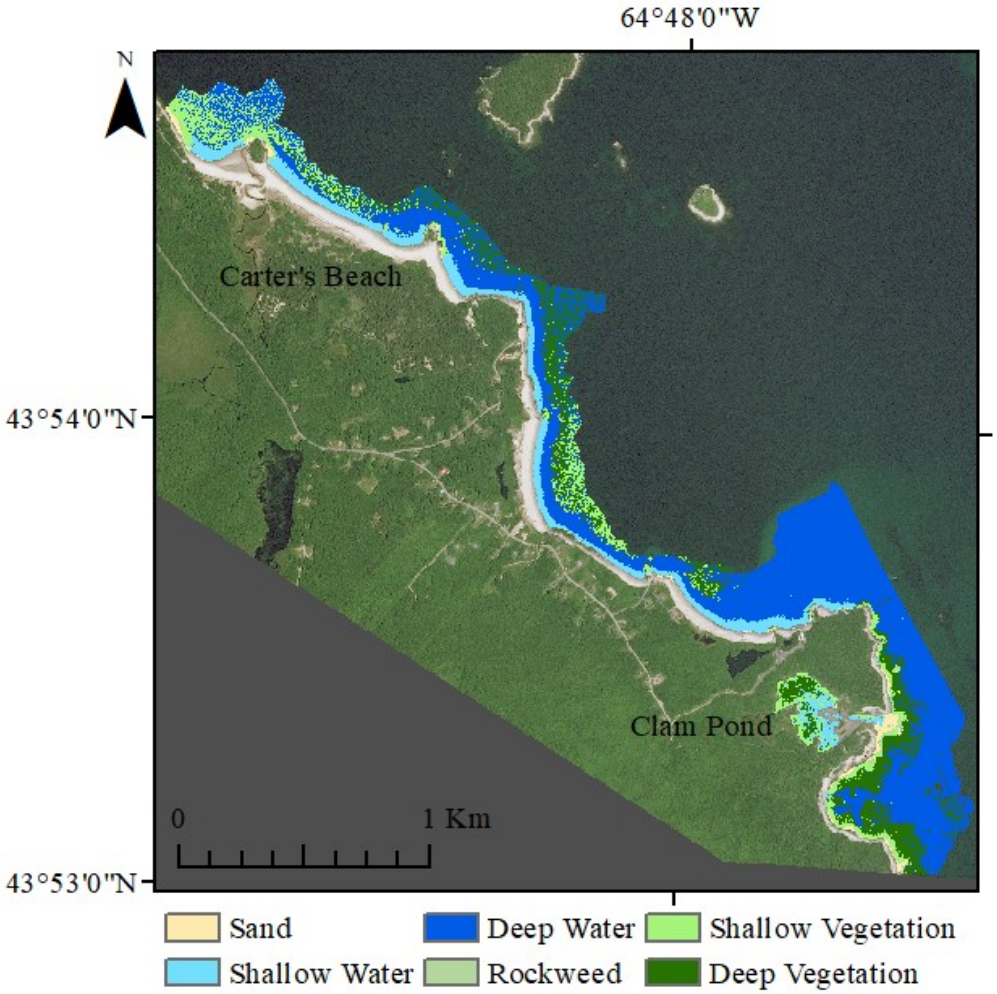

Figure E.14 Second iteration of the unsupervised classification in Port Mouton showing the results of a maximum likelihood classification, based on training sites created with ISOCLUST for Segment two. The classification was run on all four bands which were atmospherically corrected, run through a 3x3 majority filter, land and deep water (>8m) masked out run through a 3x3 majority filter. The classification was overlaid over a true colour composite. Dark grey is background data outside the satellite imagery bounds.

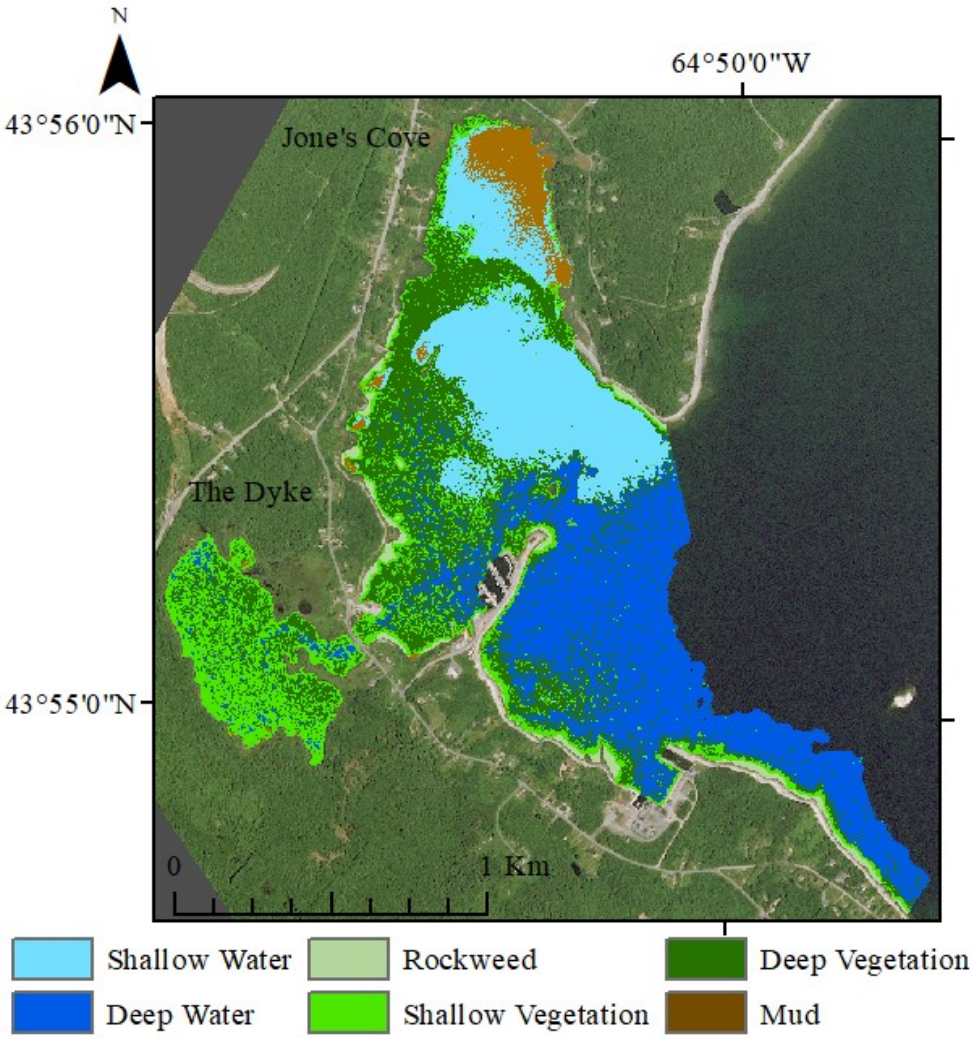

Figure E.15 Second iteration of the unsupervised classification in Port Mouton showing the results of a maximum likelihood classification, based on training sites created with ISOCLUST for Segment three. The classification was run on all four bands which were atmospherically corrected, run through a 3x3 majority filter, land and deep water (>8m) masked out run through a 3x3 majority filter. The classification was overlaid over a true colour composite. Dark grey is background data outside the satellite imagery bounds.

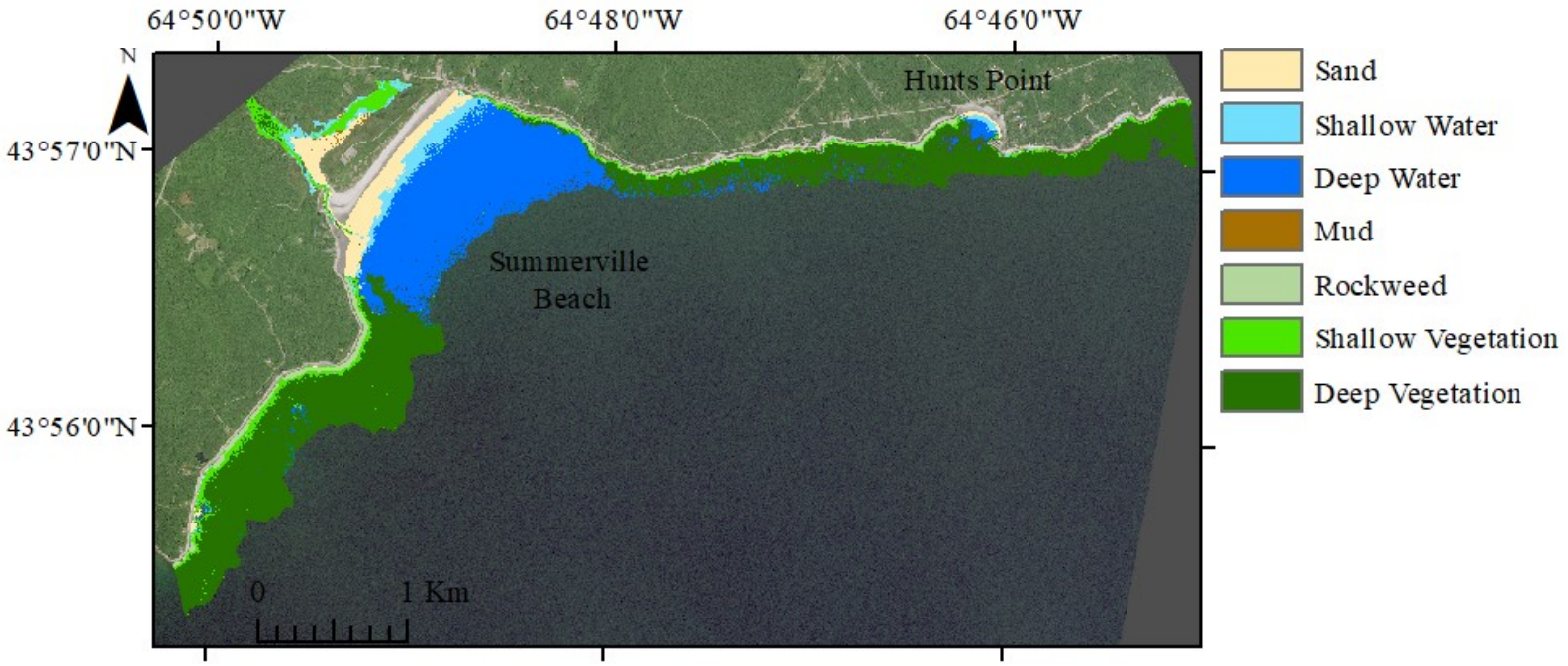

Figure E.16 Second iteration of the unsupervised classification in Port Mouton showing the results of a maximum likelihood classification, based on training sites created with ISOCLUST for Segment four. The classification was run on all four bands which were atmospherically corrected, run through a 3x3 majority filter, land and deep water (>8m) masked out run through a 3x3 majority filter. The classification was overlaid over a true colour composite. Dark grey is background data outside the satellite imagery bounds..

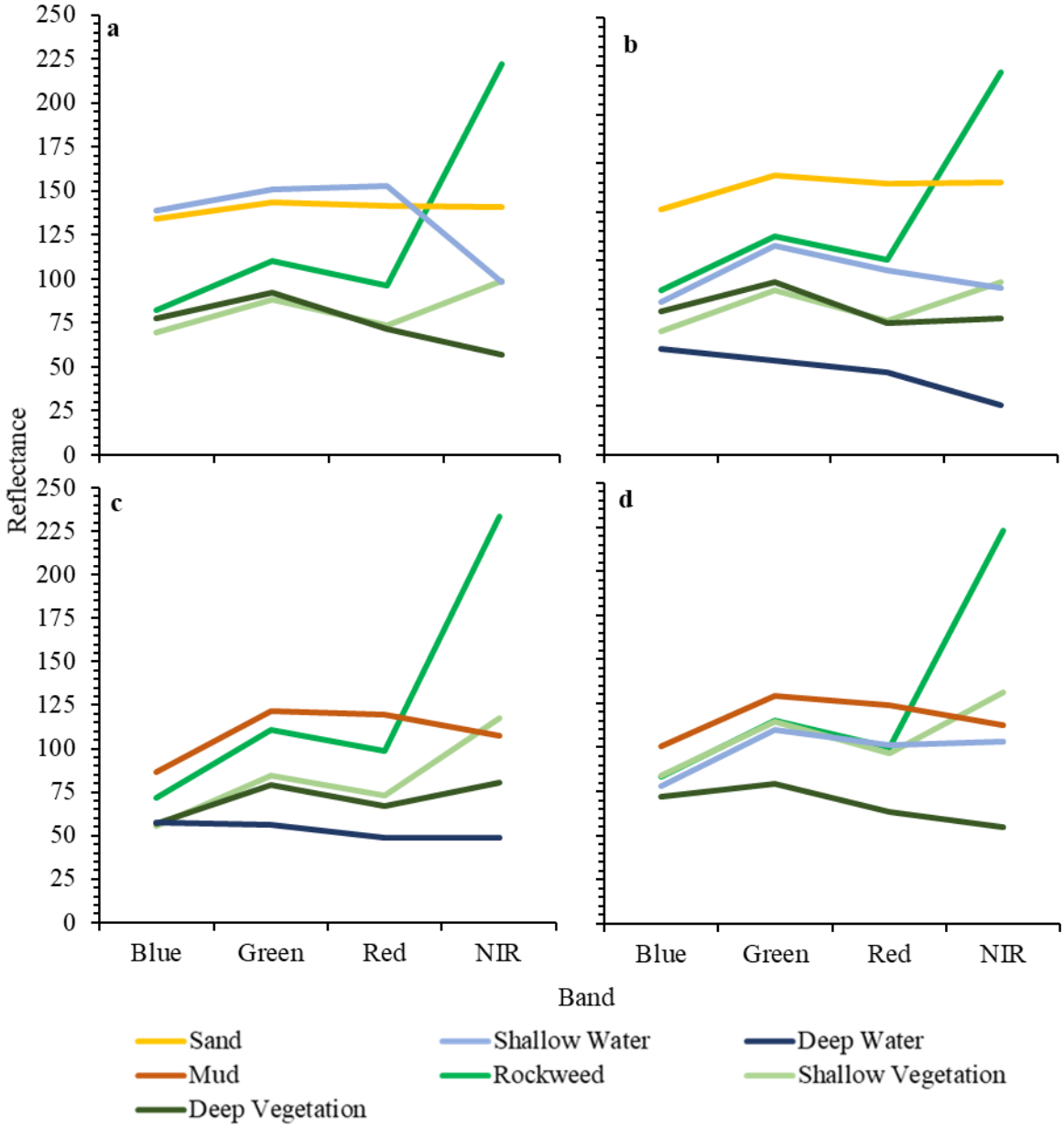

Figure E.17 Training sites spectral signature plots for the training sites created with ISOCLUST to be used in the maximum likelihood classification for the second iteration of the unsupervised classification for **a** Segment one, **b** two, **c** three, and **d** four in Port Mouton.

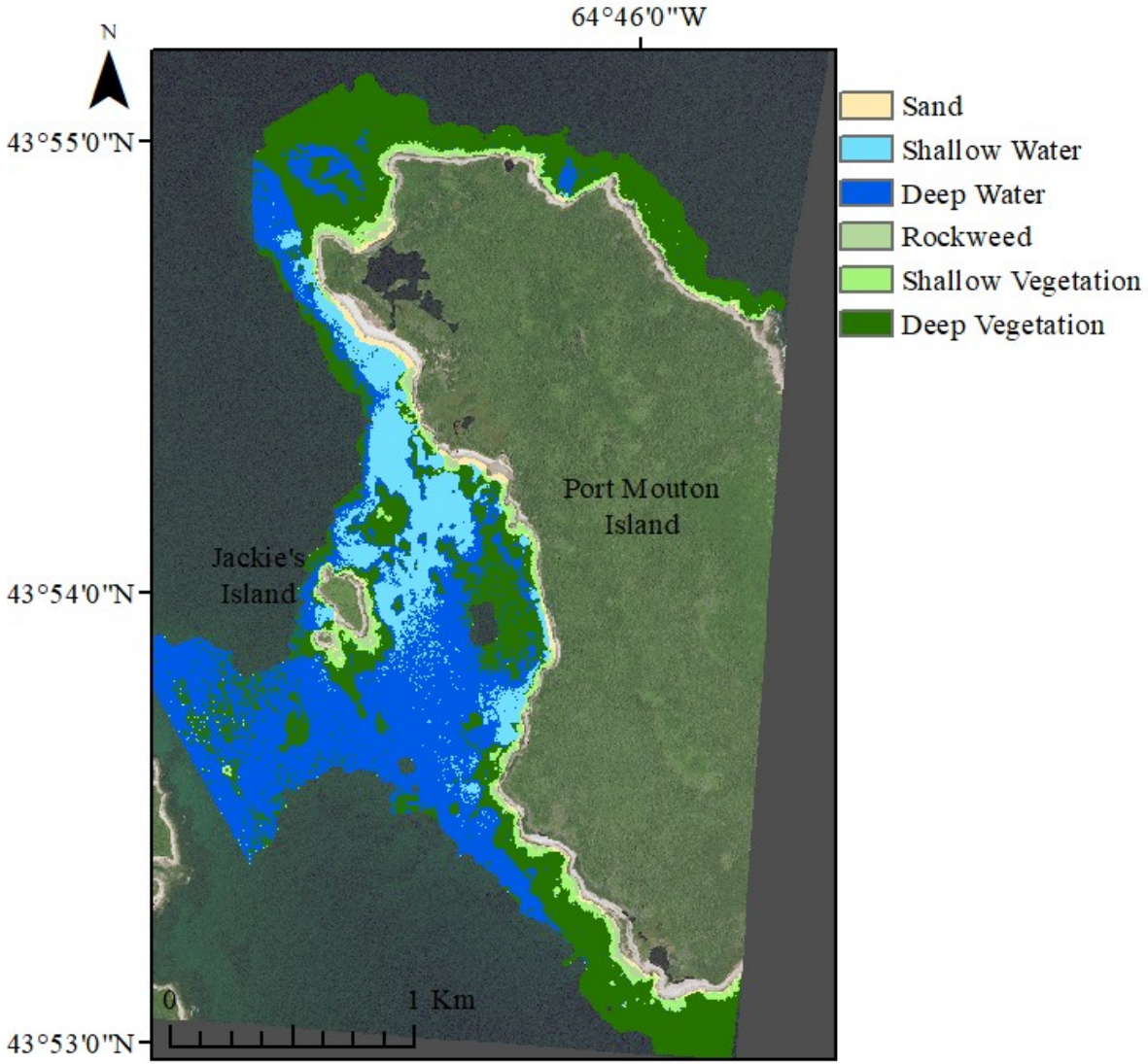

Figure E.18 Supervised maximum likelihood classification in Port Mouton for Segment one on all four bands which were atmospherically corrected, run through a 3x3 majority filter, land and deep water (>8m) masked out run through a 3x3 majority filter. The classification was overlaid over a true colour composite. Dark grey is background data outside the satellite imagery bounds.

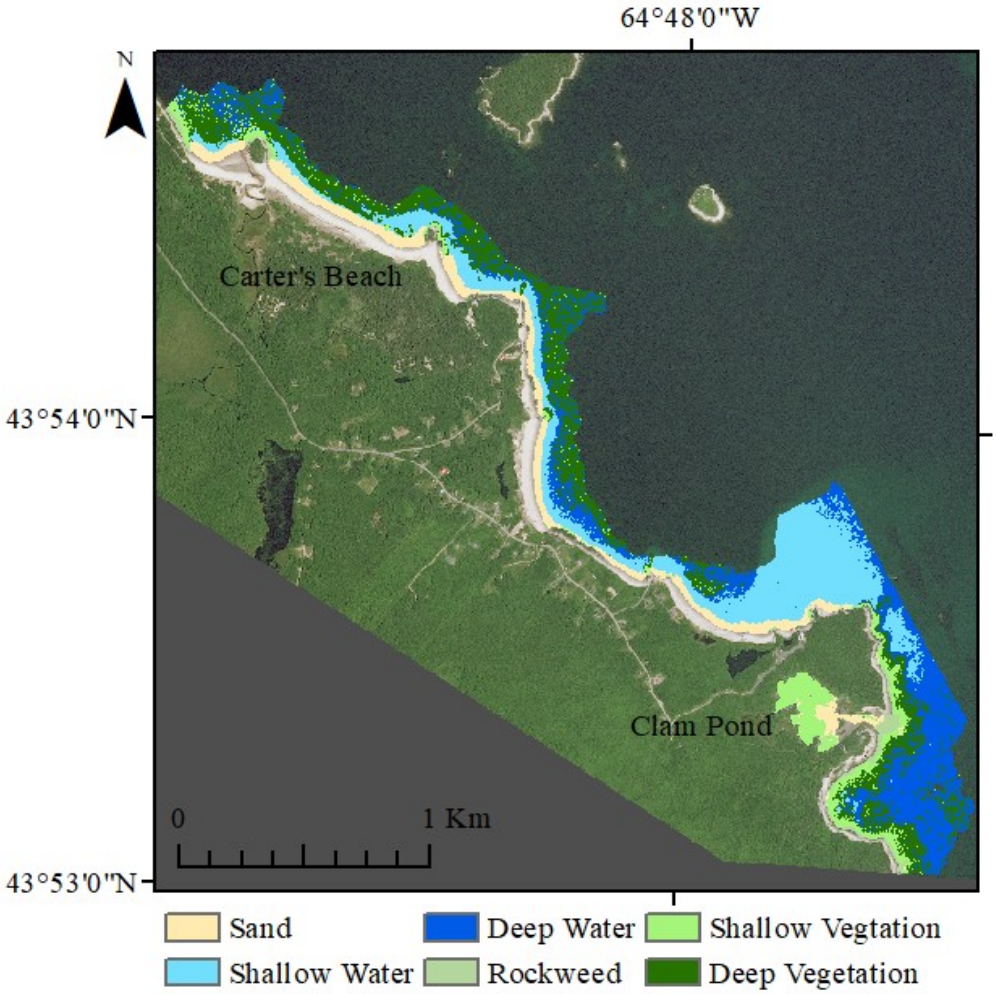

Figure E.19 Supervised maximum likelihood classification in Port Mouton for Segment two on all four bands which were atmospherically corrected, run through a 3x3 majority filter, land and deep water (>8m) masked out run through a 3x3 majority filter. The classification was overlaid over a true colour composite. Dark grey is background data outside the satellite imagery bounds.

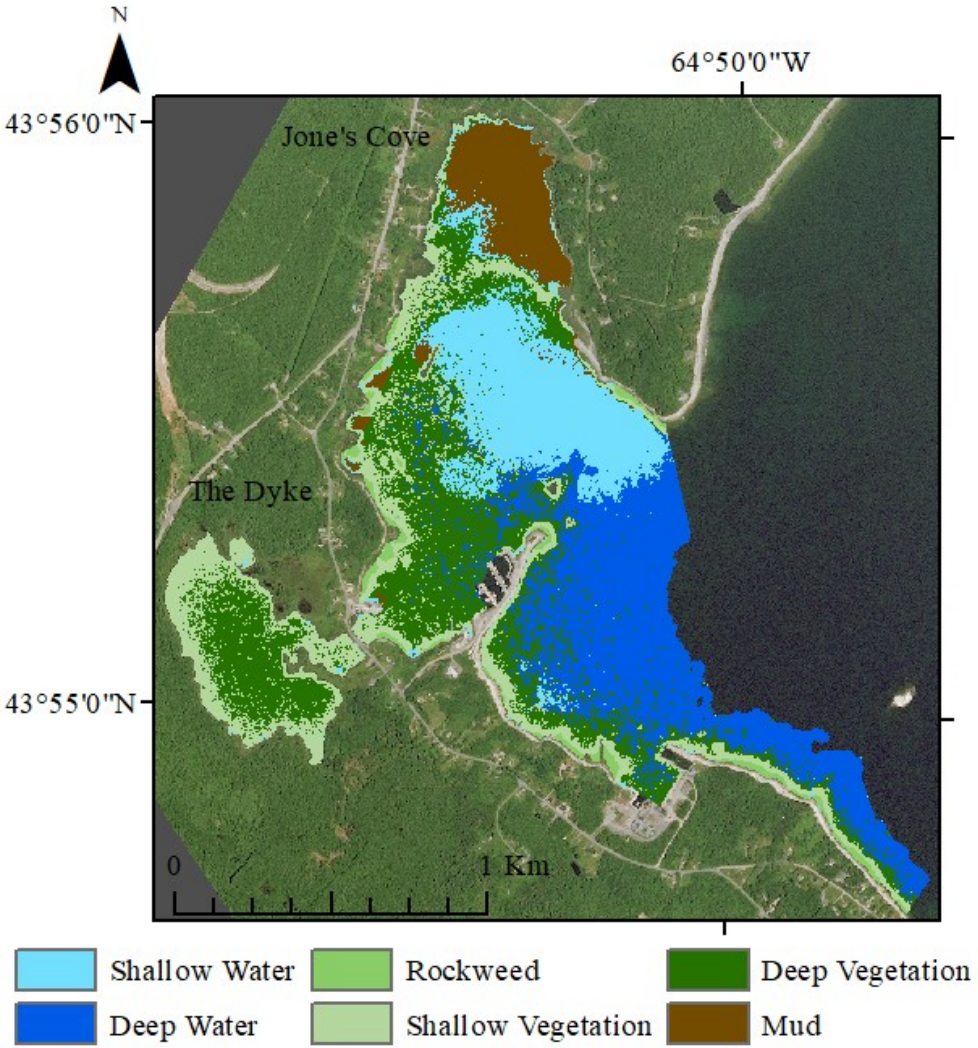

Figure E.20 Supervised maximum likelihood classification in Port Mouton for Segment three on all four bands which were atmospherically corrected, run through a 3x3 majority filter, land and deep water (>8m) masked out run through a 3x3 majority filter. The classification was overlaid over a true colour composite. Dark grey is background data outside the satellite imagery bounds.

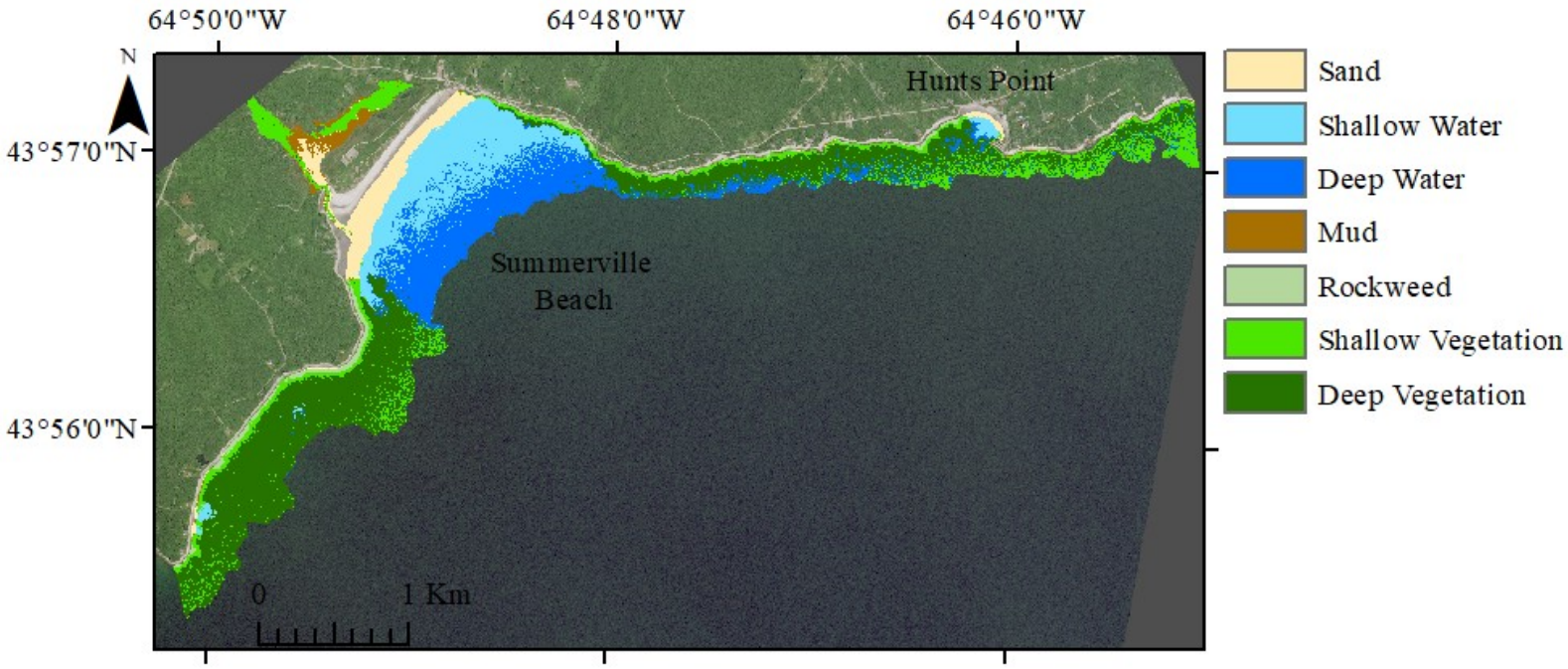

Figure E.21 Supervised maximum likelihood classification in Port Mouton for Segment four on all four bands which were atmospherically corrected, run through a 3x3 majority filter, land and deep water (>8m) masked out run through a 3x3 majority filter. The classification was overlaid over a true colour composite. Dark grey is background data outside the satellite imagery bounds..

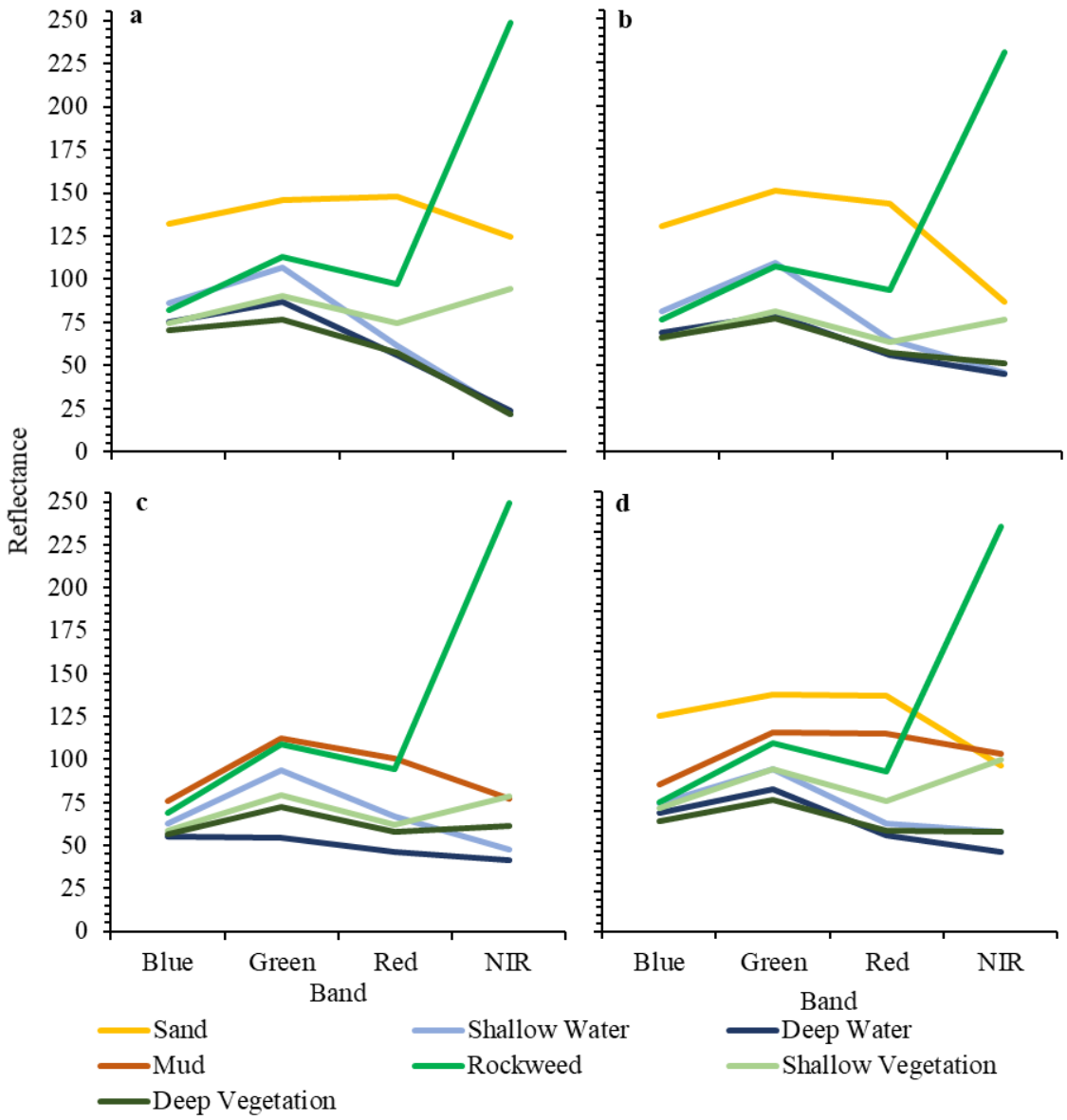

Figure E.22 Training sites spectral signature plots for the training sites created with training data to be used in the supervised maximum likelihood classification for **a** Segment one, **b** two, **c** three, and **d** four in Port Mouton.

Table E.1 Confusion matrix for classifying Port Mouton for the whole bay based on test data points for the **a** supervised classification, **b** first iteration of the unsupervised classification, and **c** full data set for the first iteration of the unsupervised classification. Submerged seaweed and rockweed band are merged into one seaweed group, and mud, sand, shallow and deep water were merged into one bare ground group for the supervised classification. All groups for NIR and the rockweed band are merged into one vegetated group for the unsupervised classification. Total map accuracy (%) in bold.

		Field Survey Reference Data			Total Correct	Total Points	User Accuracy (%)	Kappa coefficient
	Map Data	*Seagrass*	*Seaweed*	*Bare Ground*				
a	**Eelgrass**	22	2	3	22	27	81.48	0.91*
	Seaweed	0	28	1	28	29	96.55	
	Bare Ground	0	0	56	56	56	100.00	
	Total Correct	22	28	56	106			
	Total Points	22	30	60		112		
	Producer Accuracy (%)	100.00	93.33	93.33			**94.64**	
	Map Data	*Vegetated*		*Bare Ground*				
b	**Vegetated**	52		4	52	56	92.86	0.93*
	Bare Ground	0		56	56	56	100.00	
	Total Correct	52		56	108			
	Total Points	52		60		112		
	Producer Accuracy (%)	100.00		93.33			**96.43**	
	Map Data	*Vegetated*		*Bare Ground*				
c	**Vegetated**	170		16	170	186	91.40	0.89*
	Bare Ground	5		184	184	189	97.35	
	Total Correct	170		184	354			
	Total Points	175		200		375		
	Producer Accuracy (%)	97.14		92.00			**94.40**	

Appendix F: Jordan Bay Classification

Methods

Additional visually identified points could not be added to the ground survey points for Jordan Bay, outlined in section 3.2.2, as the colour composites were quiet dark in shallow areas. Furthermore, in addition to the image preprocessing outlined in section 3.2.3, Jordan Bay was subjected to a sun glint correction (Hedley et al. 2005). Lastly, the exploratory ISOCLUST did not pull out a cluster that could be used to determine a depth to set as a deep water mask. Therefore, all analysis were performed on depths shallower then 12m based on *Zostera marina* published maximum depth limit (DFO 2009).

The supervised maximum likelihood classification (section 3.2.4) was performed on all four bands (land and deep water masked out) on four levels of preprocessed data: raw output, only atmospherically corrected, atmospherically corrected with a 3 x 3 median filter, and atmospherically corrected, sun glint correction applied with a 3 x 3 median filter. All classifications were subjected to a 3 x 3 majority filter. In this initial exploratory analysis, all points were used as training data to attempt to have as much data as possible to train the classification, therefore there were no test points remaining to create the confusion matrix. These same four levels of preprocessed data were also run through an ISOCLUST analysis with 3 iterations, up to 50 clusters, and 40 minimum pixels for training sites. These clusters were analyzed in the same methods as section 3.2.4, to label a cluster as a ground cover type.

An unsupervised K-means clustering analysis was performed on the raw data, and atmospherically corrected, sun glint correction applied with a 3 x 3 median filter data, both with land and 12m depth masked out to attempt to pull out a cluster that could be

denoted as “shallow/intertidal zone”, that could then be used to run the ISOCLUST and maximum likelihood classification.

Lastly, Jordan Bay was broken up into western and eastern side, to attempt account for potential differences in spectral signatures between different areas of the bay. Spectral signature plots for ground cover were created, keeping each individual training site isolated. The west and east side of the bay were then subjected to a maximum likelihood classification, and a 3 x 3 majority filter.

Results

The maximum likelihood classification on the four levels of processed data were examined (Figures F.1-F.4), as well as the spectral signatures plot (Figure F.5). Each classification provided similar results and similar spectral curves, with strong misclassification between ground cover type.

The ISOCLUST analysis on the four levels of processed data were examined to label clusters as specific ground cover types (Figures F.6-F.9). Very few clusters could be identified as a specific ground cover type, and these clusters only corresponded to sand bars, and the rockweed band.

The k-means clustering algorithm on the raw data (Figure F.10) and atmospherically corrected, sun glint correction applied with a 3 x 3 median filter data (Figure F.11) provided similar results as the ISOCLUST analysis. No “shallow/intertidal zone” could be created from the clusters.

Examining the spectral signatures plot for each ground cover type for each individual training site, there was little difference between the west and east side of the bay (Figures F.12-F.13). Upon running a separate MLC classification for the west and

east side of the bay (Figures F.14-F.17) there was still strong misclassification between ground cover types. Therefore, based on the poor classification from these four different approaches, the imagery for Jordan Bay was deemed of too poor quality to be included as a final product of seagrass classification.

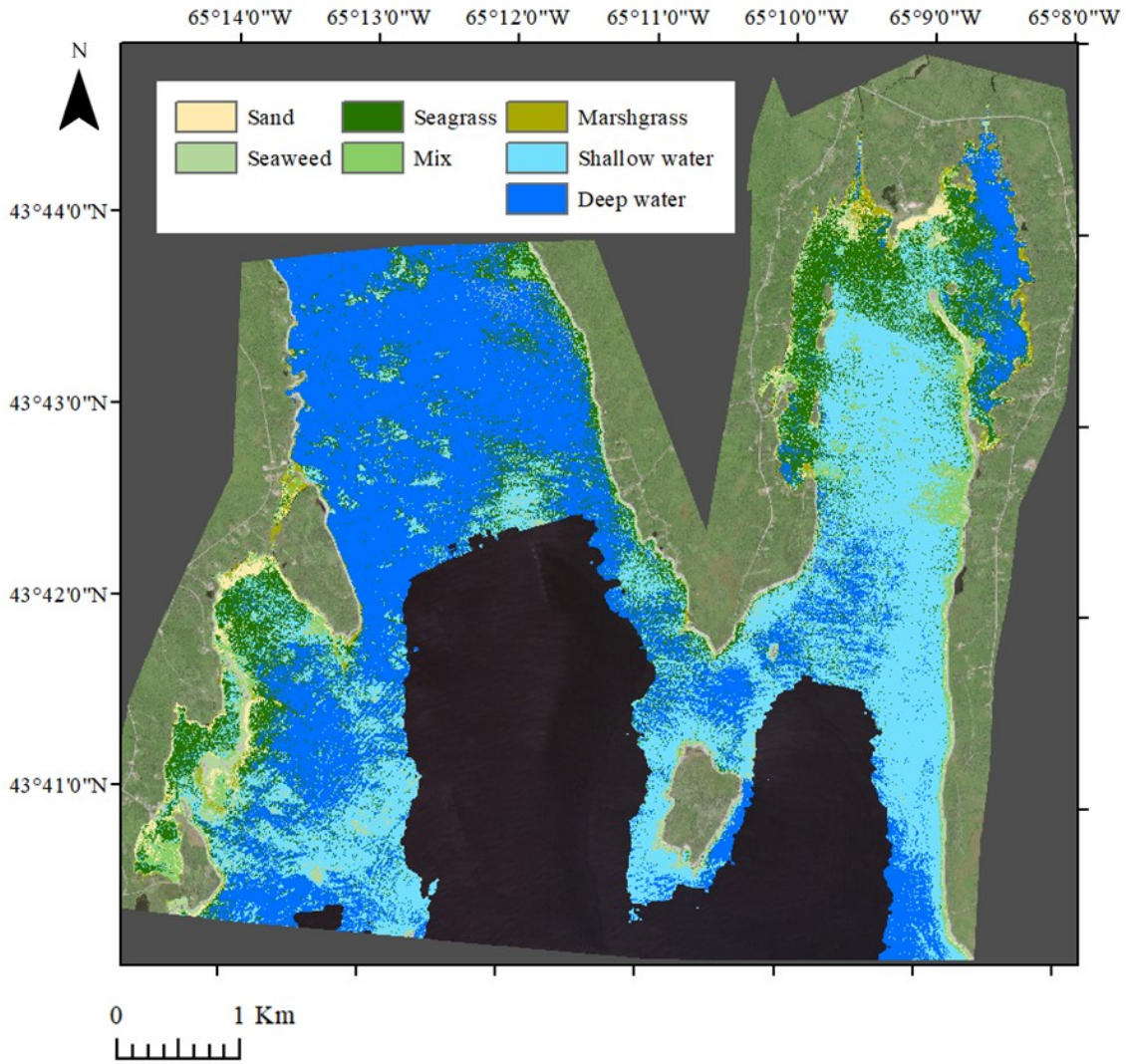

Figure F.1 Maximum likelihood classification on the raw imagery, with all four bands, land and water >12m masked out, run though a 3x3 majority filter, overlaid over the true colour composite. Dark grey is background data outside the satellite imagery bounds.

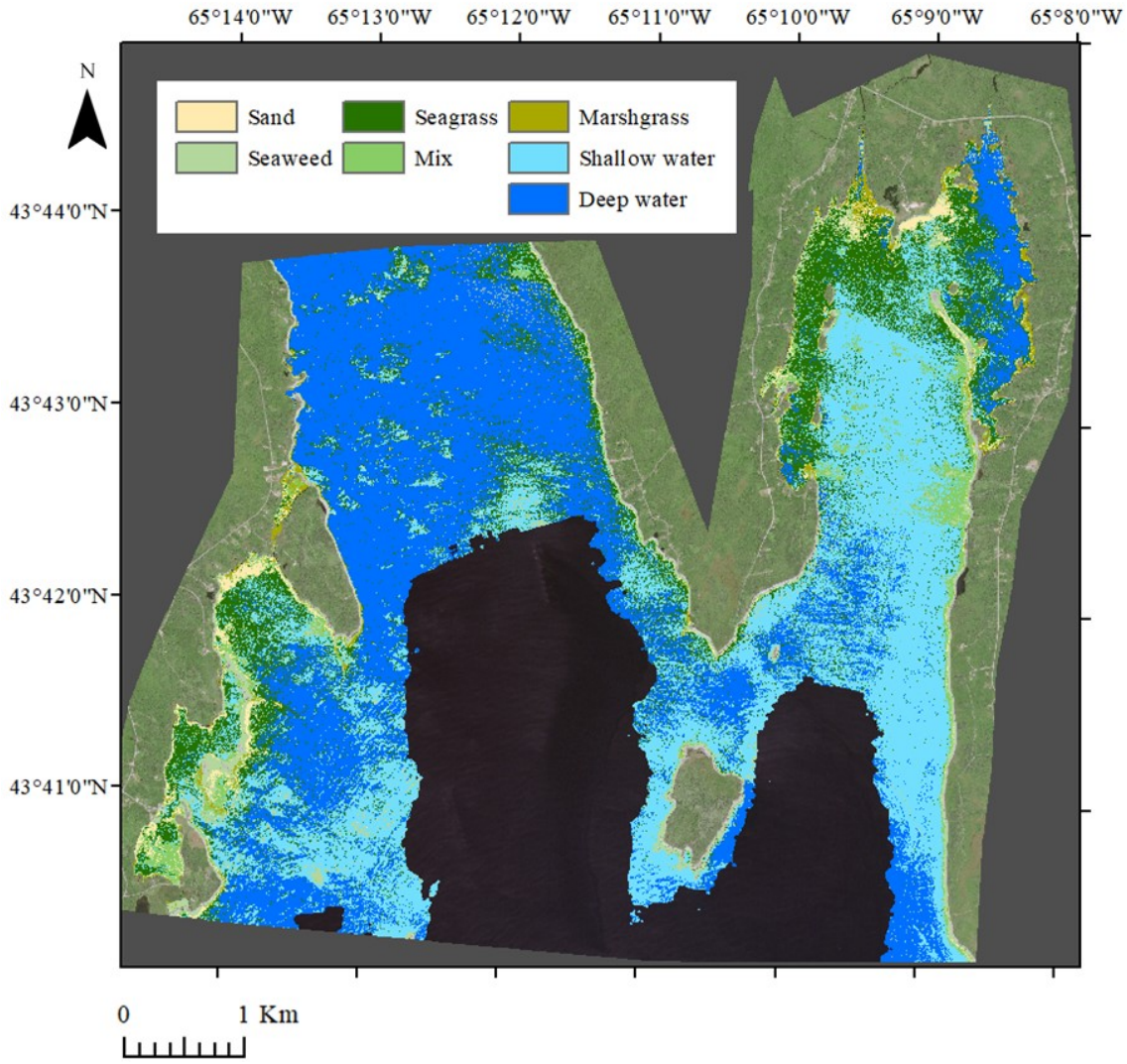

Figure F.2 Maximum likelihood classification on the atmospherically corrected imagery, with all four bands, land and water >12m masked out, run though a 3x3 majority filter, overlaid over the true colour composite. Dark grey is background data outside the satellite imagery bounds.

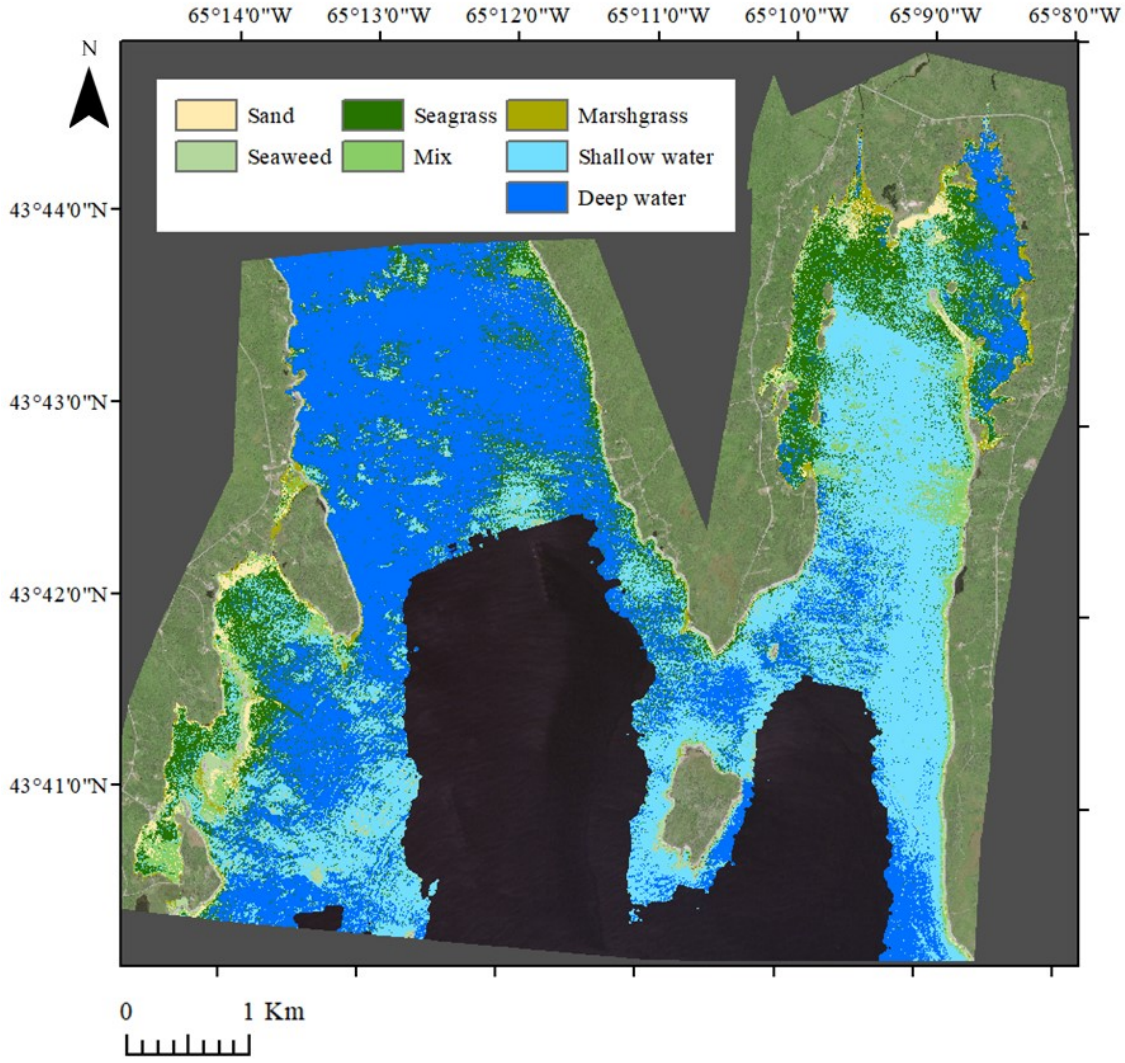

Figure F.3 Maximum likelihood classification on the atmospherically corrected, and 3x3 median filter imagery, with all four bands, land and water >12m masked out, run though a 3x3 majority filter, overlaid over the true colour composite. Dark grey is background data outside the satellite imagery bounds.

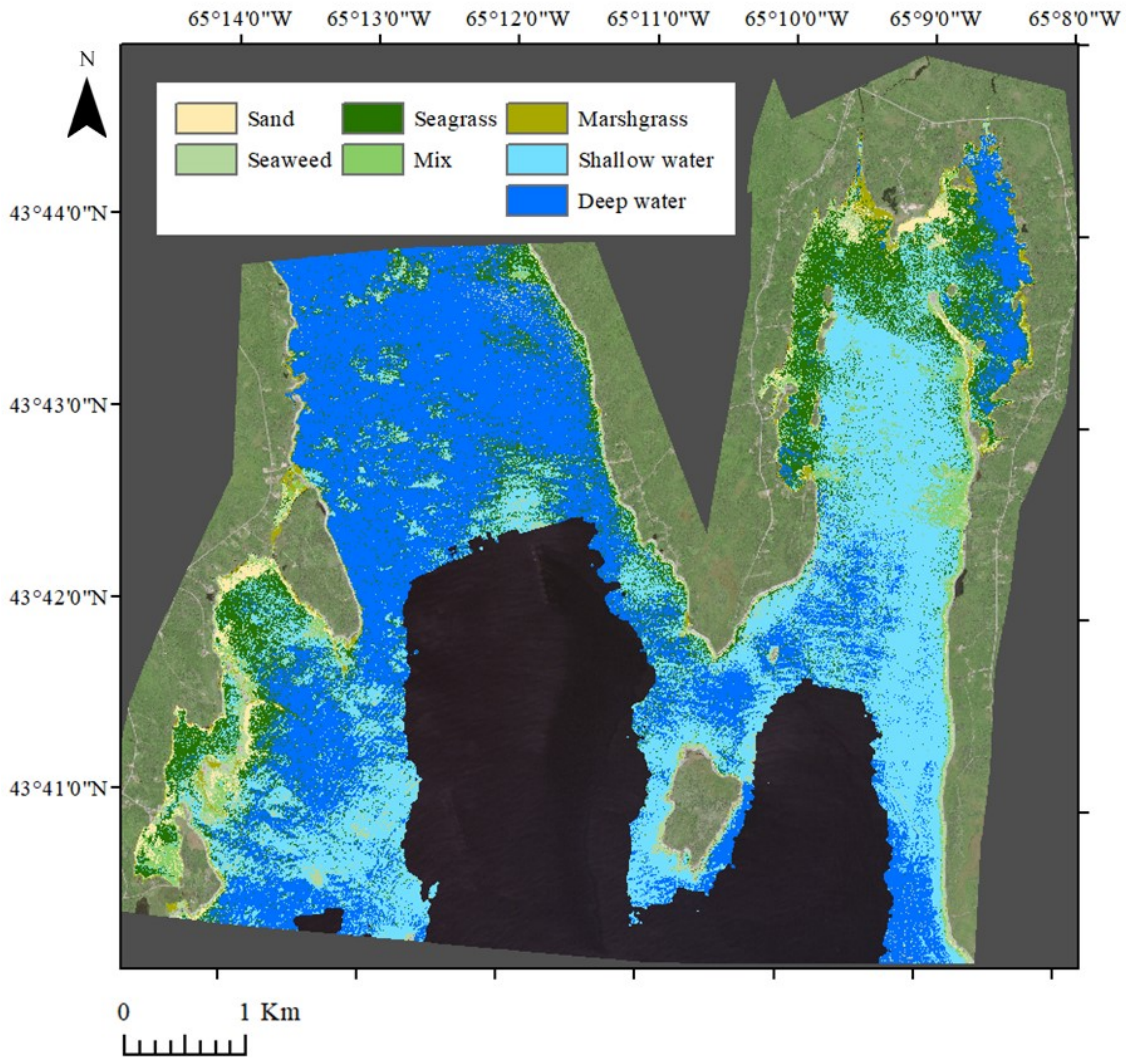

Figure F.4 Maximum likelihood classification on the atmospherically corrected, sun glint corrected, and 3x3 median filter imagery, with all four bands, land and water >12m masked out, run though a 3x3 majority filter, overlaid over the true colour composite. Dark grey is background data outside the satellite imagery bounds.

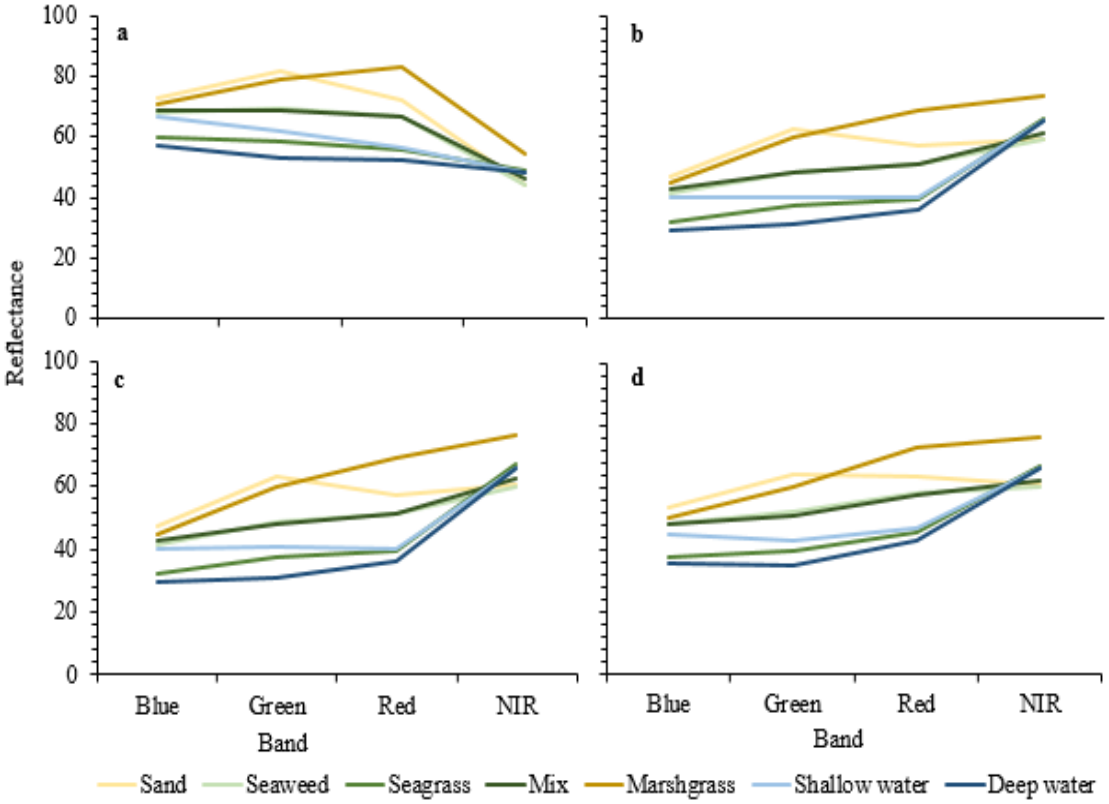

Figure F.5 Spectral signatures plot for the training sites used to create the maximum likelihood classification for **a** raw imagery, **b** only atmospherically corrected, **c** atmospherically corrected with a 3x3 median filter, and **d** atmospherically corrected, sun glint correction applied with a 3x3 median filter

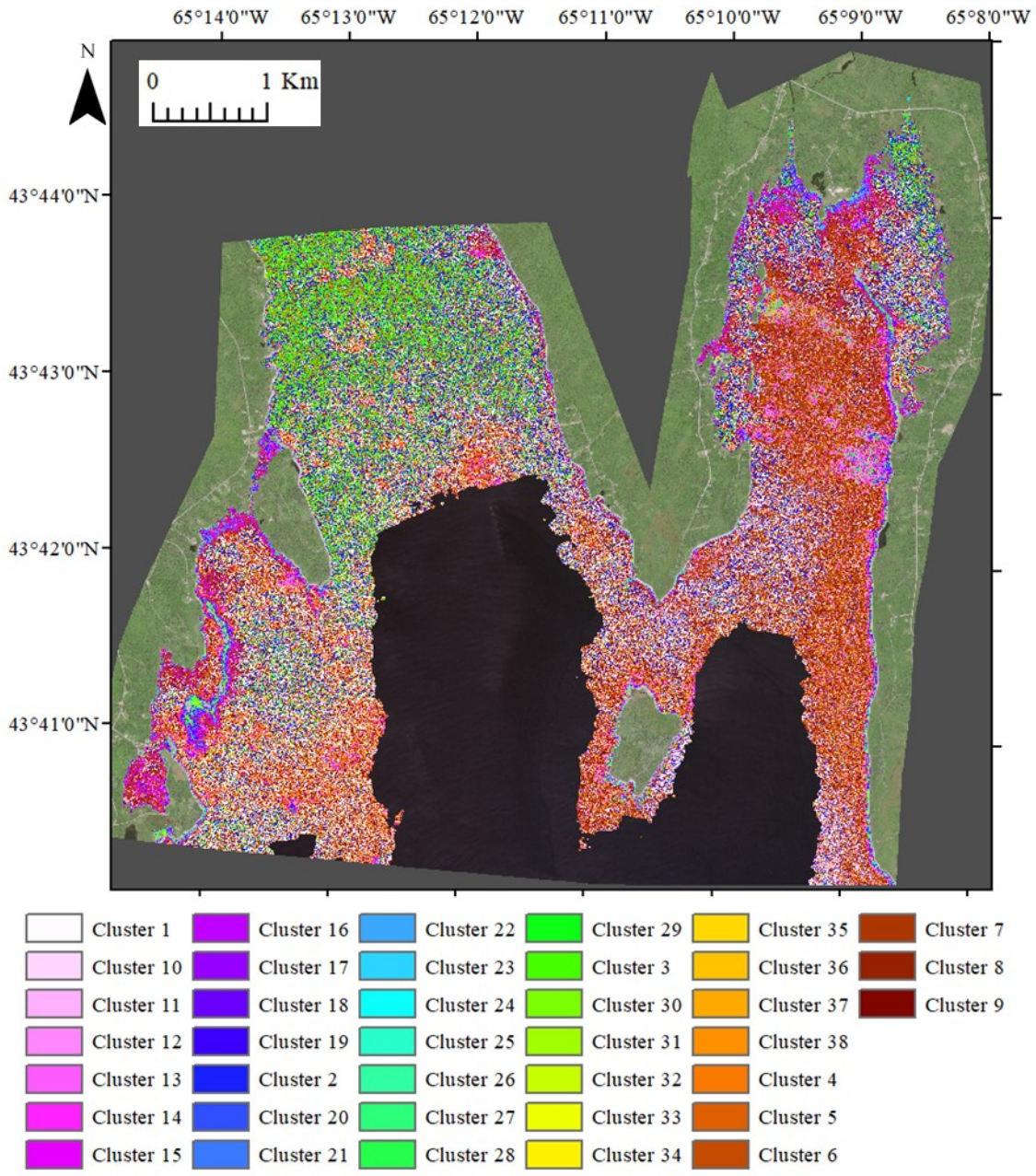

Figure F.6 ISOCLUST analysis on the raw imagery, with all four bands, land and water >12m masked out, overlaid over the true colour composite. Dark grey is background data outside the satellite imagery bounds.

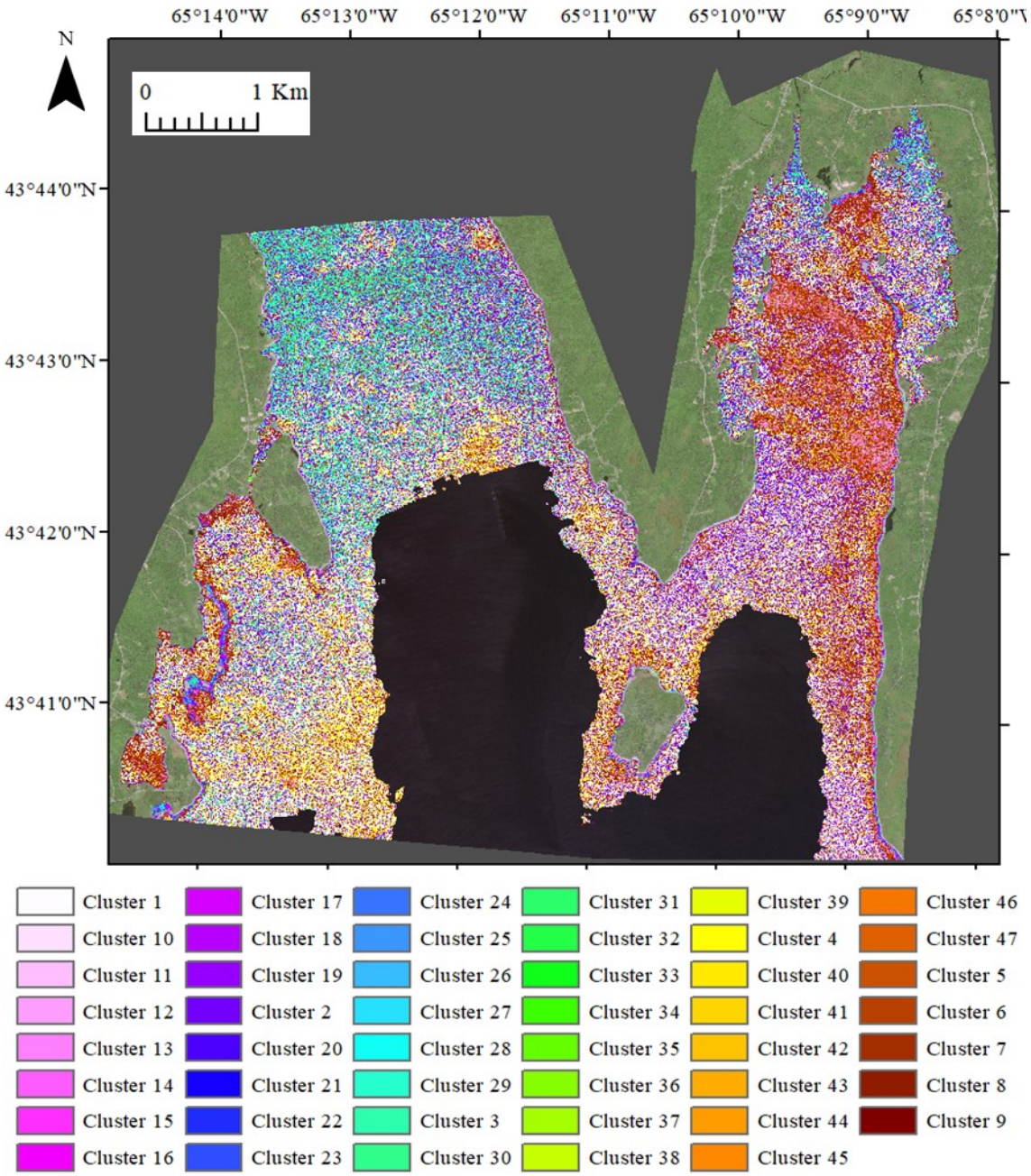

Figure F.7 ISOCLUST analysis on the atmospherically corrected imagery, with all four bands, land and water >12m masked out, overlaid over the true colour composite. Dark grey is background data outside the satellite imagery bounds.

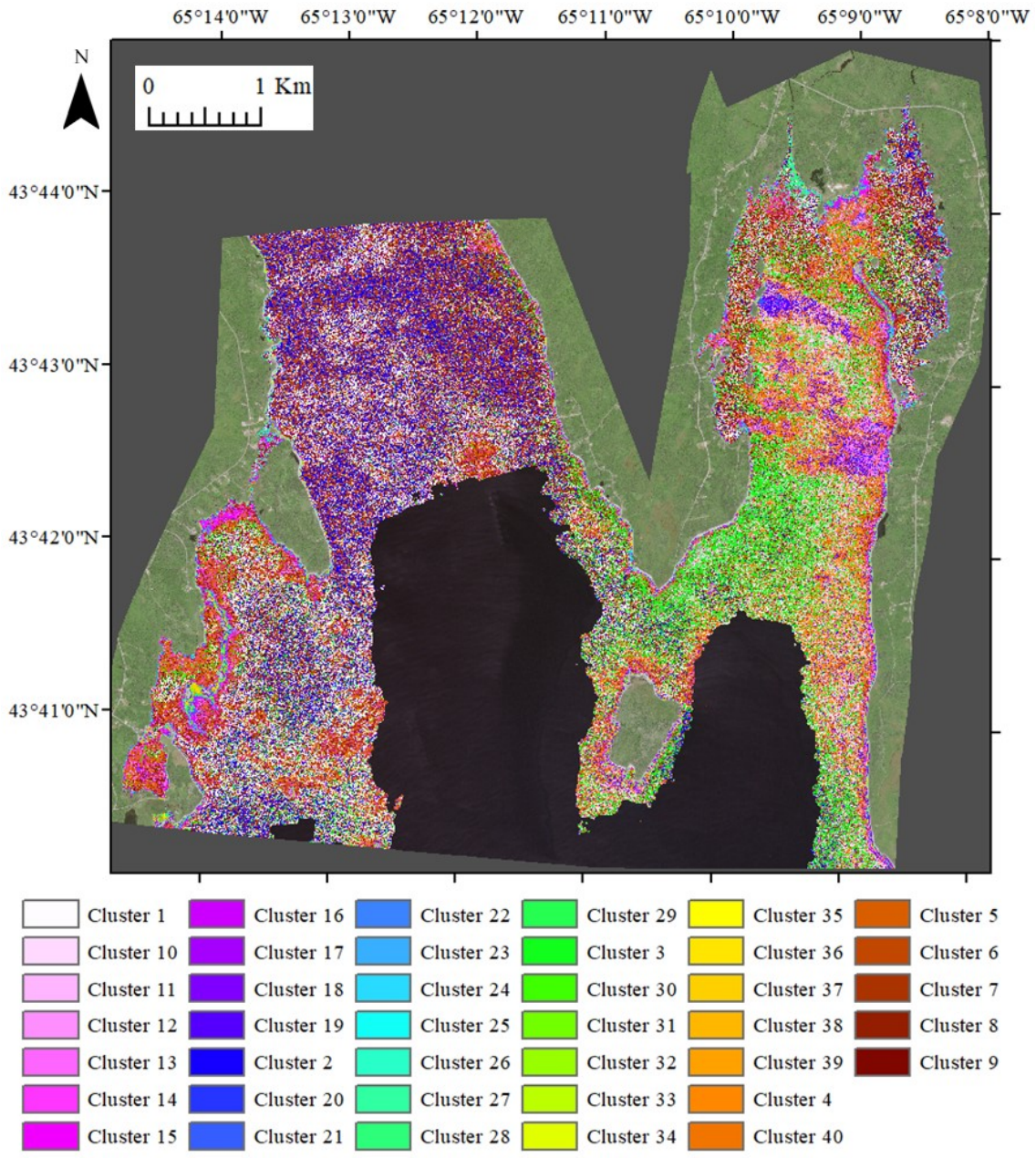

Figure F.8 ISOCLUST analysis on the atmospherically corrected, and 3x3 median filter imagery, with all four bands, land and water >12m masked out, overlaid over the true colour composite. Dark grey is background data outside the satellite imagery bounds.

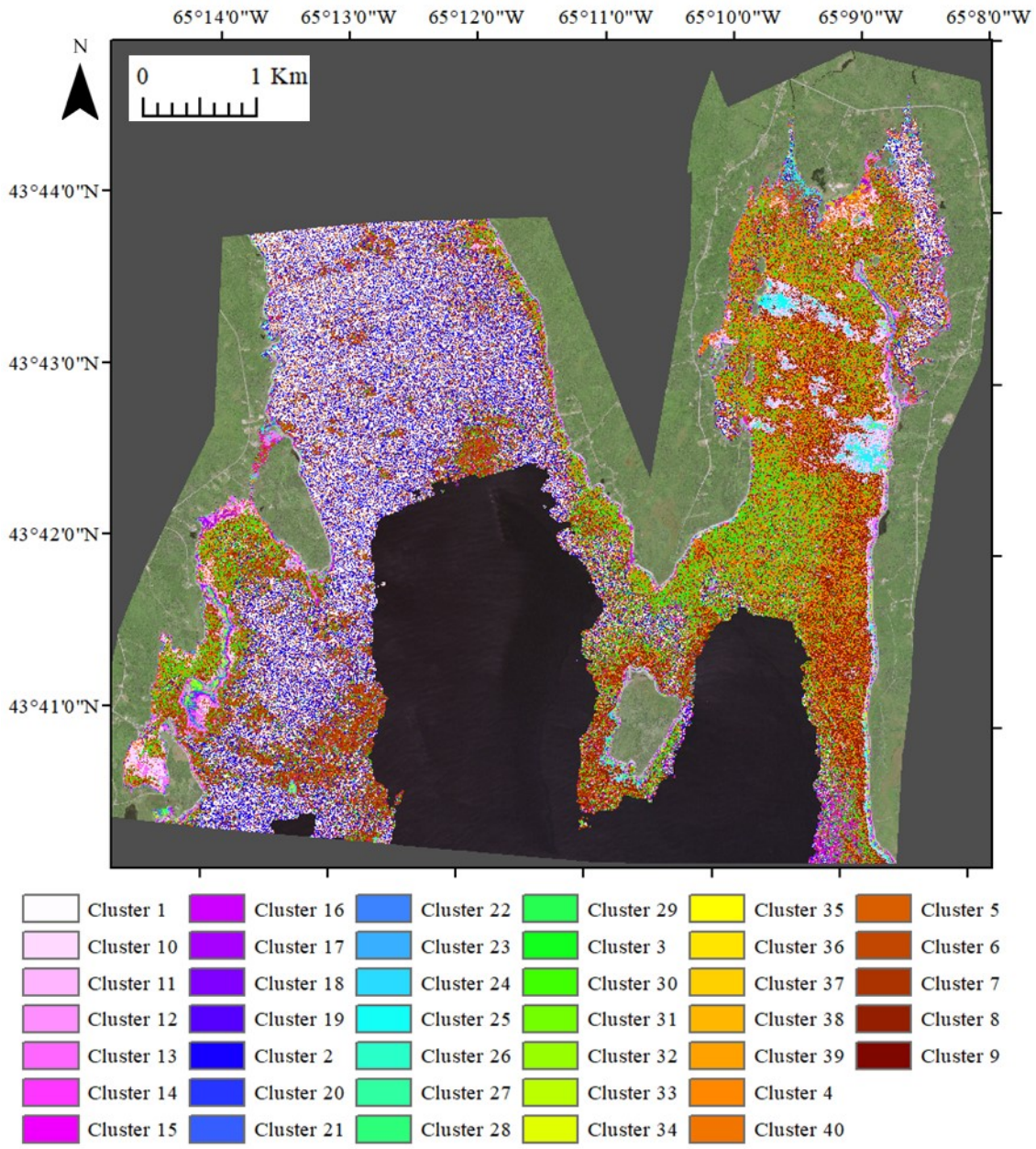

Figure F.9 ISOCLUST analysis on the atmospherically corrected, sun glint corrected, and 3x3 median filter imagery, with all four bands, land and water >12m masked out, overlaid over the true colour composite. Dark grey is background data outside the satellite imagery bounds.

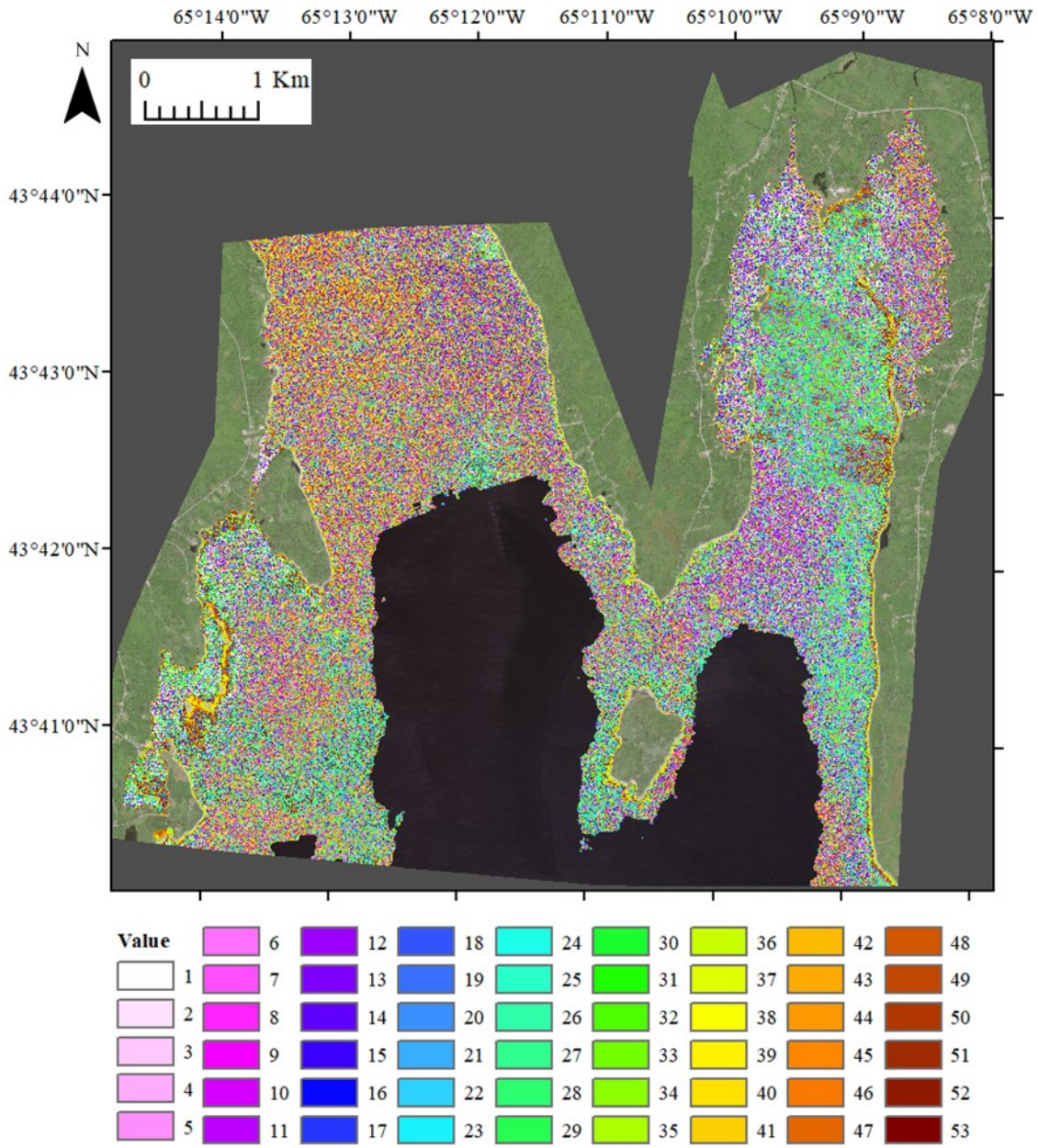

Figure F.10 K-means clustering analysis on the raw imagery, with all four bands, land and water >12m masked out, overlaid over the true colour composite. Dark grey is background data outside the satellite imagery bounds.

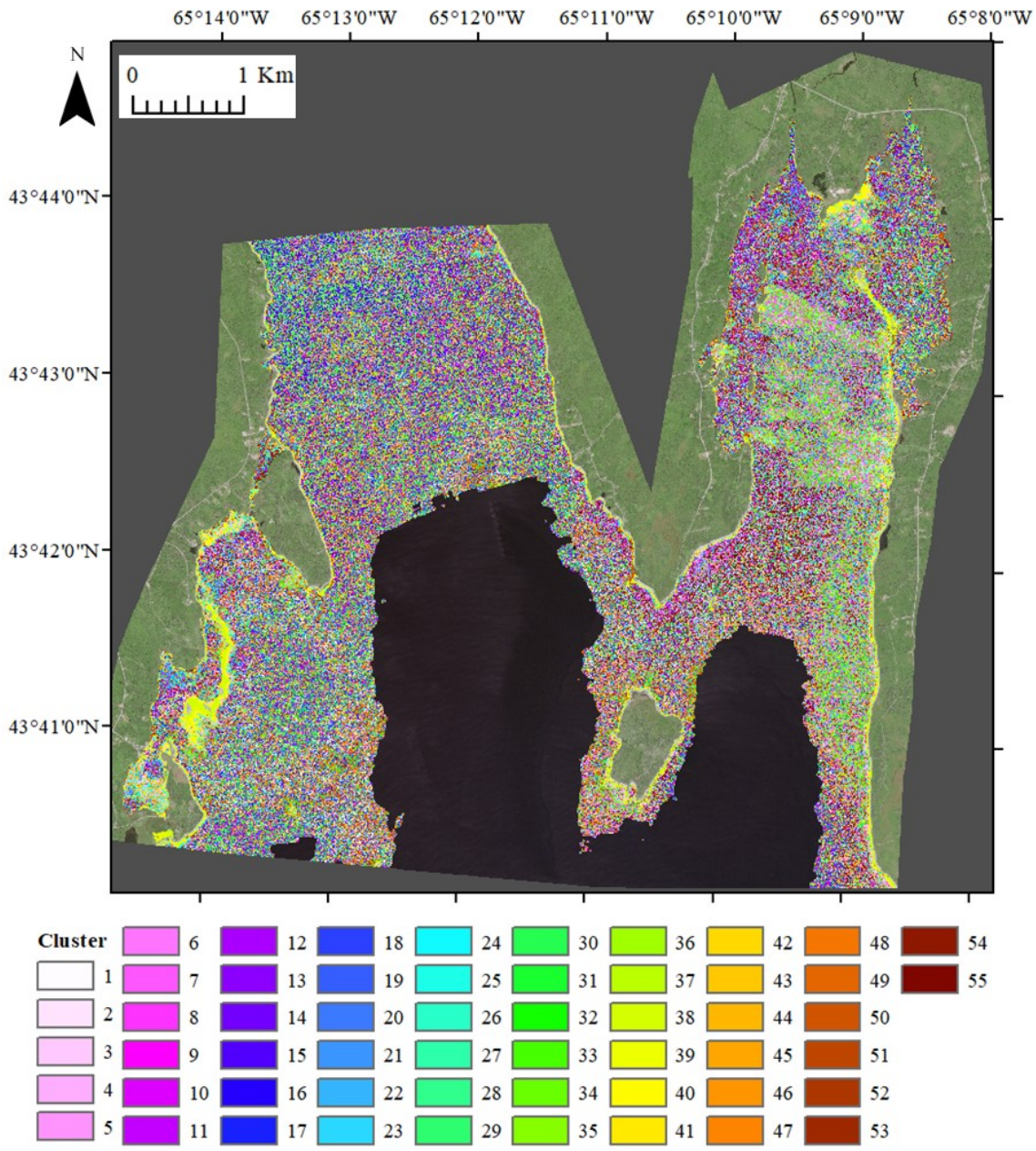

Figure F.11 K-means clustering analysis on the atmospherically corrected, sun glint corrected, and 3x3 median filter imagery, with all four bands, land and water >12m masked out, overlaid over the true colour composite. Dark grey is background data outside the satellite imagery bounds.

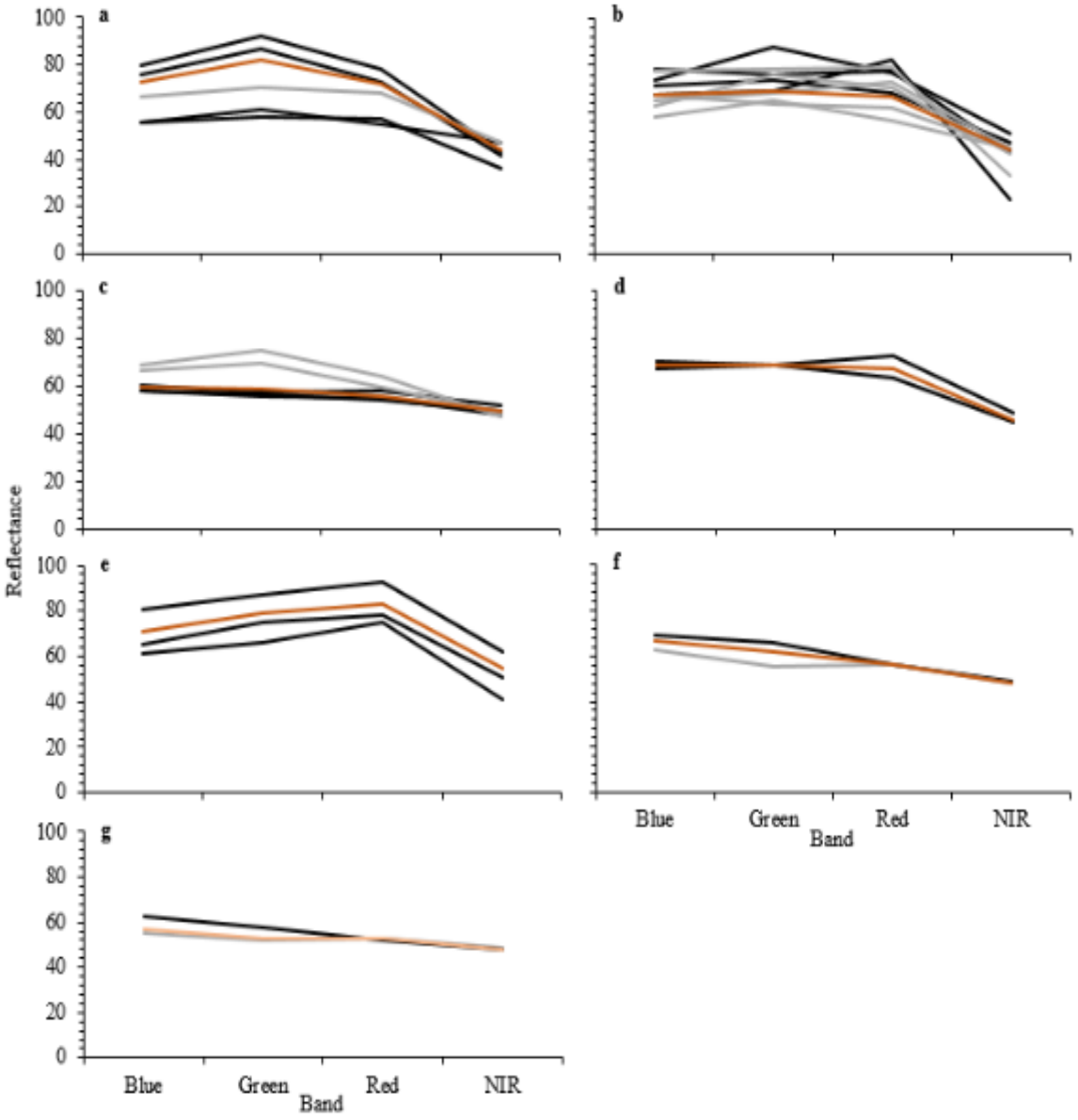

Figure F.12 Spectral signatures plot for blue, green, red, and NIR bands with land, and water >12m masked out, on raw imagery for **a** sand, **b** seaweed, **c** seagrass, **d** seaweed/seagrass mix, **e** marshgrass, **f** shallow water, and **g** deep water. Black lines indicate training sites on the east side of the bay, grey lines indicate training sites on the west side of the bay, orange line indicates the average value of the training sites as a whole

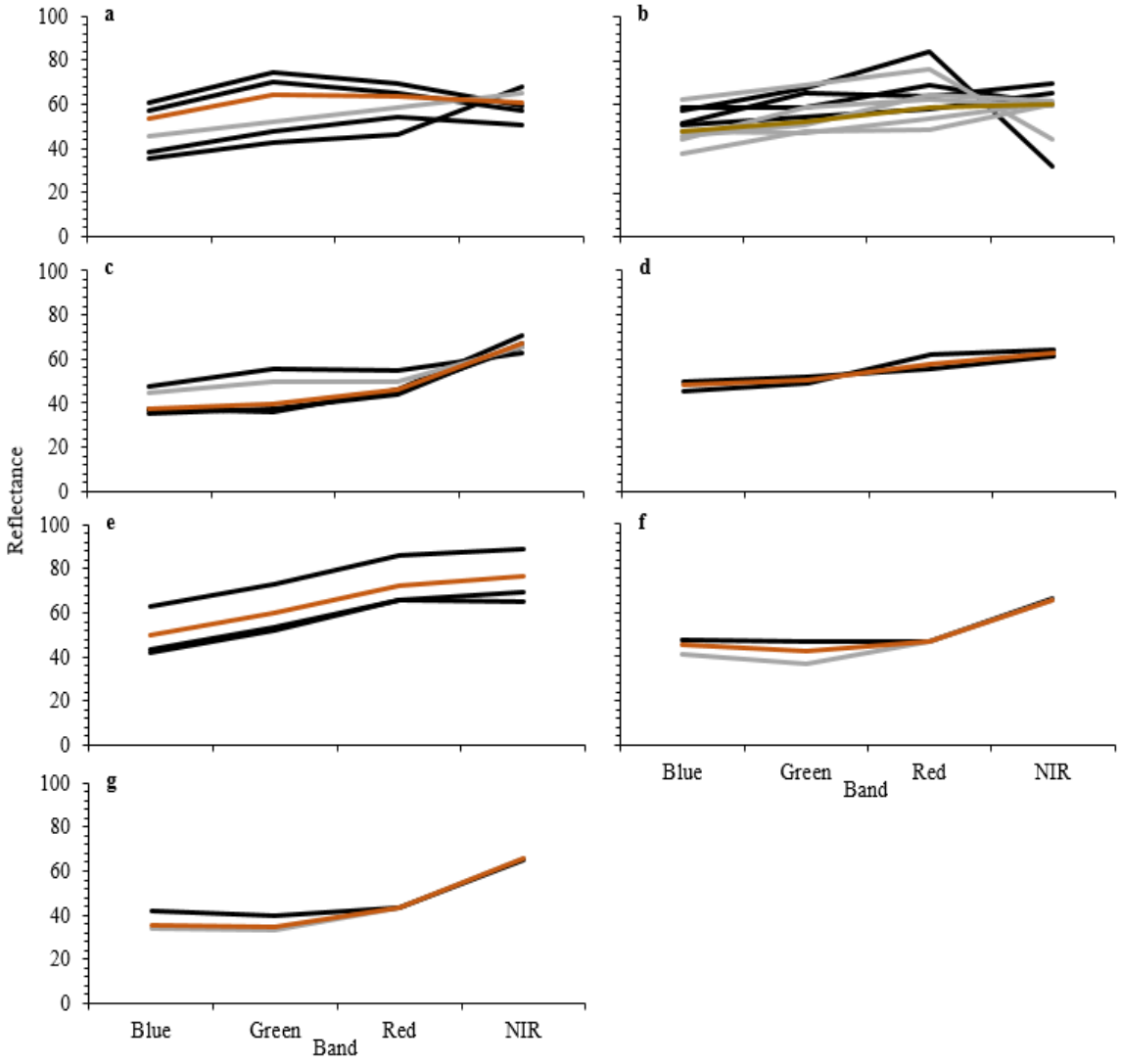

Figure F.13 Spectral signature plot for blue, green, red, and NIR bands with land, and water >12m masked out, on imagery that was atmospherically corrected, sun glint corrected, as well as run through a 3x3 median filter for **a** sand, **b** seaweed, **c** seagrass, **d** seaweed/seagrass mix, **e** marshgrass, **f** shallow water, and **g** deep water. Black lines indicate training sites on the east side of the bay, grey lines indicate training sites on the west side of the bay, orange line indicates the average value of the training sites as a whole.

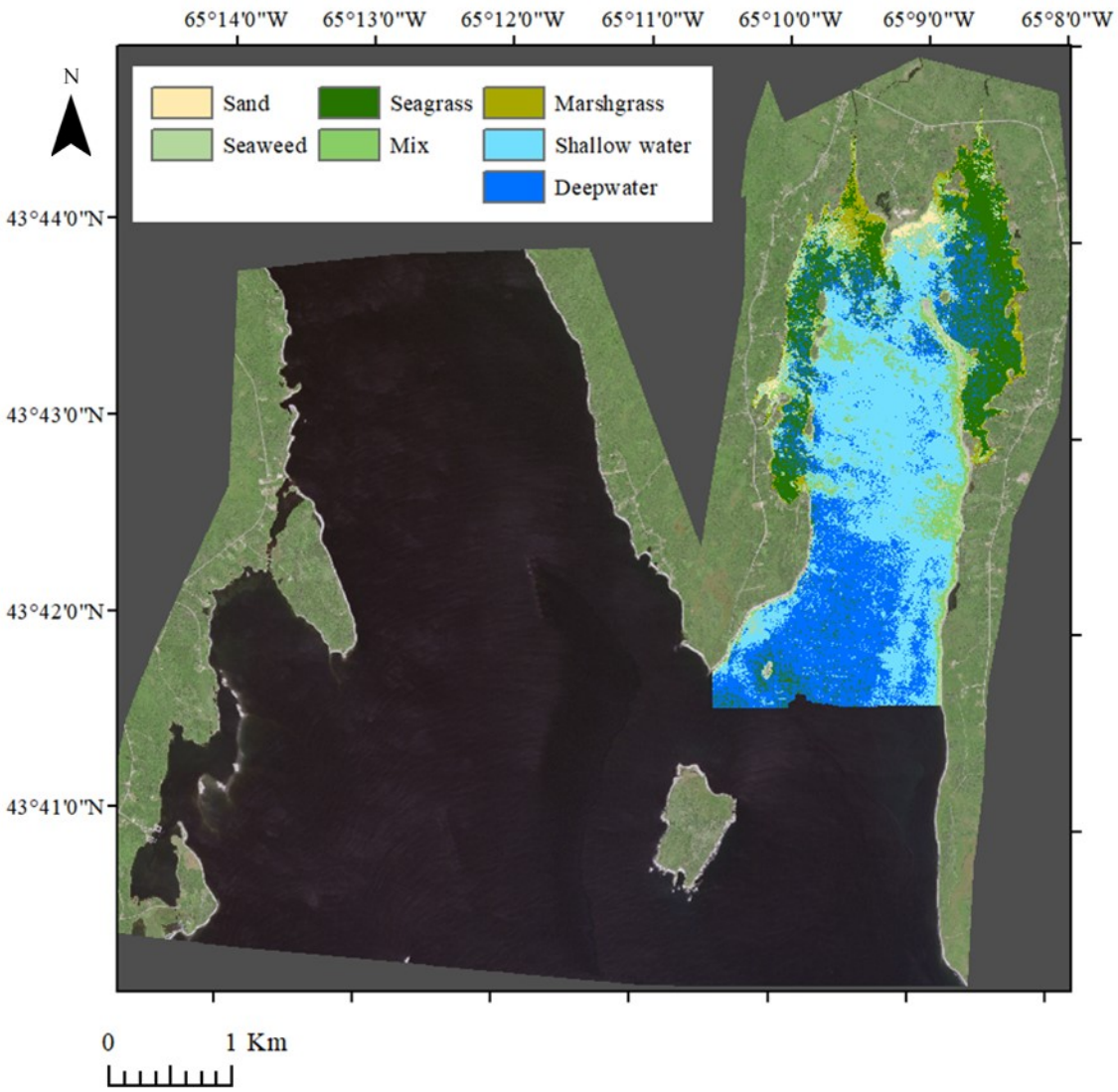

Figure F.14 Maximum likelihood classification on the raw imagery, with all four bands, land and water >12m masked out, run though a 3x3 majority filter, overlaid over the true colour composite, for the east side of the bay. Dark grey is background data outside the satellite imagery bounds.

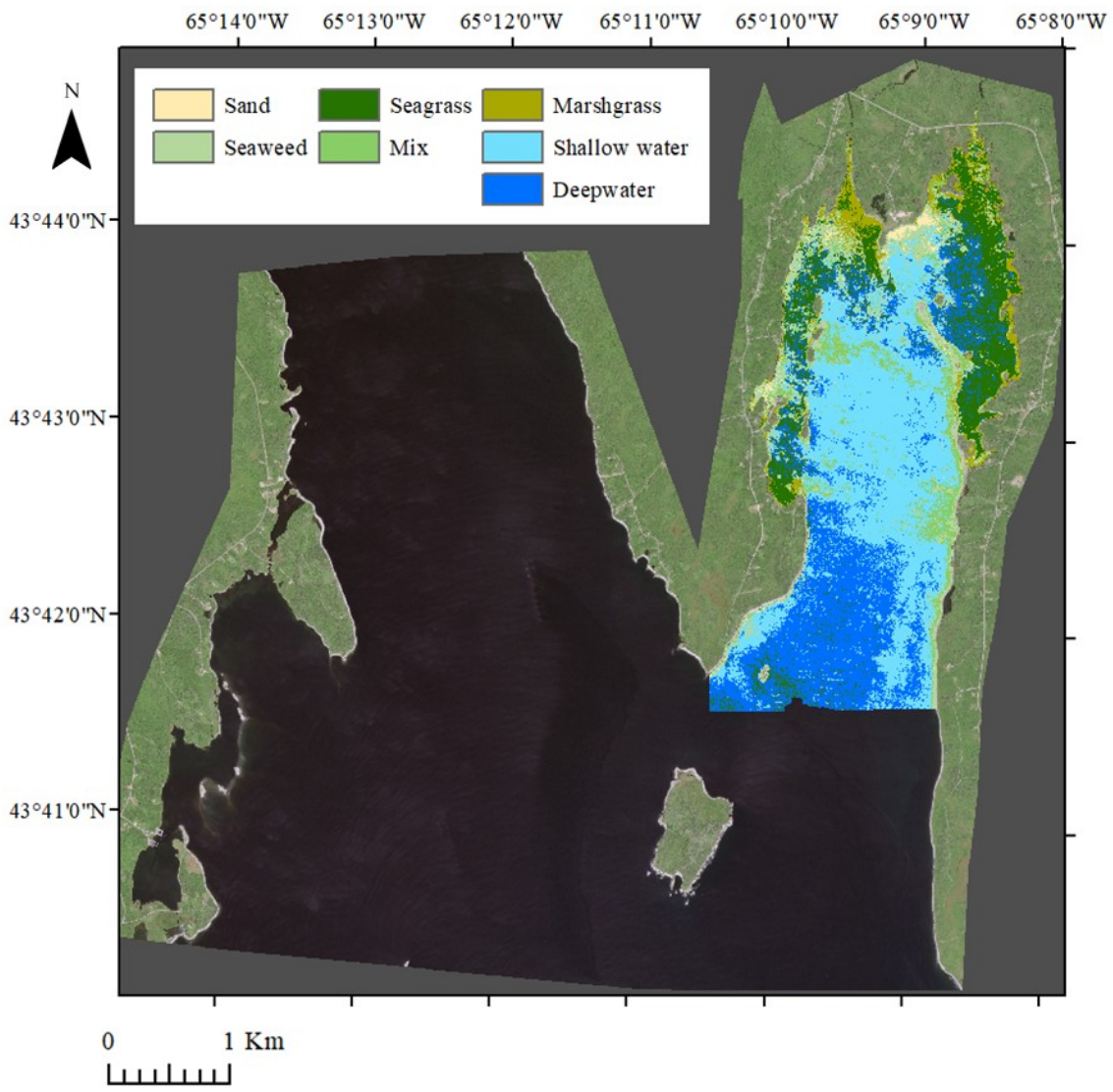

Figure F.15 Maximum likelihood classification on the atmospherically corrected, sun glint corrected, and 3x3 median filter imagery, with all four bands, land and water >12m masked out, run though a 3x3 majority filter, overlaid over the true colour composite, for the east side of the bay. Dark grey is background data outside the satellite imagery bounds.

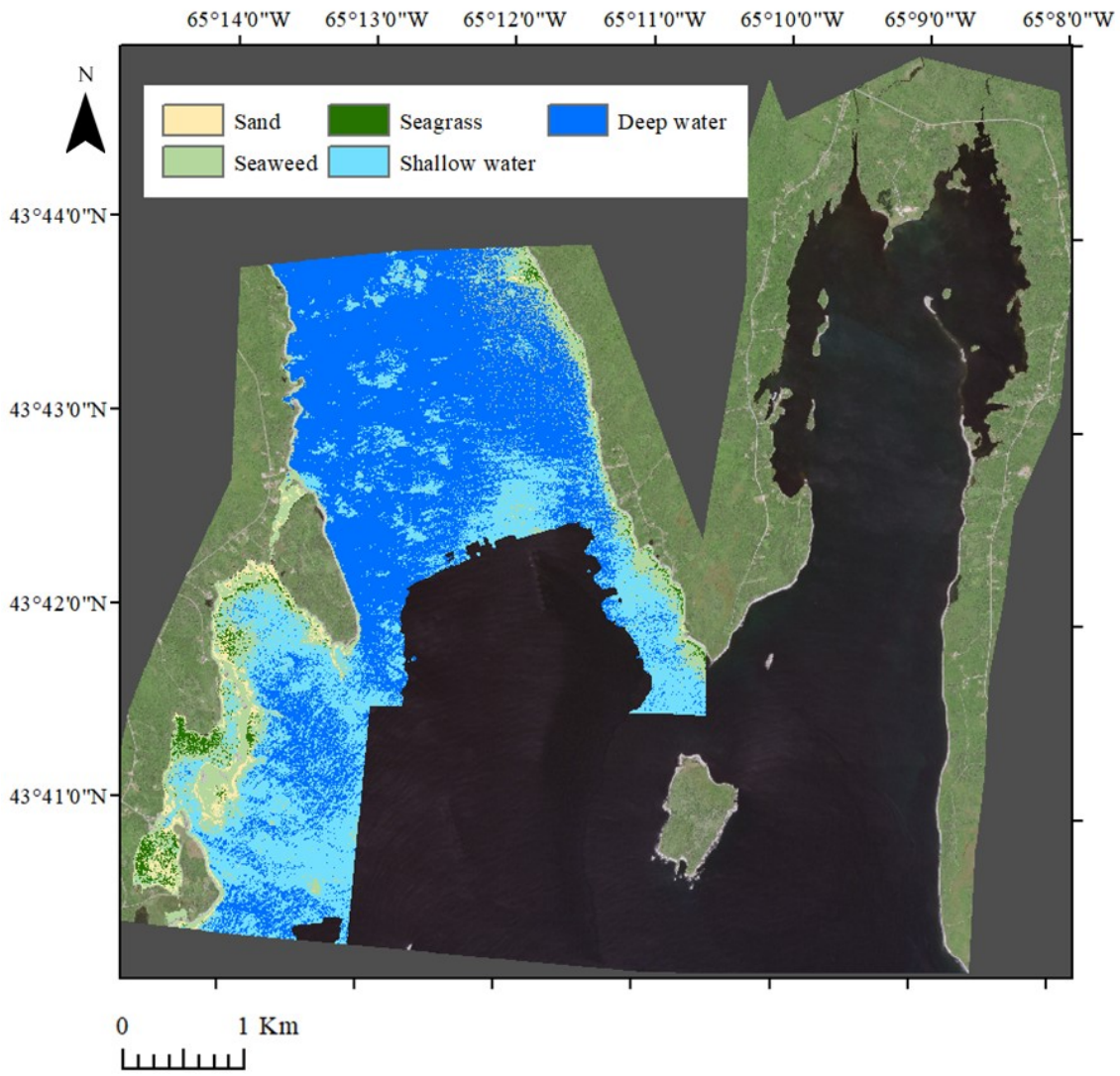

Figure F.14 Maximum likelihood classification on the raw imagery, with all four bands, land and water >12m masked out, run though a 3x3 majority filter, overlaid over the true colour composite, for the west side of the bay. Dark grey is background data outside the satellite imagery bounds.

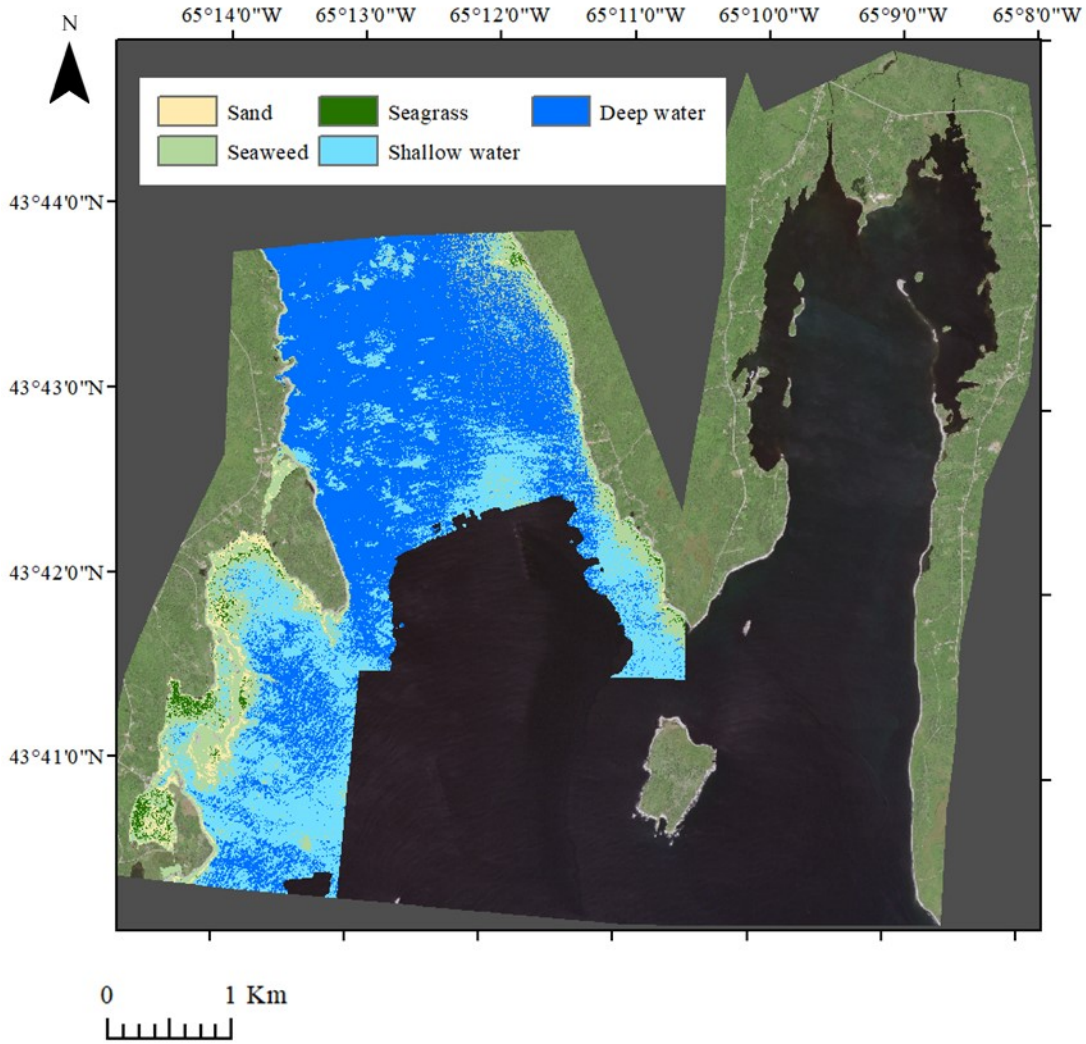

Figure F.15 Maximum likelihood classification on the atmospherically corrected, sun glint corrected, and 3x3 median filter imagery, with all four bands, land and water >12m masked out, run though a 3x3 majority filter, overlaid over the true colour composite, for the west side of the bay. Dark grey is background data outside the satellite imagery bounds.